

NASA CONTRACTOR REPORT 166258

(NASA-CR-166258) STUDY OF VTOL IN
GROUND-EFFECT FLOW FIELD INCLUDING
TEMPERATURE EFFECT Final Report (Grumman
Aerospace Corp.) 179 p HC AC9/MF A01

N82-25170

Jncias
CSCI 01A G3/01 28025

STUDY OF VTOL IN-GROUND-EFFECT FLOW FIELD
INCLUDING TEMPERATURE EFFECT

W.G. Hill
R.C. Jenkins
S.G. Kalematis
M.J. Siclari

CONTRACT NAS2- 10645
April 1982

NASA



NASA CONTRACTOR REPORT 166258

**STUDY OF VTOL IN-GROUND-EFFECT FLOW FIELD
INCLUDING TEMPERATURE EFFECT**

**W.G. Hill
R.C. Jenkins
S.G. Kalemariis
M.J. Siclari
Grumman Aerospace Corporation
Bethpage, New York 11714**

**Prepared for
Ames Research Center
Under Contract NAS2-10645**

NASA

National Aeronautics and
Space Administration

Ames Research Center
Moffett Field, California 94035

CONTENTS

Section		Page
1	SUMMARY	1
2	INTRODUCTION	2
3	SYMBOLS	3
4	EXPERIMENTAL BACKGROUND	5
	4.1 Test Facility	5
	4.2 Air Supply	5
	4.3 Settling Chamber	5
	4.4 Nozzles	7
	4.5 Ground Plane	11
	4.6 Aircraft Model	11
	4.7 Instrumentation	11
	4.7.1 Pressure	11
	4.7.2 Temperature	16
	4.7.3 Probes	16
	4.8 Experimental Techniques	19
5	RESULTS	23
	5.1 Fan-Jet Nozzles	23
	5.1.1 Nozzle Flow	23
	5.1.2 Ground Flow	31
	5.1.3 Upwash Flow	35
	5.1.4 Model Forces	35
	5.1.5 Model Surface Pressures and Temperatures	41
	5.2 Open Circular Nozzles	46
	5.2.1 Nozzle Flow	46
	5.2.2 Ground Flow without Model	50
	5.2.3 Upwash Flow without Model	59

PRECEDING PAGE BLANK NOT FILMED

CONTENTS (contd)

<u>Section</u>	<u>Page</u>
5.2.4 Effect of Model on Ground Flow	64
5.2.5 Effect of Model on Upwash	64
5.2.6 Model Forces	67
5.2.7 Model Surface Pressures and Temperatures	70
5.3 Conclusions	75
5.3.1 Fan-Jet Simulation	75
5.3.2 Open Circular Nozzles	75
6 PREDICTION METHODOLOGY	76
6.1 Theoretical Models for Non-Isothermal Jet	77
6.2 General Impingement Temperature and Velocity Equations	77
6.3 Conservation Equations	81
6.4 Heated Free-Jet Model	81
6.4.1 Potential Core Region	86
6.4.2 Transition and Fully-Developed Regions	86
6.5 Jet Deflection Region	89
6.6 Heated Wall-Jet Transition Model	93
6.7 Two-Jet Interaction Model	98
6.7.1 Maximum Pressure and Temperature Distribution along the Upwash Stagnation Line	99
6.7.2 Upwash Momentum Model	100
6.7.3 Heated Upwash Decay Model	101
6.7.4 Recirculation Model	103
7 CONCLUSIONS	109
APPENDIX - COMPUTER PROGRAM DESCRIPTION	110
REFERENCES	170

ILLUSTRATIONS

<u>Figure</u>		<u>Page</u>
1	Ram air system location plan, Plant 31	6
2	Test arrangement	7
3	Ram air system schematic	8
4	Settling chamber arrangement	9
5	Fan-jet nozzle simulation	10
6	Ground plane	12
7	1/24 scale model	15
8	Model instrumentation	17
9	Flowfield probes	18
10	Wall-jet traversing system	20
11	Position readout system	22
12	Coordinate system and nomenclature	24
13	Pitot pressure profile at fan nozzle exit, baseline pressure operation	25
14	Pitot pressure profile at core nozzle exit, baseline pressure operation	26
15	Variation of nozzle thrust with core exit temperature for baseline nozzle pressure conditions	28
16	Effect of fan and core total pressure on nozzle thrust	29
17	Free-jet pitot pressure profiles, baseline operation	30
18	Ground pressure profiles, fan-jet impingement	32
19	Ground temperature measurements	33
20	Wall jet temperature and total pressure profiles	34
21	Data from wall jet profiles resulting from fan-jet impingement . .	36
22	Pressure profiles across upwash centerline, $H_B/D_F = 1.54$. . .	37
23	Pressure profiles across upwash centerline, $H_B/D_F = 1.99$. . .	38
24	Variation of centerline upwash temperature with ground height .	39
25	Effect of fan pressure on interference forces	40
26	Effect of fan nozzle pressure on interference forces	42
27	Effect of core temperature and fan pressure ratio on interference forces, $T_{T,F} = 24^\circ\text{C}$	43

ILLUSTRATIONS (Cont.)

<u>Figure</u>		<u>Page</u>
28	Temperature distribution along model underside	44
29	Variation of model pressure and temperature with ground height	45
30a	Pressure distribution along model	47
30b	Pressure distribution across model	48
31	Model temperature distribution	49
32	Free jet total pressure surveys, $T_{SC\ NOM} = 227^{\circ}C$	51
33	Free jet total temperature surveys, $T_{SC\ NOM} = 227^{\circ}C$	54
34	Free jet properties along one flow centerline, two jets operating, open circular nozzles	56
35	Radial ground pressure distribution around one jet impingement center	57
36	Data from wall jet profiles, open jet impingement	58
37	Upwash properties at nozzle exit plane	60
38	Upwash properties between nozzle exit plane and ground, $H/D = 3$	62
39	Effect of settling chamber pressure on upwash properties at nozzle exit plane	63
40	Radial ground pressure distributions around one jet impingement center	65
41	Effect of presence of body on upwash temperature	66
42	Effect of presence of body on upwash pressures	68
43	Effect of nozzle exit temperature on ground interference forces	69
44	Effect of nozzle stagnation pressure on ground interference forces	70
45	Pressure distribution along fuselage underside.	71
46	Pressure distribution across fuselage underside	72
47	Variation of model pressure with height above ground	73
48	Pressure distribution along fuselage underside	74
49	Temperature distribution along fuselage underside	74

ILLUSTRATIONS (Cont.)

<u>Figure</u>		<u>Page</u>
50	Two-jet interacting flows - negligible deflection zone interaction	76
51	Dimensionless velocity and temperature difference profile data . .	78
52	Jet half-velocity width model	82
53	Comparison of computed heated free-jet dimensionless velocity and temperature difference decay with test data	88
54	Comparison of computed free-jet dimensionless dynamic pressure decay with test data	88
55	Comparison of computed free-jet dimensionless dynamic pressure decay with test data	89
56	Heated free-jet boundary growth characteristics	90
57	Heated free-jet boundary growth characteristics	91
58	Definition of scaling parameters for jet-impingement and wall-jet regions	92
59	Heated wall-jet dimensionless total pressure and temperature difference decay with ground radius.	98
60	Two-jet impingement without deflection zone interaction	99
61	Characteristic scaling parameters for upwash model	101
62	Heated upwash centerline decay characteristics with recirculation effects	104
63	Recirculation effects	105
64	Heated wall-jet decay characteristics with azimuthal recirculation model	106
65	Heated wall-jet decay characteristics ($\phi = 0$) versus jet spacing	107
66	Correlation of heated upwash decay characteristics ($\phi = 0$) with recirculation model.	108
66	Correlation of heated upwash decay characteristics ($\phi = 0$) with recirculation model.	108
67	Typical program input	112
68	Typical program printout	114
69	Program FORTRAN listing	140

VTOL IN GROUND EFFECT FLOWS
FOR CLOSELY SPACED JETS WITH TEMPERATURE

W.G. Hill, R.C. Jenkins, S.G. Kalemari and M.J. Siclari

Grumman Aerospace Corporation
Bethpage, New York

1 - SUMMARY

The primary purpose of this study was to obtain detailed pressure, temperature, and velocity data for twin-fan configurations in-ground-effect and to develop flow models to aid in predicting pressures and upwash forces on aircraft surfaces. For the basic experiments, 49.5mm-diameter jets were used, oriented normal to a simulated ground plane, with pressurized, heated air providing a jet. The experimental data consisted of: (1) the effect of jet height and temperature on the ground, model, and upwash pressures and temperatures, (2) the effect of simulated aircraft surfaces on the isolated flow field, (3) the jet-induced forces on a three-dimensional body with various strakes, (4) the effects of non-uniform coannular jets.

For the uniform circular jets, temperature was varied from room temperature (24°C) to 232°C. Jet total pressure was varied between 9,300 Pascals and 31,500 Pascals. For the coannular jets, intended to represent turbofan engines, fan temperature was maintained at room temperature while core temperature was varied from room temperature to 437°C. Fan and core total pressures were chosen to match the power settings most frequently used during the large-scale tests of Reference 1.

In general, the test data correlate well with the induced forces presented in Reference 1. No scale effects were found, and jet temperature and pressure did not affect the nondimensionalized induced lift. The induced lift in-ground-effect was found to be higher for the uniform circular jets than for the simulated fan jets.

Modifications to an existing wall-jet transition model adequately predict the trends with height above ground of upwash temperatures and pressures. The addition of a recirculation model is necessary to predict upwash temperatures in the presence of an aircraft.

2 - INTRODUCTION

Lift and control for V/STOL aircraft operating in-ground-effect present a critical condition in sizing the propulsion system. Ground proximity effects can result in large jet-induced lift losses or produce positive fountain lift, depending on the aeropropulsion configuration. The complexity of the resulting flow field and the sensitivity to many design parameters give rise to a large body of experimental data which model various aspects of the flow field. The primary purpose of this study was to expand the existing data base for a twin-fan V/STOL aircraft by exploring the effects of temperature and non-uniformities (temperature and pressure) in the jet. These effects were then added to an existing computerized prediction method.

Of almost equal importance, and possibly greater interest to the typical reader, this effort also investigated scale effects on jet-induced characteristics. To this end, the model used was a 1/24-scale replica of a TF 34-powered, large-scale model tested recently at NASA-Ames (Reference 1).

3 - SYMBOLS

A	=	Area; nozzle exit area
b	=	Thickness of viscous layer
D	=	Diameter; nozzle exit diameter
f	=	Analytic functions representing viscous profiles
F	=	Force; radial flux deflection function
ΔF	=	Interference force (total force on body minus thrust)
h	=	Nozzle height above ground
H	=	Heat; distance to ground
M	=	Mach number; momentum
NPR	=	Nozzle pressure ratio relative to ambient
NTR	=	Nozzle temperature ratio relative to ambient
P	=	Static pressure
q	=	Dynamic pressure
r	=	Jet radius; ground radius coordinate
r_o	=	Ground impingement radius
R	=	Radius from one jet impingement point
S	=	Jet spacing
T	=	Temperature; static temperature
V	=	Velocity
X	=	Distance perpendicular to Y and Z
Y	=	Distance from midpoint of line joining jet centerline
Z	=	Distance above ground; vertical jet or ground coordinate
Z'	=	Distance downward from nozzle exit
α	=	Exponent of profile function
γ	=	Isentropic exponent; ratio of specific heats
δ	=	Boundary layer thickness
Δ	=	Difference between local and ambient conditions
ζ	=	Non-dimensional wall thickness
η	=	Thrust efficiency factor; nondimensional thickness
θ	=	Angular orientation around one jet impingement point
ρ	=	Density
γ	=	Angle in ground polar

SUBSCRIPTS

a, A	=	Ambient
B	=	Body
C	=	Core nozzle exit conditions; potential core
F	=	Flux, fan nozzle exit conditions
FD	=	Fully-developed
g	=	Value at ground effect height
H	=	Half value
J	=	Nozzle value; jet exit conditions for open circular nozzle
m, M	=	Maximum value; viscous layer
N	=	Nozzle
PC	=	Potential core
rec	=	Recirculation
S	=	Stagnation value; static
T	=	Thermal layer; total; stagnation
u	=	Upwash
V	=	Velocity layer
W	=	Wall jet

4 - EXPERIMENTAL BACKGROUND

4.1 Test Facility

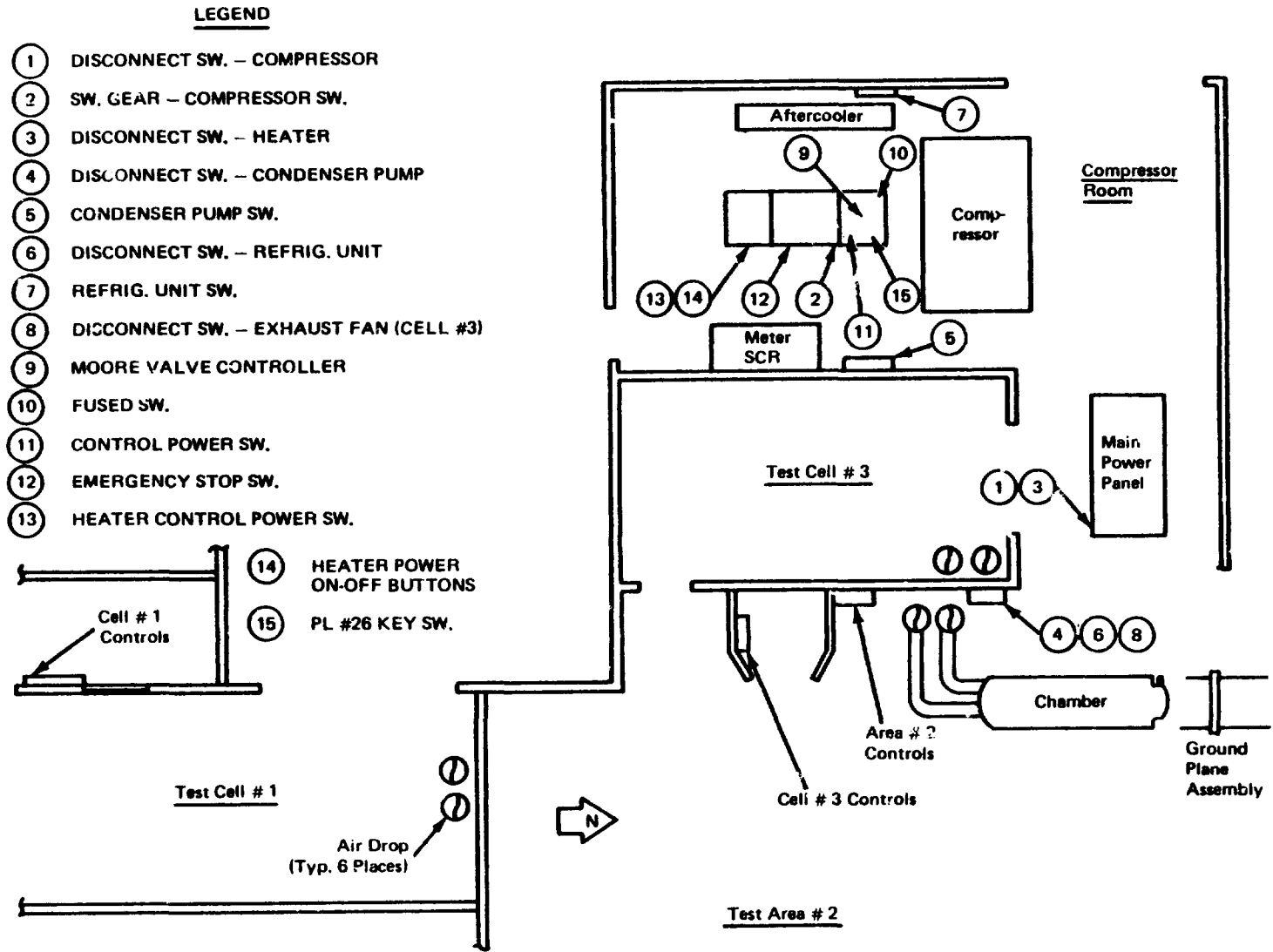
The experiments conducted under this contract were performed in the Grumman Environmental Test Facility (ETF). This facility performs a wide range of system and component testing for Grumman and has two compressor systems capable of supplying heated air: the ram air system for pressures to 110 kPag and temperatures to 232°C, and the bleed air system for pressures to 3.45 MPag and temperatures to 760°C. A general overview of the installation in this facility is given in Figure 1; a detailed photo of the test arrangement is presented in Figure 2.

4.2 Air Supply

For most of the tests, the air was compressed by a Rootes-type blower (referred to in this facility as the "ram air compressor"). Compression heating of the flow was removed and the flow divided into two piping systems. One system was then heated by a controlled resistance electrical heating system with a maximum temperature of 249°C. Both the hot and cold flows were piped to the test site by 20.3-cm diameter insulated piping systems. Supply pressure was controlled by a feedback control system at the compressor control panel and a second control valve at the user's outlet area (Figure 3). For the experiments with core temperatures above 232°C, air was supplied by a piston-type compressor and gas and electric heaters in series (bleed-air systems).

4.3 Settling Chamber

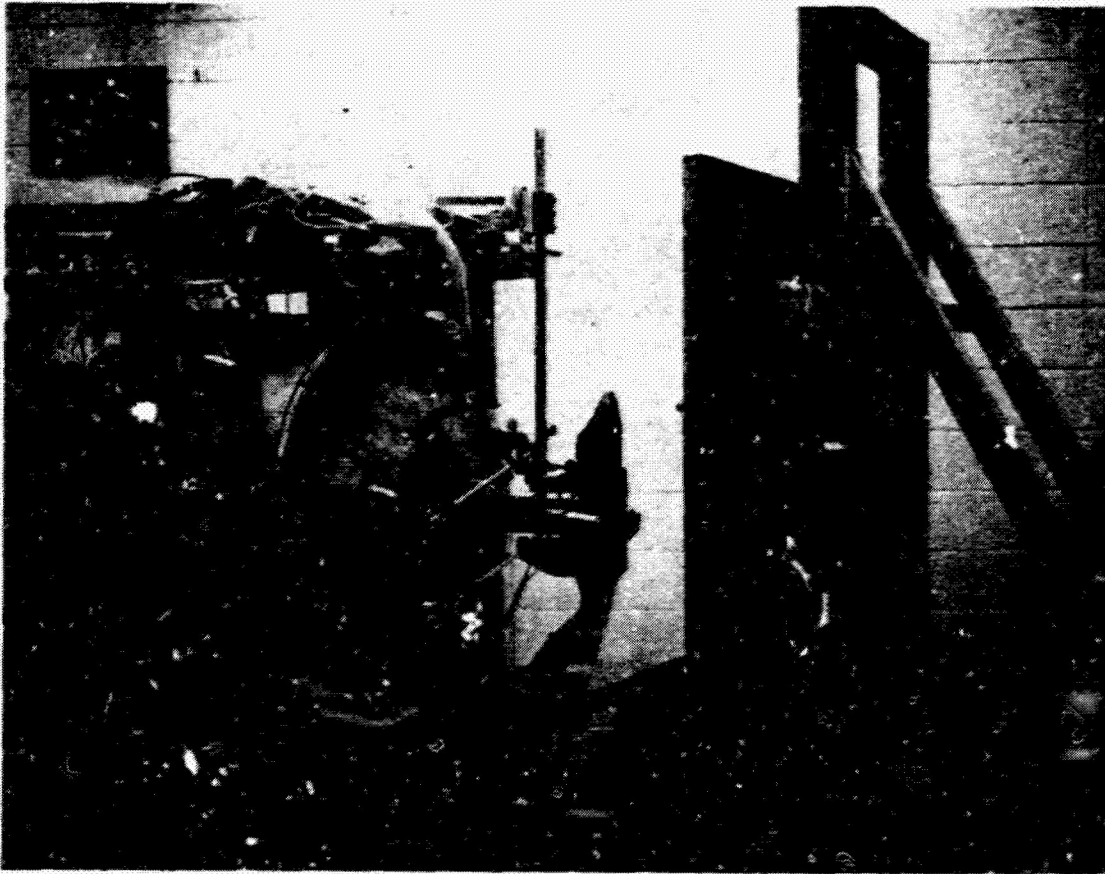
The settling chamber for the fan nozzle was a cylindrical steel tank of 76.2-cm diameter and 218.4-cm length, adapted from underwater flow research. (See Figure 4). The first 91.4 cm of this chamber are occupied by a diffuser to spread the flow from the 20.3-cm diameter inlet evenly over the chamber cross-section. This is followed by a tube bundle of 9.5-cm diameter stainless steel tubes and two fine mesh screens. The heated air supply for the core flow enters through the bottom of the chamber after a combined turn and transition from a single 20.3-cm pipe to a pair of separate 5.1-cm tubes. This supply is con-



R81-1622-001D

Figure 1 - Ram air system location plan, Plant 31.

ORIGINAL PAGE
BLACK AND WHITE PHOTOGRAPH



R81-1622-041D

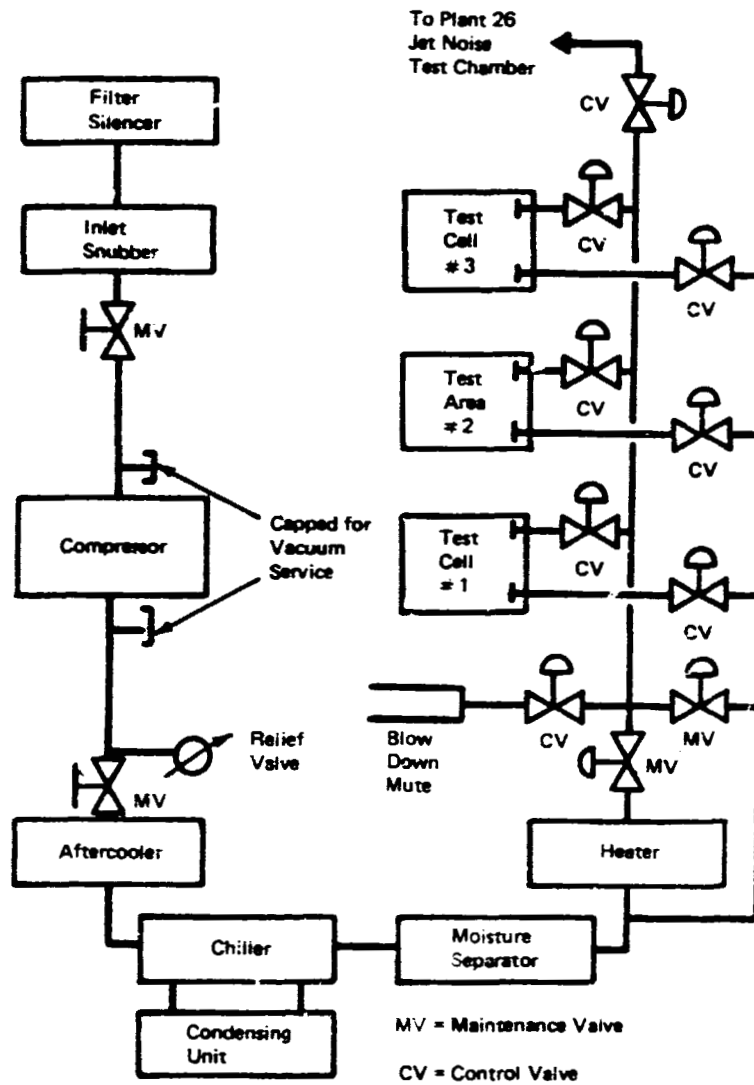
Figure 2 - Test arrangement.

tinued inside the chamber by flexible, insulated pipes to the nozzle entrances. For the open-jet experiments, this tubing system was entirely removed and the piping system was changed to bring heated air in through the diffuser inlet.

4.4 Nozzles

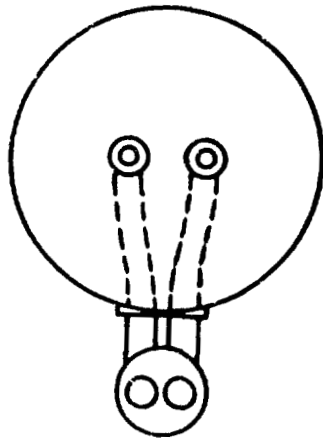
The outer fan nozzle, which is also the hardware for the open-circular-jet experiments, is an ASME elliptical profile flow metering contour with an inside diameter of 5.0 cm. (Figure 5). This nozzle is continued as a straight tube for 30.5 cm in a tradeoff of boundary layer growth and heat transfer in the nozzle flow against the need to separate the model from the front face of the chamber, thus preventing the chamber from interfering with the recirculation flow field. The inner core nozzle for the heated flow begins with a contraction from the 5.1-cm flexible supply tubes beginning 5.1 cm before the fan flow

ORIGINAL PAGE IS
OF POOR QUALITY



R81-1622-002D

Figure 3 - Ram air system schematic.



R81-1622-003D

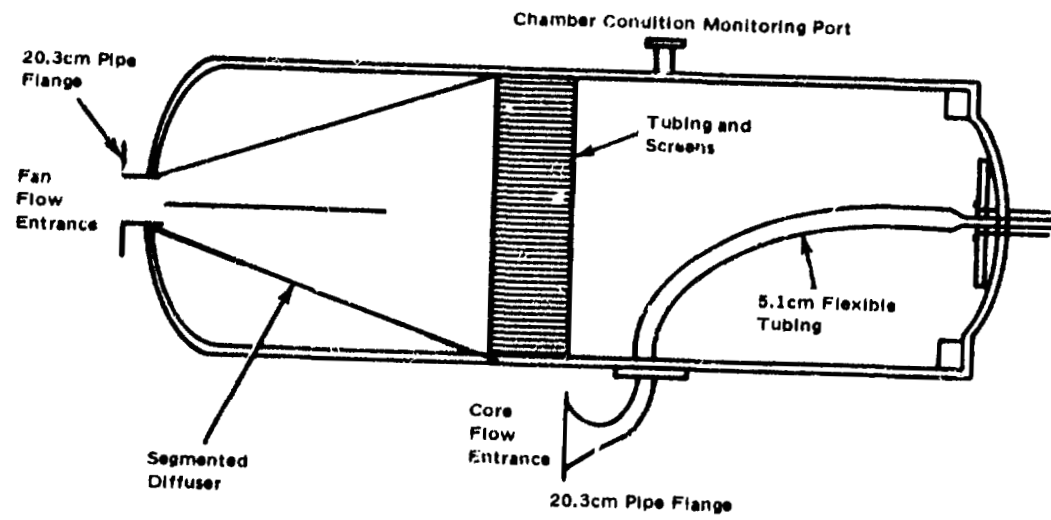
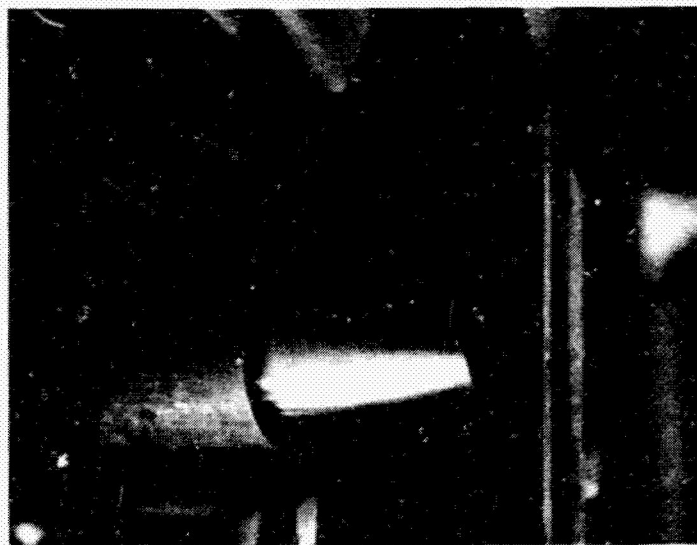
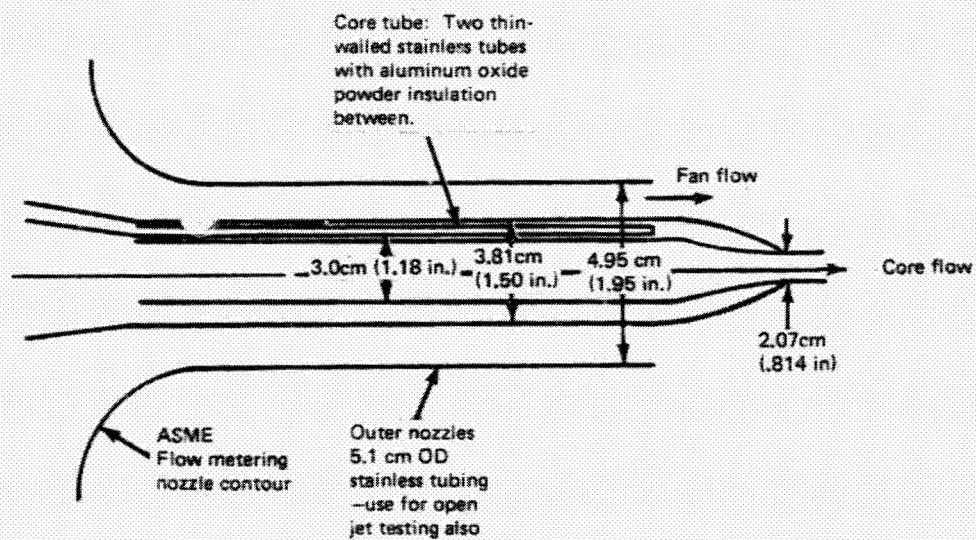


Figure 4 - Settling chamber arrangement.

ORIGINAL PAGE IS
OF POOR QUALITY

ORIGINAL PAGE
BLACK AND WHITE PHOTOGRAPH



R81-1622-042D

Figure 5 - Fan-jet nozzle simulation.

nozzle entrance. This contraction connects to a double wall tubing system with an outer diameter of 3.8 cm (the scale centerbody diameter) and an inner diameter of 3.0 cm. The area between the two walls of this contraction section and the constant area section running to the final core nozzle contraction were insulated with aluminum oxide powder. The final contraction to the 20.7-mm core exit diameter and the core centerbody outer profile are accomplished in one solid machined segment. The core-flow tube is held in place by a machine screw in the simulated core pylon, and three thin finger-type supports near the nozzle entrance.

4.5 Ground Plane

The simulated ground plane consists of a 2.5-cm thick aluminum plate 121.9-cm square, with a circular insert of steel for the pressure tap and wall jet probe mountings. (Figure 6a). This plate was mounted on a framework which rode on rails that were aligned parallel to the nozzles. The ground plane was moved by a screw that was driven by a variable speed motor/controller. The instrumentation locations are shown in Figure 6b, c, and d, (pressure taps, surface temperature thermocouples and wall jet rakes). Numbering of the instrumentation locations matches that of the full-scale ground plane (Ref. 1), with additional instrumentation designated by "R".

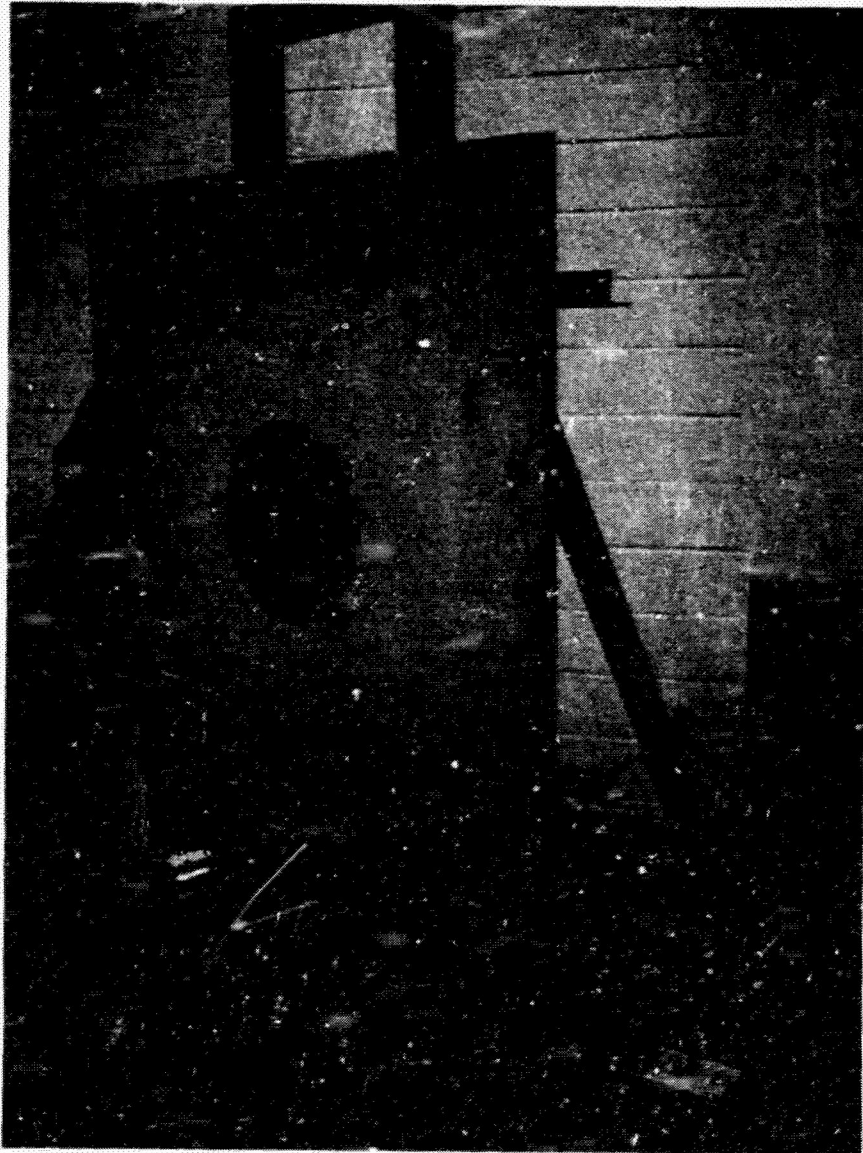
4.6 Aircraft Model

The model (Figure 7) was a 1/24 scale reproduction of the Grumman Design 698-411B tested in the NASA-Navy-Grumman full-scale demonstrator program. This model was constructed of a partially-hollow high-temperature-plastic fuselage section housing the balance and pressure/temperature lines, a metal bottom plate for pressure and temperature instrumentation, metal strakes at the fuselage chines, and separately attachable plastic wings and empennage.

4.7 Instrumentation

4.7.1 Pressure. - Pressures were measured with Validyne model DP15 or DP103 transducers, powered by single channel CD-15 or MC1-10 multichannel systems using CD18 or CD19 carrier demodulators. Transducers were calibrated versus an oil filled manometer, either singly (transducers used for probe measurements) or in groups with the manometer calibration pressure applied through a manifold (ground plane or aircraft surface).

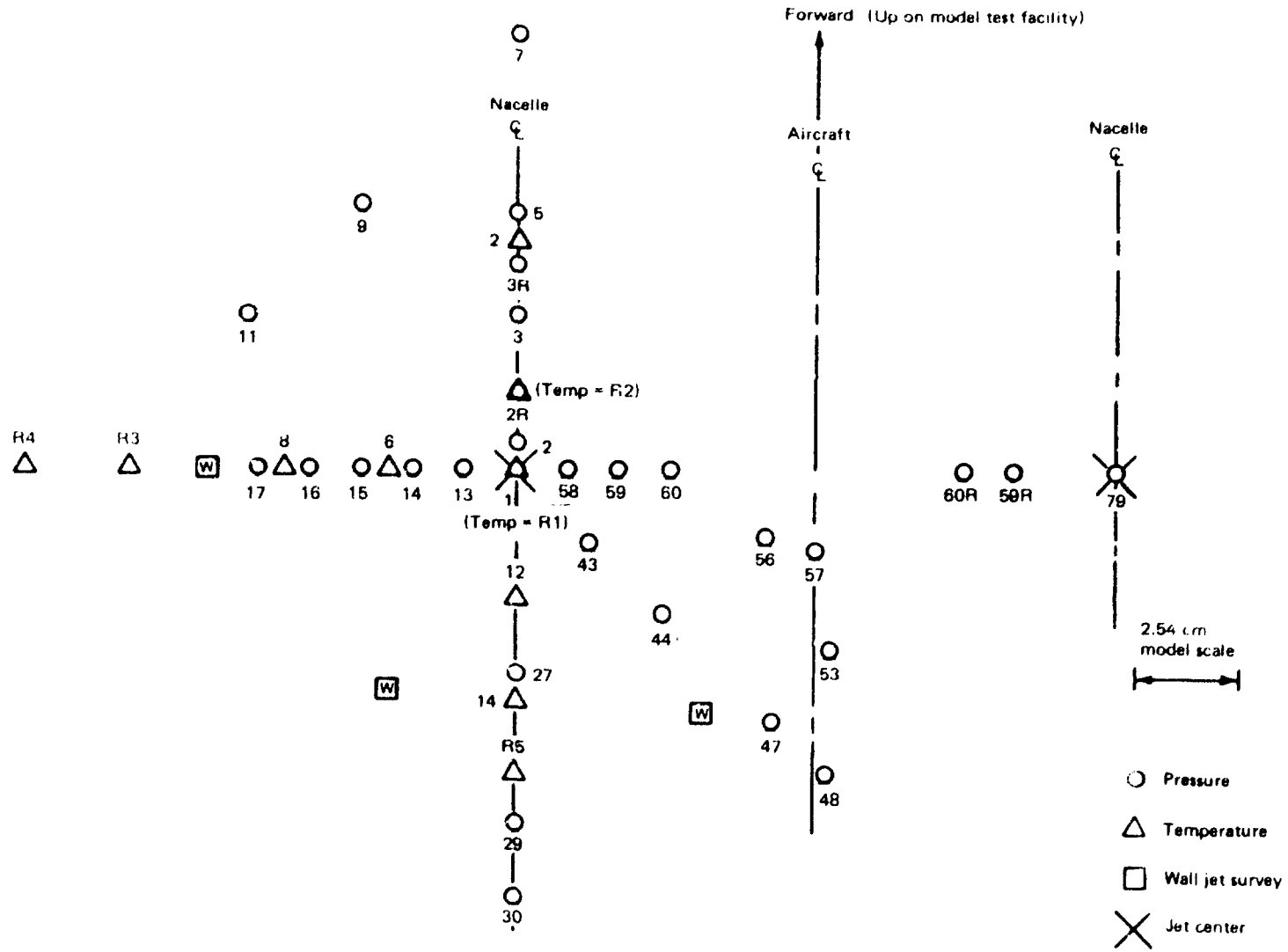
ORIGINAL PAGE
BLACK AND WHITE PHOTOGRAPH



a) Text set-up

R81-1622-043(1/3)D

Figure 6 - Ground plane.



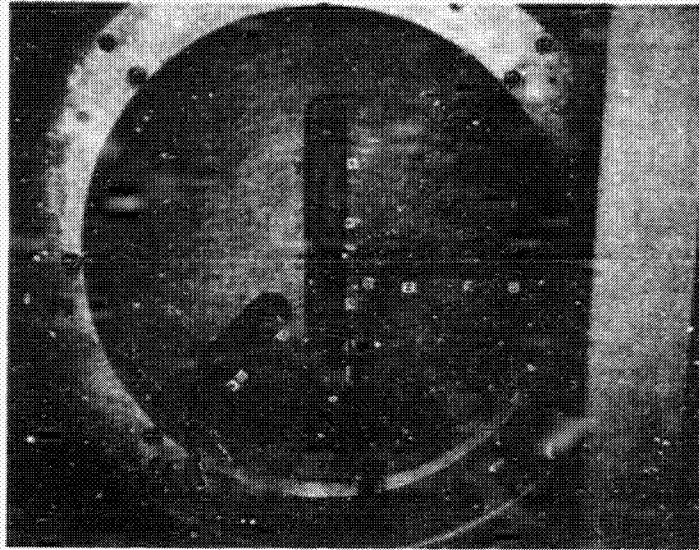
ORIGINAL PAGE IS
OF POOR QUALITY

b) Ground plane instrumentation locations

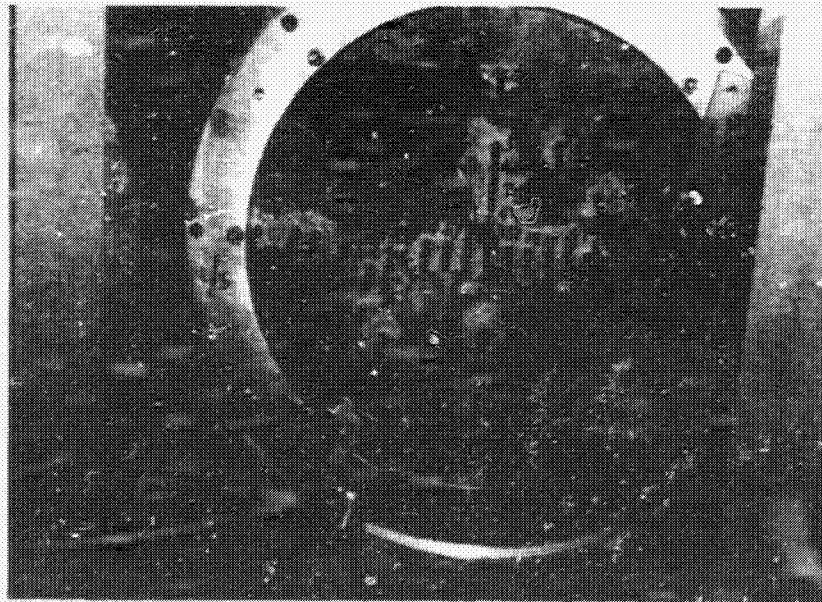
Figure 6 - (Continued.)

R81-1622-043(2/3)D

ORIGINAL PAGE
BLACK AND WHITE PHOTOGRAPH



c) Thermocouple installation

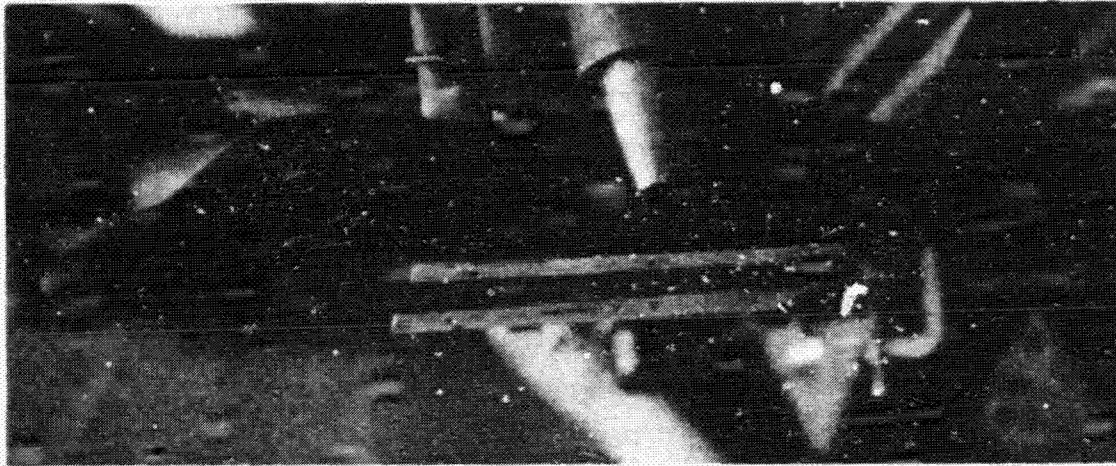


d) Pressure and wall jet instrumentation

R81-1622-043(3/3)D

Figure 6 - Concluded.

ORIGINAL PAGE
BLACK AND WHITE PHOTOGRAPH



R81-1622-044D

Figure 7 - 1/24 scale model.

Pressure tap locations on the ground plane are discussed in Section 4.5. Full-scale locations on the line connecting the nozzle impingement centerline, at 90° to the line through one jet-centerline, and at 45° were used, with a few additional locations added. The full-scale tap identification numbers were used for the model tests to aid comparisons.

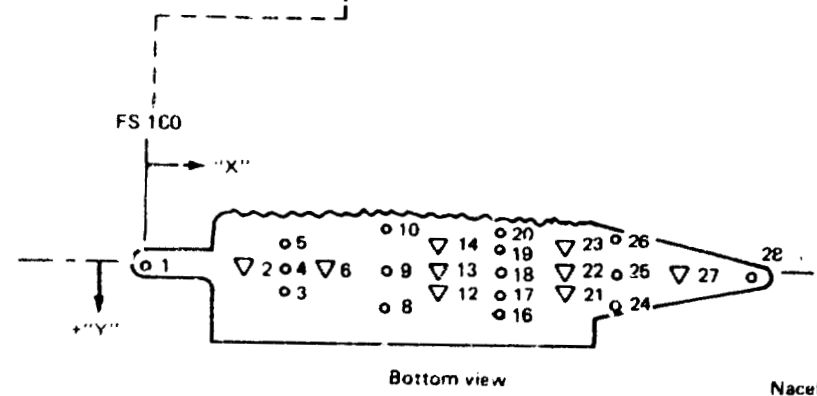
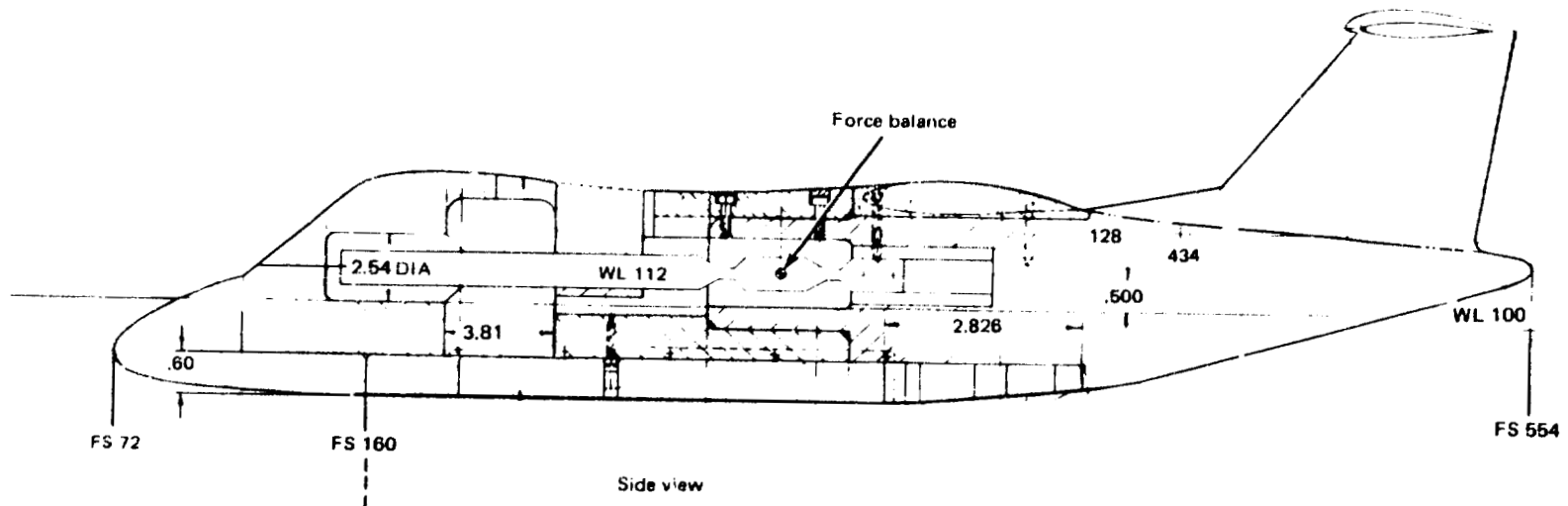
Pressure tap locations on the aircraft model are shown in Figure 8. Full scale locations were matched for many of these taps, but some taps were

relocated so that temperature (thermocouple) instrumentation could be added.

4.7.2 Temperature. - All temperature measurements were made with chromel-alumel (Type k) thermocouples connected by a multi-connection switch box to either an Omega model 2175A or a Fluke model 2166A linearized thermocouple readout amplifier. The ground plane surface temperatures and those on the flat segment of the aircraft bottom were measured with thermocouples spot welded to thin (0.4 mm) stainless steel areas. On the aircraft, the entire flat bottom was formed from one thin piece of stainless steel, and thicker pieces were spot-welded in areas for pressure tap installation. (Figure 8). The 30.5-cm diameter ground plane insert was 4.2-cm thick, and the areas for temperature measurement were machined to the 0.4-mm thickness for a distance of at least 1.3 cm from all thermocouples. (See Figure 6c). The thin skin allows greater spatial resolution in temperature measurements, which is important in small-scale testing.

4.7.3 Probes. - Three separate probe assemblies were used for measurements in the free jet, wall jet, and upwash flows (Figure 9). In each probe assembly the temperature data were taken by a bare thermocouple probe protruding from a 1.5-mm diameter stainless steel sheath that was located close to one of the pressure probes. Bare thermocouples were chosen, rather than a more conventional shielded thermocouple probe, in order to obtain good spatial resolution and time response and to avoid flow disturbances that would be associated with a housed probe. Temperature measurements with bare thermocouples require correction to account for radiation losses. Temperature corrections were acquired for the thermocouple probes in each assembly by recording output in a flow field of known temperature over a wide temperature range. We used the open jet nozzle configuration for this work. Each probe assembly was placed on the centerline of one nozzle shortly downstream of the exit and a housed thermocouple probe (United Sensor type KT-12-C/A) was placed at a corresponding point in the flow from the other nozzle.

The probe assembly used for free-jet data (Fig. 9a) consisted of 1.6-mm O.D. sharp-lipped pitot tube with a 0.5-mm diameter thermocouple displaced 2.5 mm laterally from the tip of the pitot tube. Wall jet data were taken with a



PRESS TEMP	NO.	FUZE STA	SENSOR COORDINATES	
			"X"	"Y"
	1	160	0	0
	2	200	4.22	0
	3-5	215	5.82	.71, 0, -.81
	6	238	8.26	0
	8-10	255	10.0	1.57, 0, -1.57
	12-14	280	12.7	.79, 0, -.79
	16-20	300	14.7	1.52, .76, 0, -.81, -1.68
	21-23	325	17.5	1.4, 0, -1.45
	24-26	345	18.6	1.4, 0, -1.45
	27	370	22.2	0
	28	400	25.4	0

Nacelle

NOTE: All dimensions in centimeters

ORIGINAL PAGE IS
 OF POOR QUALITY

F-31-1622-052D

Figure 8 - Model instrumentation.

ORIGINAL PAGE
BLACK AND WHITE PHOTOGRAPH



a) Free-jet probe



b) Wall-jet probe



c) Upwash probe

R81-1622-053D

Figure 9 - Flow field probes.

1.3-mm O.D. pitot tube (Fig. 9b) that was flattened to 9.5 x 1.5-mm dimensions at the tip, with a 0.5-mm diameter thermocouple that was displaced laterally 1.8 mm. The probe assembly for upwash measurements consisted of a 3.0-mm O.D. Kiel probe with a 1.6-mm O.D. static tube displaced 4.3 mm on one side, and 0.5-mm diameter thermocouple displaced 3.0 mm on the other side of the Kiel probe (Figure 9c).

The free-jet probe assembly and the upwash probe assembly were supported by a motor-driven traverse that was mounted on the same rails as the ground plane carriage. Probes were traversed in the plane containing the two jet centerlines, along paths perpendicular to those centerlines.

The support for the wall-jet probe assembly passed through a hole in the ground plane and attached to a manually driven screw traverse that was fastened to the back of the ground plane (Figure 10). The probe location relative to the wall was measured from the voltage output of a thin film linear resistance transducer that was attached to the screw drive.

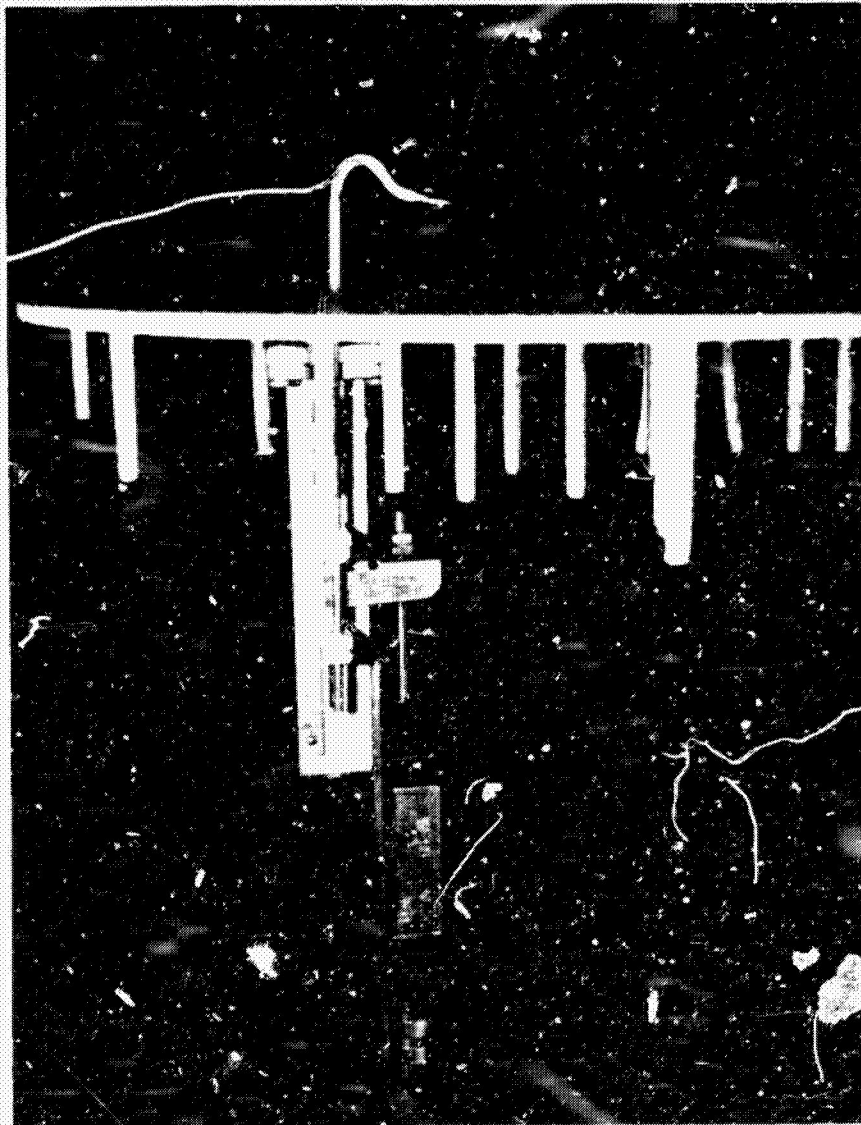
4.8 Experimental Techniques

All experiments were conducted under steady or pseudo-steady operating conditions. After initial startup time (approximately one hour) changes in pressure operating conditions took only a few minutes. Total temperature changes were much slower, primarily because of the heat capacity of the supply piping.

Under most of the operating conditions for this contract, we utilized the techniques we developed earlier (Refs. 2, 3 and 4) of continuously recording test variables versus input parameters in an analog form on an X-Y recorder. This allowed a constant monitoring of test results. Operating conditions could be changed to allow for results observed (such as gradients or fluctuations). The most frequent examples of this are the recording of interference force, ground-plane pressures, and vehicle surface pressures versus height above ground, or probe temperature and pressures versus probe position.

Probe and ground plane position were converted to voltage by a cable-

BLACK AND WHITE PHOTOGRAPH



R81-1622-045D

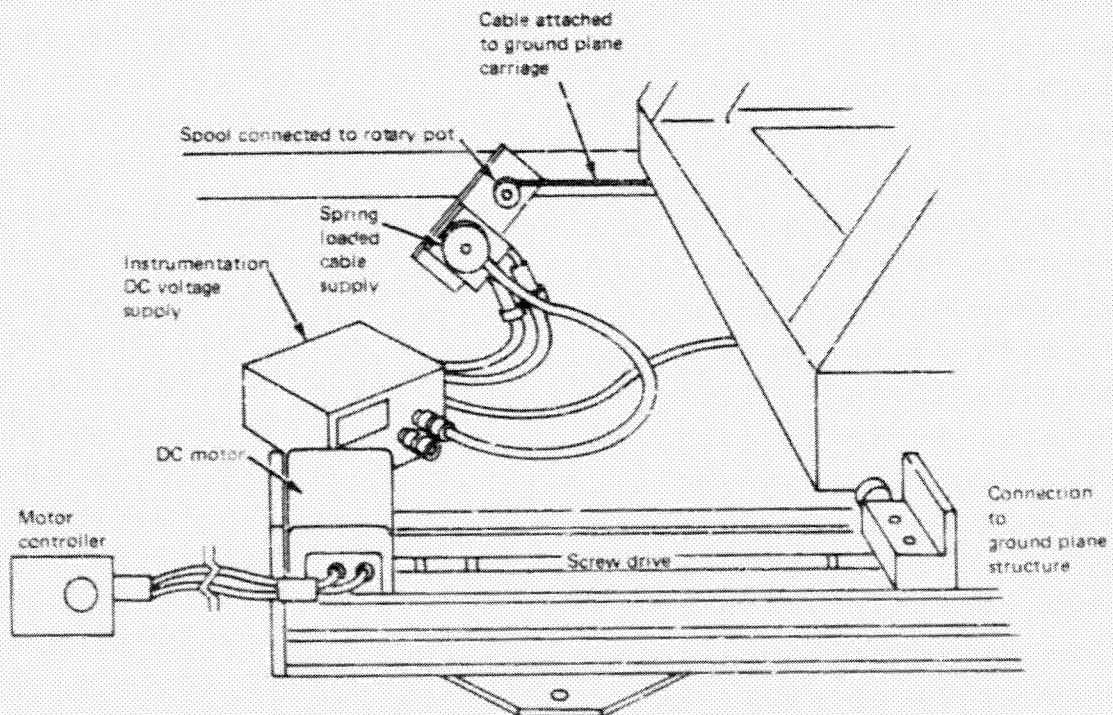
Figure 10 - Wall-jet traversing system.

driven rotary potentiometer (Figure 11) for most cases, and a linear potentiometer for the wall-jet measurements (Figure 10). Voltage was supplied by Hewlett Packard Model 6215A D. C. power supplies and adjusted so that a "calibrated" scale setting could be used on the recorder (allowing changes in scale with ease). Position was controlled by a variable speed DC motor/controller and a screw drive.

For the aspects of the experiments requiring many measurements simultaneously (such as ground plane and aircraft surface pressures) data were recorded simultaneously by an on-site minicomputer (Hewlett-Packard Model 1000(X) through A/D converters.

The aircraft force measurements were taken on separate runs from the pressure and temperature measurements because of force interference from the pressure and temperature leads which could not be eliminated. The instrumented lower surface and the instrumentation leads attached to it were removed for the force tests. A plain lower surface was fabricated to match the external contours of the instrumented lower surface and used to cover the cavity in the fuselage during the force tests.

ORIGINAL PAGE
BLACK AND WHITE PHOTOGRAPH



R81-1622-04a

Figure 11- Position readout system.

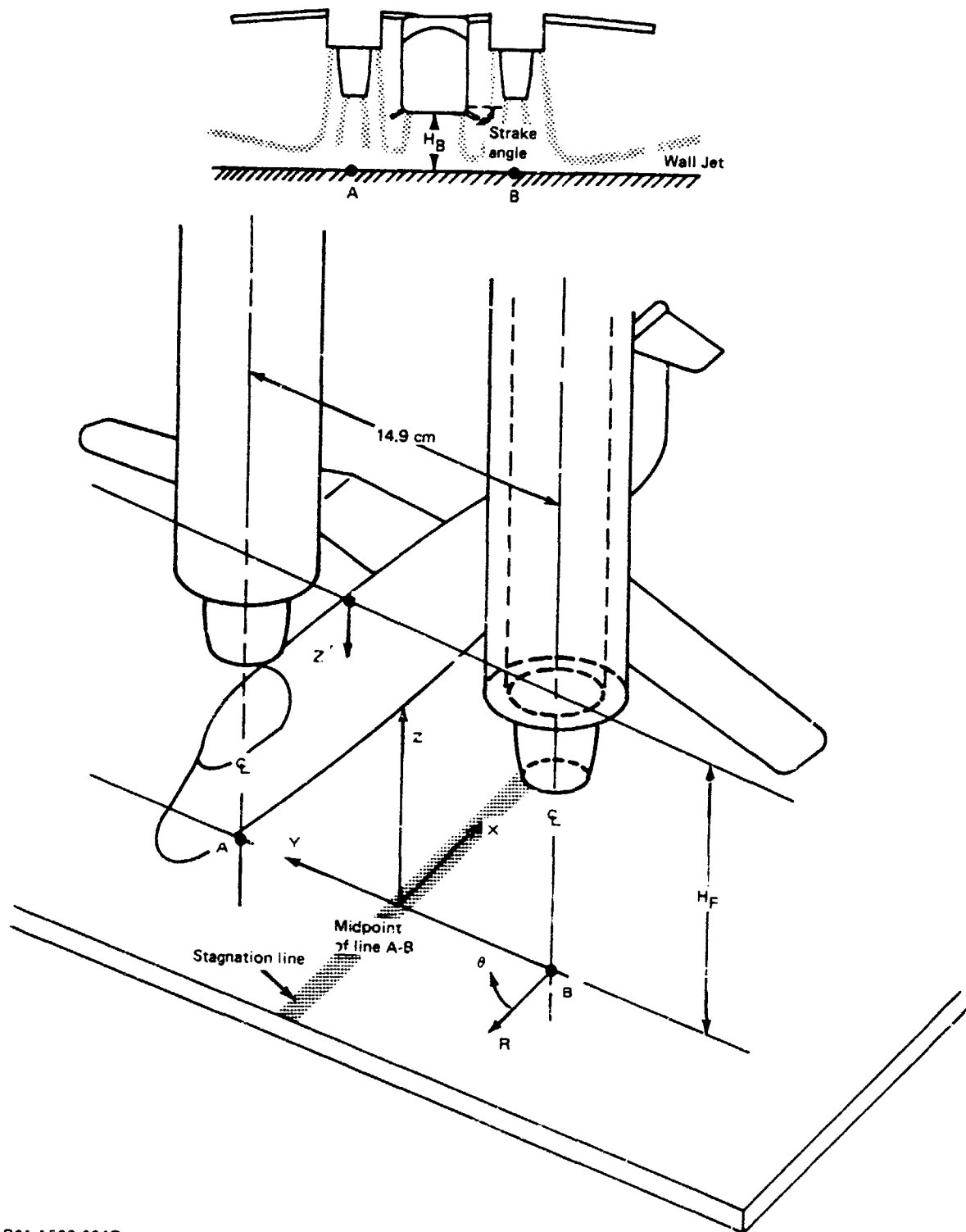
5.1 Fan-Jet Nozzles

The sketch of fan-jet impingement geometry in Fig. 12 illustrates the co-ordinate system used to describe probe and nozzle locations. All data were taken with the spacing between nozzles scaled to the full-scale model of Reference 1, with the jets normal to the ground and with the aircraft model present.

5.1.1 Nozzle Flow. - Figures 13 and 14 show pressure profiles taken across the fan and nozzle exit, with baseline pressure conditions and a 24°C total temperature in both flows. The total-pressure profile at the core exit is quite flat. The profile across the fan exit shows a well-defined maximum near the center of the annulus. The maximum value of the pitot pressure at the exits was used to define the nozzle pressure ratios (1.103 for the core and 1.195 for the fan at baseline conditions). Most of the fan-jet impingement data were taken with these nozzle pressure ratios, chosen to match those conditions most frequently used in the full-scale experiments. After the initial series of experiments, during attempts to compare full-scale and model results, it was discovered that the full-scale conditions to be matched were based on area averaged total pressures. Additional tests were conducted at the most critical conditions with the correct pressures. Non-dimensional results were found to have very little dependence on the total pressure.

Integration of the pressure profiles in Figures 13 and 14 (assuming axial symmetry) gives a value of 36.5 N thrust for one fan-jet nozzle. However, this approach provides only an approximation of the thrust because the fan flow is not truly axially symmetric (engine support pylon blockage on one side of the fan duct) and because this method of determining thrust does not account for pressure forces on the outer cowl of the core nozzle (centerbody).

A more accurate determination of nozzle thrust was made by measuring the impingement on a 0.914-meter square ground-plane plate that was instrumented with three strain beams. With baseline pressure conditions, the thrust produced by one nozzle was found to be 36.2 N. Maintaining pressure within 5% of the baseline conditions, the core exit temperature was raised from 24°C to



R81-1622-004D

Figure 12 - Coordinate system and nomenclature.

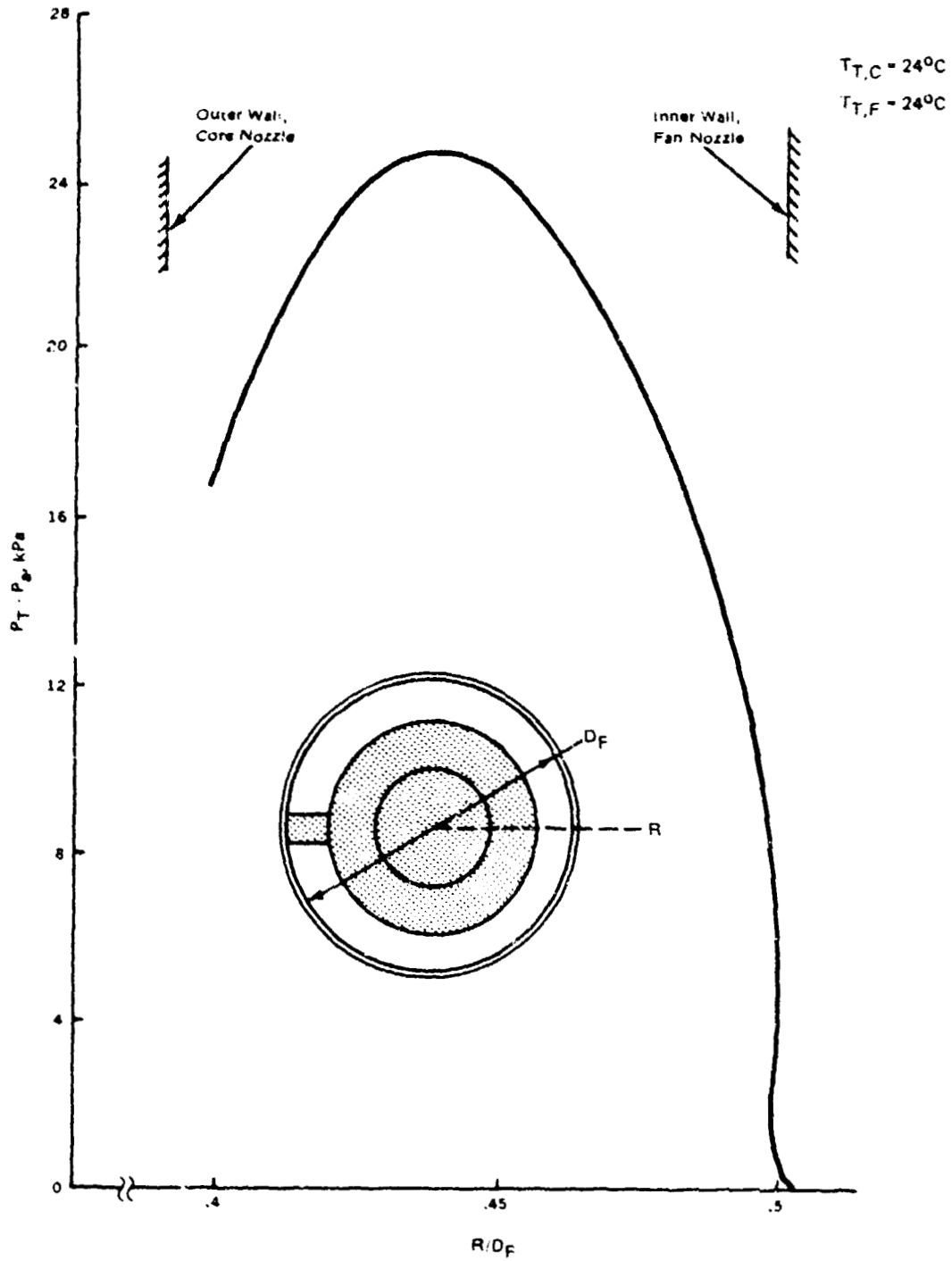


Figure 13 - Pitot pressure profile at fan nozzle exit, baseline pressure operation.

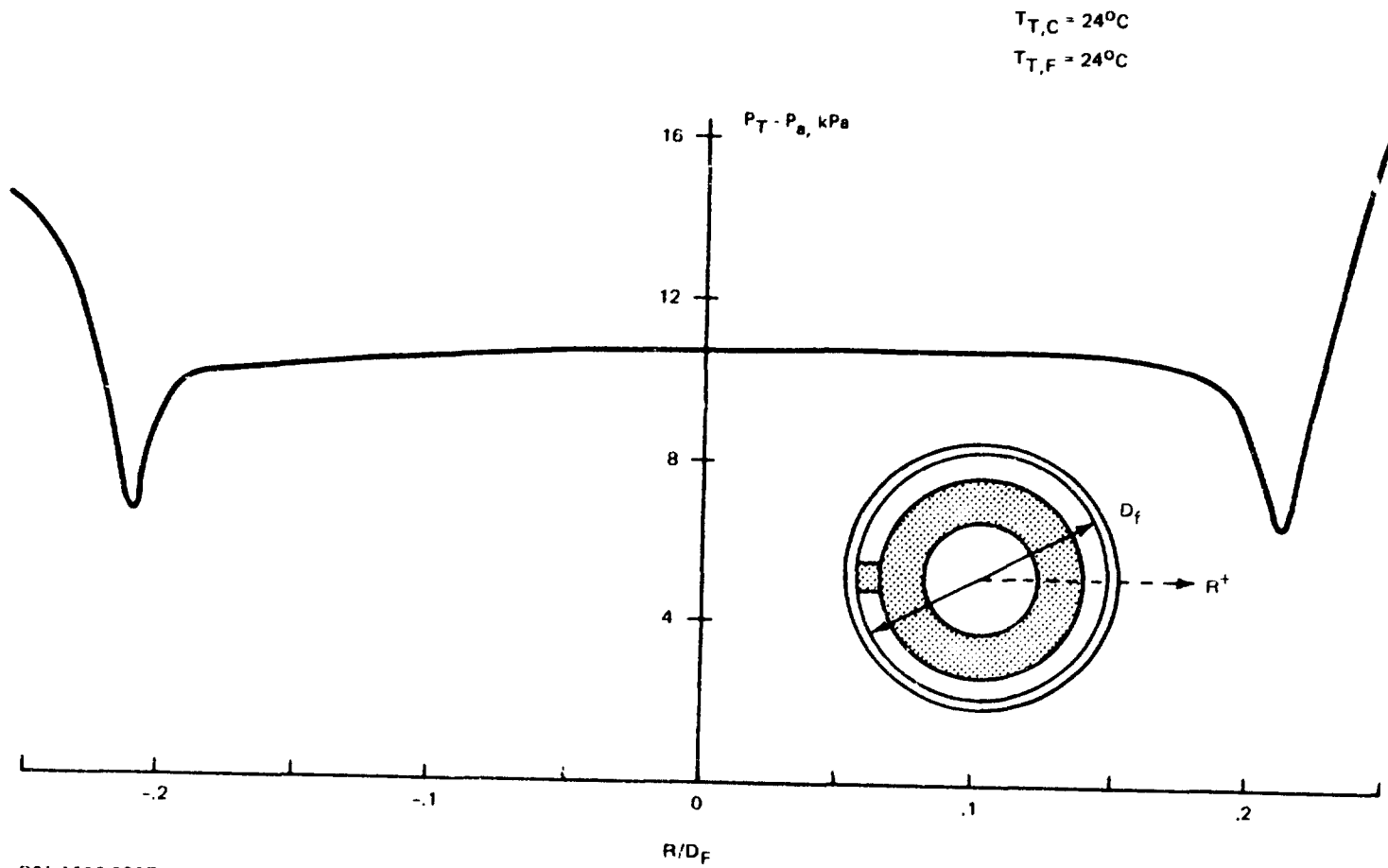


Figure 14 - Pitot pressure profile at core nozzle exit,
baseline pressure operation.

168°C. As shown in Figure 15, there was a negligible variation in nozzle thrust over this range of core exit temperatures when minor variations in total pressure at the core exit and the fan exit were taken into account.

The thrust of a fan-jet nozzle was measured for a range of both core and fan nozzle total pressures. The thrust was found to be a linear function of fan and core pressures (Figure 16). This is true over a range of pressures exceeding those used in this study. An empirical fit of the data yields $F = 1.55 q_{fan, avg.} + 0.719 q_{core} - 0.445$, in which q is in kilopascals and F is in Newtons. As an indication of the origin of this equation, the following relationship was assumed: (1)

$$F = (K_1 + K_2) 2q_{fan} A_{fan} + K_3 2q_{core} A_{core} \quad (2)$$

where K_1 and K_3 represent the relative thrust efficiencies and K_2 refers to the drag of the core centerbody in the fan flow. For the nozzles used in the study, $A_{fan} = 7.8 \text{ cm}^2$ and $A_{core} = 3.37 \text{ cm}^2$

From integration of the core nozzle exit profiles, K_3 was found to be 0.0962.

Combining the terms relative to the core, $(K_1 + K_2) \times 2 A_{fan} = K_4$

we have the relationship

$$F = K_4 \times q_{fan} + 0.650 q_{core}. \quad (3)$$

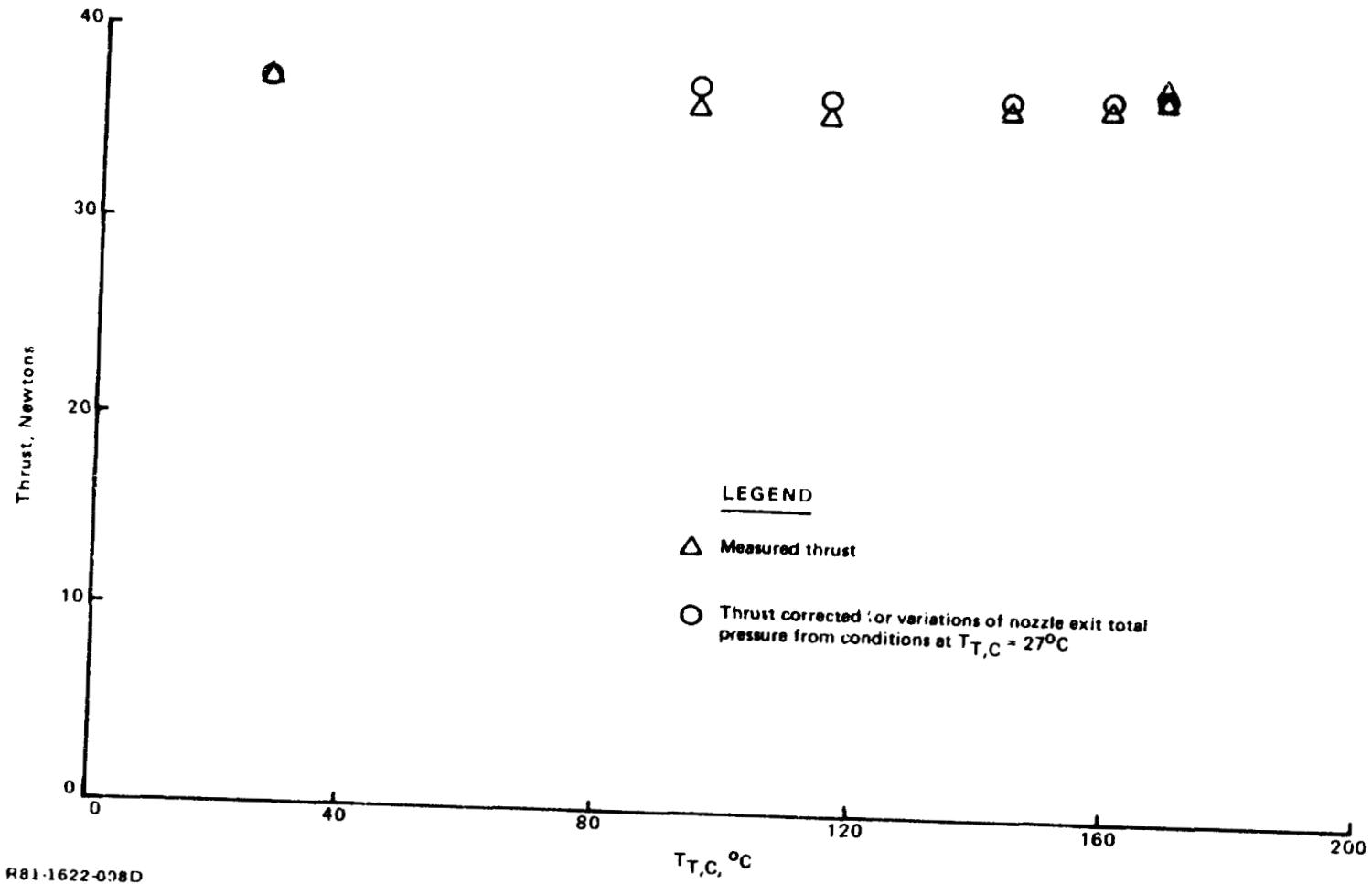
Solving for K_4 with room-temperature, baseline condition data yields $K_4 = 1.46$.

Substituting, we find

$$\Delta F = 1.46 q_{fan, avg.} + 0.650 q_{core, avg} \quad (4)$$

This agrees quite closely with the empirical relation of Eq. (1)

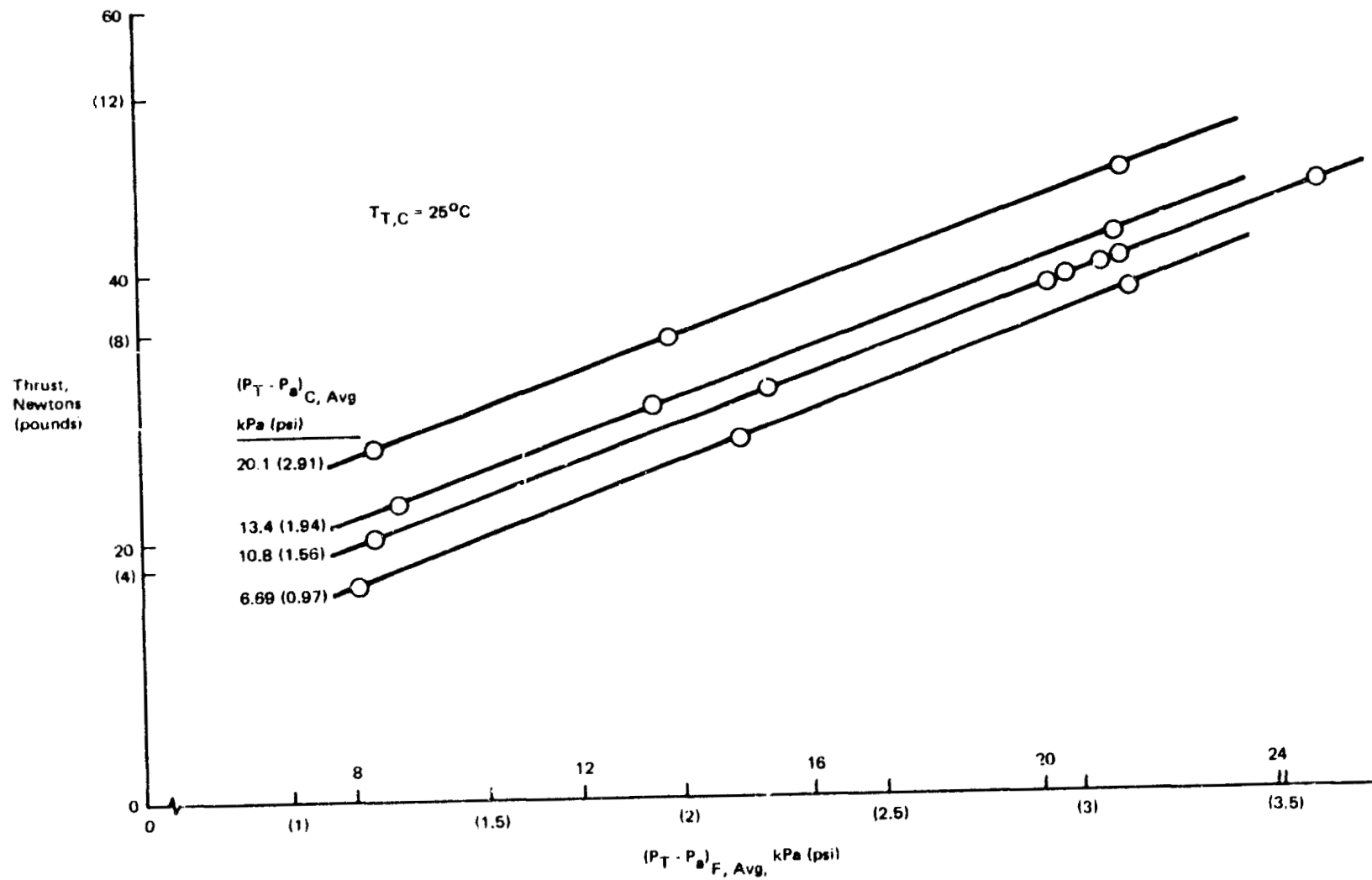
Figure 17 shows free-jet total-pressure profiles that were taken (with both fan jet nozzles operating) at successive axial stations for a total temperature at the exit of 24°C. The lack of symmetry in each of the fan flows can be attributed to the core pylon blockage in the fan nozzles. The apparent convergence of the two flows, indicated by measurement on these profiles of center-to-center distance between the two flows at several axial stations, was



R81-1622-038D

Figure 15 - Variation of nozzle thrust with core exit temperature for baseline nozzle pressure conditions.

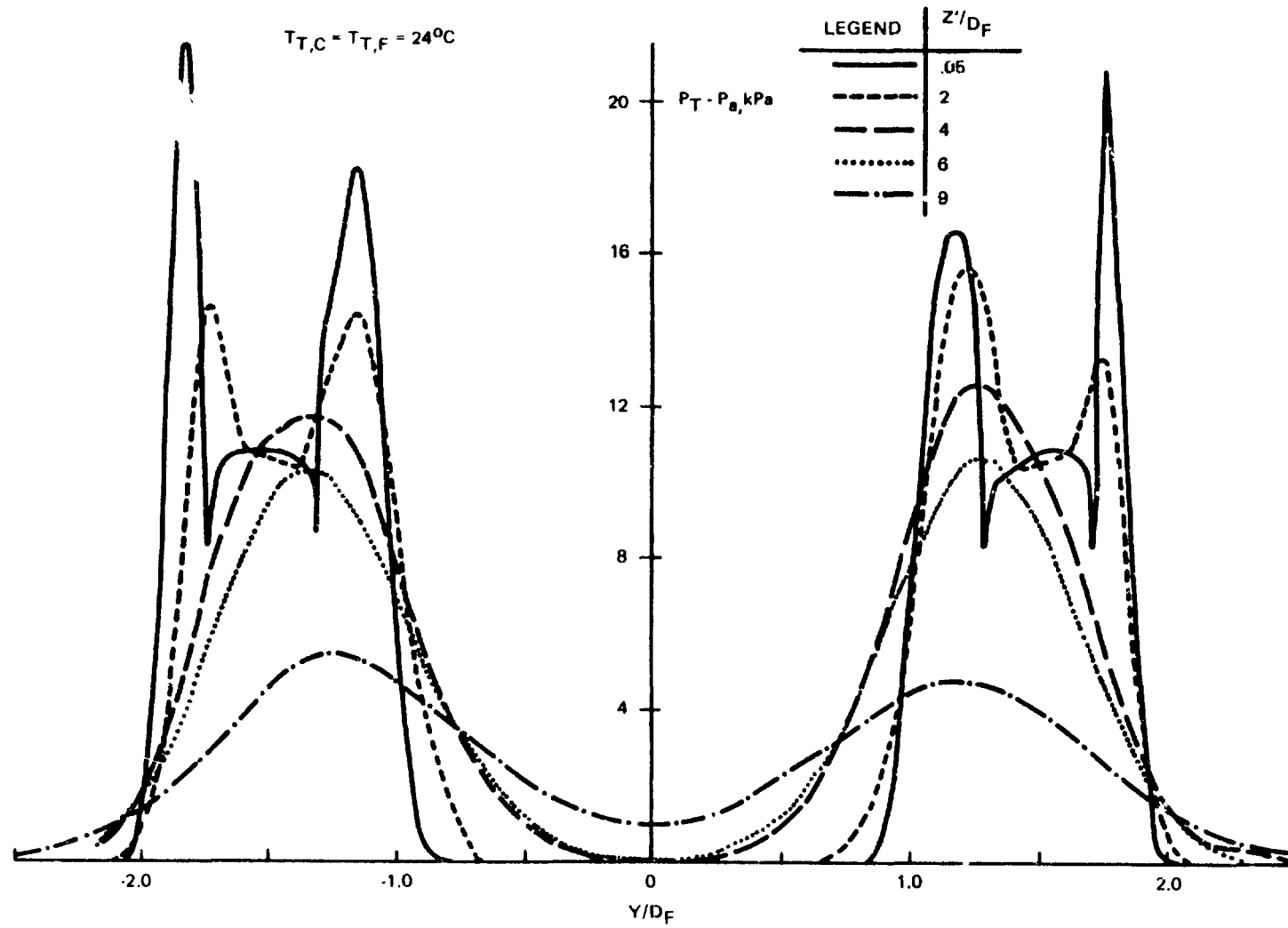
ORIGINAL PAGE IS
OF POOR QUALITY



ORIGINAL PAGE IS
 OF POOR QUALITY

RB1-1622-007D

Figure 16 - Effect of fan and core total pressure on nozzle thrust.



R81-1622-009D

Figure 17 - Free-jet pitot pressure profiles, baseline operation.

ORIGINAL PAGE IS
OF POOR QUALITY

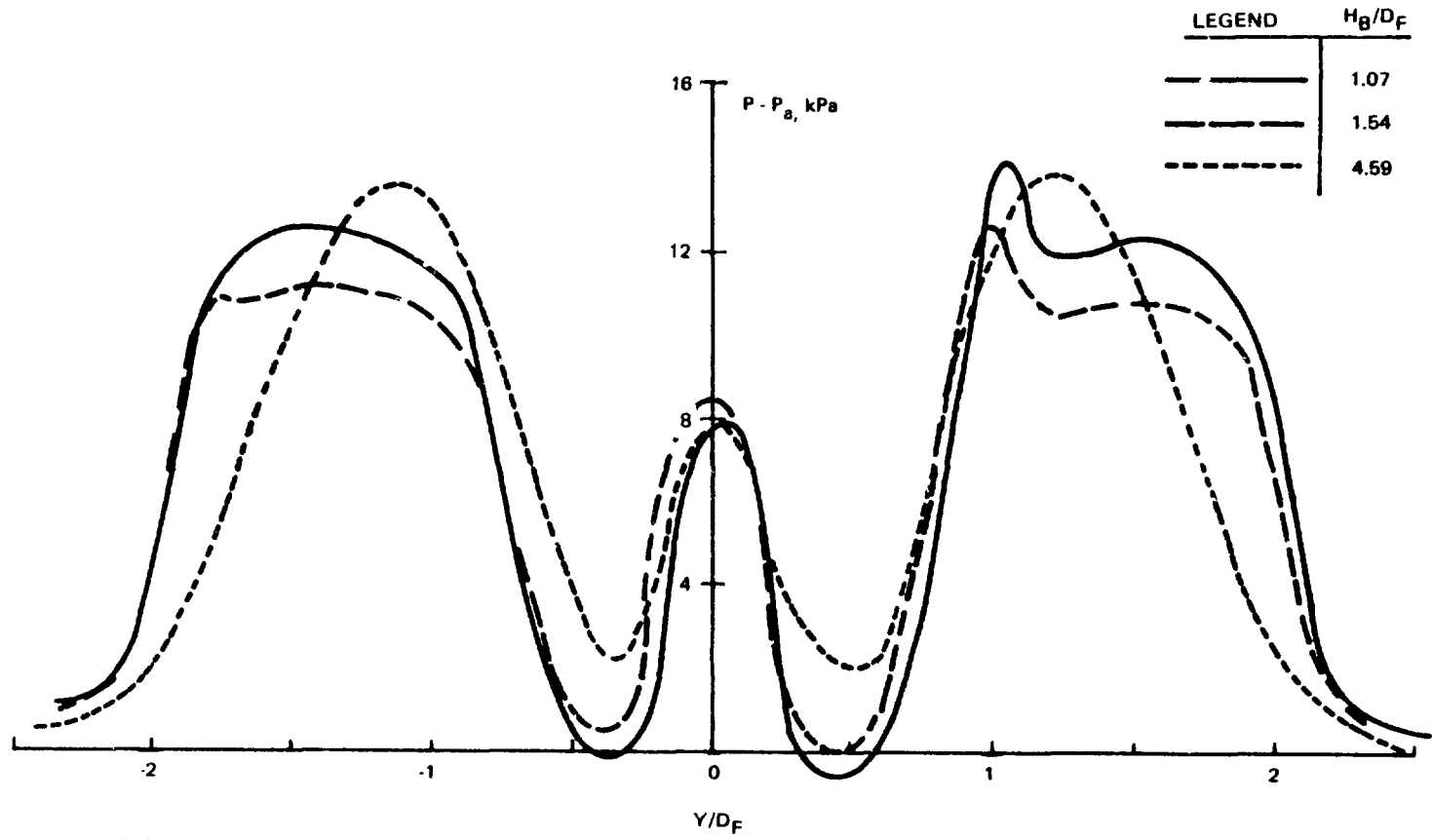
not caused by actual convergence of either the fan or core nozzle hardware. The reason for this characteristic of the free-jet pitot pressure profiles is still under active investigation, but it is assumed to be due to the pylon-induced asymmetries.

5.1.2 Ground Flow. - Pressures taken on the ground surface were recorded by a 30-channel A/D system connected to an HP-1000 minicomputer as the ground height was varied. In addition, some pressure data were taken at fixed ground heights as continuous profiles by displacing the ground plane in the y-direction. Figure 18 shows the variation of ground pressure along a line between the two jet impingement points for three body heights above ground. These ground pressure profiles were taken using baseline nozzle pressure conditions and 24°C core nozzle exit temperature. The maximum ground pressure in the stagnation line region (central section of the profiles) shows little variation with body height. The ground pressure in the impingement regions (outer sections of the profiles) shows an inward shift of the ground impingement center for each jet as ground height is increased, which is analogous to the convergence of the free jet centerlines illustrated by Figure 17.

Ground temperature measurements were taken at points around one jet impingement region for the same three heights above ground, using almost the same nozzle pressure conditions and a core exit temperature of 425°C. Figure 19 shows the ground temperature radial variation from one jet impingement point for three different angular orientations (θ). A curve was faired through the round symbols, corresponding to $\theta = 90^\circ$ (oriented in the wing spanwise direction). Note that, for $\theta = 0^\circ$, the ground temperature was lower, and for $\theta = 180^\circ$ the temperatures were higher, than this curve. The higher ground temperature under the wing may have been caused by blockage of air entrainment into the jet exhaust by the presence of the wing.

Figure 20 shows representative wall-jet profiles of total pressure and total temperature that were obtained by traversing a probe normal to the ground at the ground location scaled to rake number 6. Data were taken at the three ground heights corresponding to those run during the full-scale tests. Data were obtained at this ground location and at two other locations (rakes number

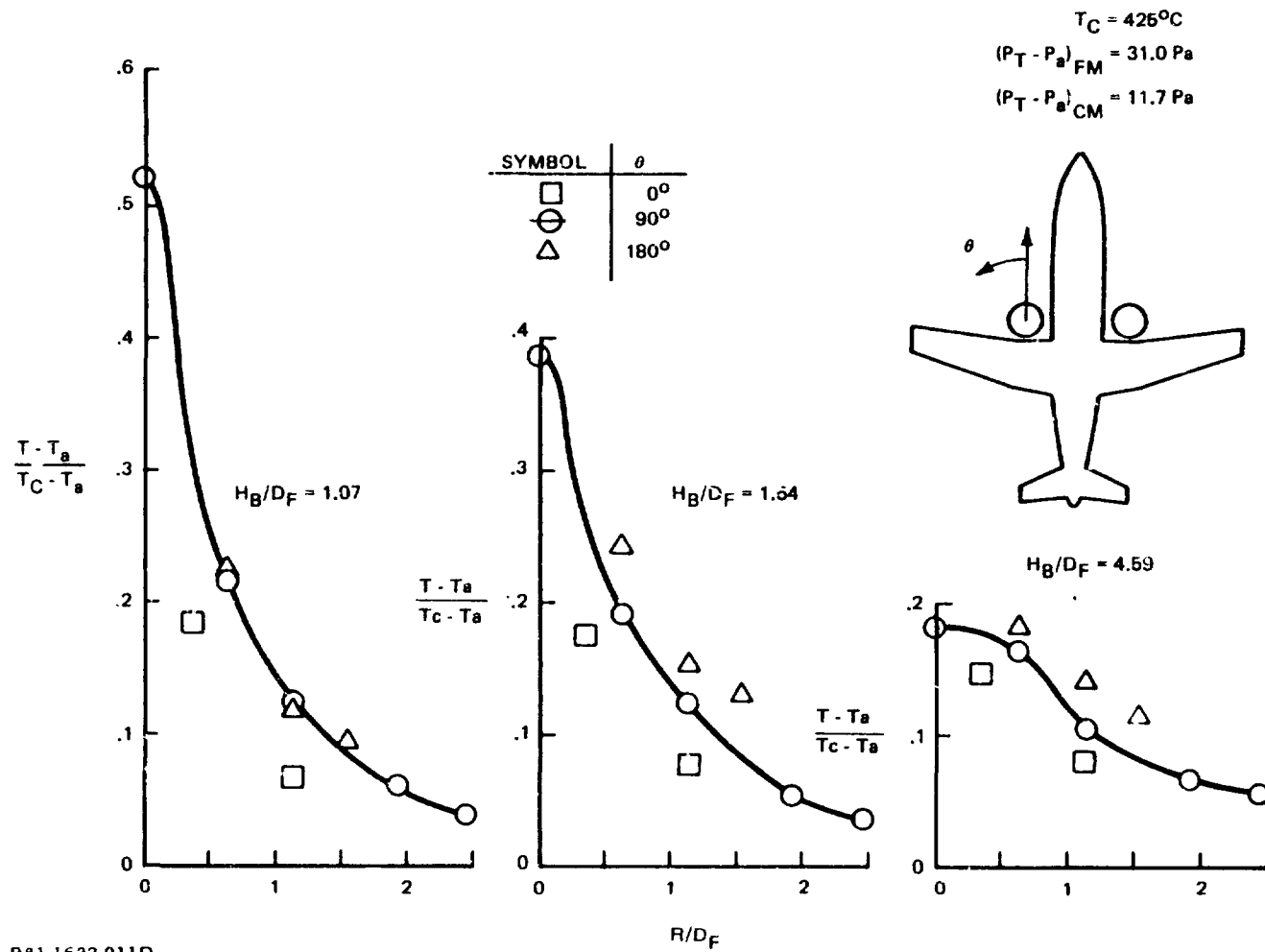
$(P_T - P_a)_{F,M} = 30.3 \text{ kPa}$
 $(P_T - P_a)_{C,M} = 10.76 \text{ kPa}$
 $T_{T,C} = 24^\circ\text{C}$



R81-1622-010D

Figure 18 - Ground pressure profiles, fan-jet impingement.

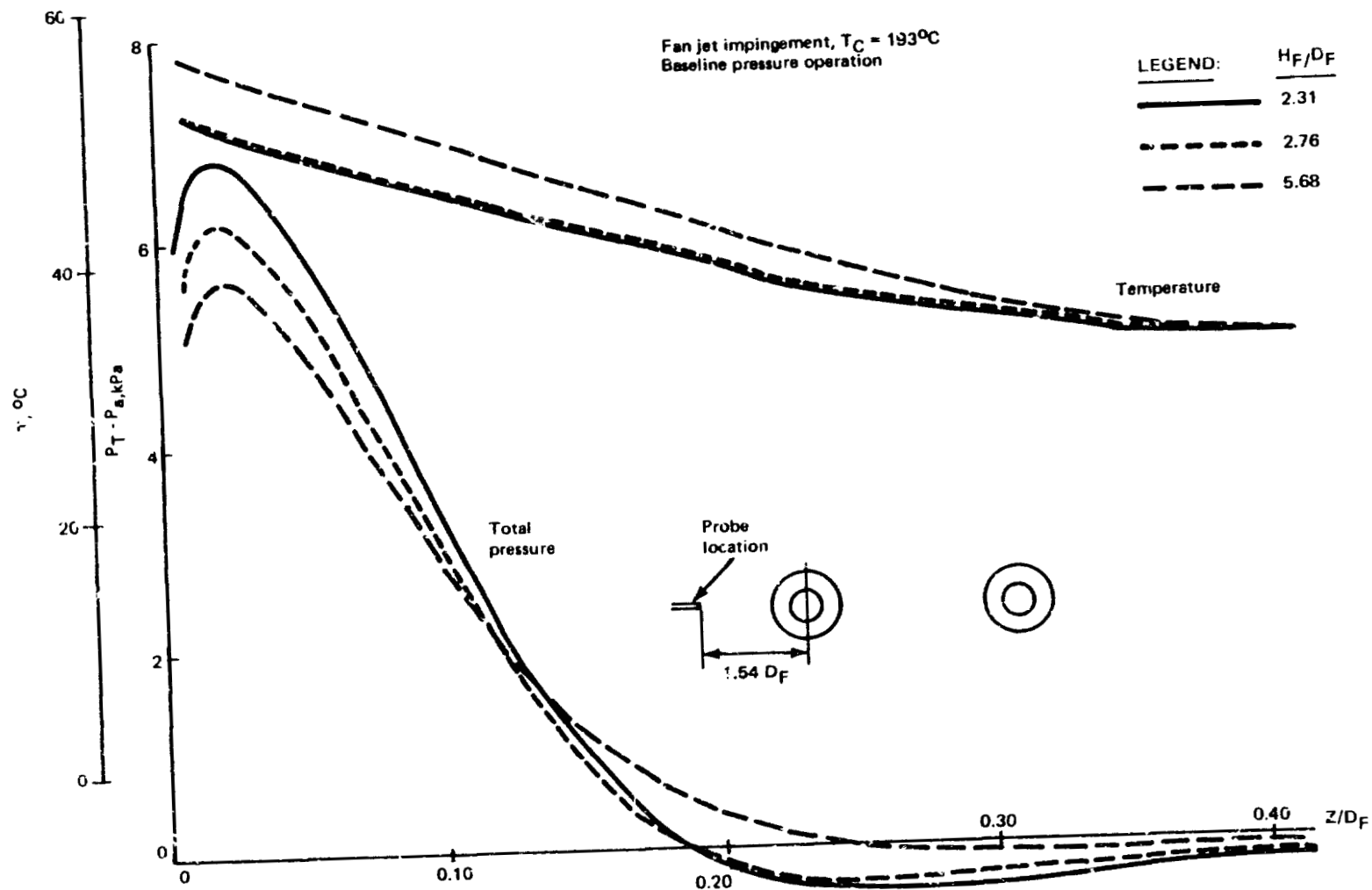
ORIGINAL PAGE IS
 OF POOR QUALITY



R81-1622-011D

Figure 19 - Ground temperature measurements.

ORIGINAL PAGE IS OF POOR QUALITY



R81-1622-012D

Figure 20 - Wall jet temperature and total pressure profiles.

ORIGINAL PAGE IS
OF POOR QUALITY

8 and 10). Figure 21 shows a tabulation of representative features of the pressure and temperature profiles taken at all three ground locations and three ground heights. In this figure, the maximum wall-jet total pressures have been normalized by the maximum total pressure at the fan exit and the wall-jet thickness (at one quarter the maximum profile dynamic pressure) has been normalized by fan-nozzle outside exit diameter.

The temperature data shown in Figure 20 were taken with a bare thermocouple that was located adjacent to the total pressure tube. These data must be corrected to account for radiation losses. The correction has been applied to the data listed in Figure 21.

5.1.3 Upwash Flow. - Flow properties in the upwash were measured by traversing a probe assembly through the centerline of the upwash in the y-direction with the model in place. The total pressure, static pressure and total temperature profiles were measured along a line $.56D$ below the model lower surface, using baseline nozzle pressure conditions and core exit temperatures of 24°C , 128°C , and 192°C . Data could not be taken at the lowest body height tested full-scale ($1.07D$) because the probe would have been in the upwash formation region. For the greatest full-scale body height ($4.59D$), the upwash was not recorded because the level was too low. Data were taken at the intermediate full-scale body height ($1.54D$), Figure 22, and at a somewhat higher body height ($1.99D$), Figure 23.

Figures 22 and 23 show the variation of total pressure and of the difference between total and static pressures across the upwash for the lowest and highest core temperatures. It was found that the upwash pressure profiles were well-centered around the midpoint between the nozzle centerlines and that they were essentially independent of core exit temperature. The temperature across the upwash was almost constant and can be represented by the centerline values plotted in Figure 24.

5.1.4 Model Forces. - Ground-induced interference forces were measured for both the 15° and 45° strake angle configuration for several nozzle pressures and temperatures. The first example, varying fan total pressure with core temperature equal to fan temperature (approximately 24°C), is shown in Figure 25.

ORIGINAL COPY
OF POOR QUALITY

H_B/D_F	Wall Jet Station	R/D_F	θ	$\frac{(P_T - P_a)_M}{(P_T - P_a)_{FM}}$	$\frac{Z_{.75}}{D_F}$	$\frac{(T_T - T_a)_M}{(T_T - T_a)_C}$
1.54	6	1.54	90°	.276	.132	.173
1.54	8	1.28	150°	.433	.122	.233
1.54	10	1.54	218°	.354	.108	.112
1.99	6	1.54	90°	.253	.130	.173
1.99	8	1.28	150°	.396	.118	.241
1.99	10	1.54	218°	.346	.113	.112
4.60	6	1.54	90°	.229	.138	.200
4.60	8	1.28	150°	.320	.138	.227
4.60	10	1.54	218°	.323	.169	.112

Notes: 1) Baseline pressure operation
2) $T_{T,C} = 193^\circ\text{C}$

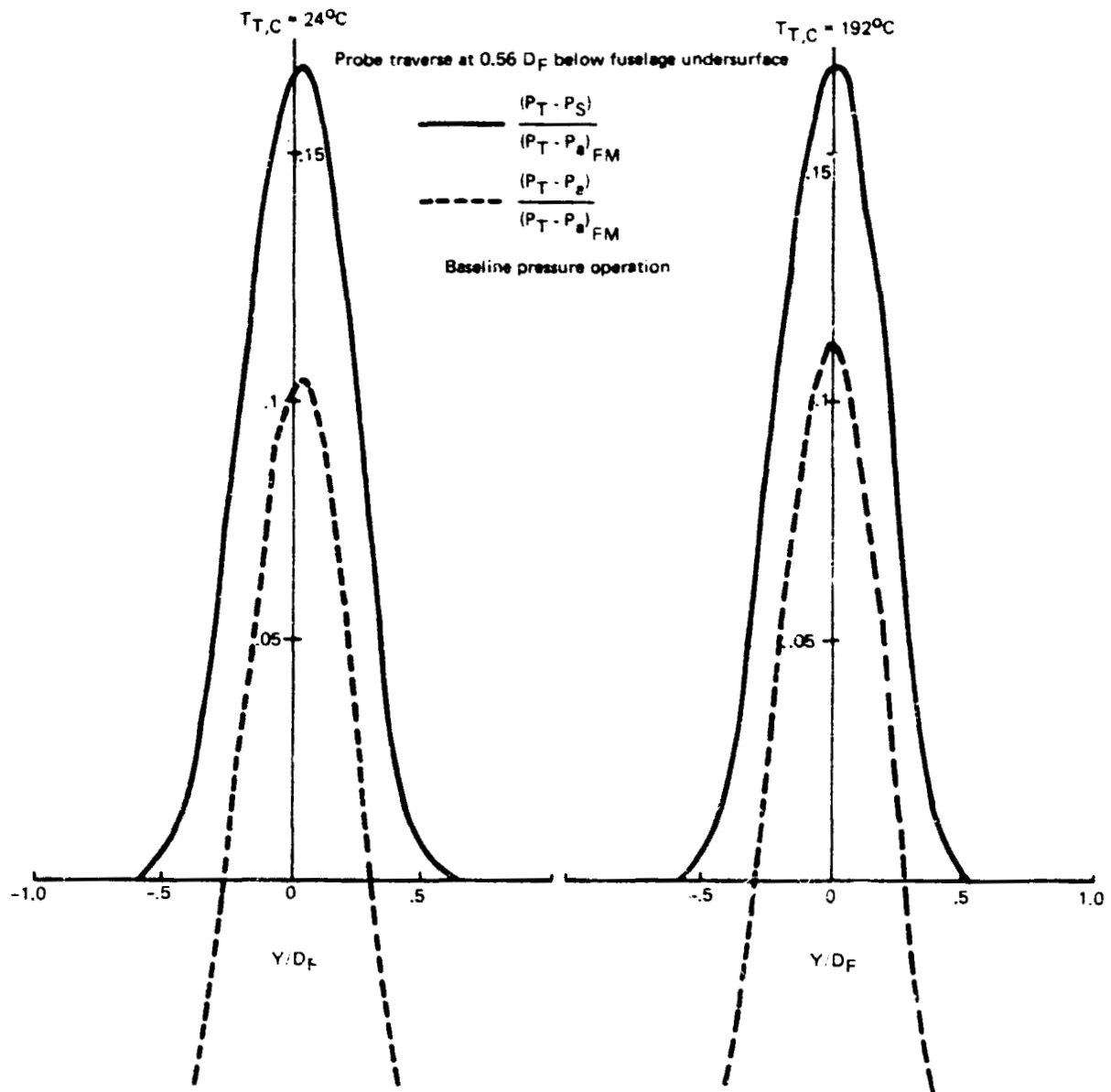
R81-1622-013D

Figure 21 - Data from wall jet profiles resulting from fan jet impingement.

For both the 15° and 45° strakes, changing fan total pressure with core total pressure held constant produced a progression of interference forces with no change in the qualitative behavior with height above ground. Note that, for all these cases, the fan total pressure was well above the core total pressure. The behavior may be changed if the core total pressure becomes equal to or larger than the fan total pressure because of changes in the impinging jet behavior.

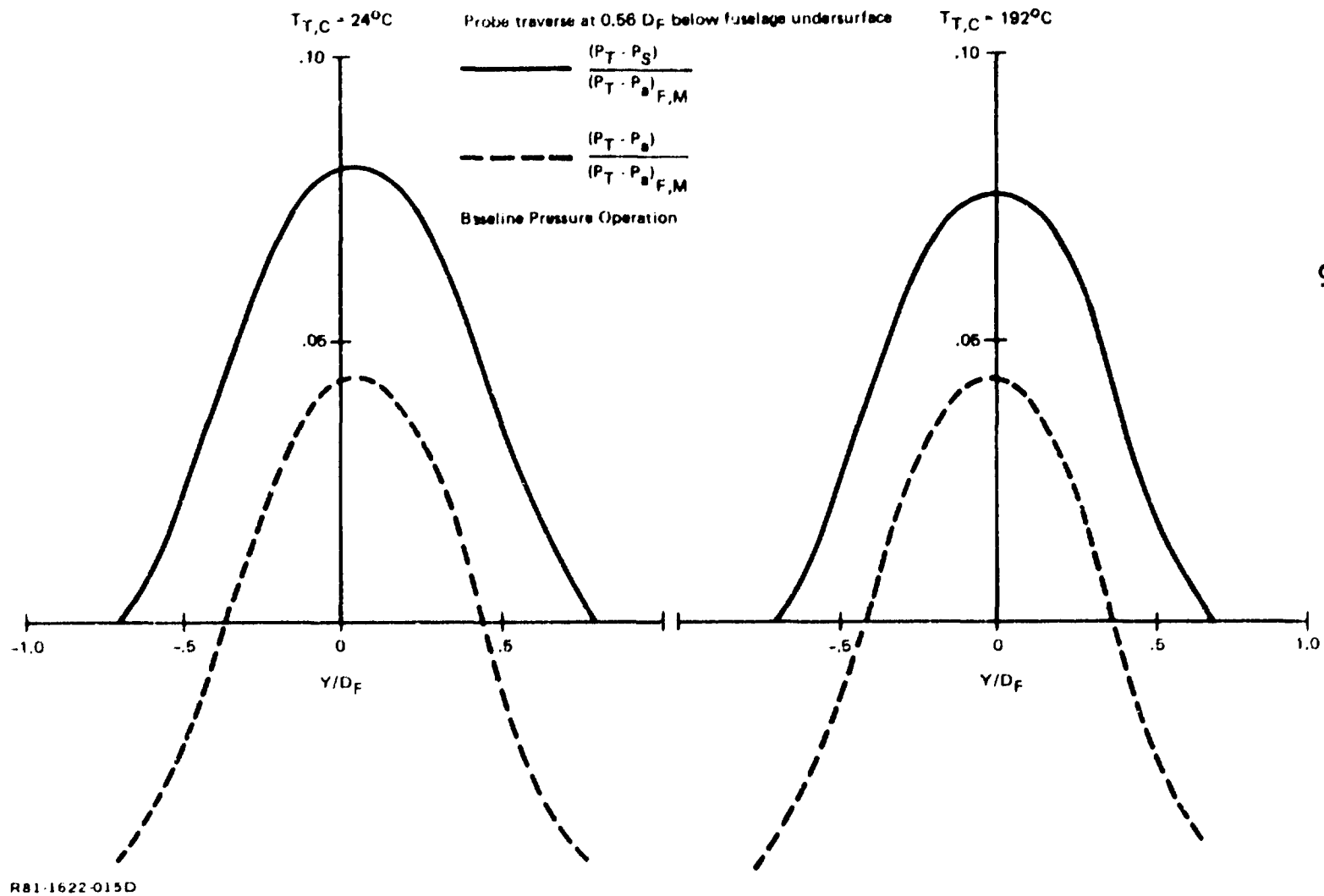
A more meaningful view of the effects of the fan total pressure can be found in the non-dimensional presentation with interference force normalized by

ORIGINAL PAGE IS
OF POOR QUALITY



R81-1622-014D

Figure 22 - Pressure profiles across upwash centerline, $H_B/D_F = 1.54$.

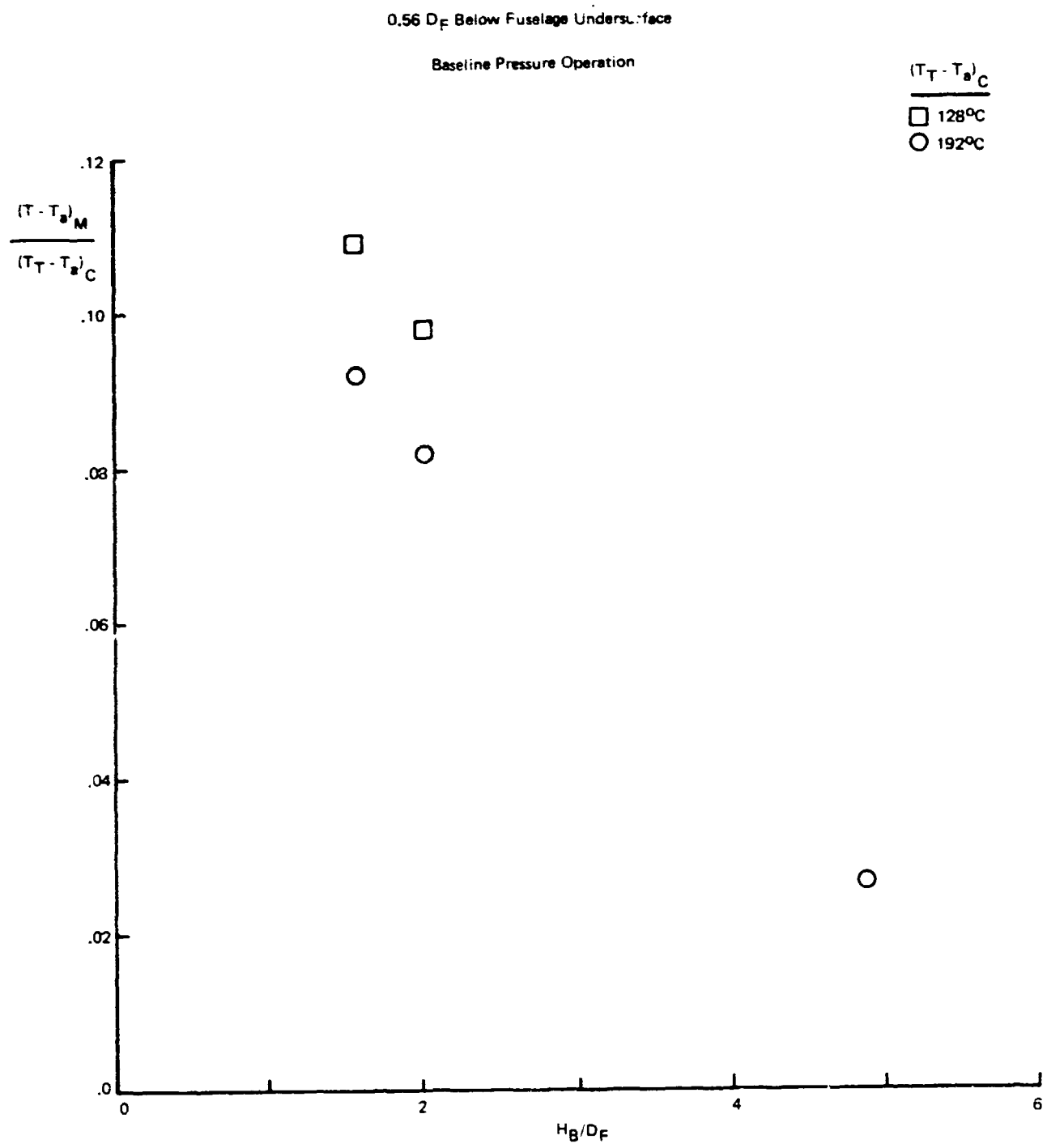


ORIGINAL PAGE IS
 OF POOR QUALITY

RB1-1622-015D

Figure 23 - Pressure profiles across upwash centerline, $H_B/D_F = 1.99$.

ORIGINAL PAGE IS
OF POOR QUALITY



R81-1622-016D

Figure 24 - Variation of centerline upwash temperature with ground height.

ORIGINAL PAGE IS
OF POOR QUALITY

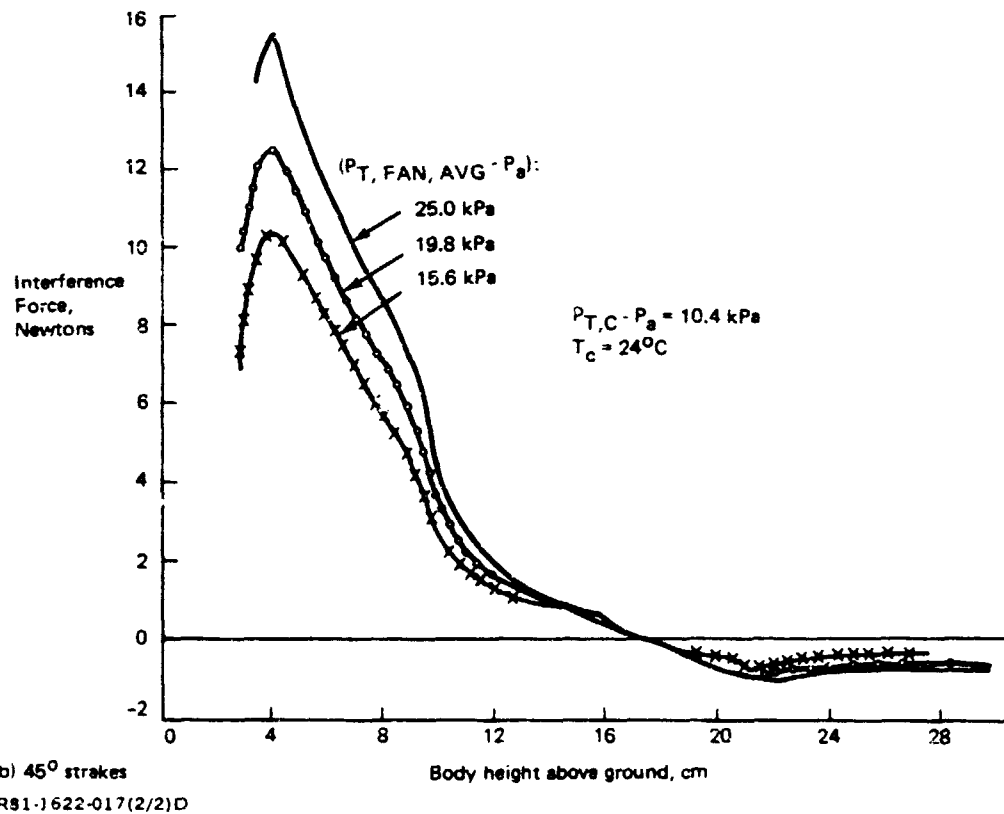
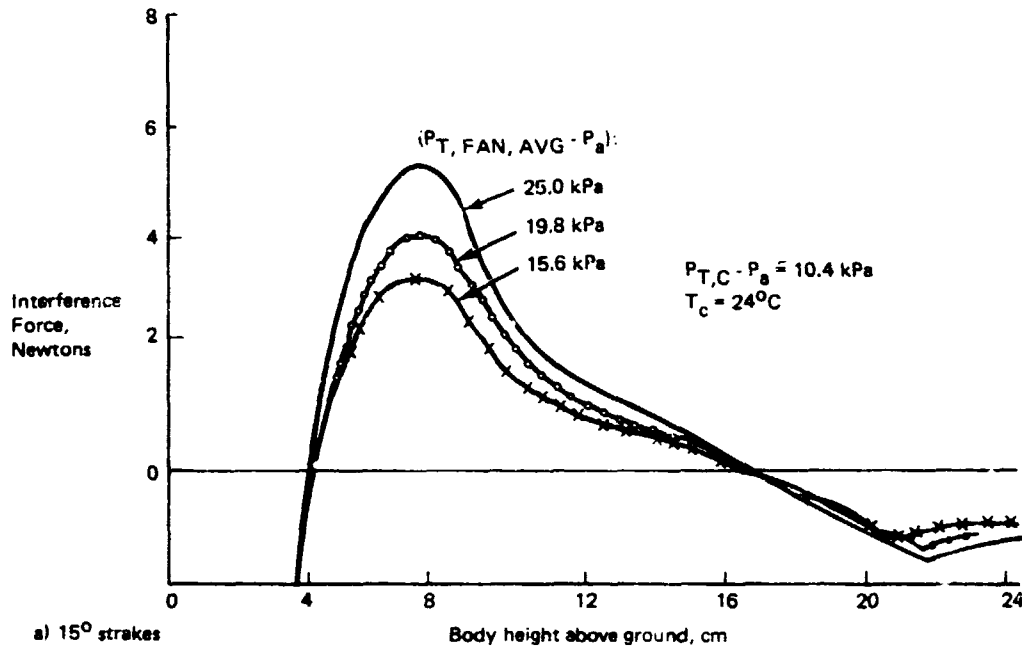


Figure 25 - Effect of fan pressure on interference forces.

the nozzle thrust shown in Figure 26. The total pressure level has no significant effect on the non-dimensional interference forces. Full scale data (from Ref. 1) are shown on this plot for reference.

At a fan average total pressure of 19.8 kPa gauge (and core total pressure, again, at 10.4 kPa gauge) five core total temperatures were run: 43°C, 104°C, 254°C, 322°C and 416°C. As shown in Figure 27, there is essentially no effect of temperature on the interference forces. Experiments were also conducted with the nozzle exit flow more closely matching the full-scale engine conditions. For a fan total pressure of 25 kPa gauge, model forces were measured with core exit temperature of 421°C and 43°C. Figure 27 shows these results compared to the full-scale data (Ref. 1). Again, there is a very small effect of temperature on interference forces. The close agreement between the model test results and the full-scale data indicates that good simulation of aircraft ground interference forces can be obtained with a 1/24th scale model even without core temperature simulation.

5.1.5 Model Surface Pressures and Temperatures. - Pressure and temperature measurements were taken on the model undersurface with the baseline nozzle pressure conditions and core nozzle exit temperatures of 128°C and 192°C. Figure 28 shows dimensionless temperature distributions along the model underside (x-direction) for three heights above ground. The temperature across the model surface (y-direction) showed little variation. Values of the surface temperature coefficient $((T - T_a) / (T_c - T_a))$ at station number 22 (0.54D aft of the nacelle centerline) are very close to values found with a probe on the upwash centerline at 0.56D below the model surface (Figure 24). This comparison provides some verification for the model surface temperature data, which were taken by thermocouples attached to the inner surface of the metallic underside of the model as described in Subsection 4.7.2. Figure 29 shows the variation of model temperature and pressure with body height above ground. The temperature was measured at station number 22 and the pressure at the midpoint between nozzles.

Model pressure and temperature data were also taken for a higher core temperature and a higher fan pressure that more closely matched the full-

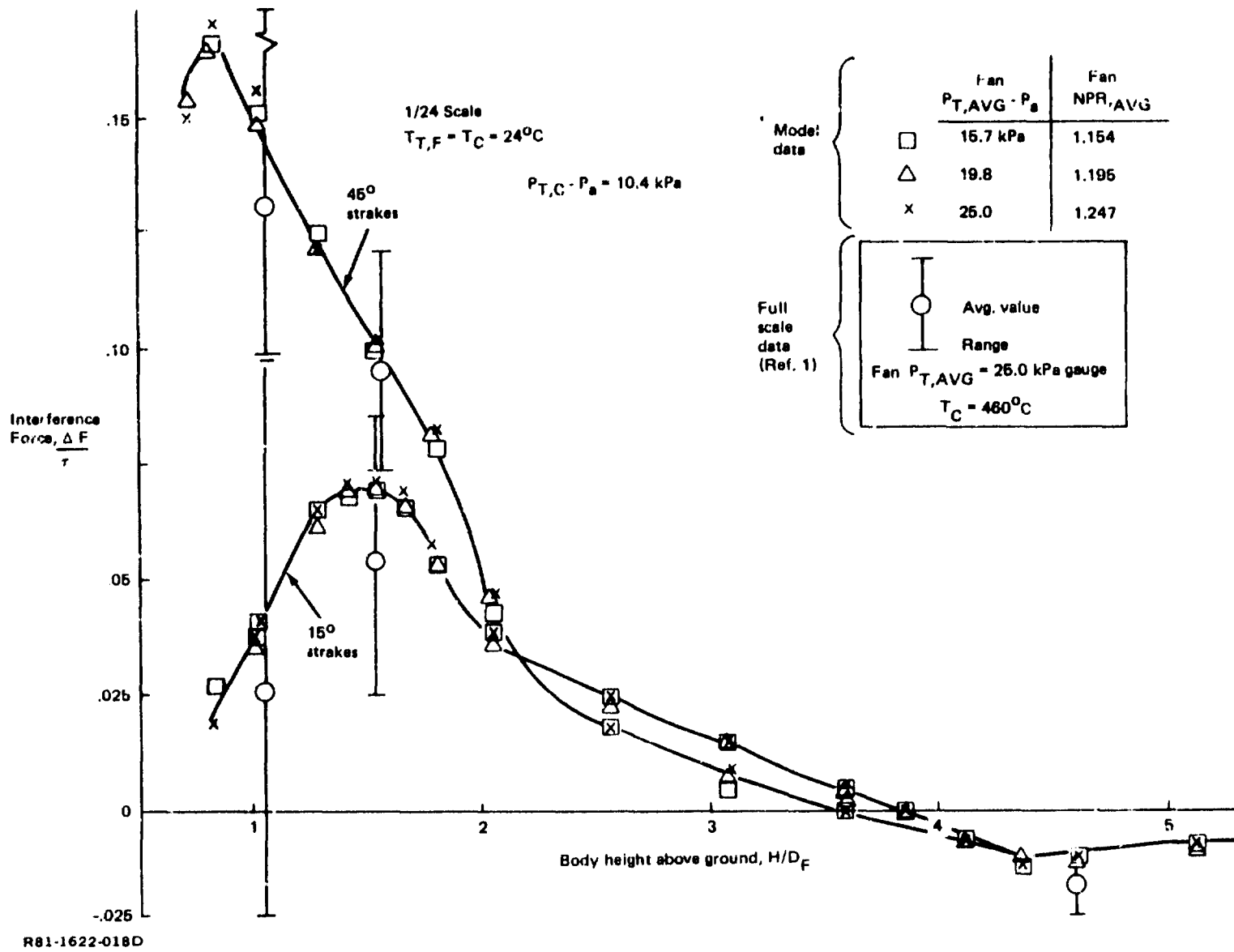
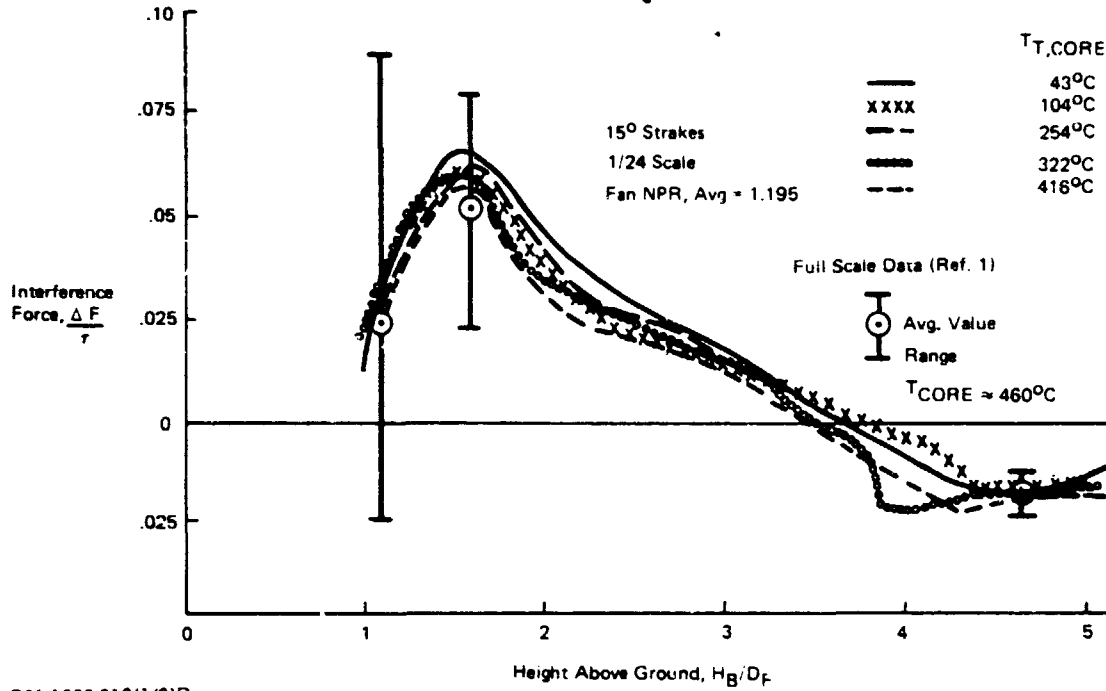


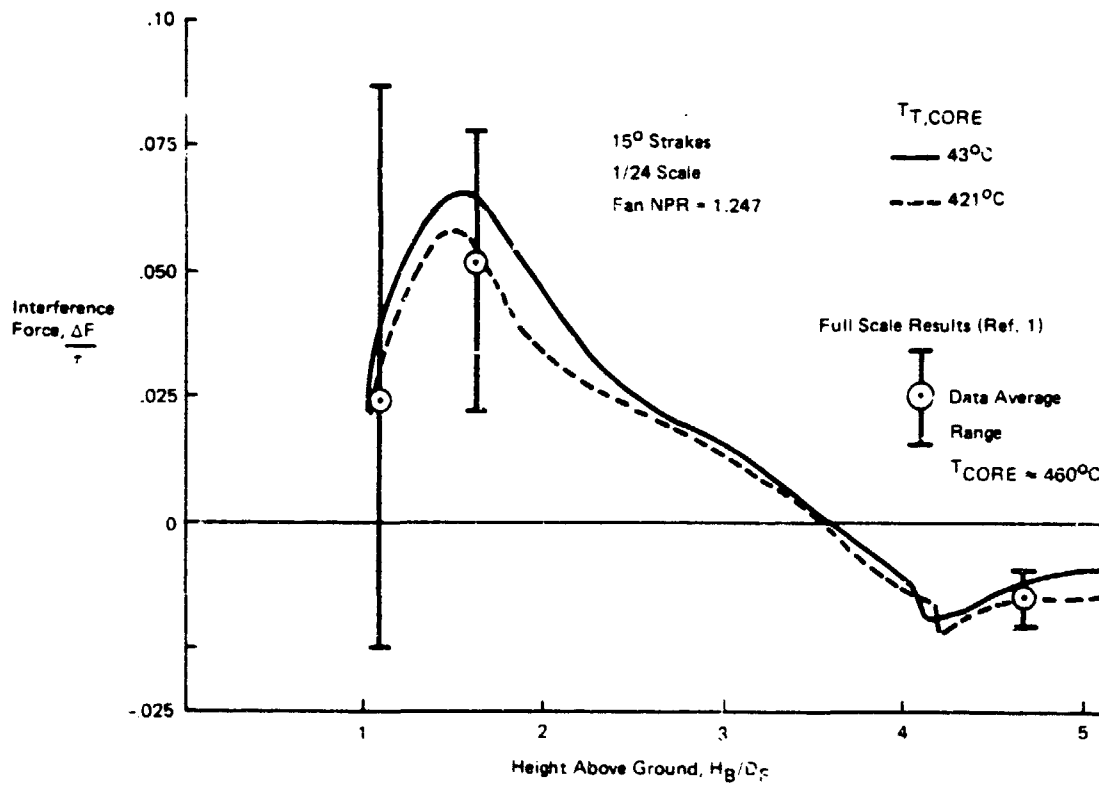
Figure 26 - Effect of fan nozzle pressure on interference forces

OFFICE OF THE
 CHIEF OF ENGINEERS
 U.S. NAVY

ORIGINAL PAGE IS
OF POOR QUALITY



R81-1622-019(1/2)D



R81-1622-019(2/2)D

Figure 27 - Effect of core temperature and fan pressure ratio on interference forces, $T_{T,F} = 24^\circ C$.

ORIGINAL PAGE IS
OF POOR QUALITY

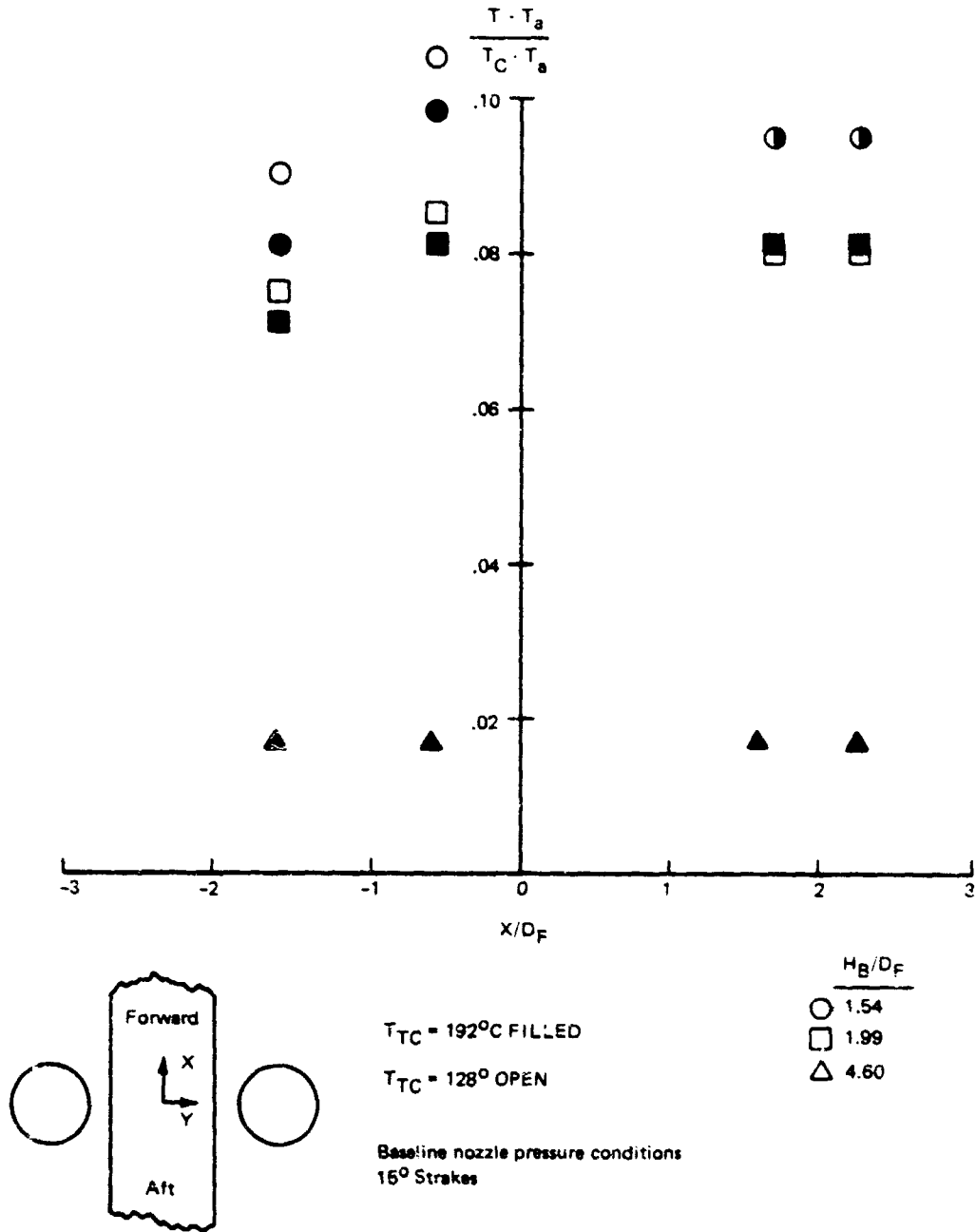
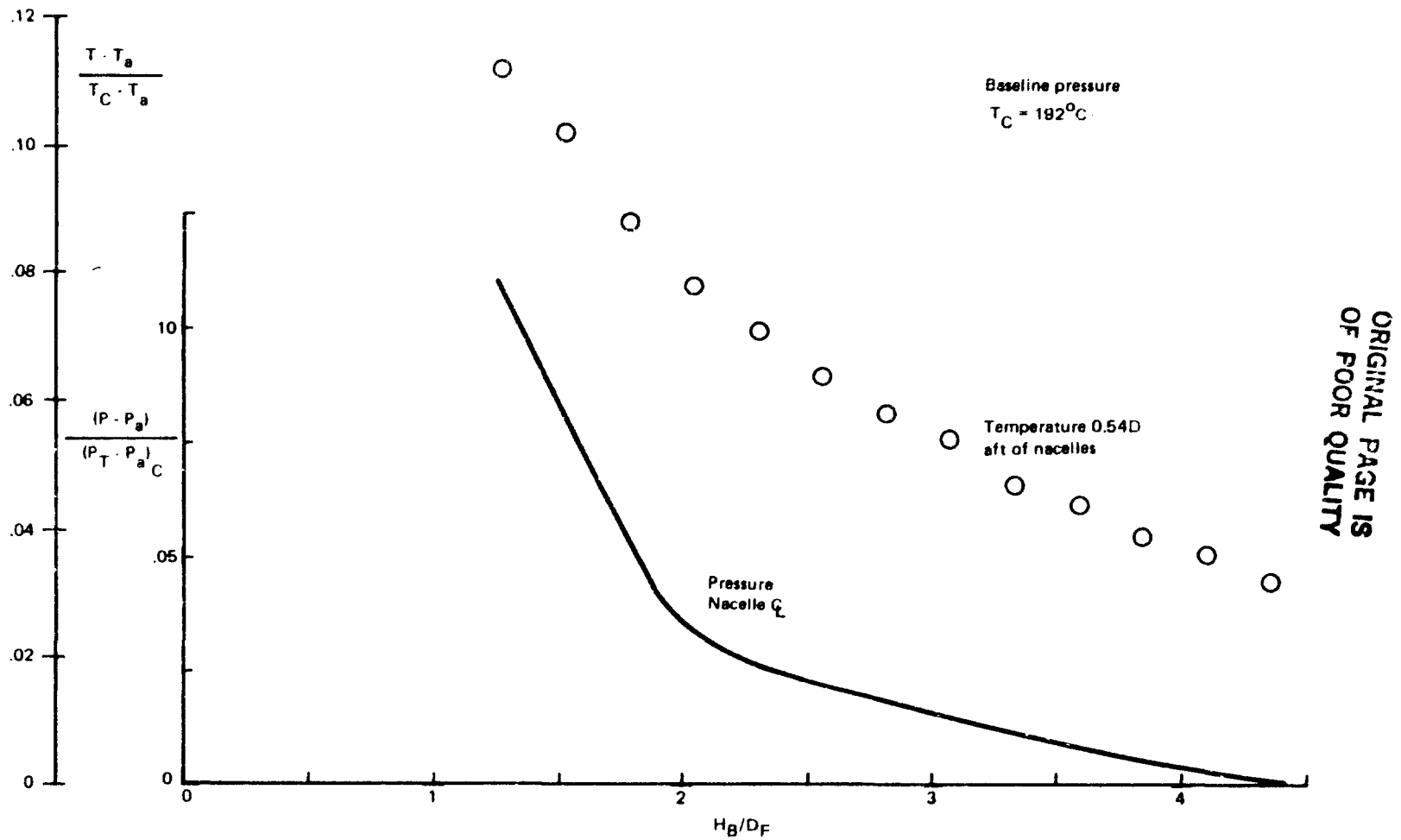


Figure 28 - Temperature distribution along model underside.



R81-1622-021C

Figure 29 - Variation of model pressure and temperature with ground height.

scale tests. Figures 30 and 31 show pressure and temperature measurements taken at three heights above ground for a core exit temperature of 427°C. The relatively low model surface temperatures shown at $X/D_F = 0.5$ in Figure 31 are not due to faulty thermocouples. Temperatures on both sides (y-direction) of this centerline thermocouple showed the same values, which verified that the temperature profile along the model had a local minimum slightly forward of the nacelle centerline. The magnitude of this local minimum varied with height above ground. This distortion did not appear in the data taken at lower core temperature (Figure 28) because this centerline thermocouple and one of the side thermocouples were inoperative during the earlier tests.

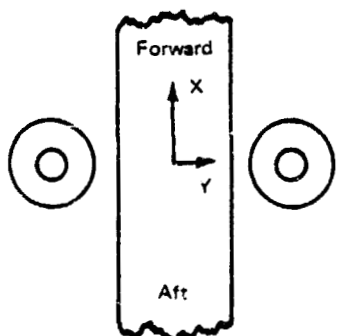
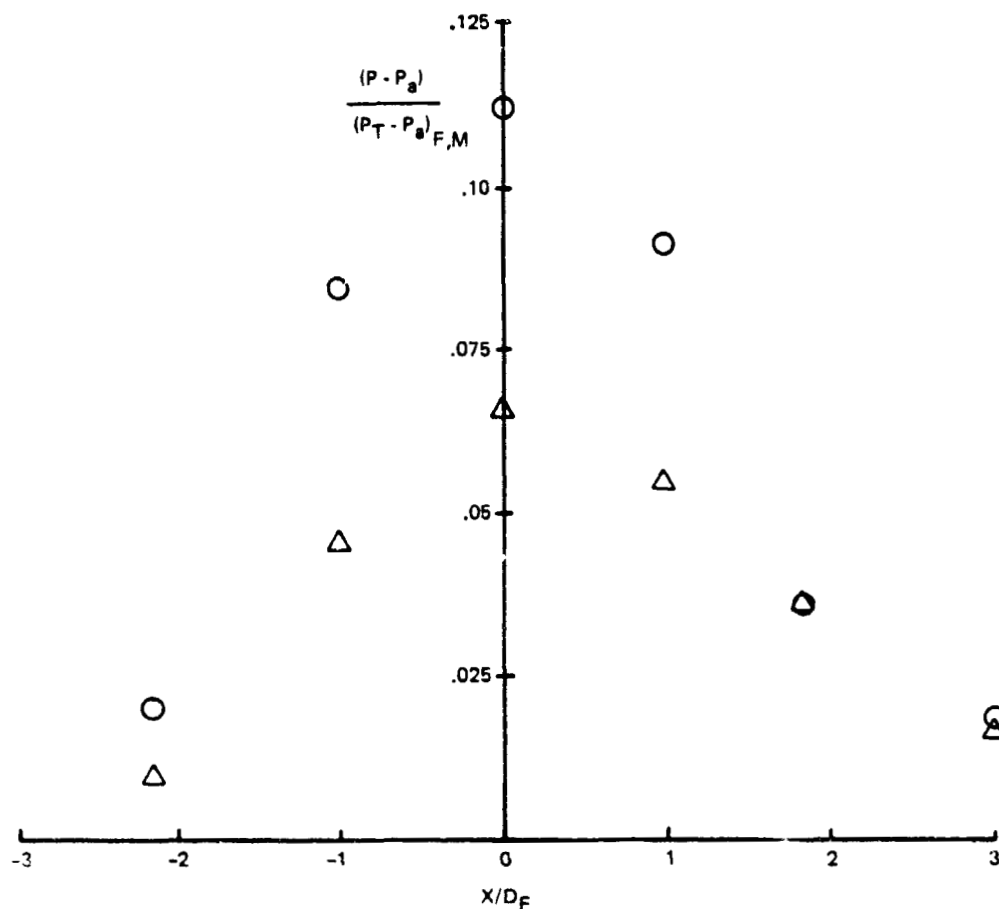
Comparison of the data shown in Figure 31 with those shown in Figure 28 indicates that the model surface temperature does not scale well with wide variations in core exit temperature. The model surface temperature coefficient decreased by more than a factor of two when the core flow temperature was raised from 128°C to 421°C. The same poor temperature scaling appeared in probe temperature measurements on the upwash centerline (Figure 24). In this case, the local temperature coefficient in the flow decreased by 15 percent when the core exit temperature was raised from 128°C to 192°C.

Probe temperature surveys were made in the area corresponding to the inlets on the full-scale model ($1.8D_F$ above the model upper surface, close to the outer surface of the fan nozzles). It was found that the temperature in this region was very close to ambient, and fluctuating greatly. The maximum temperature rise observed for a nozzle total temperature of 192°C was approximately 2°C. The strakes apparently turn the flow enough to prevent any significant amount of upflow from reaching the inlet area. The inlet suction may affect the flow field to alter this behavior, but this is not expected to happen.

5.2 Open Circular Nozzles

5.2.1 Nozzle Flow. - Free jet data were taken with the ground plane removed, using settling chamber temperatures from ambient to 232°C, and a settling chamber pressure of 27.6 kPa above ambient. Total pressure and temperature profiles were recorded for probe traverses across both jet centerlines for dis-

ORIGINAL PAGE IS
OF POOR QUALITY



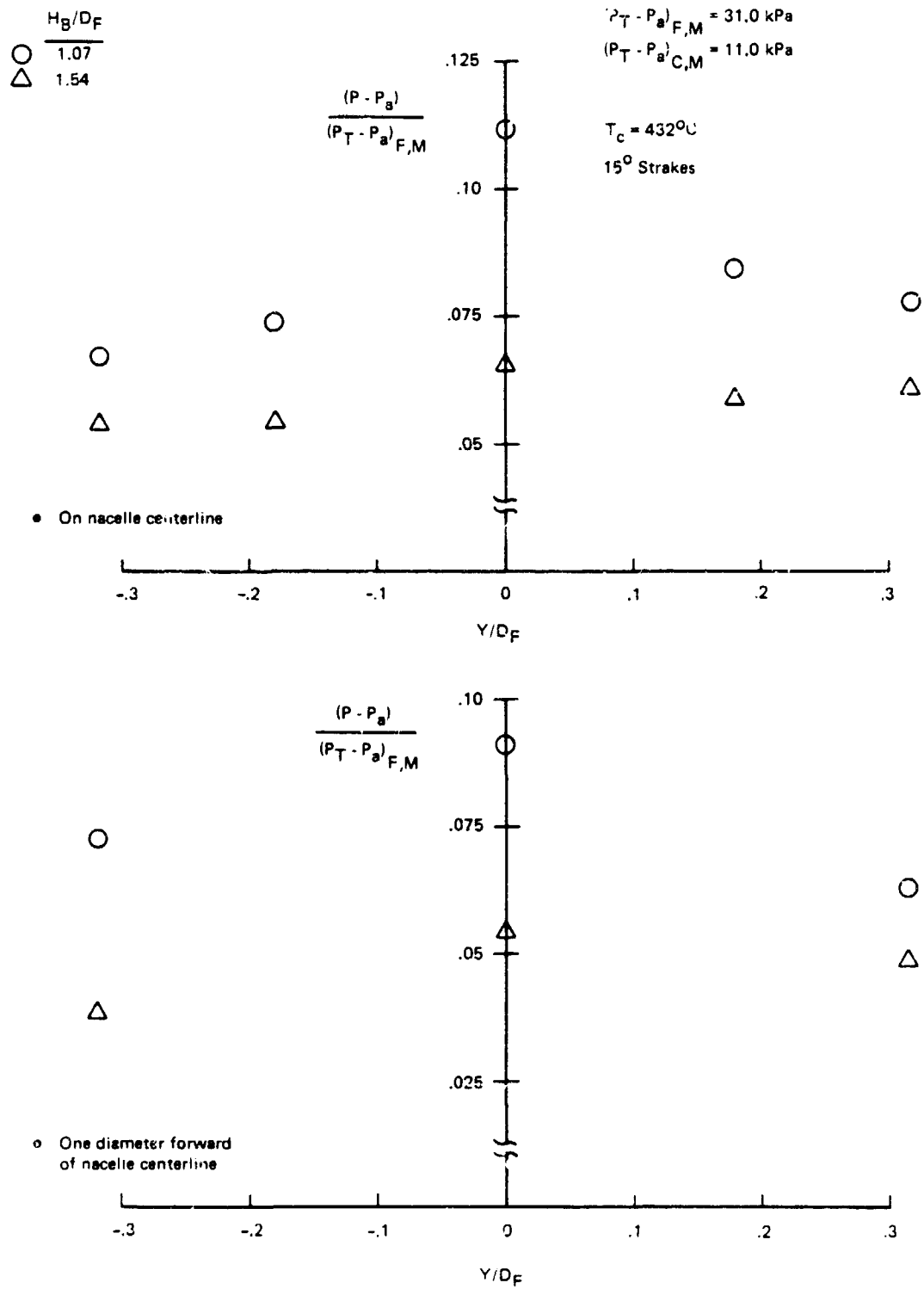
$(P_T - P_a)_{F,M} = 31.0 \text{ kPa}$
 $(P_T - P_a)_{C,M} = 11.0 \text{ kPa}$
 $T_C = 432^\circ\text{C}$
 15° Strakes

$\frac{H_B}{D_F}$
 ○ 1.07
 △ 1.54

R81-1622-022D

Figure 30a - Pressure distribution along model.

UNIVERSITY OF TORONTO
OF FLOW QUALITY



R81-1622-023D

Figure 30b - Pressure distribution across model.

ORBITAL TESTS
OF PERFORMANCE

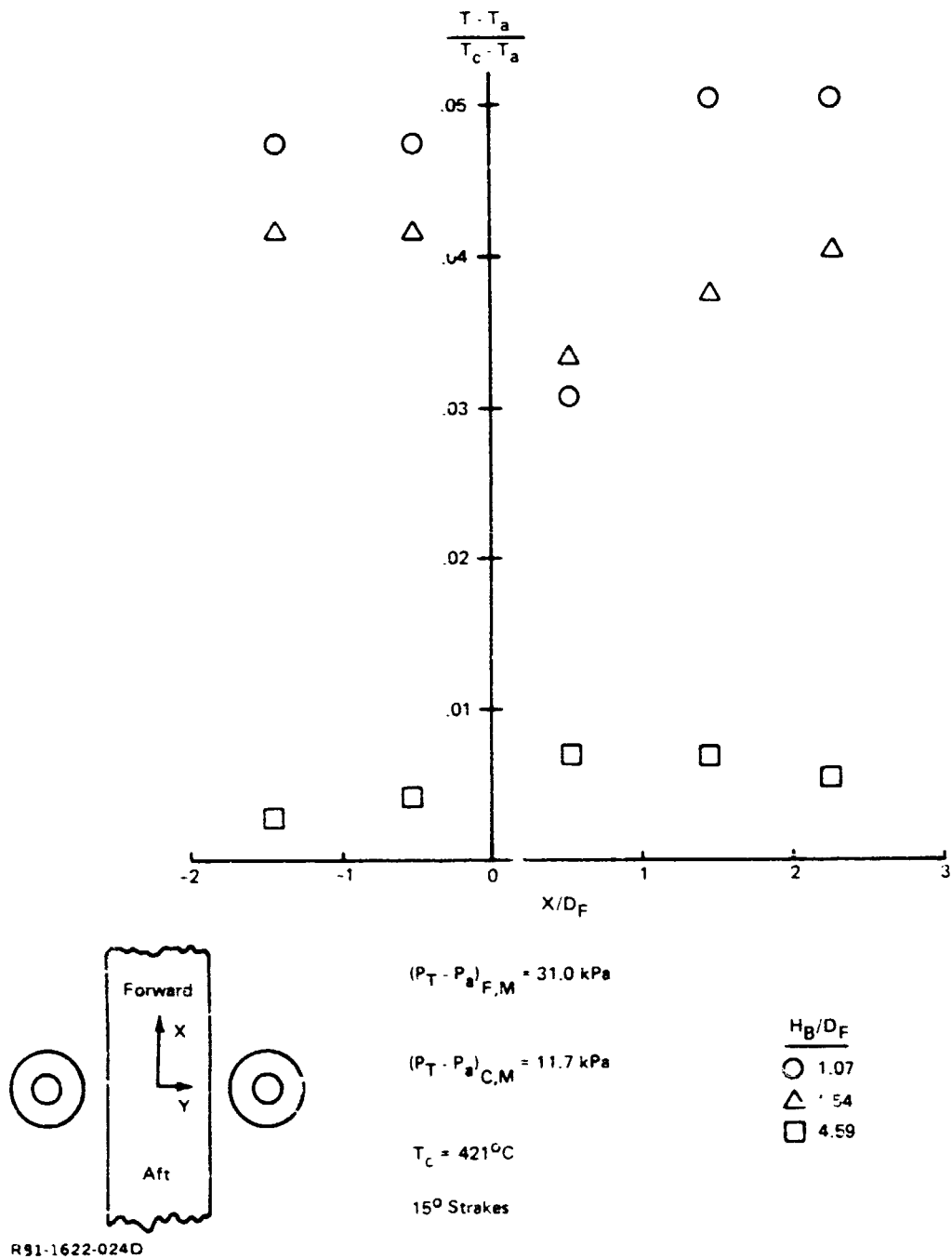


Figure 31 - Model temperature distribution.

tances (Z') from the jet exists up to 15 diameters. Figure 32 shows pitot pressure profiles obtained with a settling chamber temperature of 227°C . Profiles taken close to the exit exhibit a flat-topped profile with a 1 percent ripple that was caused by fluctuations with time of the air supply pressure. Note that there is no inward shift of the maximum pitot pressure points at large values of Z' as occurred in the free-stream data obtained with fan-jet nozzles. The corresponding temperature profiles are shown in Figure 33. These temperature data were plotted directly from the thermocouple output and have not been corrected for radiation losses. (This correction was typically of the order of 10°C .) The pressure profiles begin to merge about seven diameters from the nozzle exit. The temperature profiles show a greater radial spreading and begin to merge about five diameters from the nozzle exit.

Figure 34 shows data taken from profiles that were obtained with different settling chamber temperatures. The data show the decay of pitot pressure and temperature along one jet centerline with two jets in operation. The centerline pitot pressure decay is slightly greater for heated than for unheated jets. Several runs made with one nozzle blocked off showed no difference between the single- and dual-jet results in the centerline values of both pitot pressure and temperature out to $Z' = 15$ diameters. Hence, the decay in centerline properties obtained from two jet operation can be used to represent single-jet operation.

5.2.2 Ground Flow without Model. - Ground-pressure and wall-jet profiles were taken at three values of H/D corresponding to the full-scale test conditions. Ground pressure measurements were taken without the model to determine how closely the radial pressure distribution around one jet impingement point matched existing single-jet impingement data. Figure 35 shows the data taken along radial paths at two orientations around one jet centerline. The solid curve, taken from Ref. 2, represents an empirical approximation for the ground pressure distribution for a single jet with H/D between 2.0 and 5.0.

Wall-jet profiles (similar to those shown in Figure 20) were taken at the same values of H/D and the same ground locations used in the full-scale

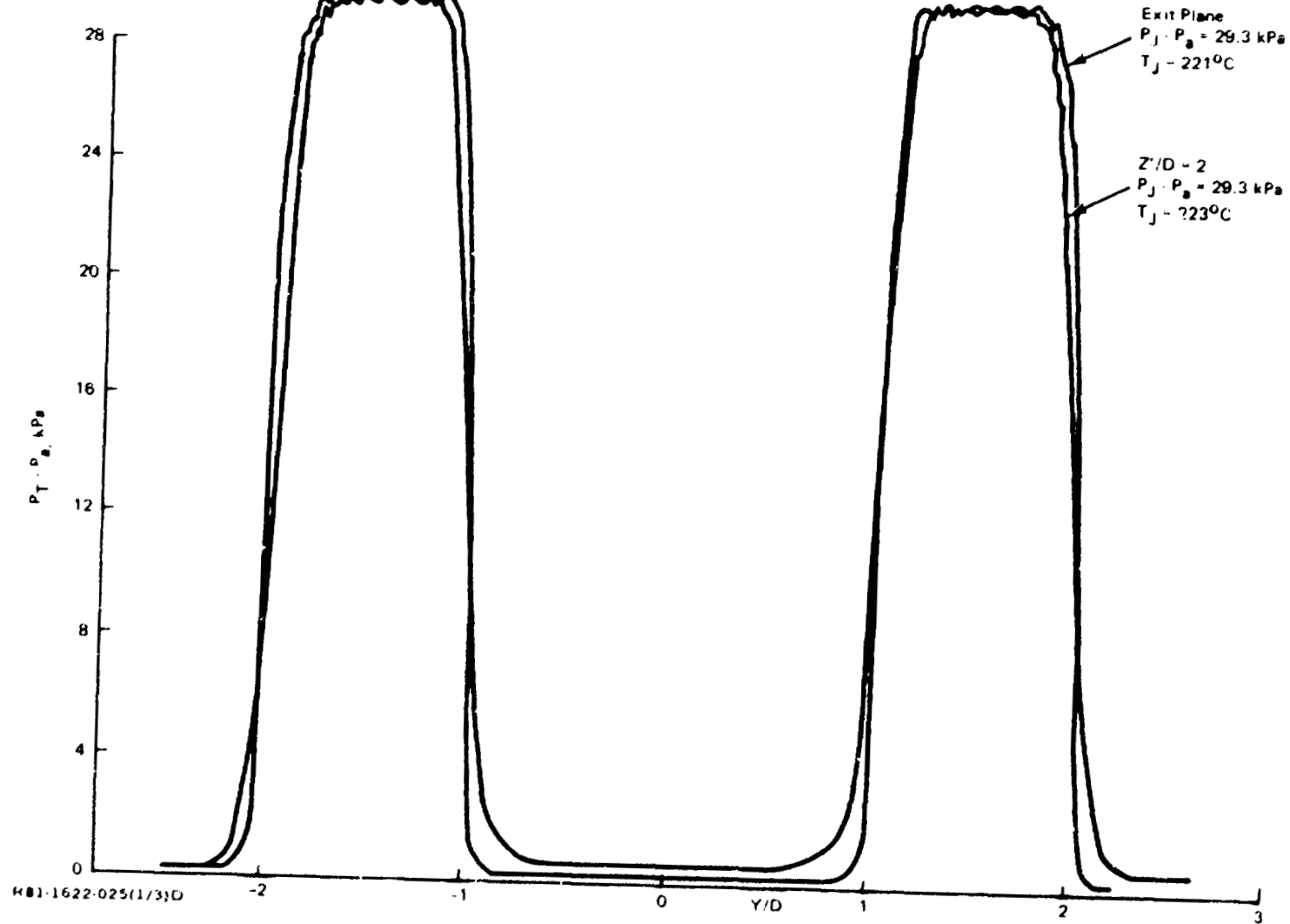


Figure 32 Free jet total pressure surveys, open circular nozzles.

ORIGINAL PAGE IS
 OF POOR QUALITY

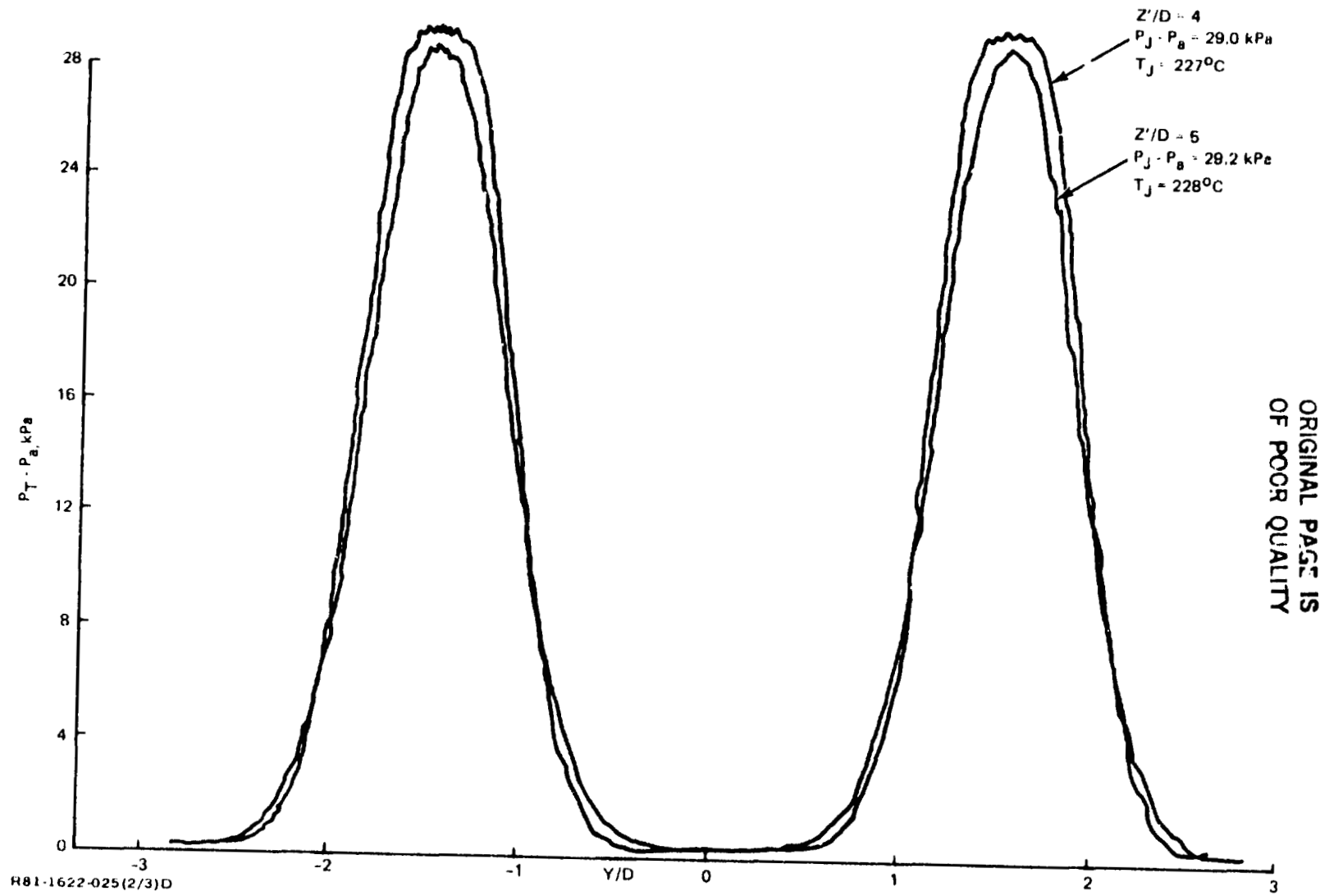


Figure 32 - (Continued).

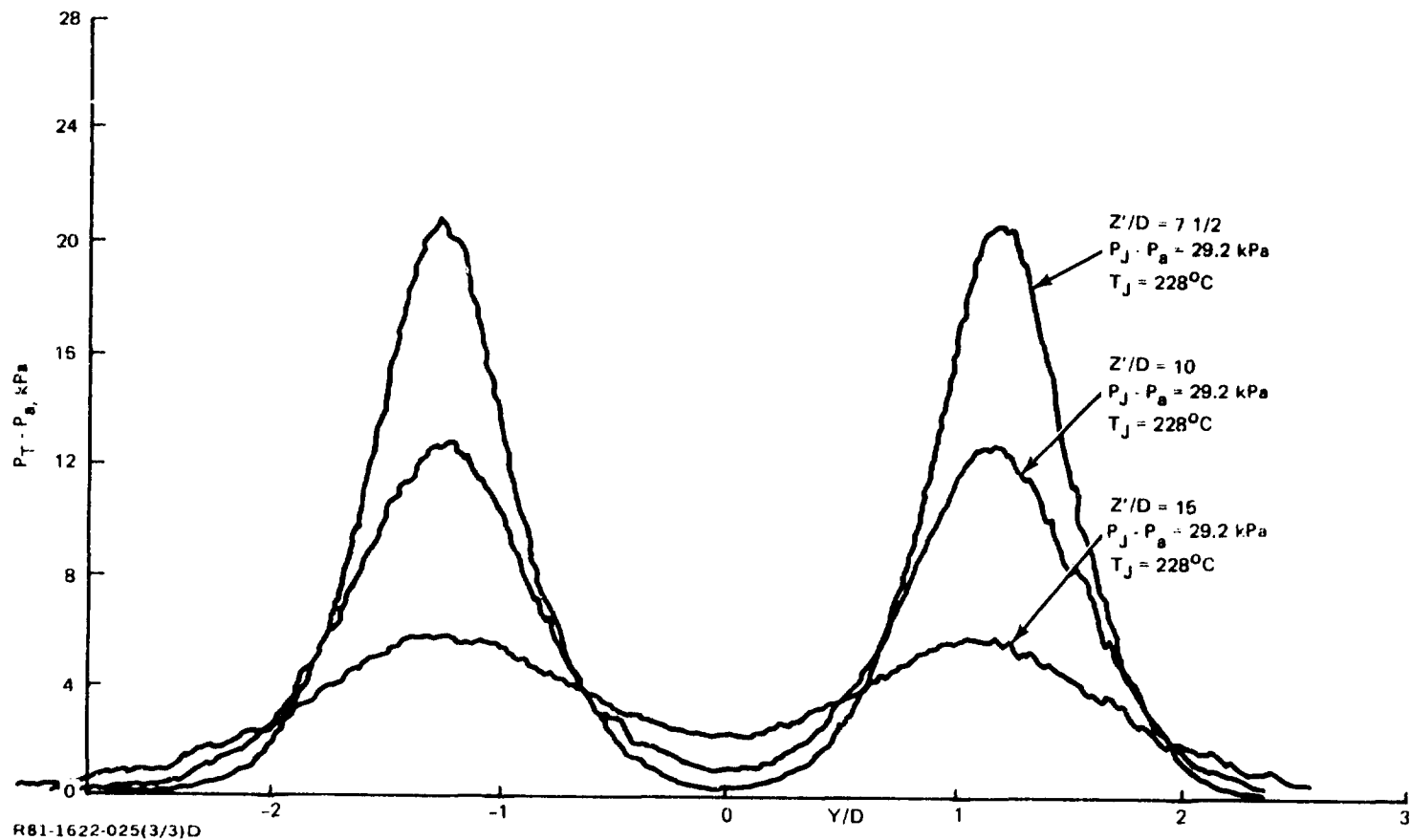


Figure 32 - (Concluded).

NATIONAL BUREAU OF STANDARDS
 GAITHERSBURG, MARYLAND

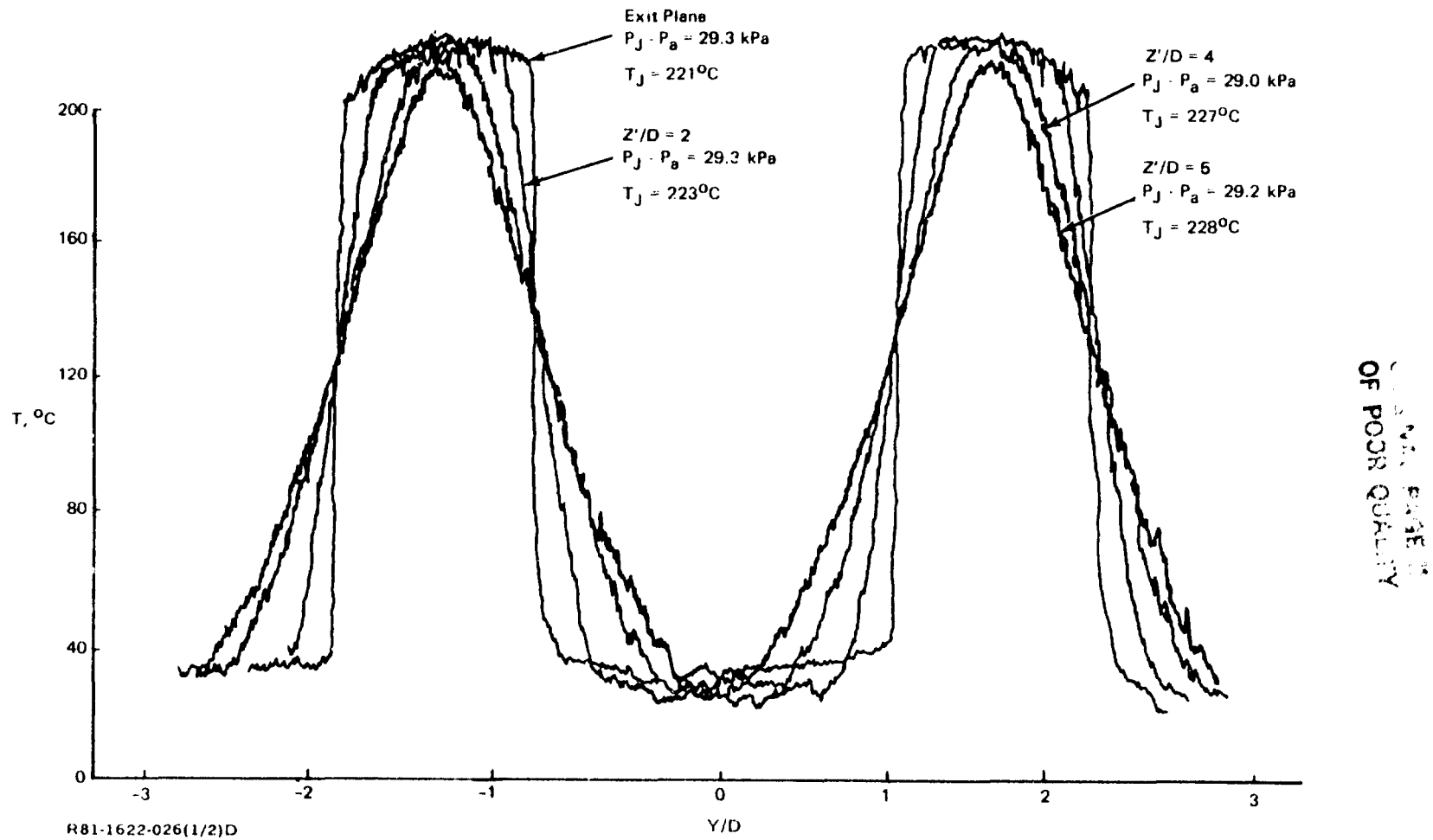


Figure 33 - Free jet total temperature surveys, open circular nozzles.

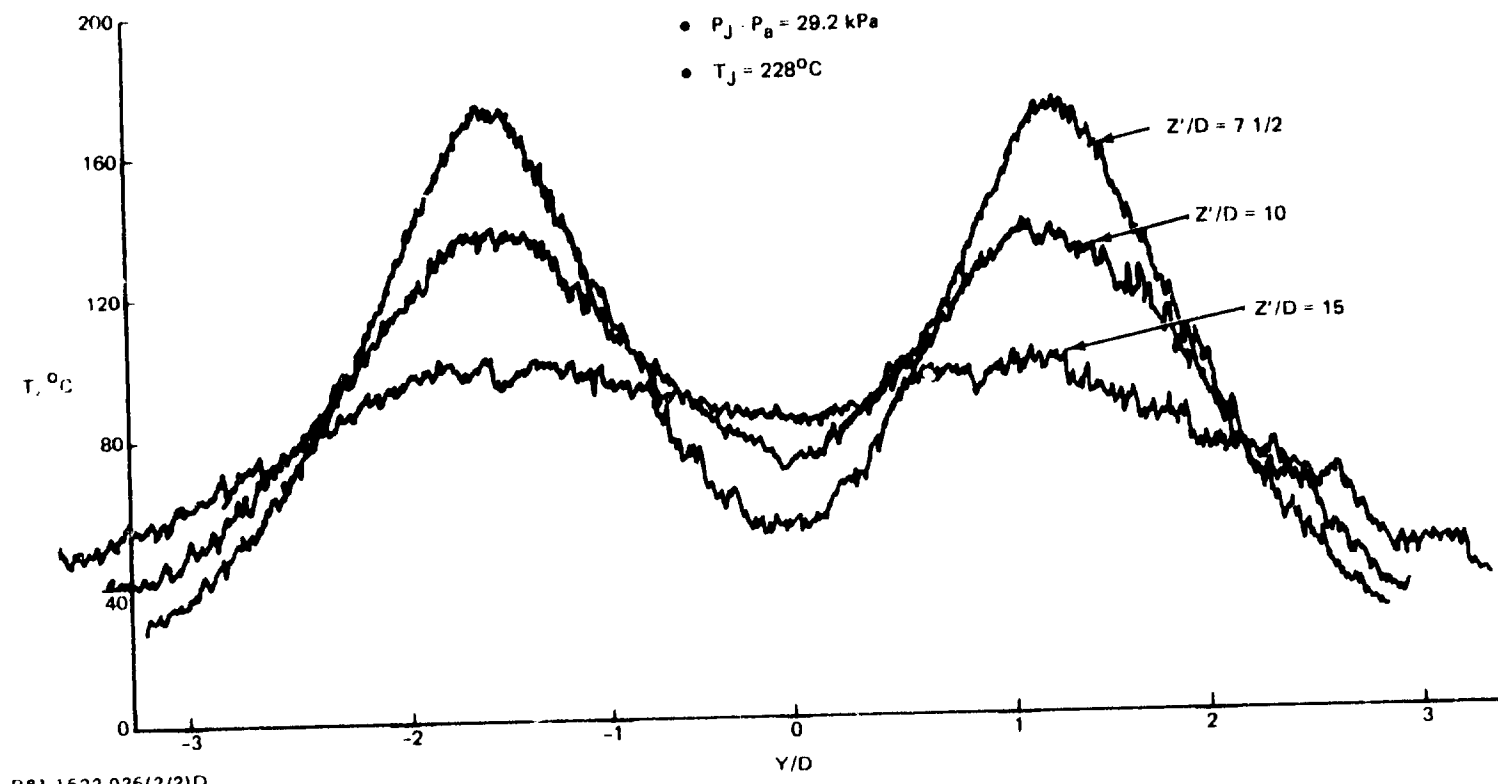
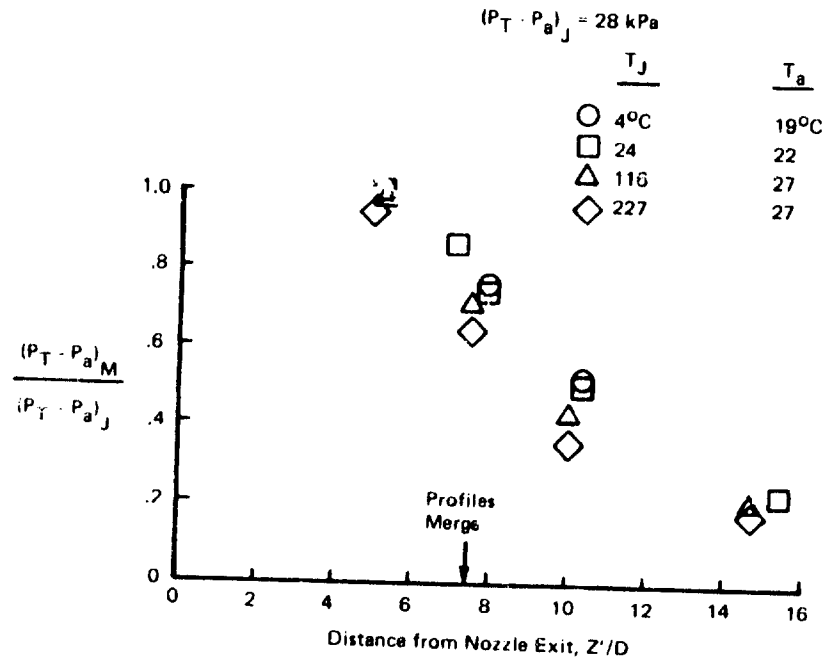
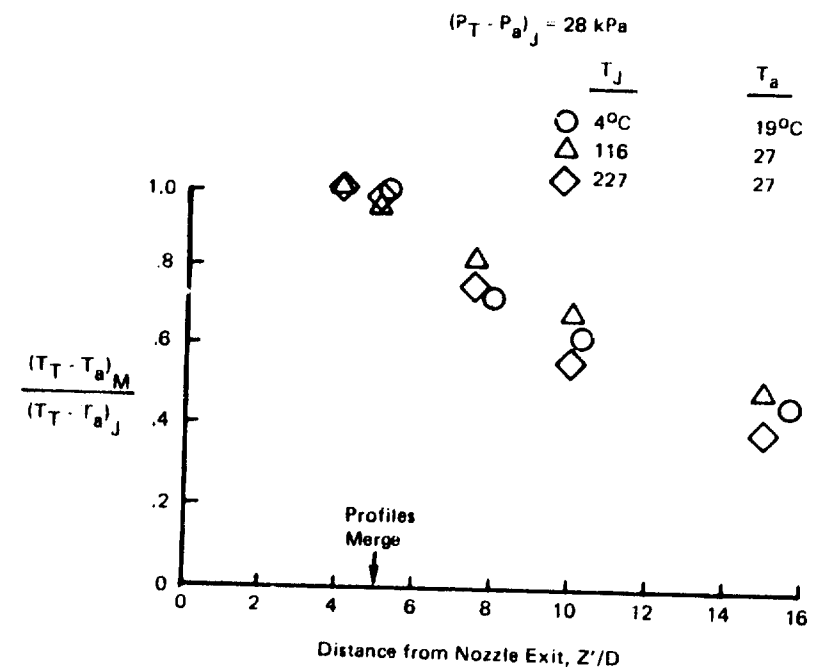


Figure 33 - (Concluded).

OF POOR QUALITY



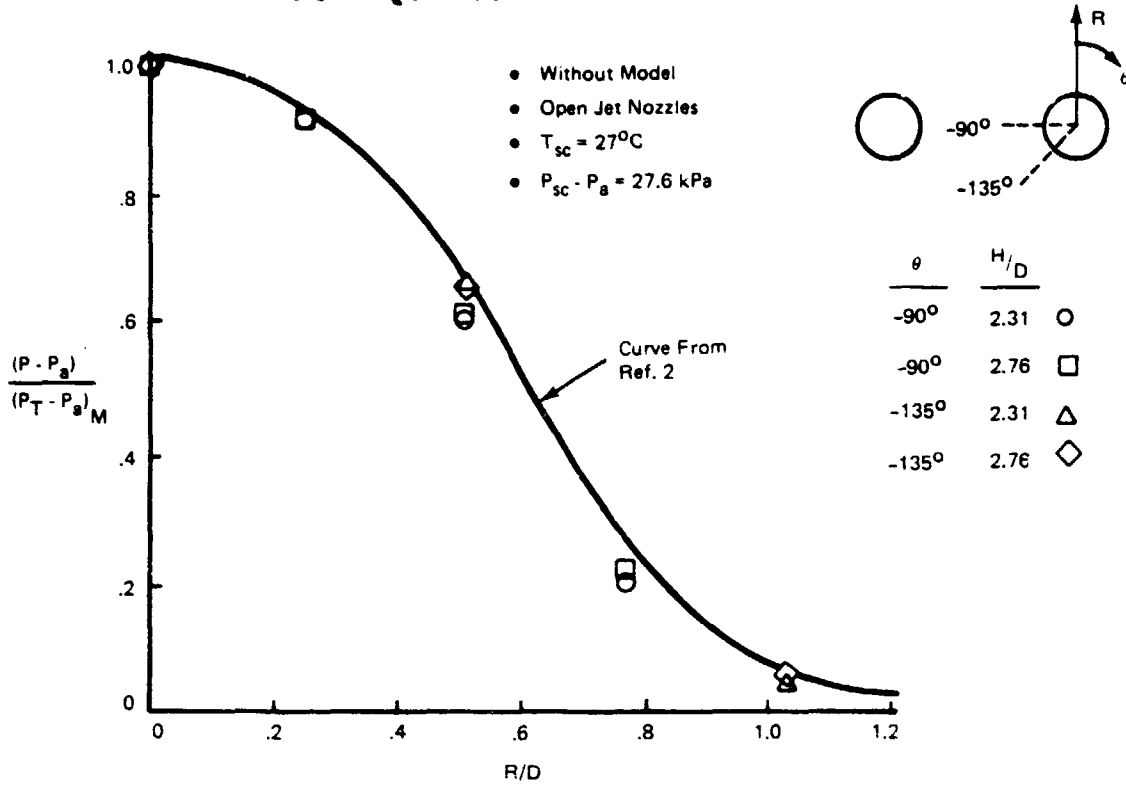
a) Pitot Pressure
R81-1622-027(1/2)D



b) Temperature
R81-1622-027(2/2)D

Figure 34 - Free jet properties along one flow centerline, two jets operating, open circular nozzles; data representative of single-jet operation.

ORIGINAL PLOTS
OF POOR QUALITY



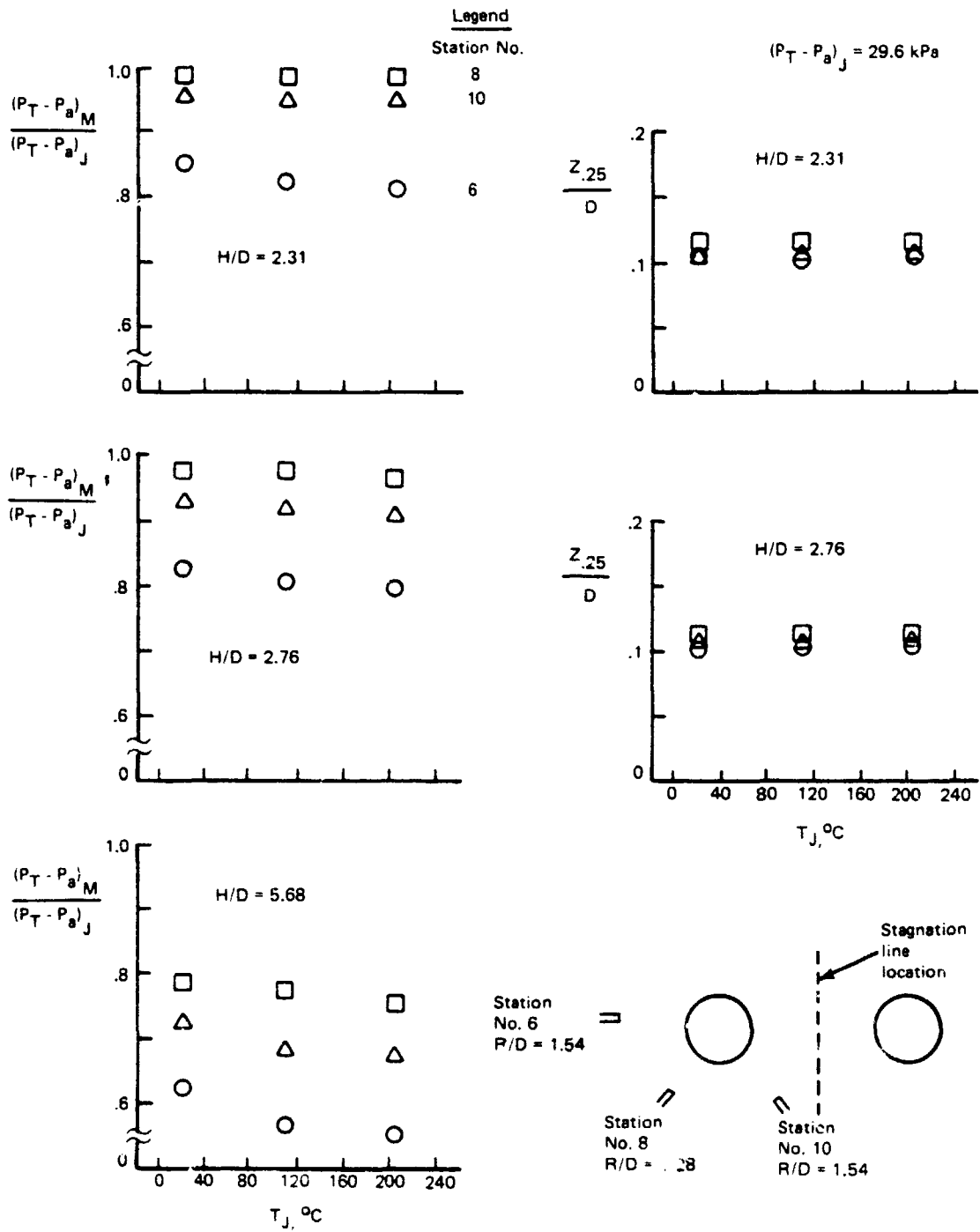
R81-1622-028D

Figure 35 - Radial ground pressure distribution around one jet impingement center.

fan-jet tests. These measurements, summarized by plots of maximum total pressure and thickness in Figure 36, show little influence of temperature on the wall-jet pressure data.

This figure suggests that the wall-jet flow was not axially symmetric around one jet impingement point. Wall-jet profiles taken at the same radius from the closest impingement center show that the flow directed toward the stagnation line has a higher peak total pressure and a greater thickness than the flow directed away from it. This trend occurs for all tested heights above the ground and all settling chamber temperatures. This apparent lack of symmetry in the wall jet data around one impinging jet is probably a real distortion of the ground flow caused by the impingement of the second jet, but may have been caused by interference of the probe support with the upwash formation region when it was located at Station No. 10 (see sketch in Figure 36).

ORIGINAL PAGE IS
OF POOR QUALITY



R81-1622-029D

Figure 36 - Data from wall jet profiles, open jet impingement.

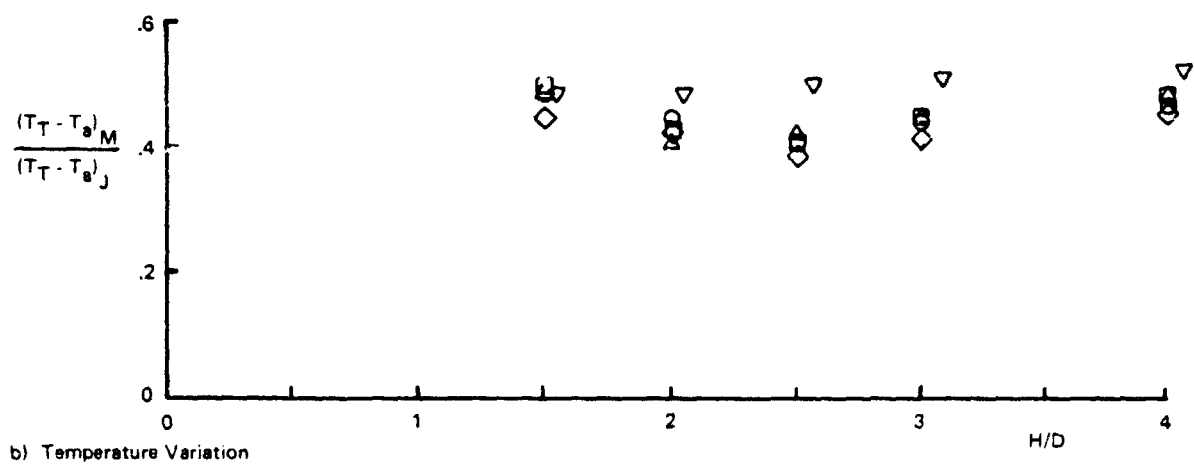
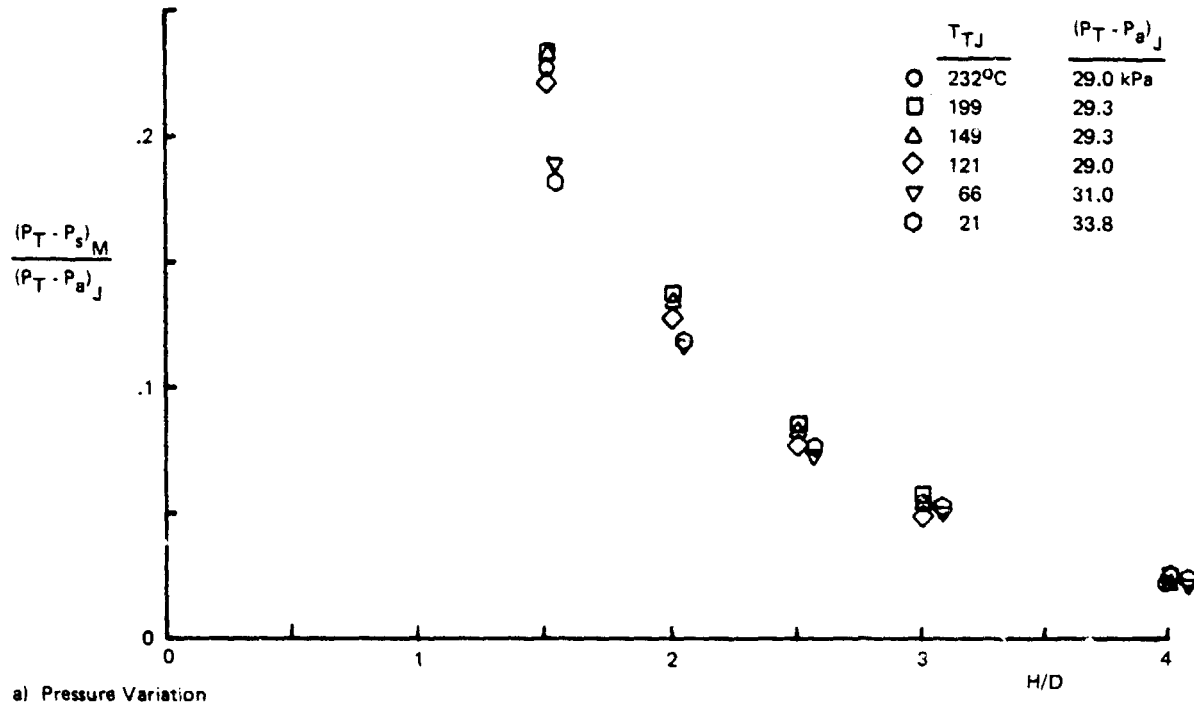
5.2.3 Upwash Flow without Model. - Measurements were taken in the upwash without the model to evaluate flow properties in the absence of model blockage effects. The probes were traversed through the upwash at the nozzle exit plane for several values of H/D and a range of settling chamber temperatures. The results are summarized by the centerline values of upwash properties at the nozzle exit plane that are plotted in Figure 37. The data obtained from the pressure probes were essentially unaffected by temperature. Temperature profiles across the upwash were almost flat, and the exit plane temperatures show little variation with ground height out to H/D = 4.

Additional upwash surveys were made at a fixed nozzle height above ground by traversing the probe through the upwash at various probe heights above ground. The results are summarized in Figure 38 which shows the variation of temperature and pressure along the upwash centerline for H/D = 3. These pressure plots also show little influence of jet exit temperature.

The effect of settling chamber pressure on upwash properties with jet temperature equal to ambient was investigated by conducting exit-plane probe traverses at various ground heights. Figure 39 shows that the centerline properties at the nozzle exit plane, for ground heights of 2-1/2 nozzle diameters or greater, vary linearly with settling chamber pressure over a wide range. Furthermore, these measurements agree with past data taken at this jet spacing in our low-pressure facility. The lack of pressure scaling at low ground heights may be caused by the influence of the ground interaction flow on nozzle exit conditions. As brought out in Ref. 3, the pressure distribution inside the nozzles close to the exit (for this jet spacing) becomes non-uniform when the ground is brought closer than 2-1/2 diameters to the nozzle exit.

The magnitude of the upwash pressure data shown in Figure 39 illustrates that the upwash flow at the nozzle exit plane can be treated as an incompressible flow for all of the nozzle exit conditions and all of the ground heights, even though the nozzle exit flow itself was in the compressible flow range. Flow with a dynamic pressure less than about 5 kPa (corresponding to airflow velocity less than 90 m/sec) can be considered incompressible without a loss in accuracy. Below this value, the dynamic pressure can be found from the difference between total and static pressures. Dynamic pressure much

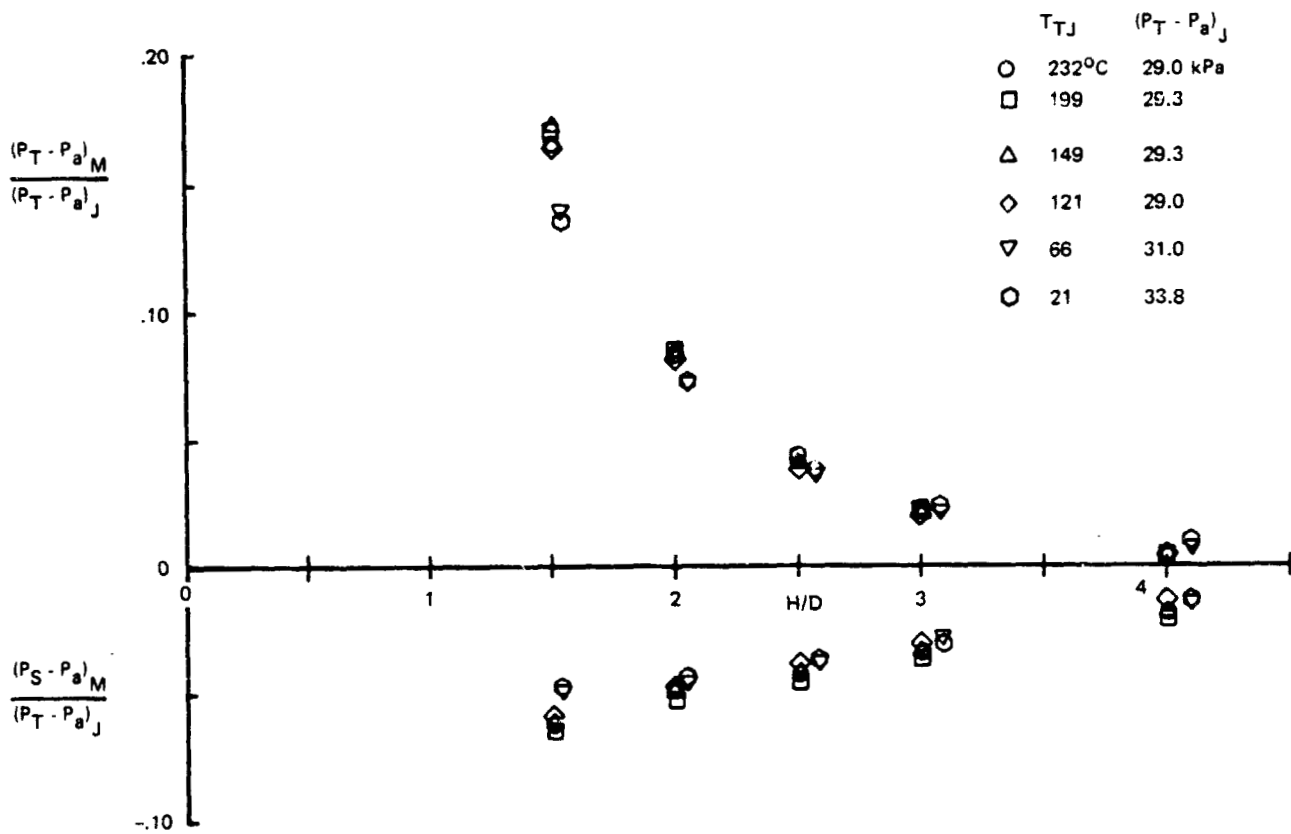
ORIGINAL COPY IS
OF POOR QUALITY



Re1-1622-030(1/2)D

Figure 37 - Upwash properties at nozzle exit plane.

ORIGINAL PAGE IS
OF POOR QUALITY



c) Total and Static Pressure

R61-1622-030(2/2)D

Figure 37 - (Concluded).

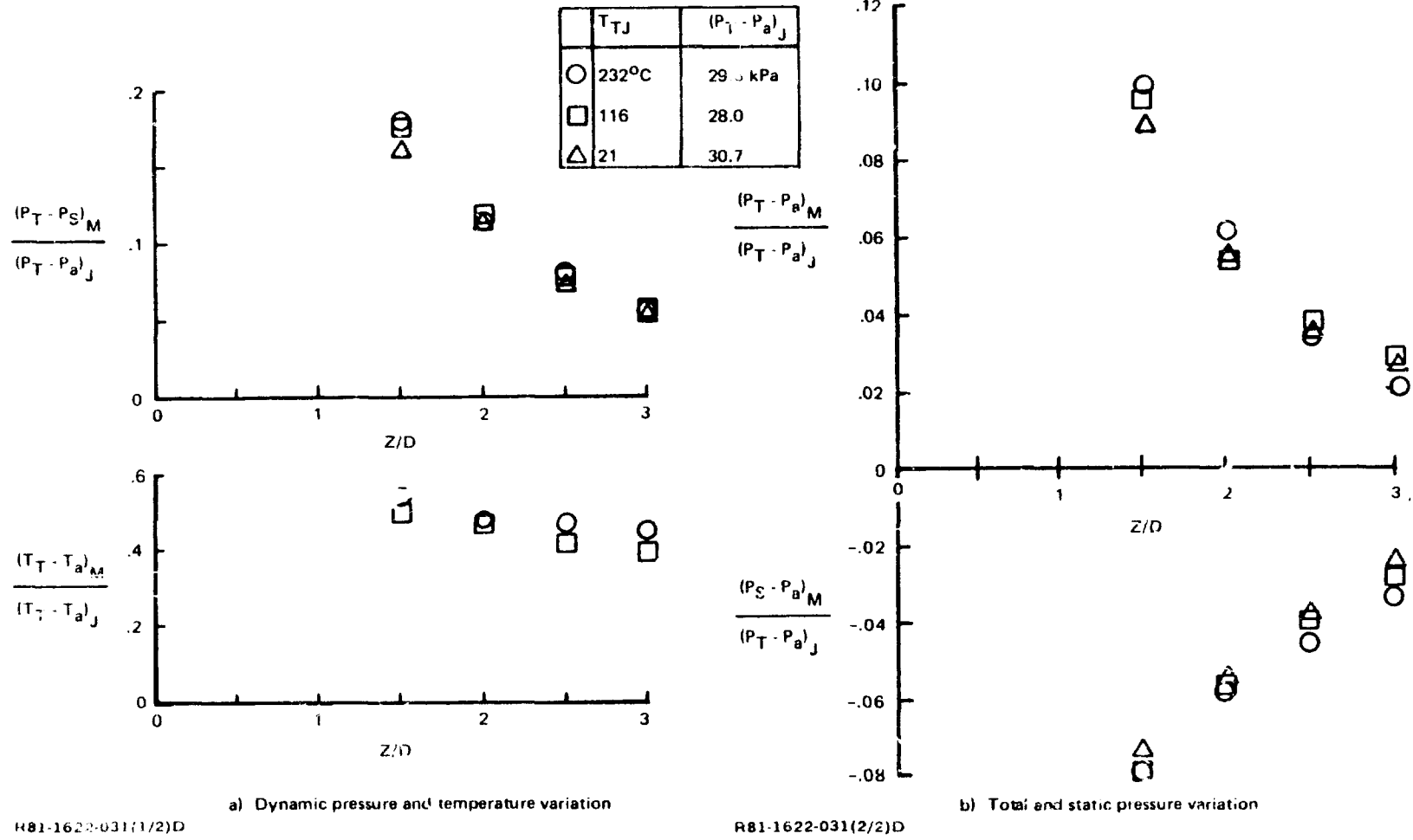
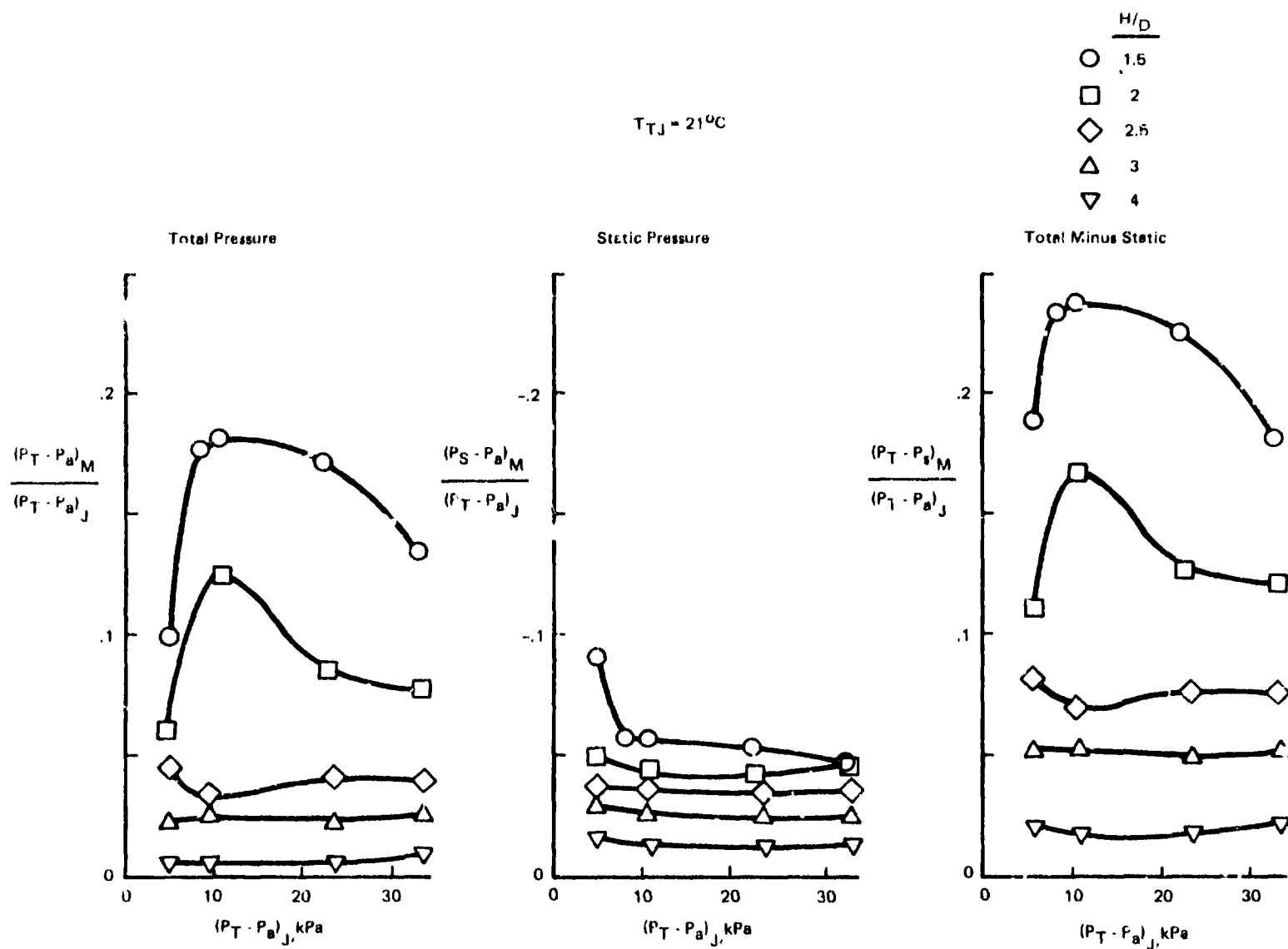


Figure 38 - Upwash properties between nozzle exit plane and ground, H/D = 3.

ORIGINAL PAGE IS
OF POOR QUALITY



RB1-1622-032D

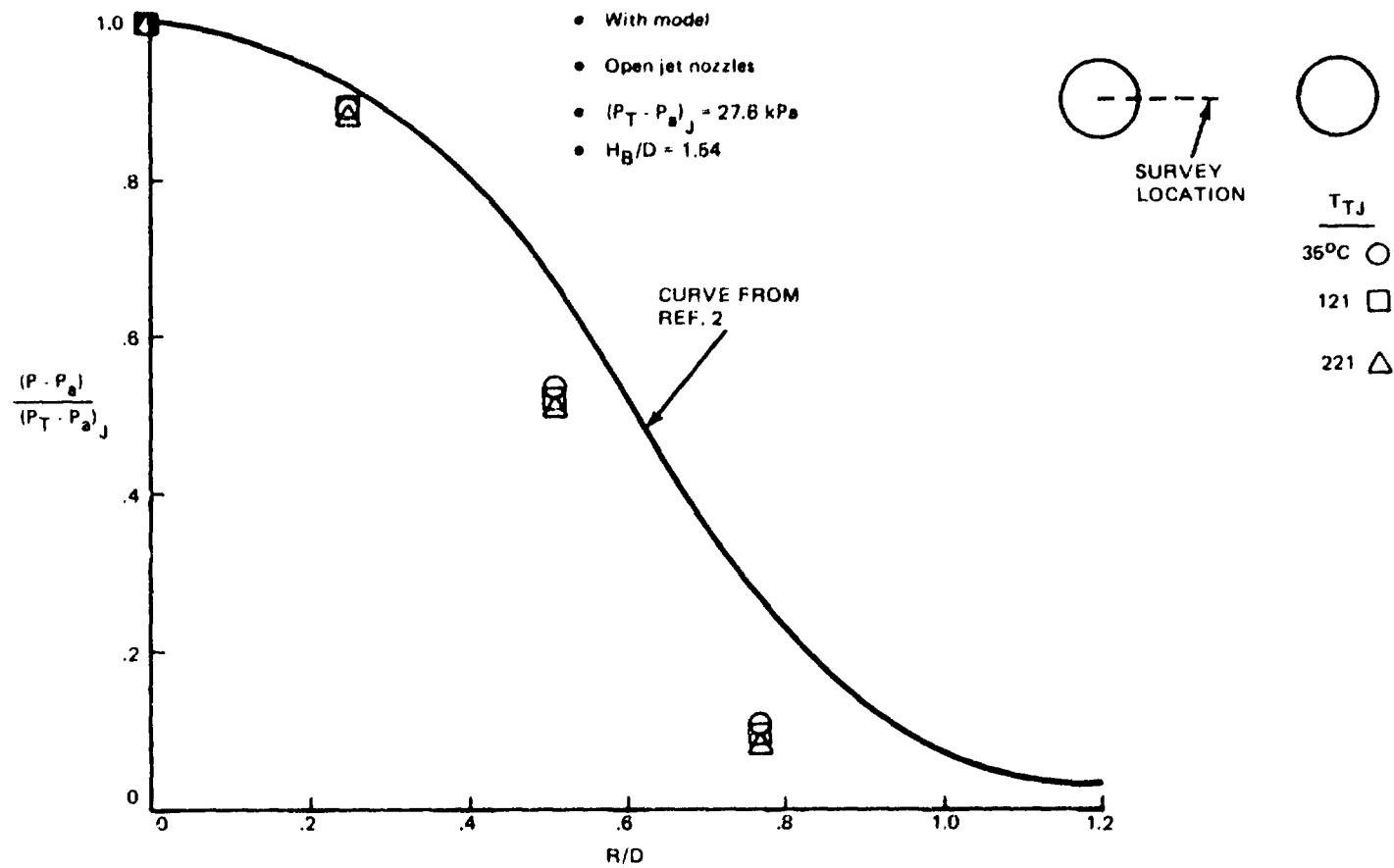
Figure 39 - Effect of settling chamber pressure on upwash properties at nozzle exit plane.

higher than this (somewhat arbitrary) 5kPa level requires a compressible flow approach to determine dynamic pressure, since it cannot be found by subtracting static pressure from total pressure. Nozzle exit total pressure was greater than 5 kPa for almost all of our experimental work.

Therefore, for all of the data shown in Figure 39, the quantity $(P_T - P_S)$ represents the upwash dynamic pressure on the centerline at the nozzle exit plane, and the flow velocity corresponding to this dynamic pressure can be evaluated with incompressible flow relations. Total pressures were measured with a Kiel probe and static pressures with a static probe aligned with the mean flow direction (probe dimensions are given in Subsection 4.7.3). Traversing both probes through the flow simultaneously (with fixed inter-probe distance, Y') provided direct plots of the total and static pressure profiles. When overlaid and shifted a distance, Y' , one can trace a profile of $(P_T - P_S)$. Data shown as $(P_T - P_S)_M$ in Figure 37, 38 and 39 were all obtained from the peak value of such tracings.

5.2.4 Effect of Model on Ground Flow. - Ground pressure measurements taken with and without the model in place showed that the model had little influence on the pressure close to the stagnation line but did change the pressure in the jet impingement region. Figure 40 shows the distribution of ground pressure in one of the jet impingement regions along a line connecting the two jet centerlines. The solid curve represents an empirical approximation for the ground pressure distribution for single jet impingement. Comparison with data taken at the same locations without the model (Figure 24) shows that the model reduces the pressure in this part of the impingement region. Data in Figure 40 for different jet temperatures show no significant temperature effect.

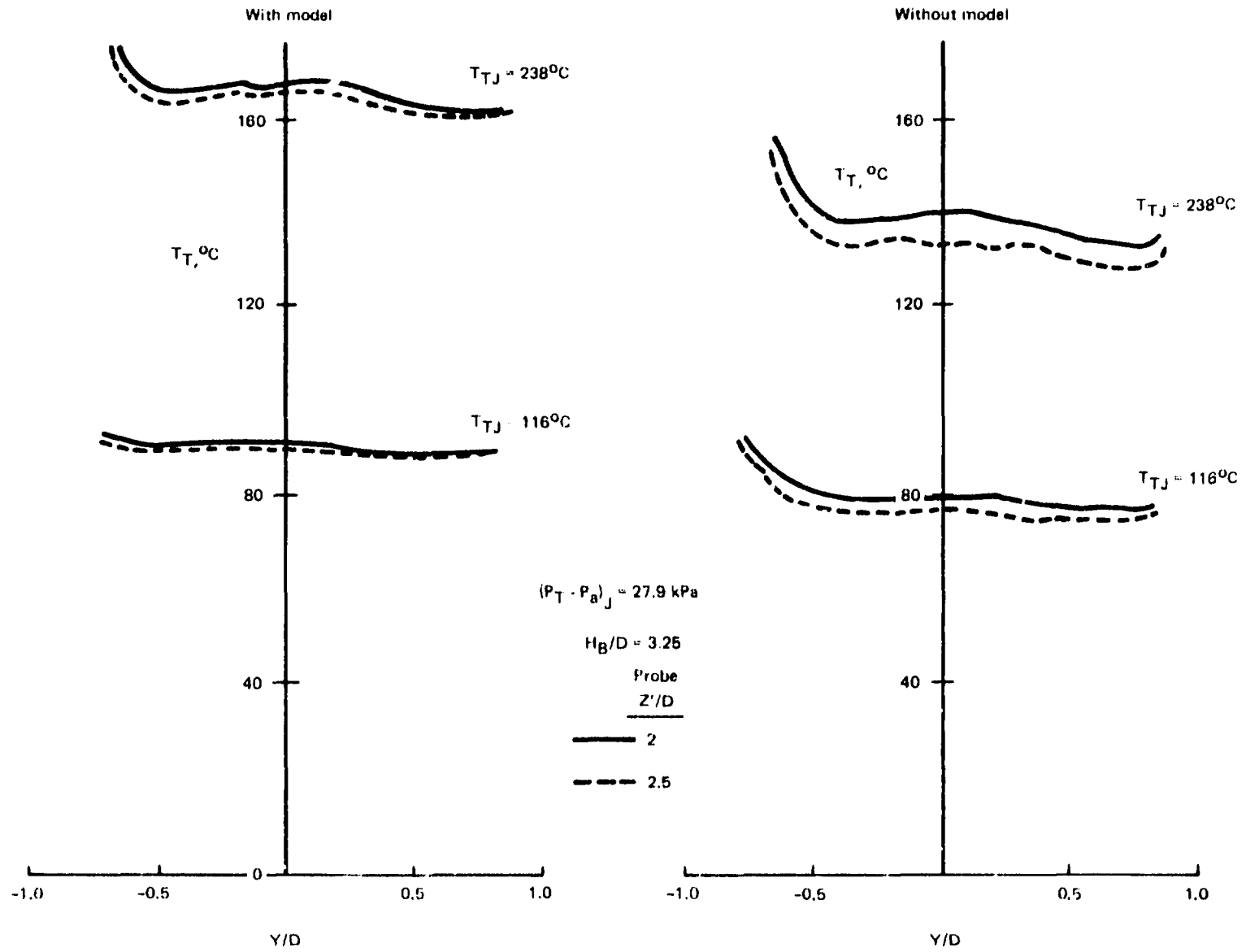
5.2.5 Effect of Model on Upwash. - Probe traverses were taken across the upwash with and without the model in place to determine the influence of the model on upwash properties. The temperature profiles across the upwash presented in Figure 41 show that the presence of the model raises the temperature of the upwash approaching the model. The increased upwash temperature with the model in place indicates a recirculating flow entrainment caused by model blockage.



RB1-1622-033D

Figure 40 - Radial ground pressure distribution around one jet impingement center.

ORIGINAL PAGE IS
OF POOR QUALITY



R81-1622-034D

Figure 41 - Effect of presence of body on upwash temperatures.

ORIGINAL PAGE IS
OF POOR QUALITY

Figure 42 shows pressure profiles taken across the upwash with and without the model for the same nozzle height above ground. These profiles were taken far enough from the model undersurface so that the increased upwash dynamic pressure caused by the presence of the model was not a local flow disturbance involving flow around the model. The dynamic pressure (and hence flow velocity) throughout the entire upwash was affected by model blockage. This change is significant for flow modelling. The cause of this change is not understood at present. The data in Figure 42 were taken with a jet exit temperature of 238°C. Data taken at temperatures of 116°C and 24°C showed almost identical profiles with and without the model, again illustrating that jet exit temperature has little influence on the pressure measurements in the upwash.

5.2.6 Model Forces. - The thrust of one of the open circular nozzles was determined from the relation

$$\text{Thrust} = 2 q \eta A ,$$

where q is the dynamic pressure associated with the nozzle pressure ratio, A is the nozzle exit area and η is a thrust efficiency factor that accounts for momentum loss in the nozzle boundary layer. Based on thrust measurements made earlier on this 5-cm diameter nozzle, we found $\eta = .90$ for the open circular nozzles.

$$\text{Using } q = \frac{\gamma}{2} P M^2 \text{ and } M^2 = 5 \left[\left(\frac{P_T}{P_S} \right)^{2/7} - 1 \right] \text{ for air.}$$

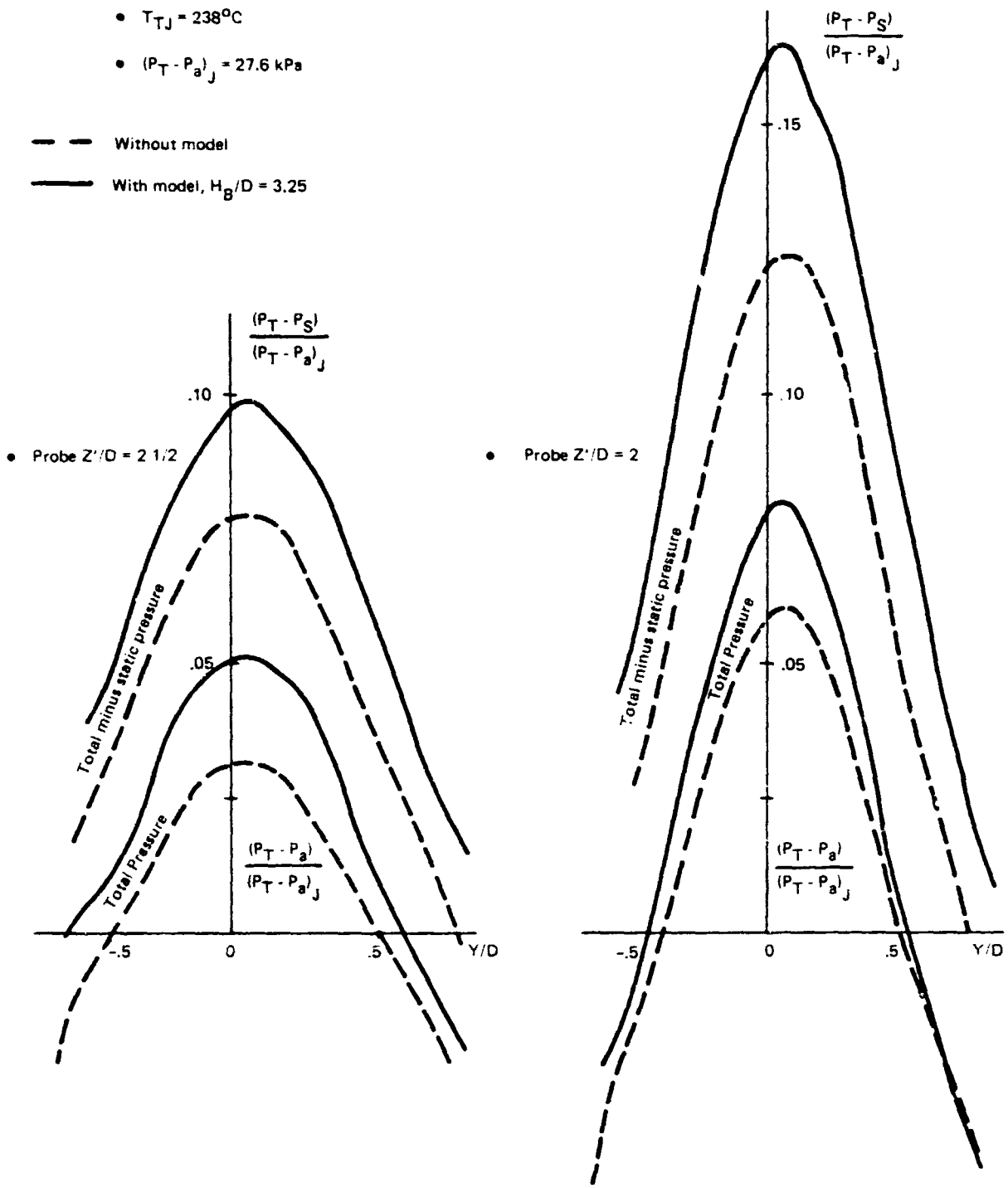
the thrust developed by one circular nozzle can be found as a function of P_{TJ} (settling chamber pressure):

$$\text{Thrust} = 6.30 \left[\left(\frac{P_{TJ}}{P_a} \right)^{2/7} - 1 \right] A P_a$$

Force data taken with the open circular nozzles were normalized by twice the value of nozzle thrust.

Forces were measured on the model with 15° strakes for a range of settling-chamber temperatures and pressures. Figure 43 shows the variation of model interference force with height above ground for a settling chamber pressure of 27.6kPa gauge and jet temperatures of 24°C, 116°C and 240°C. These

ORIGINAL PAGE IS
OF POOR QUALITY



R81-1622-035D

Figure 42 - Effect of presence of body on upwash pressures.

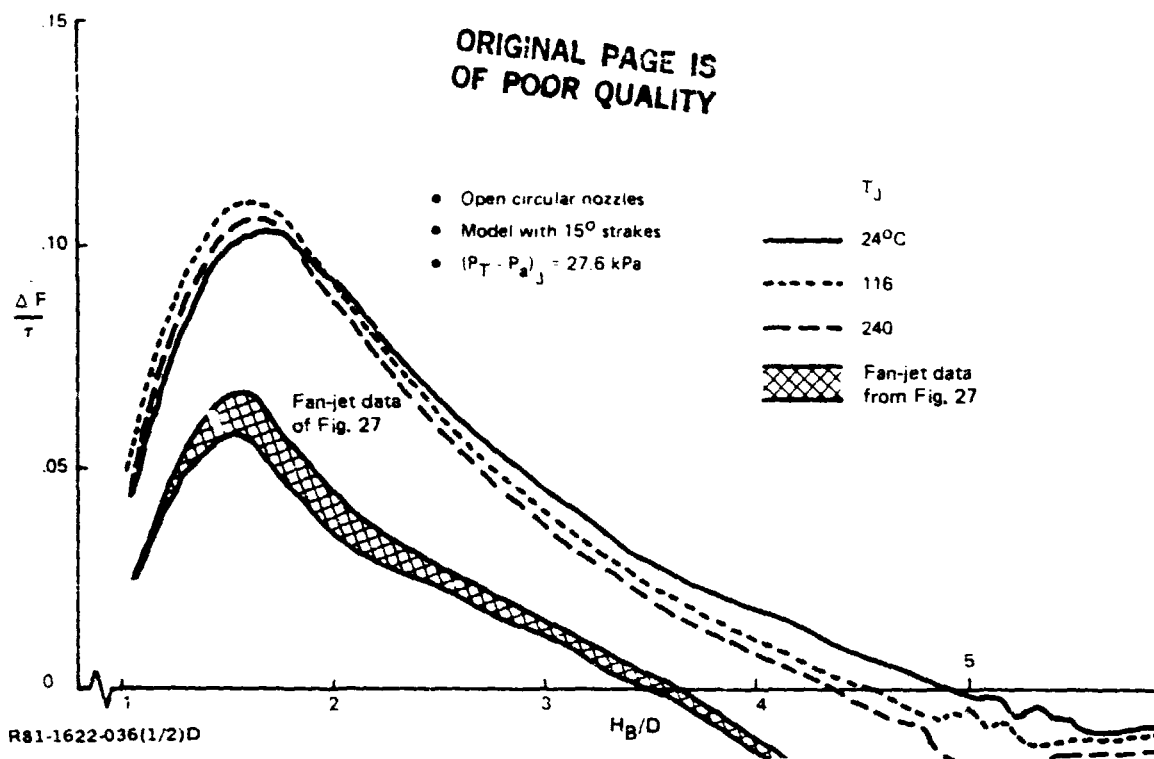


Figure 43 - Effect of nozzle exit temperature on ground interference forces.

three curves are quite similar, having small differences that appear to show a progression with temperature. Further investigation showed that differences in the force curves in Figure 43 are more likely to represent scatter attributable to slight differences in model alignment between runs. Subsequent measurements were taken at a fixed height above ground ($H/D = 3.2$) as the settling chamber temperature was raised from 24° to 221°C . Testing in this manner, essentially no change was found in interference force with jet exit temperature. The non-dimensional forces for the fan-jet simulation (Figure 27) are also shown and are much lower than those of the present section.

Figure 44 shows the variation of model force with height above ground for different settling chamber pressures and a jet exit temperature of 24°C . While these curves are qualitatively the same, they show some variation with settling chamber pressure. These data were all taken without disturbing alignment between tests.

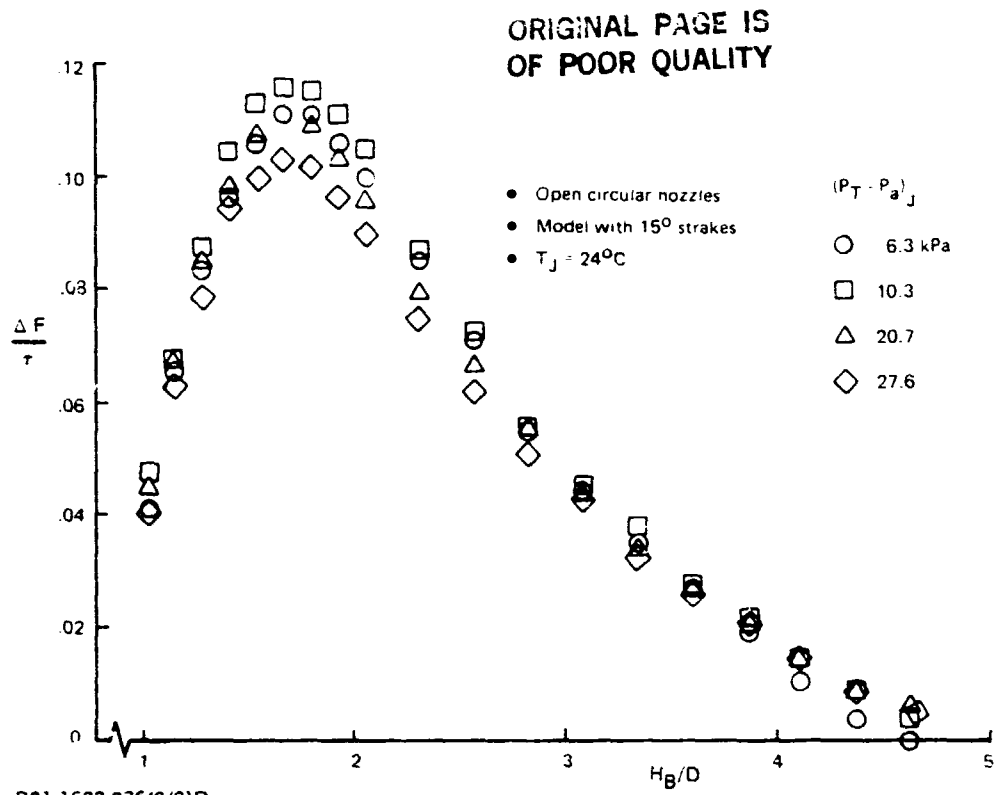
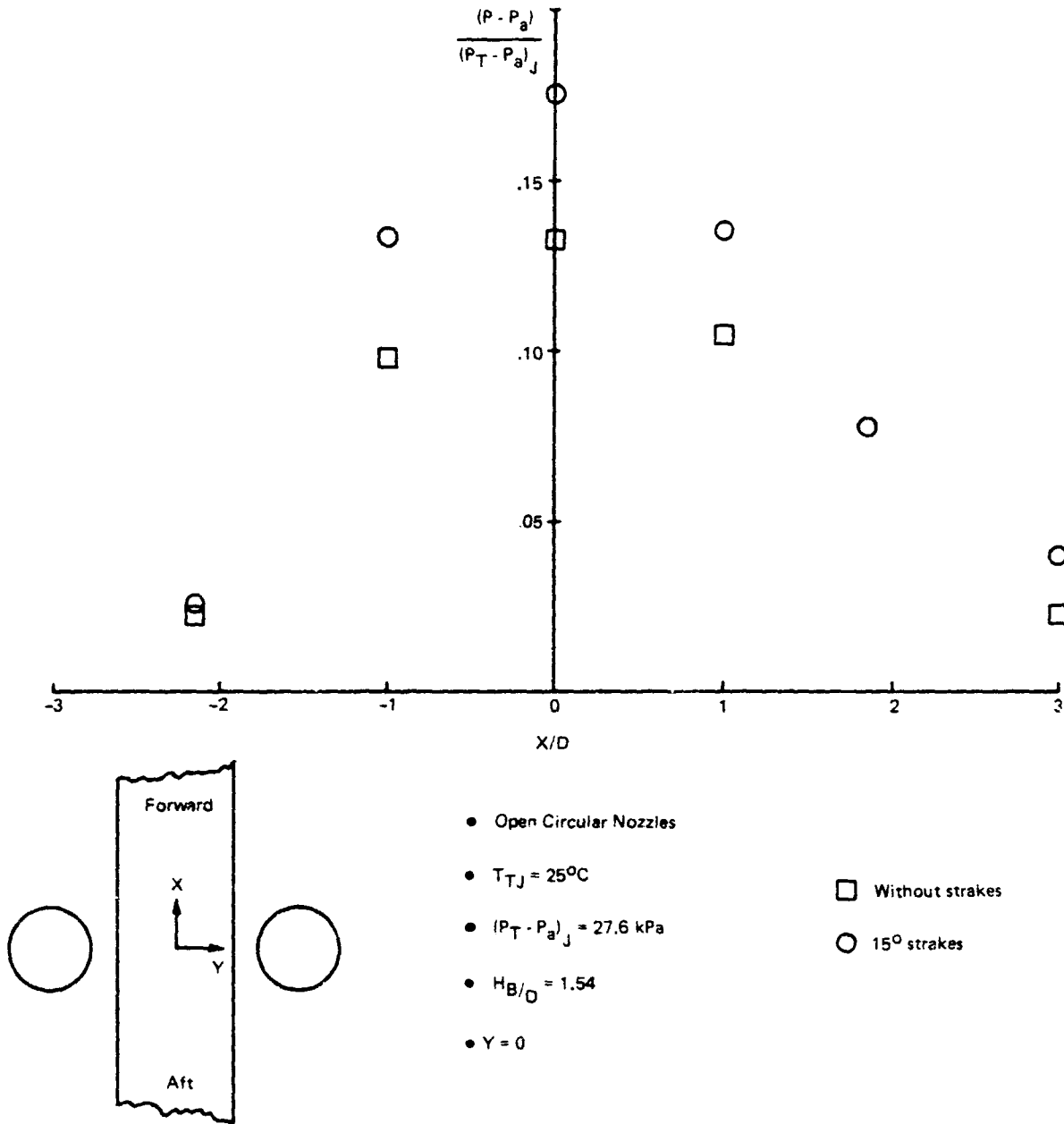


Figure 44 - Effect of nozzle stagnation pressure on ground interference forces.

5.2.7 Model Surface Pressure and Temperature. - Model surface pressures were measured with and without the 15° strakes for 24°C nozzle exit temperatures. At higher jet temperatures, the data were taken only with the strakes attached. Figure 45 shows the effect of the strakes on the pressure distribution along the fuselage undersurface. The pressure distribution across the model is shown in Figure 46. The presence of the strakes raises the surface pressure level and flattens the profile across the undersurface. Figure 47 shows the variation with height above ground of model pressure at three centerline taps for the model with strakes. The pressure on the fan nacelle centerline (from Figure 29) is shown for comparison, and is much lower. Figure 48 shows that the pressures along the model at a fixed height above ground are not significantly affected by jet temperature.

The temperature distribution along the model is shown in Figure 49. For $H/D = 1.54$, the temperature coefficient at a point between the nozzles was approximately 0.8, which is considerably higher than values measured with probes (range of 0.5) on the upwash centerline without the model (see Figures

ORIGINAL PAGE IS
OF POOR QUALITY



R81-1622-037(1/2)D

Figure 45 - Pressure distribution along fuselage underside.

ORIGINAL PAGE IS
OF POOR QUALITY

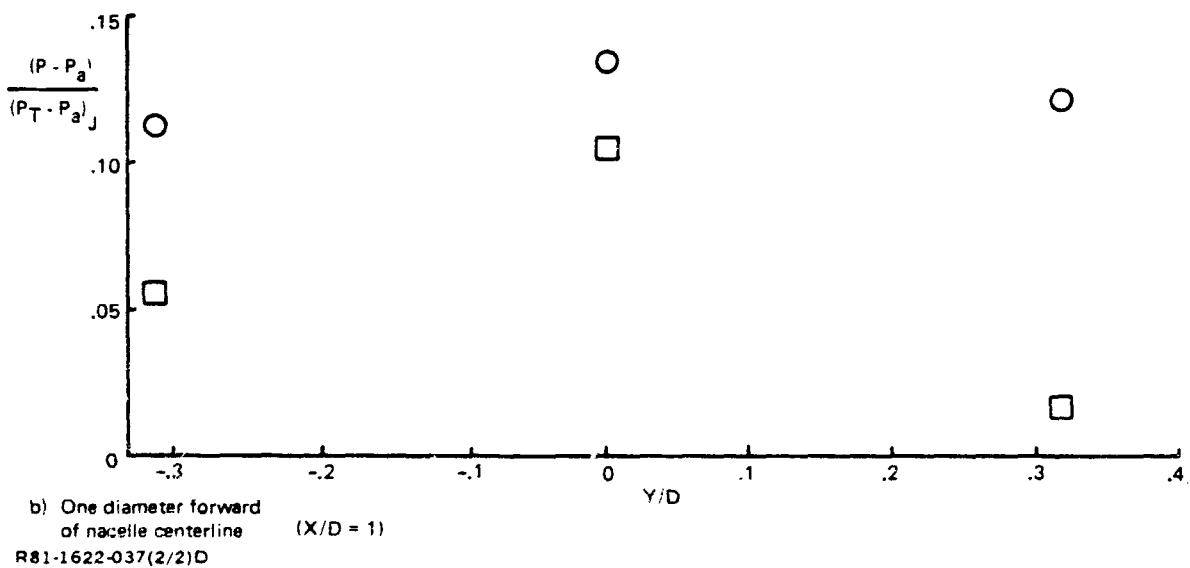
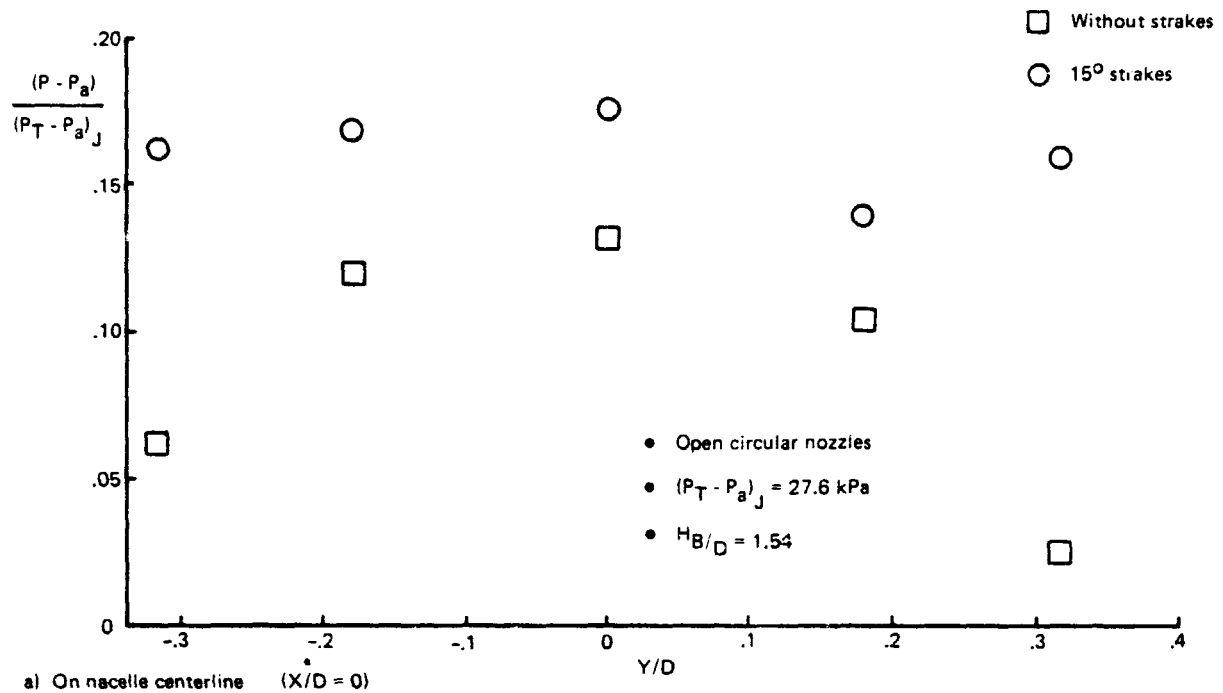
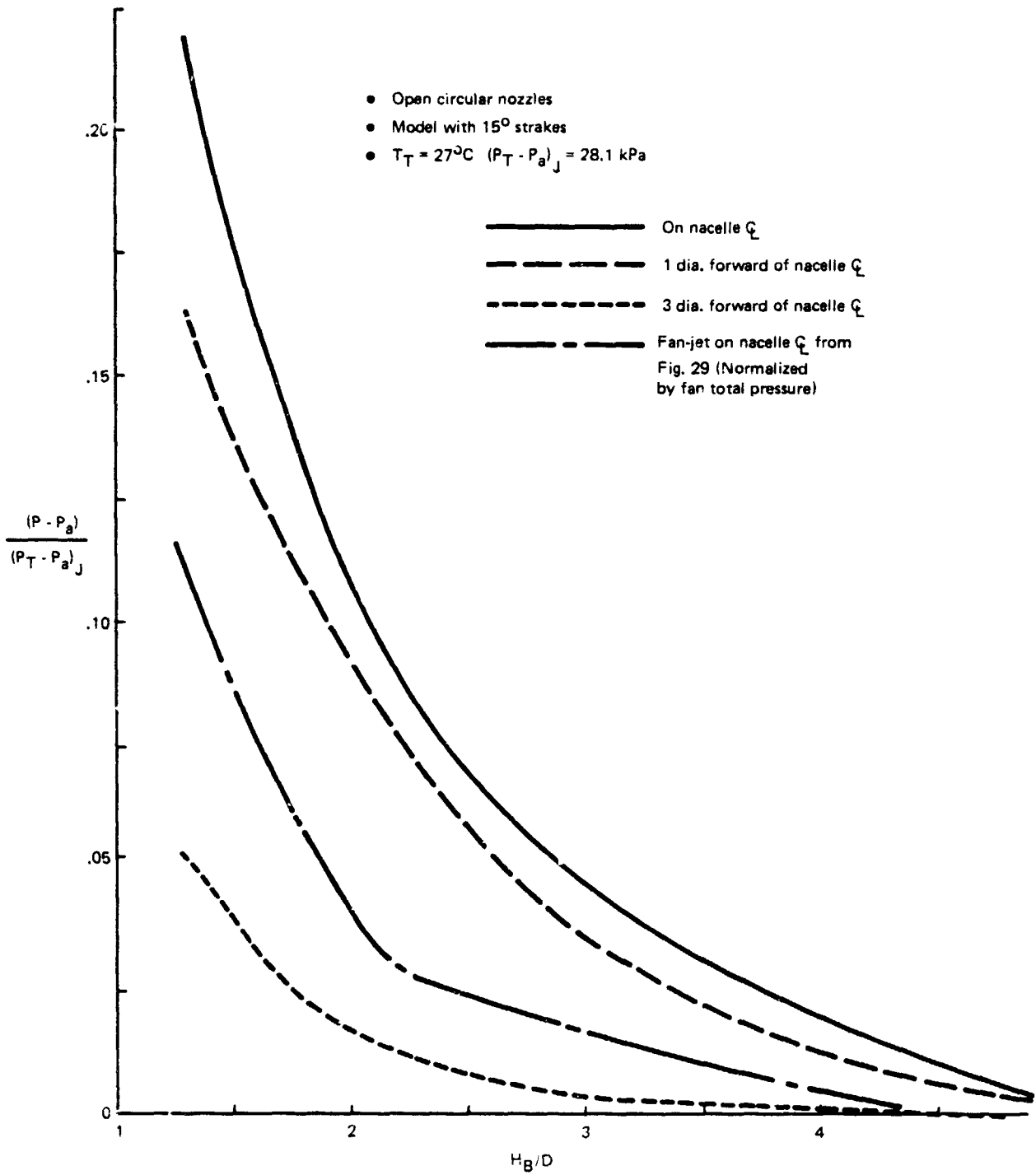


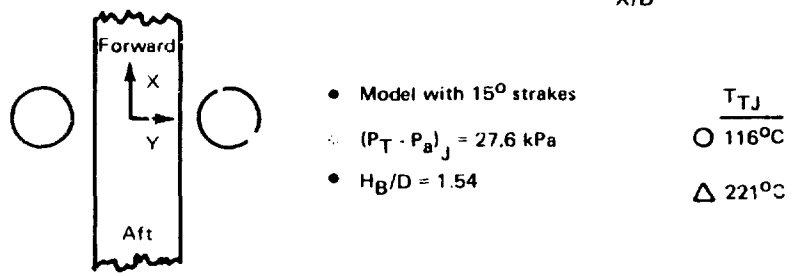
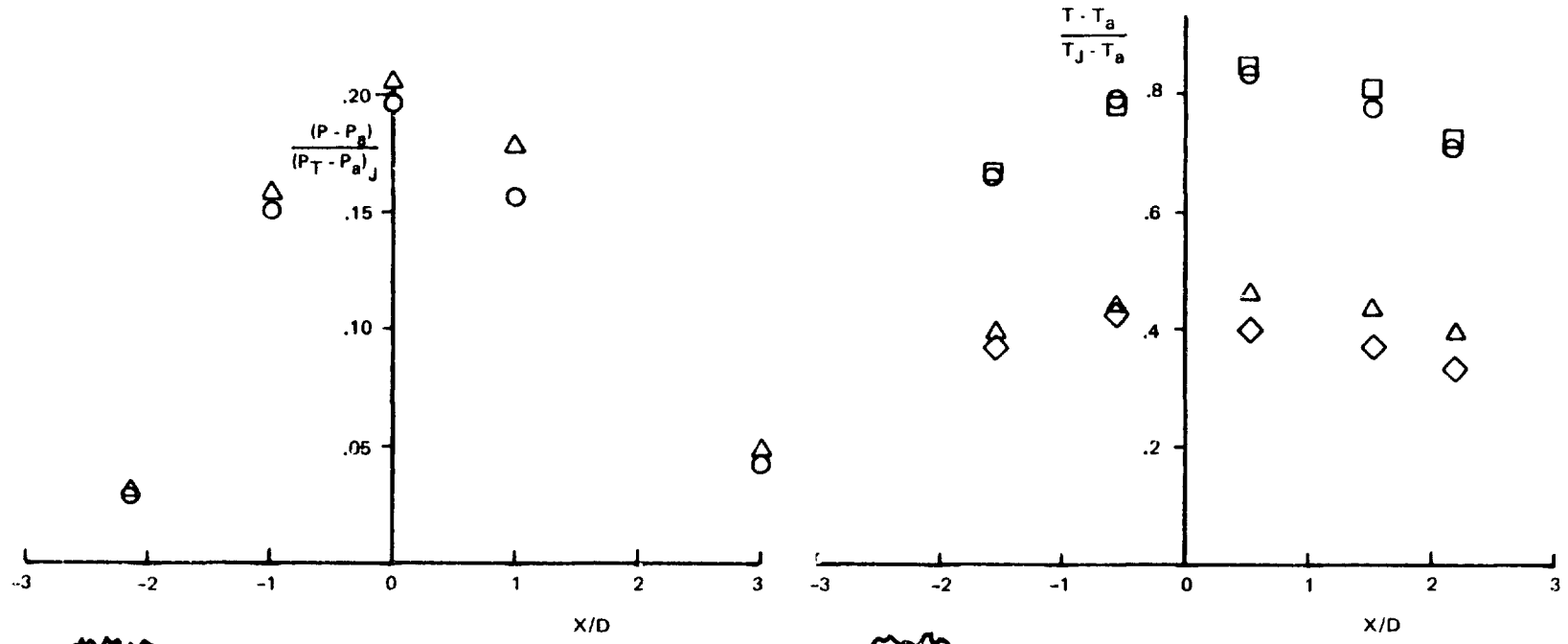
Figure 46 - Pressure distribution across fuselage underside.

ORIGINAL PAGE IS
OF POOR QUALITY



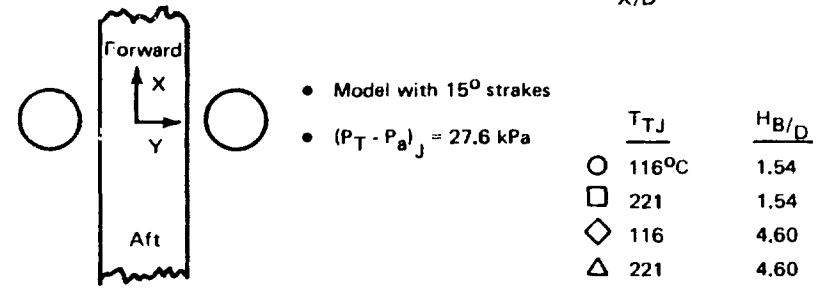
R81-1622-038D

Figure 47 - Variation of model pressure with height above ground.



R81-1622-039(1/2)D

Figure 48 - Pressure distribution along fuselage underside.



R81-1622-039(2/2)D

Figure 49 - Temperature distribution along fuselage underside.

ORIGINAL PAGE IS OF POOR QUALITY

37b and 38a). The high model temperature appears to be caused by blockage of the entrainment flow brought about by the presence of the model. As discussed in Subsection 5.2.5, higher temperatures were measured in the upwash with the model in place than without it.

The model temperature distributions in Figure 49 do not show a local temperature minimum just forward of the nacelle centerline that was found using the fan jet nozzles (Figure 31). In addition, comparison of Figure 49 with Figures 31 and 28 shows that the model temperature coefficients appear to scale better with jet exit temperature using the open circular nozzles than using the fan-jet nozzles, where only the core flow was heated. Temperature data taken in the upwash using the open circular nozzles (Figure 37b and 38a) also showed better temperature scaling than the fan-jet data (Figure 24).

5.3 Conclusions

5.3.1 Fan-Jet Simulation. - The primary conclusion of this experimental study is that a geometrically correct small-scale model testing program can predict V/STOL aircraft hover performance quite well. Interference force results of the 1/24-scale experiments matched full scale results closely. Pressure ratio changes (in this case with subsonic jet exit conditions) produced a negligible effect. Core nozzle exit temperature produced a small effect, easily compensated for by empirical scaling. Aircraft lower surface temperatures did not scale well with core nozzle exit temperature.

5.3.2 Open Circular Nozzles. - The normalized interference forces resulting from operation with open circular nozzles were much larger (approximately a factor of two) than those found with the fan jets. The qualitative behavior with height above ground was the same. As with the fan-jet nozzles, there was a small change in the force with changes in stagnation temperature. There was also a small change in normalized force with total pressure in the region of highest forces ($H/D \sim 1\frac{1}{2}$), which did not occur for the fan-jet case. Aircraft lower surface temperature did scale well with nozzle exit temperature, a different result than that obtained with the fan-jet nozzles.

The presence of the model was found to raise significantly the temperature in the upwash. Unexpectedly, model presence also raised the total pressure in the upwash.

6 - PREDICTION METHODOLOGY

The establishment of a vertical jet impingement model is the basis for the prediction of the behavior of two jets impinging on a ground plane. A sketch of the flow problem is shown in Figure 50. Figure 50a shows the vertical plane containing the jet stagnation points and the ground plane. Each jet impinges on the ground plane and deflects to form radial-wall jets. The wall jets then interact and form an upwash deflection zone where the wall jets collide and are turned upward on leaving the ground plane. The stagnation line lies on the ground in the vertical plane of symmetry between the two impinging jets. The maximum upwash stagnation pressure occurs at the midpoint of the line connecting the two jet stagnation points on the ground. The ground pressure then drops off with lateral distance along the stagnation line. Figure 50b shows the radial streamline pattern that has been observed (Ref. 5, 6 & 7) both in the ground plane and in the vertical upwash plane of symmetry between the two jets. This flow situation only exists when the jets are spaced far enough

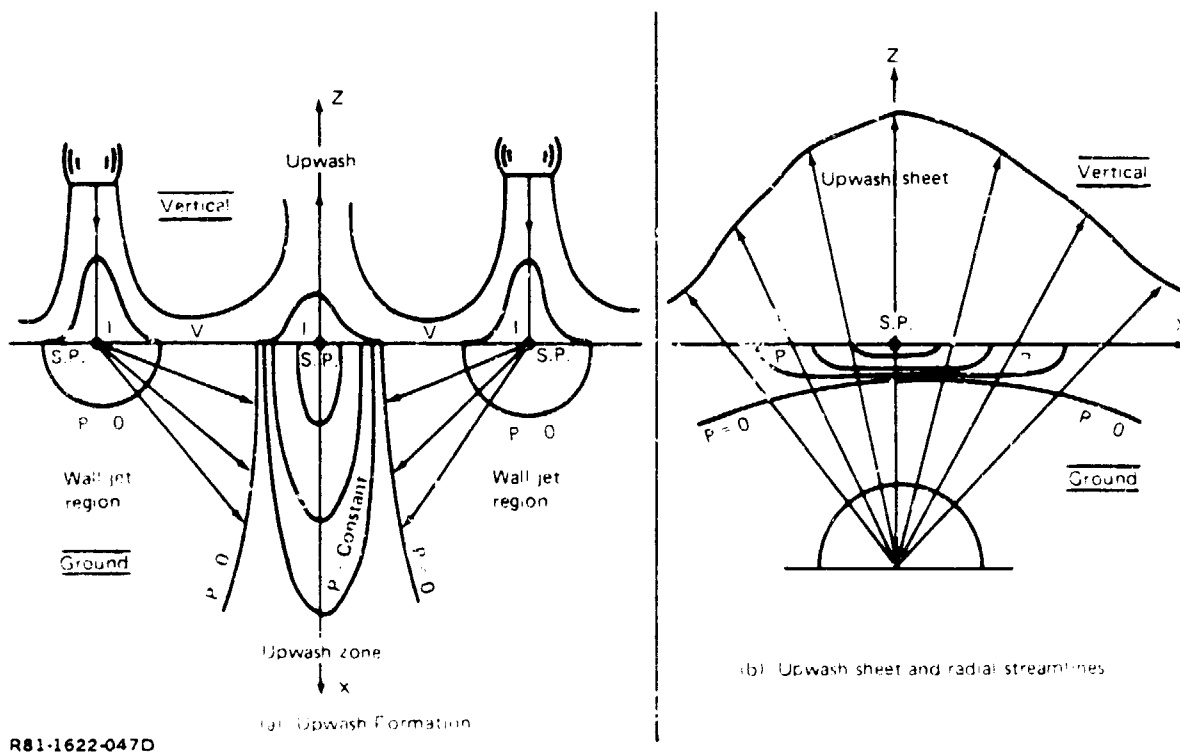


Figure 50 - Two-jet interacting flows - negligible deflection zone interaction.

apart so that the jet impingement zone does not interact or has a negligible affect on the upwash deflection zone. (Ref. 3).

6.1 Theoretical Models for Non-Isothermal Jet Impingement

In Ref. 3, semi-empirical analytical models were formulated to simulate the global behavior of two incompressible jets impinging on a ground plane. Models were generated for the behavior of the free and wall jets and, finally, the upwash sheet generated by the interaction of the opposing wall jets. The effect of jet proximity is considered in Ref. 3, leading to the development of upwash momentum models.

These incompressible models are extended, in the present study, to include temperature or density effects. The flowfield is divided into three major regions where viscous or turbulent mixing effects dominate, being:

- Free jet
- Wall jet
- Upwash.

Subdomains of these regions include the jet and upwash deflection zones. In these smaller regions, the flow changes from an inviscid behavior to a shear flow along with streamline deflections, causing a change in static pressure due to the stagnation and acceleration of the flow.

6.2 General Temperature and Velocity Equations

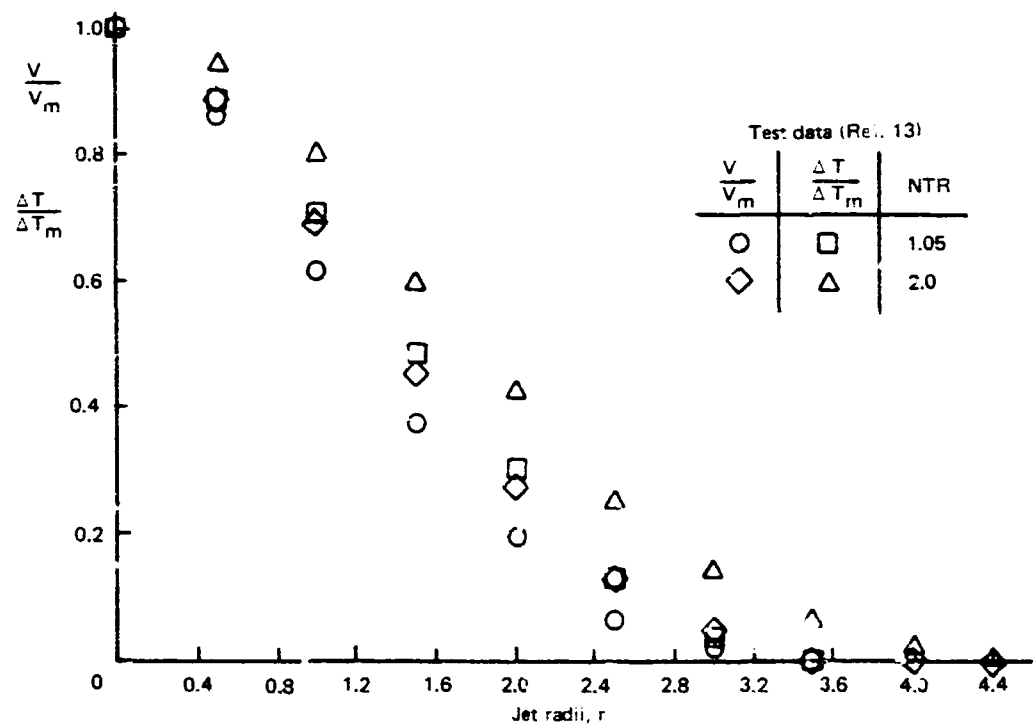
The transport or diffusion of heat in a free jet is much like the transport of momentum. The viscous mixing and entrainment of ambient air causes a shear layer of momentum (velocity) and heat to occur. Schlichting (Ref. 8), in quoting the experimental and theoretical observations of Reichardt (Ref. 9), implies that the temperature profile distribution of a two-dimensional jet behaves like the square root of the velocity distribution. Taylor's Free Turbulence Theory, as quoted by Abramovich (Ref. 10), arrives at this result for the thermal layer by a turbulence theory that is based on vorticity transfer rather than momentum. In Ref. 10, the temperature profile in a jet is obtained by a "New Prandtl-Gortler Theory of Turbulence". The following relationship is obtained between the temperature and velocity:

ORIGINAL COPY IS
OF POOR QUALITY.

$$\frac{\Delta T}{\Delta T_M} = \left(\frac{V}{V_M} \right)^{\frac{1}{\delta}} \quad (1)$$

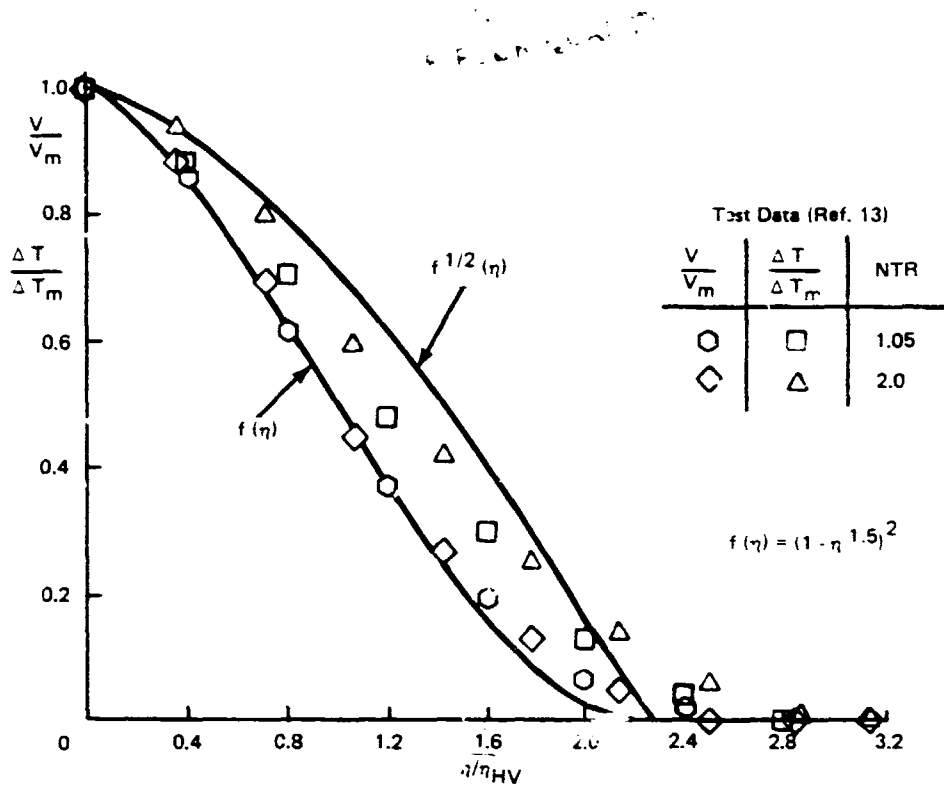
where δ is some constant. If $\delta = 1$, the dimensionless temperature and velocity profile coincide. It has been observed experimentally that this behavior does not hold. For $\delta = 2$, Taylor's analytical result is obtained as well as Reichardt's experimental observations.

Experimental observations indicate that the thermal layer spreads faster than the dynamic (velocity) layer. In order to establish an empirical value for δ in eq. (1), some non-isothermal profile data are plotted in Figure 51a for a circular jet. Similarity is not obtained if the temperature data are related to the velocity half widths as shown in Figure 51b. In addition, the data do not seem to confirm the square root of the velocity relationship. If, on the other hand,



a) Related to jet radius.
...81-1622-040(1/3)D

Figure 51 - Dimensionless velocity and temperature difference profile data.



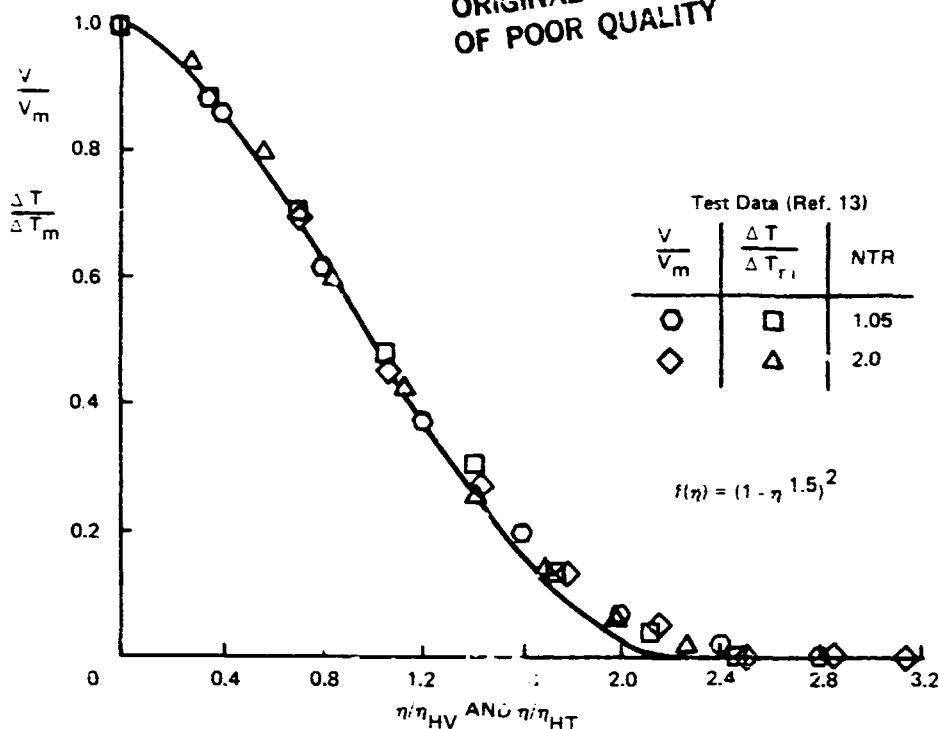
b) Related to jet radius non-dimensionalized by velocity half-width.
R81-1622-040(2/3)D

Figure 51 - (Continued).

the velocity and temperature difference data are plotted dimensionless to their respective half-velocity and half-temperature difference lengths, the data fall on one dimensionless curve as illustrated in Figure 51c. This result was also observed in Ref. 11 and in Ref. 12 for wall jets. It seems to be clear from the available data that the thermal layer persists beyond the point where a measurable velocity exists. The form of eq. (1) implies that the dynamic and thermal layers have the same scale length. If an exponential or infinite layer is assumed for the velocity profile and, hence, the thermal layer, then eq. (1) would yield results consistent with measured data. Indeed, if such a relationship as eq. (1) exists, the exponent may be a function of the nozzle thermal conditions.

In the models to be developed, it is more convenient to assume a finite thickness to the various layers to facilitate the various integrations involved in computing the velocity and temperature decay rates. Equation (1) is not

ORIGINAL PAGE IS
OF POOR QUALITY



c) Related to jet radius non-dimensionalized by velocity and temperature half-widths.
R81-1622-040(3/3)D

Figure 51 - (Concluded).

used in the following models but the relationship depicted by Figure 51c is used instead:

$$\frac{T - T_A}{T_M - T_A} = f_T(r_T) \quad (2)$$

$$\frac{V}{V_M} = f_V(r_V)$$

where $r_T = \frac{r}{b_T}$, $r_V = \frac{r}{b_V}$ and $f = \left(1 - \eta^2\right)^2$

The dimensionless forms (i.e., velocity and temperature each have their own scale lengths, b_V and b_T) of the velocity and temperature difference profiles as depicted in eq. (2) are assumed identical. The relationship between the thermal and dynamic (velocity) layers can be simply expressed by the ratio

of the half widths of the two layers:

$$\lambda = \frac{b_{HT}}{b_{NV}} > 1 \quad (3)$$

Hence, the thermal and dynamic layers do not have the same scale. The velocity goes to zero while the temperature persists beyond a measurable velocity.

6.3 Conservation Equations

The basic governing equation to model the behavior of jets is the conservation of momentum equation. To account for non-isothermal or temperature effects, an additional equation is required. The conservation of excess heat content is used as the governing equation to account for heat diffusion or temperature effects. These two integral equations can be expressed as:

Momentum -
$$M_J = \rho_N V_N^2 A_N = \int \int \rho V^2 dA \quad (4)$$

Heat Flux
$$H_F = \rho_N V_N (\Delta T_N) A_N = \iint \rho V \Delta T dA \quad (5)$$

where $\Delta T_N = T_N - T_A$, T_N is the nozzle temperature, and A_N is the nozzle area.

Equations (4) and (5) yield two expressions for the two unknowns, maximum centerline temperature and velocity. Unfortunately, more than two unknowns exist, namely, the profile shapes and growth rates of the various shear layers. These additional parameters must be given by empirical observations. The spreading models of Ref. 3 are used with the addition of eq. (5) and the further complication of the density or temperature occurring in eq. (4) which necessitates the simultaneous solution of eqs. (4) and (5).

6.4 Heated Free-Jet Model

The nozzle exit conditions of a free jet can be specified by two parameters, the nozzle exit stagnation pressure ratio (NPR) and temperature ratio (NTR). The exit Mach number of the jet is purely a function of NPR. A compressibility correction is included in the incompressible models, based upon an approximate Mach number computed using Bernoulli's equation.

$$M_N \sim \sqrt{\frac{2}{\gamma} (NPR-1)}$$

To be consistent with an incompressible approximation, the nozzle exit static temperature is assumed equal to the nozzle stagnation temperature,
or

$$T_N \sim NTR$$

The free jet is subdivided into three regions, as shown in Figure 52:

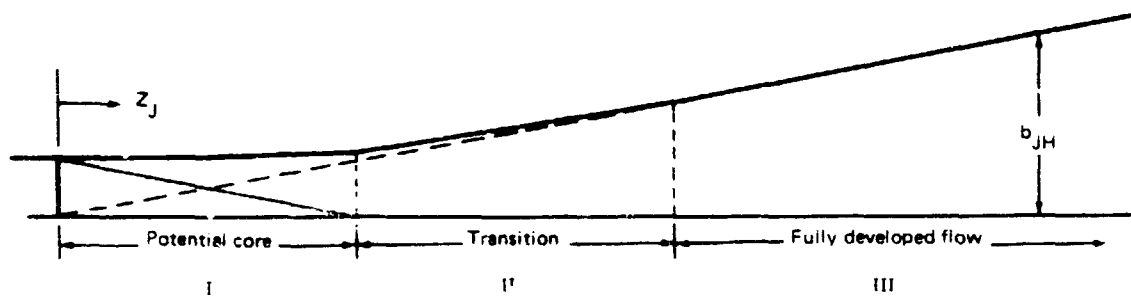
- Potential core, Region I
- Transition, Region II
- Fully developed, Region III.

In order to solve eqs. (4) and (5), some information about the half-velocity boundary growth behavior must be assumed to be known from experimental data. To be consistent with the models of Ref. 3, and for the sake of simplicity, the jet radius model assumes a simple linear boundary growth in each region.

$$\text{Region I:} \quad \frac{b_{VH}}{r_N} = a_1 \left(\frac{Z}{r_N} \right) + 1$$

$$\text{Region II:} \quad \frac{b_{VH}}{r_N} = a_2 \left(\frac{Z}{r_N} \right) + b_2$$

$$\text{Region III:} \quad \frac{b_{VH}}{r_N} = a_3 \left(\frac{Z}{r_N} \right)$$



R81-1622-048D

Figure 52 - Jet half-velocity width model.

The constants (a_1, a_2, a_3) governing the half-velocity boundary growth in the transition and fully-developed regions are determined empirically. The potential core length (Z_{PC}) and the exponent α_{FD} governing the shape of the shear profile in the fully developed region also must be specified. These constants vary slightly as functions of nozzle Mach number and temperature ratio. Suitable values have been determined as:

$$a_3 = .09 \left\{ 1 + \ln \left(\frac{2}{1 + \frac{1}{T_N \beta_3}} \right) \right\} \left\{ 1 - .16 M_N \right\}$$

where $\beta_3 \sim 0.50$.

The potential core length is approximated by:

$$\frac{Z_{PC}}{D} = \frac{8.55}{2} \left[\frac{1 + 1}{T_N} \beta_c \right]$$

where $\beta_c \sim 0.75$, and is also slightly a function of the nozzle temperature ratio.

The growth constant of the half-velocity boundary in the potential core region is determined by matching the boundaries at the end of the potential core, yielding,

$$a_1 = \left(\frac{b_2 - 1}{Z_{PC}/r_N} \right) a_2$$

In addition, a linear decay in potential core radius r_c , is assumed:

$$\frac{r_c}{b_V} = 1 - \frac{Z_J}{Z_{PC}}$$

The beginning of the fully developed region of flow, denoted by the length parameter Z_{FD} , is determined by matching the boundaries between the transition and fully developed regions,

$$\frac{Z_{FD}}{r_N} = \frac{b_2}{(a_3 - a_2)}$$

The momentum and heat flux equations become, for a circular jet,

$$M_J = \frac{2\pi P_A}{R_G} \int \frac{V^2 r}{T} dr \quad (6)$$

$$H_F = \frac{2\pi P_A}{R_G} \int \frac{V \Delta T}{T} r dr \quad (7)$$

using $P_A = \rho R_G T$ to eliminate density.

The velocity and temperature profiles are represented by the following dimensionless self-similar quantities:

$$\frac{V}{V_M} = f_V(\eta_V) ; \eta_V = \frac{r}{b_V} \quad (8)$$

$$\frac{\Delta T}{\Delta T_M} = f_T(\eta_T) ; \eta_T = \frac{r}{b_T} \quad (9)$$

Since finite profile functions will be used in the modeling, the velocity and temperature scale lengths, as represented by b_V and b_T , are not equal.

Substituting eqs. (8) and (9) into eqs. (6) and (7), and rearranging, yields,

$$\text{Momentum} \quad \frac{T_M}{T_N} = 2 \left(\frac{V_M}{V_N} \right)^2 \left(\frac{b_V}{r_N} \right)^2 \int_0^1 \frac{f_V^2 \eta_V d\eta_V}{\left[f_T \frac{1-f_T}{\bar{T}_M} \right]} \quad (10)$$

$$\text{Heat} - \quad \frac{T_M}{T_N} = 2 \left(\frac{V_M}{V_N} \right) \left(\frac{b_V}{r_N} \right)^2 \frac{\Delta T_M}{\Delta T_N} \int_0^1 \frac{f_V f_T \eta_V d\eta_V}{\left[f_T + \frac{(1-f_T)}{\bar{T}_M} \right]} \quad (11)$$

$$\text{where } \bar{T}_M = \frac{T_M}{T_A}$$

Unfortunately, bringing the density into the integrands makes the profile integrals functions of the maximum centerline temperature ratio. Hence, simple

geometrical similarity does not exist for non-isothermal jets. The velocity scale length η_V is used in the integration since there can be no contribution to eq.

(10) or eq. (11) beyond the dynamic (velocity) layer. The integrals in the above equations do not lend themselves necessarily to analytical integration, and are defined as:

$$C_M(\bar{T}_M) = \int_0^1 \frac{f_V^2 \eta_V d\eta_V}{\left[f_T + \frac{(1-f_T)}{\bar{T}_M} \right]} \quad (12)$$

$$C_T(\bar{T}_M) = \int_0^1 \frac{f_V f_T \eta_V d\eta_V}{\left[f_T + \frac{(1-f_T)}{\bar{T}_M} \right]} \quad (13)$$

Equations (10) and (11) can be rewritten simply as

$$\frac{T_M}{T_N} = 2 \left(\frac{V_M}{V_N} \right)^2 \left(\frac{b_V}{r_N} \right)^2 C_M(\bar{T}_M) \quad (14)$$

$$\frac{T_M}{T_N} = 2 \left(\frac{V_M}{V_N} \right) \left(\frac{b_V}{r_N} \right)^2 \frac{\Delta T_M}{\Delta T_N} C_T(\bar{T}_M) \quad (15)$$

The values of the integrals C_M and C_T are also functions of the profile characteristics. In general, it is assumed that

$$\frac{v}{V_M} = f_V(\eta_V) = \left[1 - \left(\frac{\eta_V - \eta_c}{1 - \eta_c} \right)^\alpha \right]^2 \quad (16)$$

and

$$\frac{\Delta T}{\Delta T_M} = \left[1 - \left(\frac{\eta_T - \eta_c}{1 - \eta_c} \right)^\alpha \right]^2 = f_T(\eta_T) \quad (17)$$

where $\eta_c = r_C/b_V$.

Since the dimensionless velocity and temperature profile functions have the same form, then

$$\eta_T = \left(\frac{b_{VH}}{b_{TH}} \right) \eta_V \quad (18)$$

In general, it is assumed that

$$\lambda_T \equiv \frac{b_{TH}}{b_{VH}} > 1 \quad (19)$$

Hence:

$$\eta_T = \frac{\eta_V}{\lambda_T} \quad (20)$$

and the temperature scale length can be directly related to the scale length of the dynamic layer.

6.4.1 Potential core region - In the potential core region, the maximum temperature and velocity are known and are equal to the nozzle values. The momentum and heat equations, (14) and (15), can be reduced to,

$$\frac{1}{2} R_V^2(\alpha) - \left(\frac{b_{VH}}{r_N} \right)^2 C_M(\alpha, \lambda_T) = 0 \quad (21)$$

$$\frac{1}{2} R_V^2(\alpha) - \left(\frac{b_{VH}}{r_N} \right)^2 C_T(\alpha, \lambda_T) = 0 \quad (22)$$

where $R_V = \frac{b_{VH}}{b_V} = \eta_c - (1 - \eta_c) \left(\frac{2 - \sqrt{2}}{2} \right)^{\frac{1}{\alpha}}$

Equations (21) and (22) are solved simultaneously for the exponent α and the thermal-to-dynamic layer ratio λ_T . For simplicity, the thermal and dynamic cores are assumed identical.

6.4.2 Transition and fully-developed regions - The conservation equations can now be written as:

$$\frac{1}{2} R_V^2 \left(\frac{T_M}{T_N} \right) - \left(\frac{V_M}{V_N} \right)^2 \left(\frac{b_{VH}}{r_N} \right)^2 C_M(\bar{T}_M) = 0 \quad (23)$$

$$\frac{1}{2} R_V^2 \left(\frac{T_M}{T_N} \right) \left(\frac{T_N}{T_A} - 1 \right) - \left(\frac{V_M}{V_N} \right) \left(\frac{T_M}{T_N} \cdot \frac{T_N}{T_A} - 1 \right) \left(\frac{b_{VH}}{r_N} \right)^2 C_T(\bar{T}_M) = 0 \quad (24)$$

The above equations are solved simultaneously for the dimensionless maximum temperature ratio, $\frac{T_M}{T_N}$, and maximum velocity ratio, $\frac{V_M}{V_N}$, given values for the exponent α and λ_T . Suitable values based on empirical data are assigned to these parameters in the fully developed regions as

$$\alpha_{FD} = 1.5$$

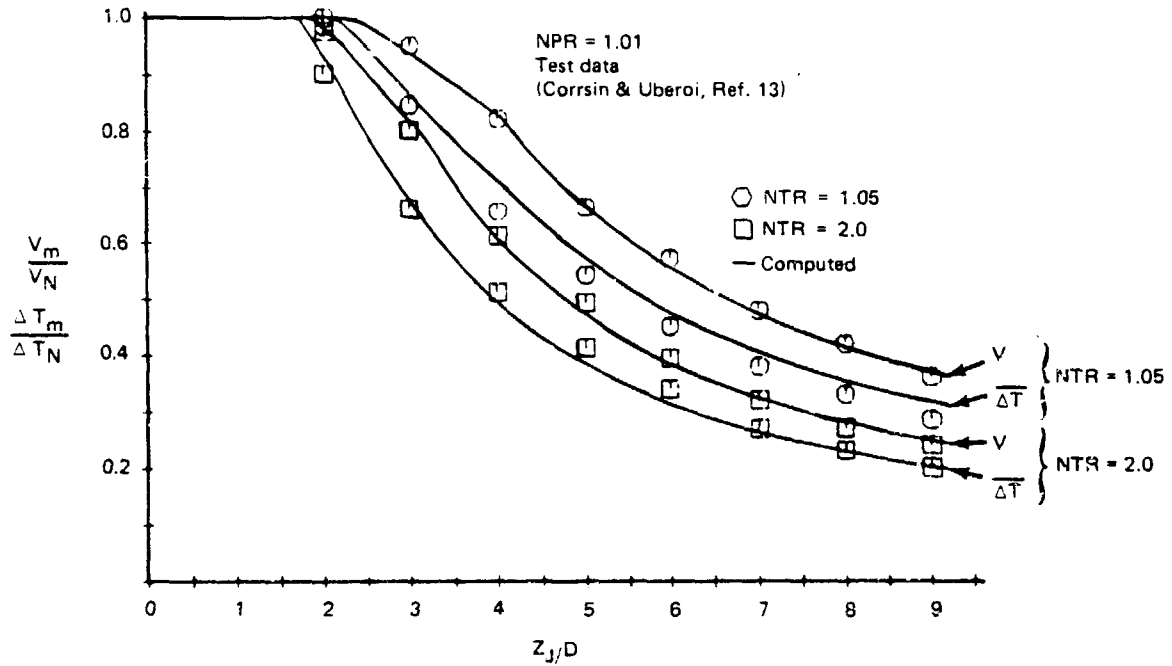
$$\lambda_T = 1 + 0.185 T_N^{\beta_\lambda} \quad \text{where } \beta_\lambda \sim 0.50,$$

and a linear variation from potential core values to the fully developed ones is assumed.

Some typical results are shown in Figures 53 through 57 and compared to the test data of Corrsin & Uberoi (Ref. 13) for low Mach number or basically incompressible jets. Figure 53 shows the relationship between the dimensionless velocity and temperature decay rates for a slightly-heated jet (NTR = 1.05) and a significantly-heated jet (NTR = 2.0). Both the velocity and temperature decay rates are enhanced due to an increase in heat content of the jet. The temperature decays faster than the velocity. Figure 54 shows the dynamic pressure or total pressure decay for the two different temperature ratios. The total pressure decays faster for the hotter jet. Figure 55 shows the relationship between the dynamic pressure and total temperature decay. Unlike the velocity and temperature, the pressure and temperature curves cross each other. The

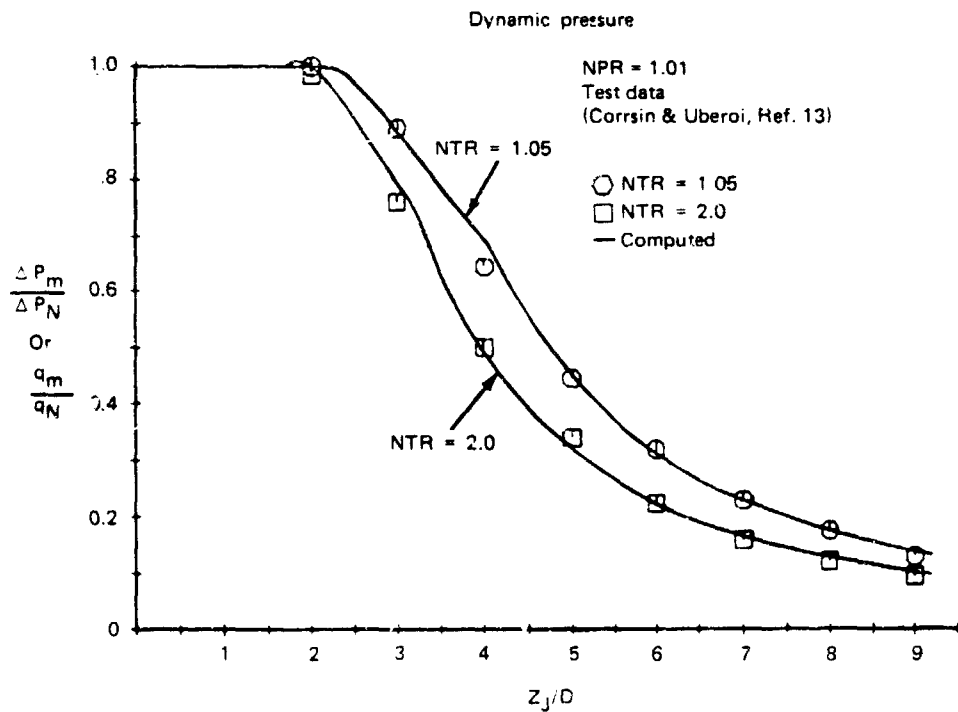
dynamic pressure is computed as $\left(\frac{V_M}{V_N} \right)^2 / (T_M/T_N)$. Figure 56a and b shows the relationship between the half dynamic pressure (q), half velocity (V_M/V_N) and half dimensionless temperature $(T_M - T_A / T_N - T_A)$ boundaries for the two nozzle

ORIGINAL PAGE IS
OF POOR QUALITY



R81-1622-057(1/2)D

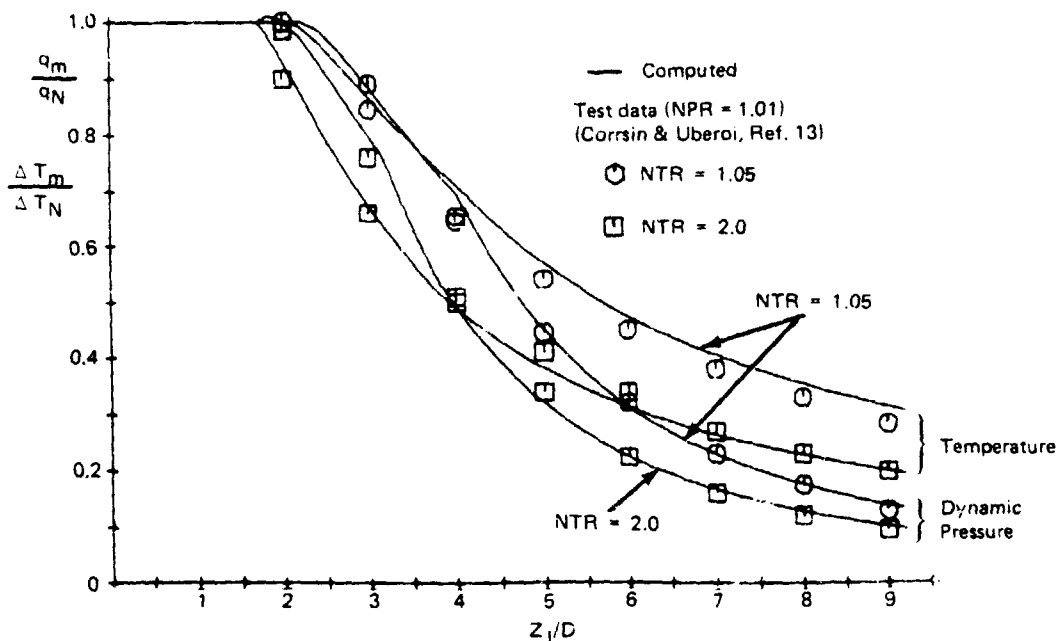
Figure 53 - Comparison of computed free-jet dimensionless velocity and temperature difference decay with test data.



R81-1622-057(2/2)D

Figure 54 - Comparison of computed free-jet dimensionless dynamic pressure decay with test data.

ORIGINAL PAGE IS
OF POOR QUALITY



R81-1622-058(D)

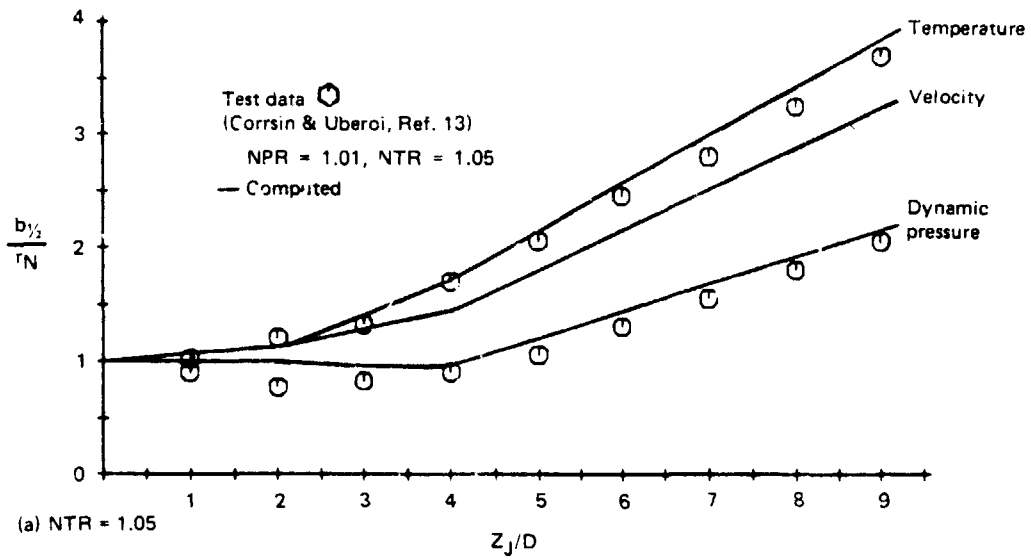
Figure 55 - Comparison of computed free-jet dimensionless dynamic pressure and temperature difference decay with test data.

temperature ratios. The half dynamic pressure boundary exhibits a contraction in the potential core region ($Z_{PC} \sim 4D$). The half velocity boundary lies between the half dynamic pressure and temperature boundaries. The half temperature boundary being significantly wider than the half velocity boundary as the nozzle temperature is increased. Figure 57 shows a comparison of the half q and half temperature boundaries for the two nozzle temperature ratios. Hence, heating the jets causes an increase in the jet half boundaries, which is consistent with the higher decay rate exhibited by the hotter jet in the previous figures.

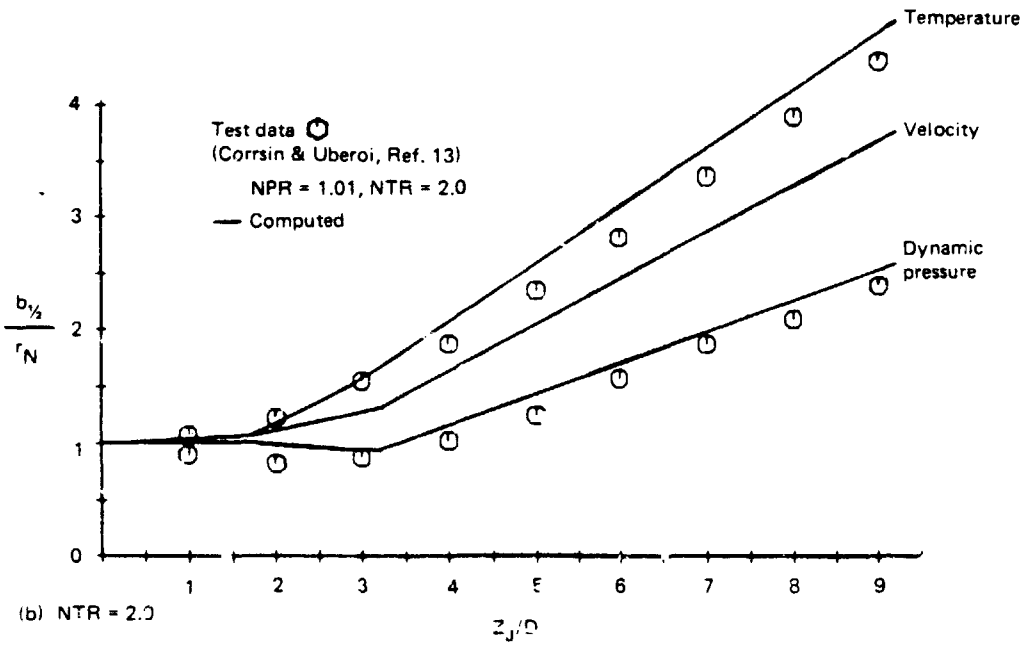
6.5 Jet Deflection Region

A schematic of the wall jet impingement model is shown in Figure 58. The jet begins to stagnate at some ground effect height given by Δ_j . Values for Δ_j are given in Ref. 14. The ground stagnation pressure and temperature is then determined by the jet properties at the ground effect height denoted by

ORIGINAL PAGE 13
OF POOR QUALITY



R81-1622-059(1/2)D



R81-1622-059(2/2)D

Figure 56 - Heated free-jet boundary growth characteristics.

ORIGINAL PAGE IS
OF POOR QUALITY

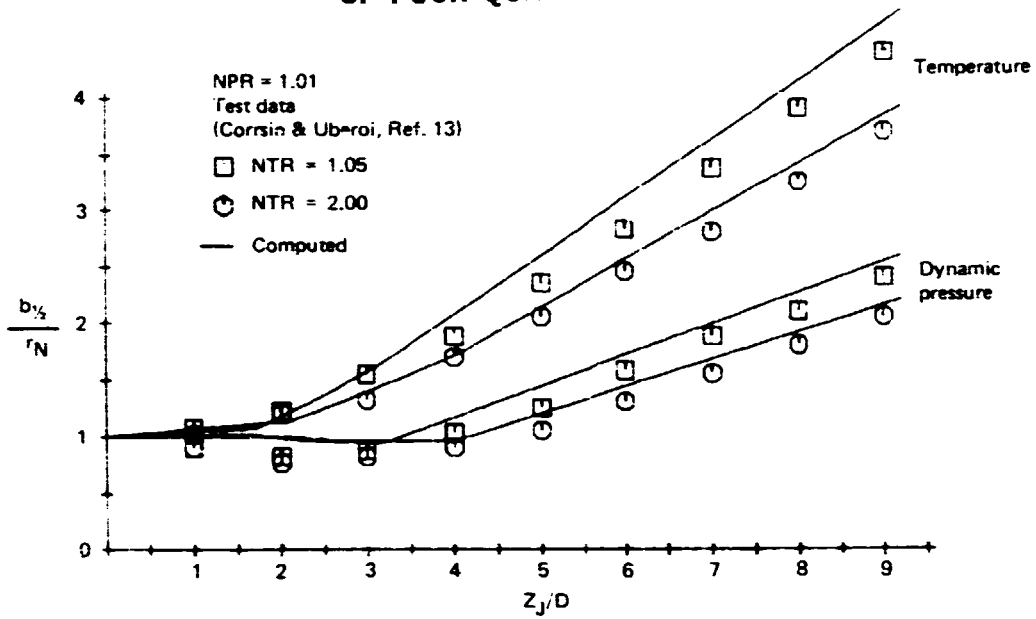


Figure 57 - Heated free-jet boundary growth characteristics.

the subscript (g), or:

$$\frac{\Delta P_S}{\Delta P_N} = \left(\frac{V_g}{V_N} \right)^2 \left(\frac{T_g}{T_N} \right) : \quad (25)$$

$$\frac{T_S}{T_A} = \frac{T_g}{T_A}$$

The ground pressure distribution in the impingement region is obtained in the same fashion as for an isothermal jet. A momentum balance is performed with the integral of the ground pressure equal to the momentum or thrust of the incident jet.

$$\frac{M_J}{4} = \int_0^{r_0} \int_0^{\pi/2} \Delta P r dr d\phi \quad (26)$$

The ground pressure distribution is assumed to have the form:

$$\frac{\Delta P}{\Delta P_S} = f_g(r_W) = \left(1 - r_W^2 \right)^4 \quad (27)$$

where $r_W = \frac{r}{r_0}$.

2-2

ORIGINAL PAGE IS
OF POOR QUALITY

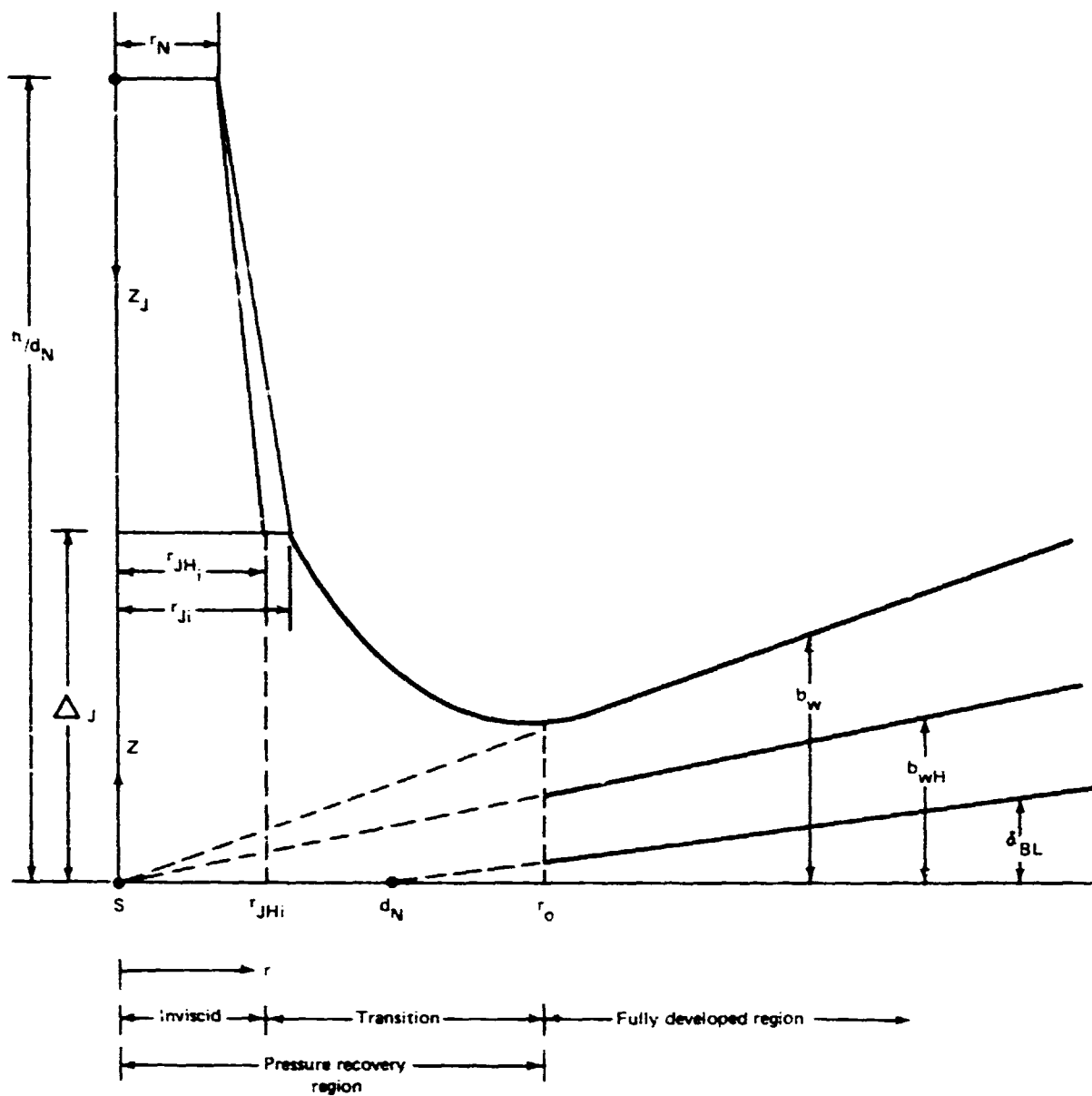


Figure 58 - Definition of scaling parameters for jet impingement and wall jet regions.

Equation (26) can be rewritten as,

$$1 = \left(\frac{r_o}{r_N} \right)^2 \left(\frac{V_g}{V_N} \right)^2 C_{sp}(\alpha_g) / (T_g / T_N) \quad (28)$$

where $C_{sp}(\alpha_g) = \int_0^1 f_g(r_W) r_W dr_W$.

Given the impingement radius r_o , equation (28) can be solved for the exponent α_g governing the shape of the ground pressure distribution. The deflection radius r_o is estimated empirically and is based upon the incident half velocity radius (b_{VH}) of the jet:

$$2.9 \leq \frac{r_o}{b_{VHi}} \leq 3.6 ; 1.2 \leq \frac{h}{D} \leq 3.0$$

$$\frac{r_o}{b_{VHi}} = 3.6 ; \frac{h}{D} > 3.0$$

6.6 Heated Wall-Jet Transition Model

Figure 58 shows a schematic of the wall-jet model. The wall-jet transition model developed in Ref. 3 consists of three subregions:

- i) Inviscid deflection region where the effects of viscosity are assumed to be negligible except in a region close to the wall and near the edge of the deflected flow. In this region, the inner boundary layer is established as governed by axially-symmetric stagnation flow.
- ii) Transition region where the effects of viscosity are beginning to dominate and the inner boundary layer and outer shear flow changes to the fully-developed turbulent wall-jet.
- iii) Fully-developed flow, where the effects of turbulent viscosity dominate and the static pressure through the wall layer is considered ambient, or fully recovered. In this region, the nearly similar wall-jet develops.

The addition of heat to the wall-jet requires the introduction of a radial

heat flux equation into the model of the isothermal wall-jet. The two conservation equations (assuming negligible losses) applied to the wall jet are:

$$\text{Momentum - } M_F = \int_0^{b_W} (\rho V^2 + \Delta P) r dz \quad (29)$$

$$\text{Heat - } H_F = \int_0^{b_W} \rho V \Delta T r dz \quad (30)$$

where b_W is the height or thickness of the dynamic (velocity) layer.

Before being able to apply eqs. (29) and (30) to the wall layer, the velocity, pressure and temperature profile behavior must be approximated. Two sublayers are assumed, an inner boundary layer and an outer shear layer. Adiabatic wall conditions are assumed and the thermal and dynamic boundary layers are also assumed to coincide.

Inner Boundary Layer

$$\frac{V}{V_M} = \left(\frac{\zeta_V}{K_\delta} \right)^{\frac{1}{N}} \quad \text{where } \zeta_V = \frac{z}{b_W}, \quad K_\delta = \frac{\delta}{b_W} \quad (31)$$

$$\frac{\Delta P}{\Delta P_M} = 1 \quad (\text{constant pressure through boundary layer})$$

$$\frac{\Delta T}{\Delta T_M} = 1 \quad (\text{adiabatic wall, constant temperature through boundary layer})$$

where $7 \leq N \leq 15$.

Outer Shear Layer

$$\frac{V}{V_M} = f_V(\zeta_V) = \left[1 - \left(\frac{\zeta_V - K_\delta}{1 - K_\delta} \right)^\alpha \right]^2 \quad (32)$$

$$\frac{\Delta P}{\Delta P_M} = f_p(\zeta_V) = f_V^2(\zeta_V) = \left[1 - \left(\frac{\zeta_V - K_\delta}{1 - K_\delta} \right)^\alpha \right]^4$$

$$\frac{\Delta T}{\Delta T_M} = f_T(\zeta_T) = \left[1 - \left(\frac{\zeta_T - K_\delta}{1 - K_\delta} \right)^\alpha \right]^2$$

where $\zeta_T = \frac{z}{b_T}$ and b_T is the height or thickness of the thermal layer. The

dynamic and thermal layers are assumed to be related by:

$$\frac{b_{TH}}{b_{VH}} = \frac{b_T}{b_W} \equiv \lambda_T > 1 \quad (33)$$

The introduction of equations (30) and (31) into eqs. (28) and (29) lead to the development of several profile integral expressions.

The momentum integral has a velocity squared and a pressure term. The pressure term contributes to the momentum until pressure recovery occurs. Substitution of the profile expressions into the velocity term of the integral yields the following integrals for the two layers:

$$C_M(\bar{T}_M) = \int_0^{K_\delta} \left(\frac{\zeta_V}{K_\delta}\right)^{\frac{2}{N}} d\zeta_V + \int_{K_\delta}^1 \frac{f_V^2(\zeta_V) \left[f_p(\zeta_V) + \left\langle 1 - \frac{f_p(\zeta_V)}{\bar{P}_M} \right\rangle \right]}{\left[f_T(\zeta_T) + \left(1 - \frac{f_T(\zeta_T)}{\bar{T}_M} \right) \right]} d\zeta_V \quad (34)$$

where $\bar{T}_M = \frac{T_M}{T_A}$ and $\bar{P}_M = \frac{P_M}{P_A}$

The pressure term leads to a simpler expression:

$$C_p = K_\delta + \int_{K_\delta}^1 f_p d\zeta_V \quad (35)$$

which can be integrated analytically.

The heat equation leads to integrals similar to eq. (34):

$$C_T (\bar{T}_M) = \int_0^{K_\delta} \left(\frac{\zeta_V}{K_\delta} \right)^{\frac{1}{N}} d\zeta_V + \int_{K_\delta}^1 \frac{f_V(\zeta_V) f_T(\zeta_T) \langle f_p(\zeta_V) + [1-f_p(\zeta_V)] \rangle d\zeta_V}{\left[\frac{f_T(\zeta_T) + \langle 1-f_T(\zeta_T) \rangle}{\bar{T}_M} \right]} \quad (36)$$

The pressure distribution along the wall was defined previously as:

$$\Delta P_M = \Delta P_S f_g(\eta_W) \quad (37)$$

Equations (29) and (30) can now be expressed as

Momentum -

$$F_M(\eta_W) F_{VIS}(r) = \left(\frac{r}{r_N} \right) \left(\frac{b_W}{r_N} \right) \left[\frac{2\bar{P}_M \left(\frac{V_M}{V_A} \right)^2}{\frac{T_M}{T_N}} C_M + \frac{\Delta P_S}{\Delta P_N} f_g(\eta_W) C_P \right] \quad (38)$$

Heat Flux -

$$F_T(\eta_W) = 2 \left(\frac{r}{r_N} \right) \left(\frac{b_W}{r_N} \right) \bar{P}_M \left(\frac{V_M}{V_N} \right) \left(\frac{\Delta T_M}{\Delta T_N} \right) C_T / \left(\frac{T_M}{T_N} \right) \quad (39)$$

The terms on the left side of eqs. (38) and (39), F_M and F_T , reflect the gain in radial momentum or heat flux as the jet deflects and becomes parallel to the wall. These functions are made proportional to the pressure recovery function, or

$$F_M(\eta_W) = F_T(\eta_W) = 1 - f_g(\eta_W) \quad (40)$$

since little or no empirical data are available in the deflection region. Hence, the radial momentum and heat flux reach a maximum at pressure recovery, and for

$$\eta_W = \frac{r}{r_0} \geq 1, \quad F_M = F_T = 1$$

The term $F_{VIS}(r)$ reflects the loss of momentum due to frictional losses at the

wall, and
$$F_{\text{VIS}}(r) = \frac{1}{\left(\frac{r}{D}\right)^{\alpha_{\text{VIS}}}}, \text{ where } \alpha_{\text{VIS}} = 0.15-0.25. \quad (41)$$

Equations (38) and (39) represent two simultaneous equations for the two unknowns, V_M and T_M . The values of the integrals C_M , C_p and C_T , which arise from the profile functions, are determined numerically and are, in general, a function of the maximum temperature ratio $\left(\frac{T_M}{T_A}\right)$.

The inviscid deflection region is assumed to occur under the half velocity width (b_{VHi}) of the incident jet profile. Constant total pressure and total temperature is assumed throughout the inviscid layer to be equal to the incident jet values. The wall-jet properties at the beginning of the wall-jet transition region are obtained from the inviscid values. The initial velocity at the end of the inviscid region is defined from the static pressure and Bernoulli's equation.

Equations (38) and (39) are used to determine the initial values of the exponent α , governing the wall-jet profiles in the shear layer, and the initial ratio, λ_{T_i} , of the thermal-to-dynamic layer thickness. The wall layer is now completely initialized upon prescription of the initial boundary layer characteristics. Fully developed values for the exponent α and the ratio λ_T are now prescribed and a linear variation between the initial values at the beginning of the transition to the fully developed region is assumed. Equations (38) and (39) can then be solved simultaneously for the maximum temperature and velocity throughout the wall-jet, given a prescribed behavior for the half-velocity thickness.

For the fully developed wall-jet region, the boundary and shear layers are assumed to have a simple linear behavior:

$$\frac{b_{\text{WH}}}{r_N} = a_{W_3} \left(\frac{r}{r_N}\right) \quad (42)$$

$$\frac{\delta_{\text{bL}}}{D} = a_{\text{bL}_3} \left(\frac{r}{D}\right) \quad (43)$$

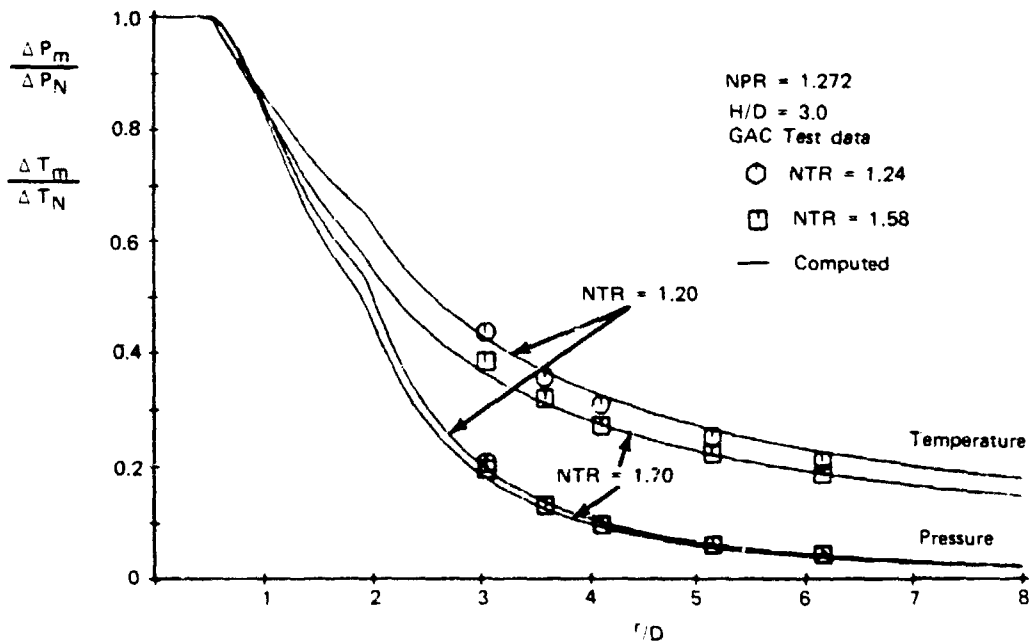
where
$$a_{W_3} = 0.9 \left[1 + \ln \left(\frac{2}{1 + \frac{1}{T_N^{\beta_W}}} \right) \right] \left[1 - .16M_S \right]; \beta_W \sim 0.50$$

$$a_{DL_3} = 0.0175$$

and M_S is the stagnation Mach number of the jet. The wall jet thickness in the transition region is obtained by a linear variation between the initial and fully developed values. Some total pressure and temperature decay data is shown in Figure 59 for single circular jet impingement into a radial wall-jet. The wall-jet pressure decay is only slightly influenced by the nozzle temperature ratio for the range tested. The temperature decay shows a greater dependence on the nozzle temperature. Both the temperature and pressure decays more rapidly with an increase in nozzle temperature.

6.7 Two-Jet Interaction Model

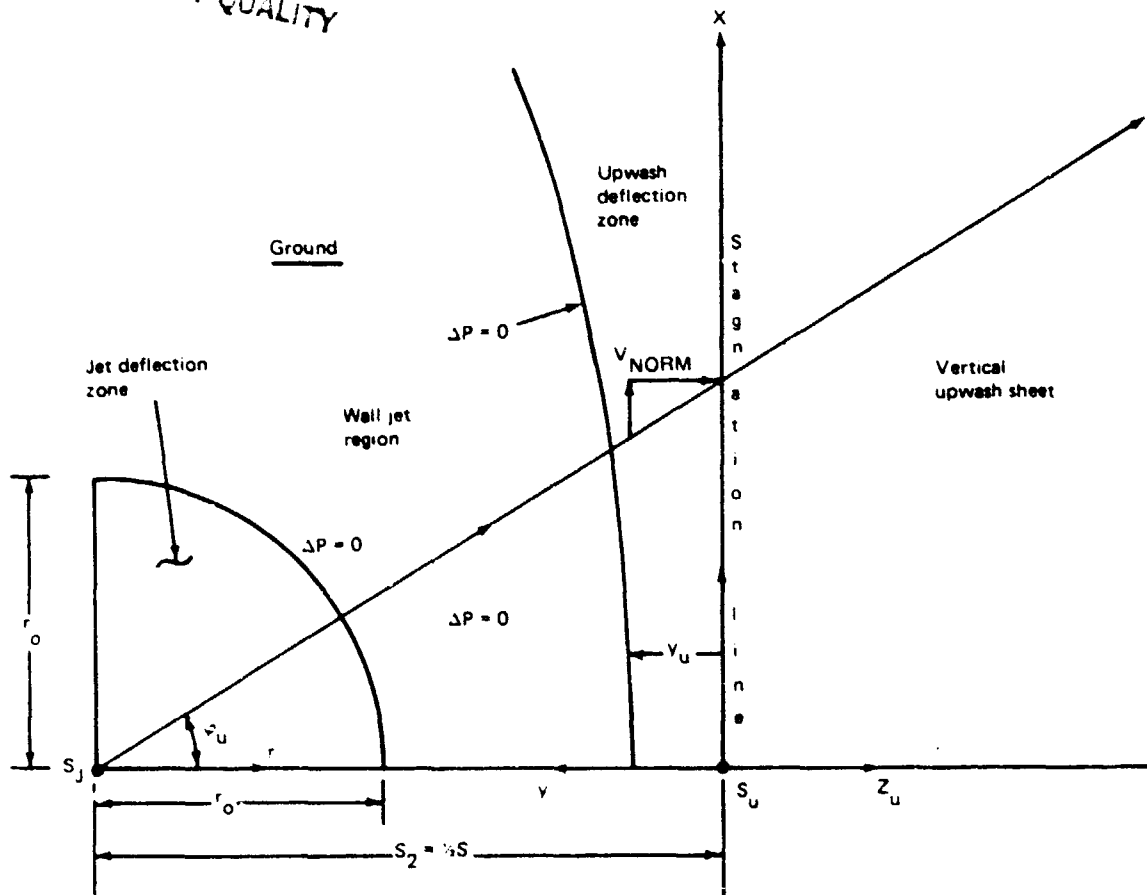
Figure 60 shows a sketch of the ground plane coordinate systems for the two jet impingement interaction problem. The jets stagnate on the ground, de-



R81-1622-061D

Figure 59 - Heated wall-jet dimensionless total pressure and temperature difference decay with ground radius.

ORIGINAL SOURCE IS
OF POOR QUALITY



R81-1622-050D

Figure 60 - Two-jet impingement without deflection zone interaction.

flect into radial wall jets and collide along their plane of symmetry. The formation of an upwash stagnation zone is a result of the upward deflection of the wall jet flow. The point S_u , on the line joining the jet centers, is the only true stagnation point where the flow comes to rest and deflects vertically. At points off of the center, the flow is deflected at an angle such that the pressure is representative of the stagnation of the normal component of the maximum wall jet velocity.

6.7.1 Maximum pressure and temperature distribution along the upwash stagnation line - To estimate the upwash stagnation line ground pressure and temperature distribution, the maximum velocity of the wall jet normal to the stagnation line is computed:

$$V_{\text{NORM}} = V_{\text{MW}} \cos \varphi_u \quad (44)$$

The maximum pressure along the stagnation line is computed from the static plus the contribution of the normal velocity of the wall jet.

Pressure -

$$\Delta P_{\text{umg}} = \Delta P_{\text{MW}} + \frac{1}{2} \frac{P_{\text{MW}}}{R_G T_{\text{MW}}} V_{\text{MW}}^2 \cos^2 \varphi_u \quad (45)$$

Dividing by the nozzle pressure given by

$$\frac{\Delta P_{\text{SN}}}{P_A} = \text{NPR} - 1 = \frac{1}{2} \frac{V_N^2}{R_G T_N} \quad (46)$$

yields

$$\frac{\Delta P_{\text{umg}}}{\Delta P_{\text{SN}}} = \frac{\Delta P_{\text{MW}}}{\Delta P_{\text{SN}}} + \left(\frac{P_{\text{MW}}}{P_A} \right) \left(\frac{V_M}{V_N} \right)^2 \cos^2 \varphi_u \quad (47)$$

$$\left(\frac{T_M}{T_N} \right)$$

Temperature -

$$\frac{T_{\text{umg}}}{T_A} = \frac{T_{\text{MW}}}{T_A} \quad (48)$$

The maximum temperature along the stagnation line is then just equal to the maximum temperature of the wall-jet at the stagnation line location, $X = \frac{S}{2}$

The pressure along the stagnation line given by eq. (47) uses the maximum temperature, velocity, and static pressure of the wall-jet evaluated at the stagnation line location.

6.7.2 Upwash momentum models - The upwash momentum model, including the effects of close jet spacing, remains unchanged in principle due to temperature effects and are those described in Ref. 3. The addition of temperature effects has a slight effect on the ground pressure distribution since the addition of heat to the flow somewhat affects the overall decay rates of the various regions. The overall upwash momentum can then be related to the integral of the upwash ground pressure distribution as described in detail in Ref. 3.

6.7.3 Heated upwash decay model - Figure 61 shows a schematic of the upwash sheet model and the characteristic scaling parameters. The upwash sheet is assumed to be a reflection of the wall-jet flow into the vertical plane of symmetry lying between the jets. The radial streamline pattern of the wall layer is assumed to continue into the upwash sheet and, to a first approximation, be unperturbed by the turning region. The wall-jet flow is assumed to enter the upwash deflection region with a characteristic profile, half velocity width and maximum velocity or total pressure. The characteristic length scale in the upwash sheet is the half velocity width of the incident wall-jet layer estimated at the wall location. The pressure recovery region in the upwash sheet is assumed to be approximately three times the half velocity width of the incident wall jet profile. The magnitude of the momentum flux in the resulting upwash streamline is assumed equal to that of the incident wall-jet. Hence, the upwash sheet is treated in a similar fashion as the wall-jet with a few exceptions.

Due to the high turbulence levels typically measured in the upwash sheet, the flow is considered to be fully turbulent and similar. The upwash velocity profile is taken to be that of a free shear profile with no internal momentum defect due to the wall layer. The upwash sheet growth rate is assumed to be

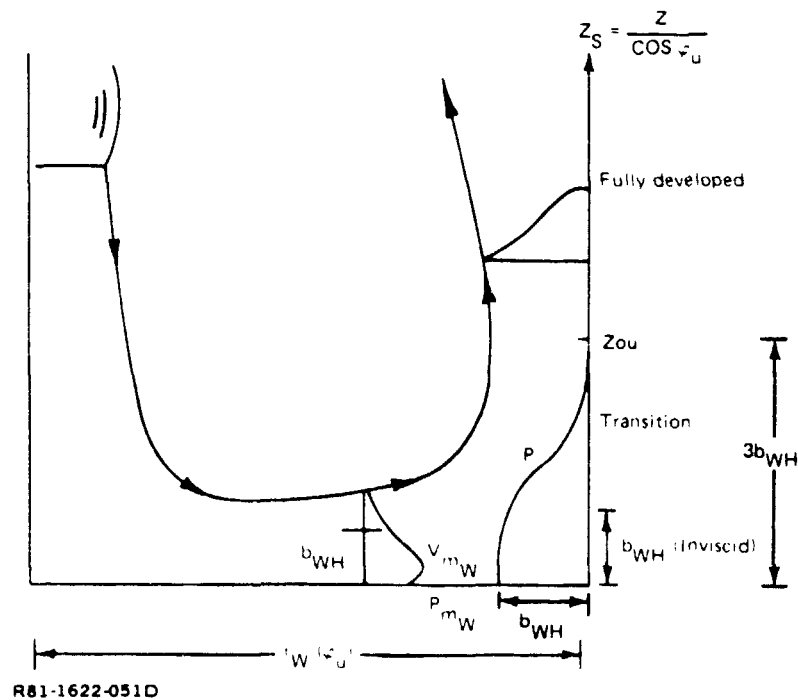


Figure 61 - Characteristic scaling parameters for upwash model.

constant without any initial transition phase. It is also assumed that the magnitude of the momentum flux distribution in the upwash sheet is given by the previously discussed momentum models. Expressions for the momentum and heat flux similar to those for the wall jet can be derived for the upwash flow:

Momentum -

$$f_{Mu}(\varphi) \left[1 - f_{Pu}(\varphi) \right] = \left[\left(\frac{r_W + Z_S}{r_N} \right) \frac{b_u}{r_N} \right] \left[\frac{2 \left(\frac{P_{uM}}{P_A} \right) \left(\frac{V_{Mu}}{V_N} \right)^2}{\left(\frac{T_{Mu}}{T_N} \right)} C_{Mu}(\bar{T}_{Mu}) + \frac{\Delta P_{uM}}{\Delta P_N} C_{Pu}(\bar{T}_{Mu}) \right] \quad (49)$$

where $\Delta P_{Mu} = \Delta P_{MUG}(\varphi) f_{Pu}(\varphi)$

Heat Flux -

$$f_{Mu}(\varphi) \left[1 - f_{Pu}(\varphi) \right] = 2 \left(\frac{r_W + Z_S}{r_N} \right) \left(\frac{b_u}{r_N} \right) \left(\frac{P_{Mu}}{P_A} \right) \left(\frac{V_{Mu}}{V_N} \right) \left(\frac{\Delta T_{Mu}}{\Delta T_N} \right) \frac{C_{Tu} \bar{T}_{Mu}}{T_M / T_N} \quad (50)$$

where

$$C_{Mu} = \int_0^1 f_V^2 \frac{\left[f_p + \frac{(1-f_p)}{\bar{P}_M} \right]}{\left[f_T + \frac{(1-f_T)}{\bar{T}_M} \right]} d\eta_V \quad (51)$$

$$C_{Pu} = \int_0^1 f_p d\eta_V \quad (52)$$

$$C_{Tu} = \int_0^1 \frac{f_V(\eta_V) f_T(\eta_T) \left[f_p + \frac{(1-f_p)}{\bar{P}_M} \right] d\eta_V}{\left[f_T + \frac{(1-f_T)}{\bar{T}_M} \right]} \quad (53)$$

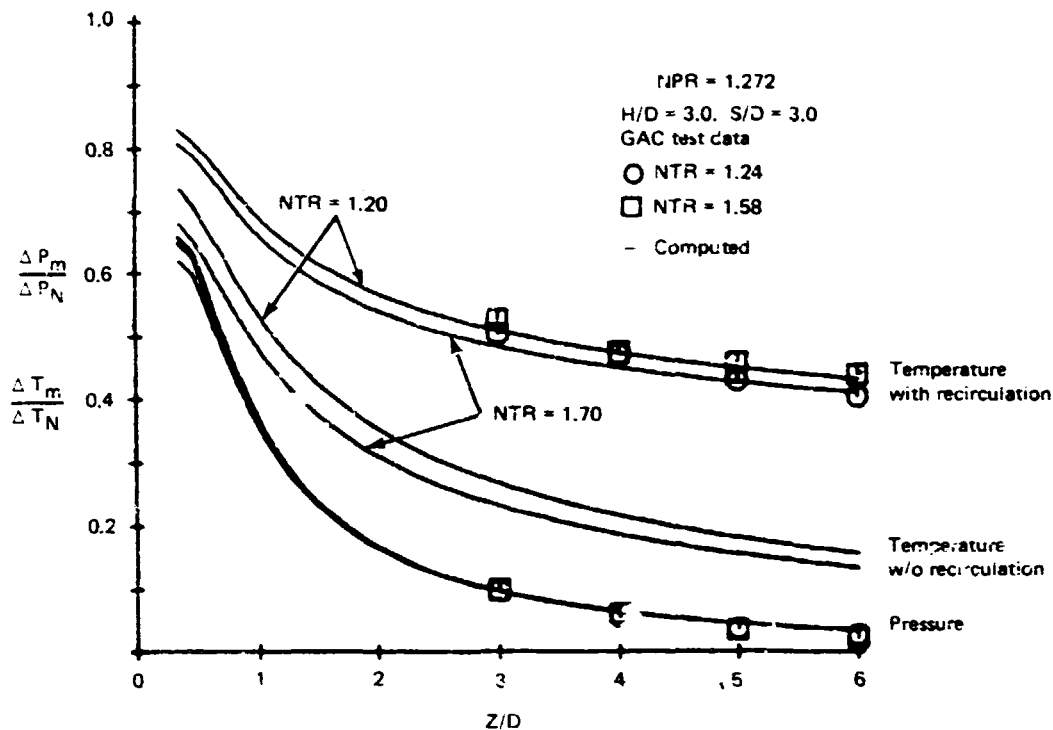
$$\zeta = \frac{z_S}{z_{SO}}, \quad \eta_V = \frac{y}{b_u}, \quad \eta_T = \frac{y}{b_{uT}}$$

The pressure terms in eqs. (49) and (50) only have a contribution in the upwash deflection regions. The above integrals, as with the wall-jet and jet flows, are carried out over the width of the dynamic layer given by b_u . The thermal layer is considered to be somewhat wider and is given by:

$$b_{uT} = \lambda_T b_u$$

The growth rate of the upwash flow is assumed to be approximately three times the rate of the wall-jet due to the higher turbulence. Equations (49) and (50) are then solved simultaneously for the temperature and velocity. Initial application of this model to the heated upwash led to the results shown in Figure 62 for the pressure and temperature decay. The pressure correlates well with the test data but the temperature decays too rapidly. The wall-jet and upwash temperature behavior for two interacting impinging jets is significantly different from a single isolated jet impinging to form a wall-jet. Recirculation effects dominate for multi-jet impingement. These effects are due to several aspects of the two-jet problem. Hot upwash flow tends to recirculate back into the free jet and wall jet regions, altering their effective temperature decay. Confinement of the region between the free jet and upwash flow tends to heat the ambient flow or restrict the influx of cooler ambient air into this region to be entrained by the wall jet and upwash flow. As a result of these effects, in order to be able to estimate the temperature behavior of wall-jets and upwash flow, a recirculation model must be established.

6.7.4 Recirculation model - As a preliminary attempt at estimating recirculation effects, a model was generated for both the wall-jet and upwash flows. The



R81-1622-054(1/2)D

Figure 62 - Heated upwash centerline decay characteristics with recirculation effects.

basic principle of such a model is demonstrated in Figure 63. The model takes into account that the wall jet and upwash streamlines do not effectively entrain air at the reference ambient condition. This situation is most extreme along the inner wall-jet and upwash streamline ($\varphi=0^\circ$) and is enhanced as the jet spacing is reduced. The recirculation effect is also assumed to be negligible along the outermost ray ($\varphi=\pi$). In reality, the outermost ray may also be affected if the free jet decay has been altered. This is neglected in the present study. In order to quantify the recirculation effect, it is assumed that it results in a local change in ambient conditions represented by:

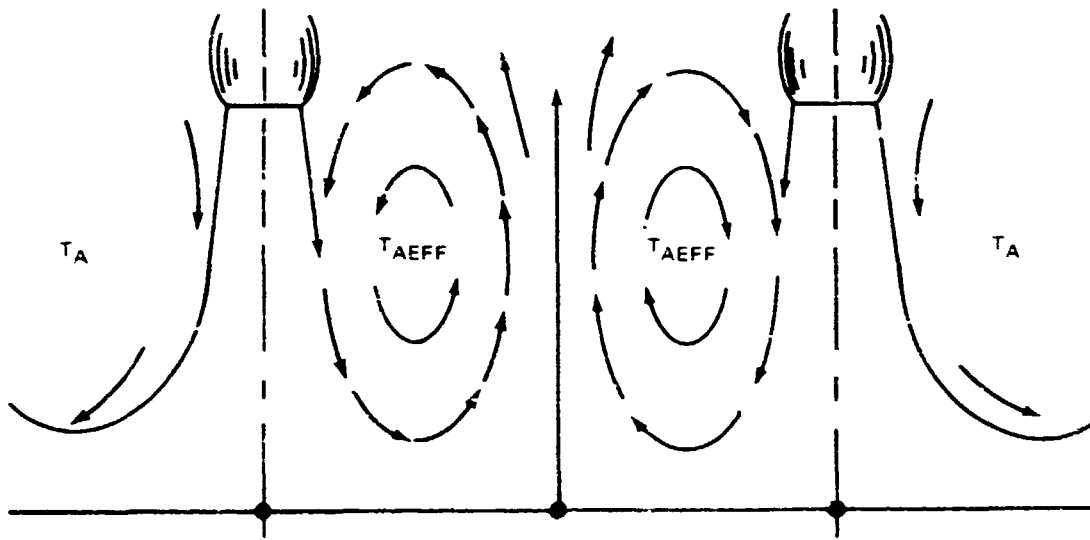
$$\frac{T}{T_A} A_{\text{eff}} = 1 + A_{\text{rec}} \cos^2\left(\frac{\varphi}{2}\right) \Delta T_g \quad (54)$$

where

$$A_{\text{rec}} = \left[\frac{r_g}{(S/2)} \right]^{\alpha_{\text{rec}}}, \quad \alpha_{\text{rec}} \sim 1.30$$

and ΔT_g is the ground stagnation temperature of the incident jet.

ORIGINAL
OF POOR QUALITY



R81-1622-054(2/2)G

Figure 63 - Recirculation effects.

Essentially, the amount of excess heat flux in any given layer is then altered by the effective local ambient condition:

$$H_F - \dot{q}_N = T_N - T_{Aeff}$$

Hence, if the effective or local ambient temperature is equal to the nozzle temperature, the excess heat flux will be zero and no temperature decay will take place as a result of the heat equation.

If the incident radius (r_g) of the impinging jet is equal to the half spacing of the jets, then the effective ambient temperature (T_{Aeff}) becomes equal to the $\frac{T_A}{2}$

incident temperature ratio of the jet along the stream, $\psi = 0^\circ$ and no further temperature decay will occur. Figures 64a and 64b demonstrate the effect of this model on the wall jet decay rates for two jets with $S/D = 3.0$ and $H/D = 3.0$, and two different nozzle temperature ratios. In this figure, the decay is computed until the wall jet interacts with the stagnation line. For $\psi > \pi/2$, the wall-jet decay is computed to a fixed radius of three diameters. The least temperature decay occurs along the inner ($\psi = 0^\circ$) streamline. The wall-jet decays more rapidly as the outermost ray is approached and, at $\psi = \pi$, the decay of the wall-jet becomes equal to the isolated impingement value.

ORIGINAL COPY
OF POOR QUALITY

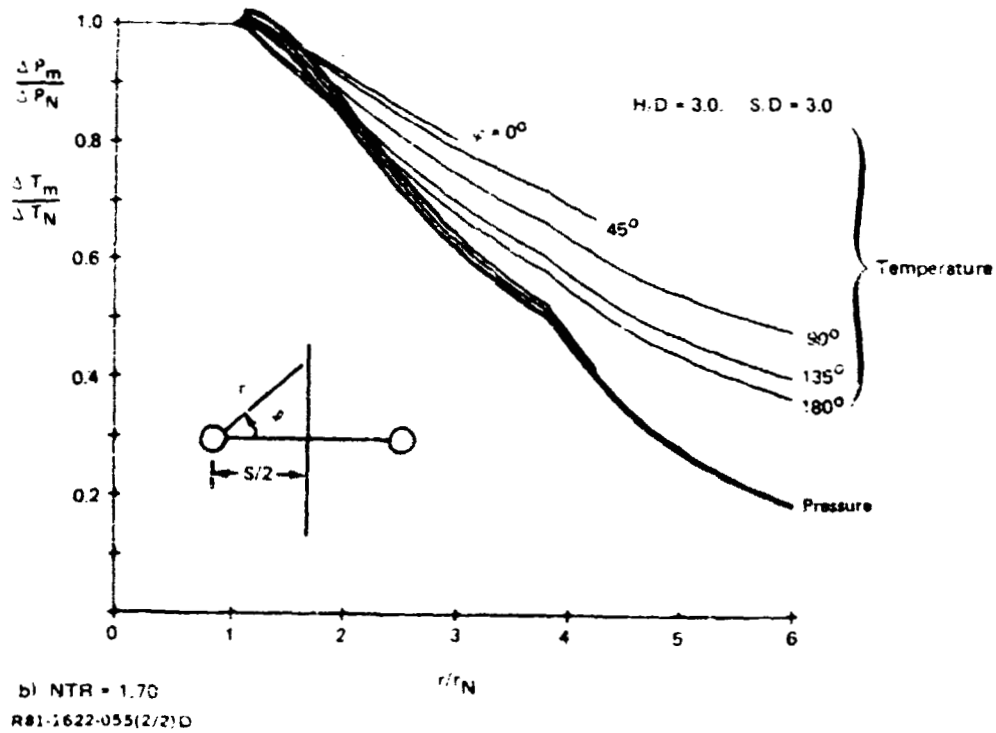
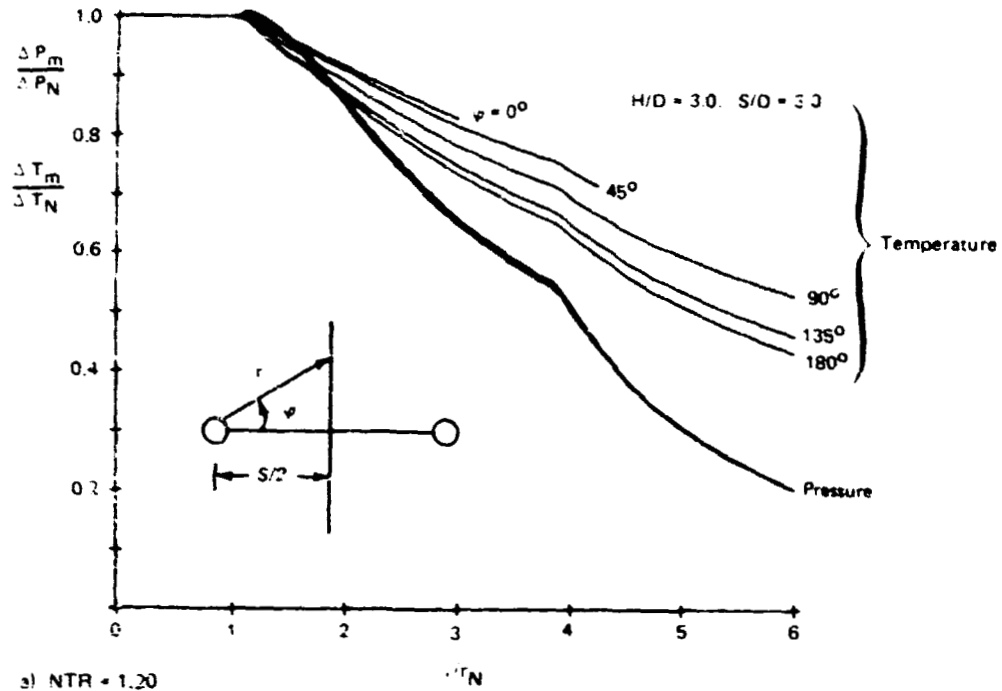
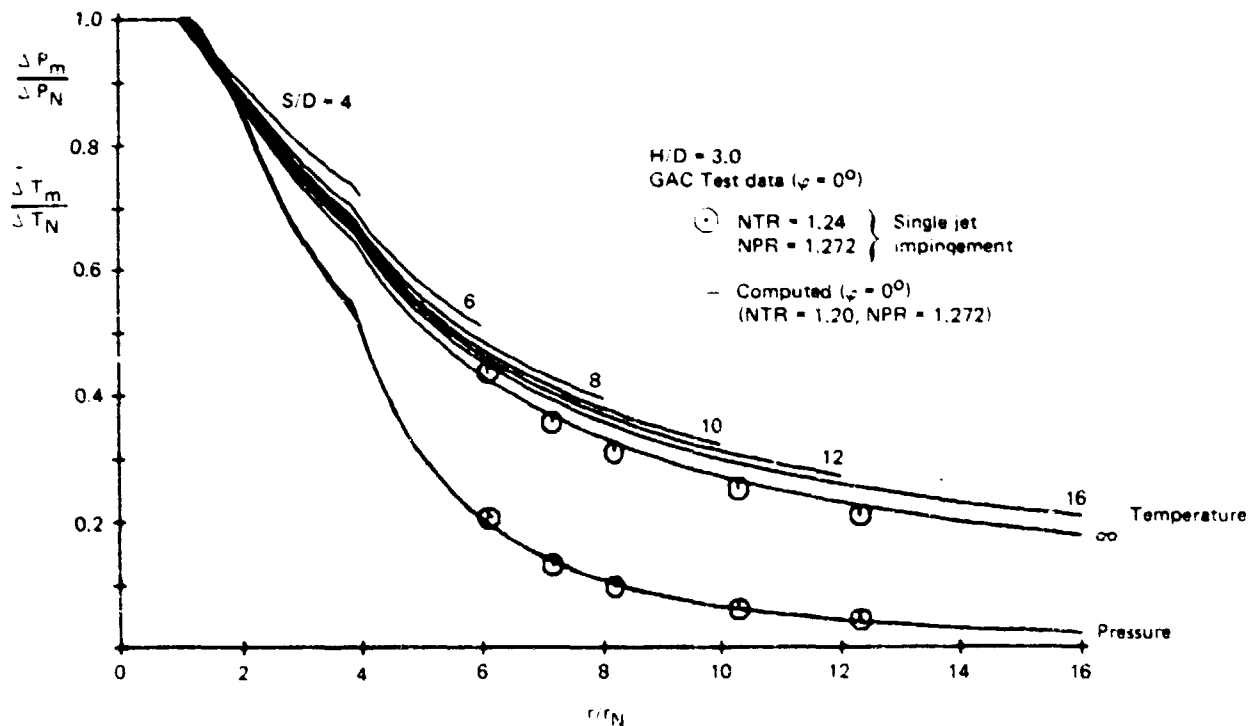


Figure 64 - Heated wall jet decay characteristics with azimuthal recirculation model.

ORIGINAL PAGES
OF POOR QUALITY

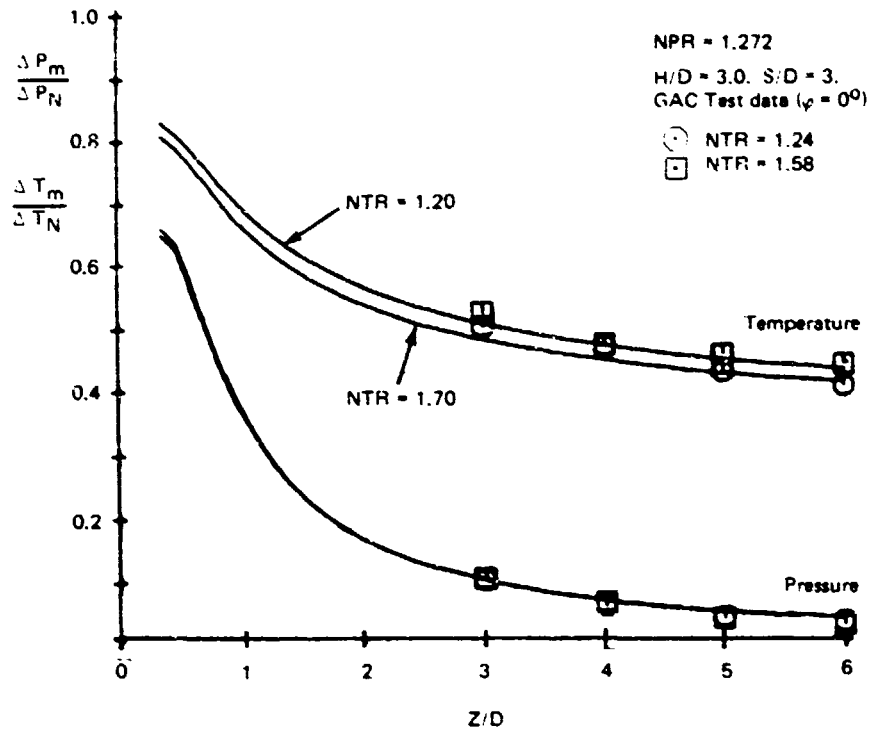
A slight overshoot of the values occur at the end of the inviscid region due to a mismatch either in the radius of the inviscid region or in the thickness of the wall layer. Even though an effective change in ambient temperature conditions affects the temperature decay rate dramatically, it only affects the total pressure decay slightly as indicated by the figures. Figure 65 more clearly demonstrates the effect of the recirculation model as a function of jet spacing. the decay of the innermost streamline ($\phi=0$) is plotted as a function of jet spacing. As the spacing increases, the wall-jet temperature decays more rapidly and, as $S/D \rightarrow \infty$, the decay rate of the interacting wall jet approaches the isolated or single jet impingement behavior. The recirculation effect on the wall-jet feeds into the upwash as an alteration of the initial upwash temperature as well as changing the upwash decay rate. Figure 66 shows the improved correlation in the upwash temperature decay with the implementation of the recirculation model in comparison with Figure 62. Obviously, more detailed correlation is required really to be able to quantify this effect. It is also expected that the presence of a confining plate or vehicle will significantly alter or enhance the recirculation effects.



R81-1622-056(1/2)D

Figure 65 - Heated-wall jet decay characteristics ($\phi = 0^\circ$) vs. jet spacing.

ORIGINAL COPY
OF POOR QUALITY



R81-1622-056(2/2)D

Figure 66 - Correlation of heated upwash decay characteristics ($\psi = 0^\circ$) with recirculation model.

7 - CONCLUSIONS

For the configuration considered in this investigation, small-scale models can be used to predict full-scale induced forces. No scale effects were found, and jet temperature and pressure did not affect the nondimensionalized induced lift. The induced lift in-ground-effect was found to be higher for the uniform circular jets than for the simulated fan jets.

Modifications to an existing wall-jet transition model adequately predict the trends with height above ground of upwash temperatures and pressures. The addition of a recirculation model is necessary to predict upwash temperatures in the presence of an aircraft.

APPENDIX
COMPUTER PROGRAM DESCRIPTION

PROGRAM NAME: GRUMHOT2

PURPOSE: VTOL TWO-JET IMPINGEMENT INTERACTION PROBLEM

This program is designed to estimate the dynamic and thermal flow characteristics associated with two vertically-impinging and equal-strength hot jets. This program is specifically oriented towards the problem of closely-spaced jet interaction, where the deflection regions interact until eventually jet coalescence occurs.

Aside from the basic flow characteristics, the program assumes the symmetrical placement of a slender fuselage in the upwash flow. The upwash lift force is then computed for a cylindrical fuselage of constant cross-sectional shape. The body parameters, in terms of width and depth, do not vary longitudinally. The program estimates the force on the basis of a rectangular and a circular cross section. Two planes of symmetry are assumed and all output applies to one quadrant of the flow field (ie. equal jets and nozzles located at the midpoint of the fuselage). Jet entrainment effects may be significant but are neglected in this program. Hence, the force is only that due to upwash impingement. Some residual programming exists in the code for a parabolic body of revolution. These cards have been commented out but may be used if desired.

INPUT DESCRIPTION

Note: All input parameters are in terms of nozzle diameters.

<u>Card No.</u>	<u>Code Names</u>	<u>Format</u>
1	NPR, NTR	2F10.5
<u>Name</u>	<u>Definition</u>	
NPR	Nozzle pressure ratio	
NTR	Nozzle temperature ratio	

<u>Card No.</u>	<u>Code Names</u>	<u>Format</u>
2	HD, SD, ZPLD, DZPL, ZFINAL	5F10.5

<u>Name</u>	<u>Definition</u>
HD	Nozzle height above ground
SD	Nozzle spacing

Note: The program will compute one or several positions of the fuselage relative to the ground for a fixed nozzle height above ground.

ZPLD	Initial fuselage height above ground
DZPL	Increment in fuselage ΔZ above ground
ZFINAL	Final Z coordinate of fuselage height relative to ground plane.

<u>Card No.</u>	<u>Code Names</u>	<u>Format</u>
3	XL2, WCON, ZCON	3F10.5

<u>Names</u>	<u>Definition</u>
XL2	Fuselage Length
WCON	Fuselage Width
ZCON	Fuselage Depth

Note: ZCON determines position of fuselage underside relative to its ZPLD location. Bottom of fuselage will be located at ZPLD-ZCON at first computed location. The upwash sheet properties are also computed at this Z location.

<u>Card No.</u>	<u>Code Names</u>	<u>Format</u>
4	IPBAR	I1

<u>Name</u>	<u>Definition</u>
IPBAR	Integer controlling the output of ground pressure pattern: IPBAR = 0, no pressure pattern output IPBAR = 1, pressure pattern output is desired

Note: Card No. 4 is not required if IPBAR = 0.

<u>Card No.</u>	<u>Code Name</u>	<u>Format</u>
5	NU	I2

<u>Name</u>	<u>Definition</u>
NU	Number of pressure values to be input for computation of ground isobar pattern NU < 25

Note: Card No. 5 is repeated NU times.

<u>Card No.</u>	<u>Code Name</u>	<u>Format</u>
6	PU	F10.5

<u>Name</u>	<u>Definition</u>
PU	Nondimensional pressure for isobar pattern $0.0 \leq \text{PU} < 1.0$

Figure 67 shows a typical input set.

```

TOF:
                                INPUT DATA
*****
1.007      2.00
4.00      3.000      2.00      1.00      4.00
8.00      1.00      9.0
1
10
.9
.8
.7
.60
.50
.4
.3
.2
.10
.05
*****
EOF:
R01-1622-062D

```

Figure 67 Typical program input.

PRINTED OUTPUT DESCRIPTION

Figure 68 shows a typical computer printout. Most of the geometrical output quantities are nondimensionalized by the nozzle radius. All velocities and pressure are initially nondimensionalized by the nozzle exit velocity and stagnation pressure. All pressures are relative to ambient conditions.

Note: RN and D refer to nozzle exit radius and diameter. VN refers to nozzle exit velocity.

Input Parameters

The first set of output echoes the input parameters.

<u>Output Titles</u>	<u>Definitions</u>
NPR	Nozzle pressure ratio
NTR	Nozzle temperature ratio
Mach No.	Mach number computed from NPR and NTR
TN	Nozzle temperature ratio (NTR) relative to ambient or TN/TA
H/D	Nozzle height above ground
S/D	Nozzle spacing, distance between jet centerlines
Z/D	Initial fuselage height
DZ/D	Increment in fuselage position
ZFINAL/D	Final location of fuselage
L/D	Body Length
W/D	Body Width
ZB/D	Location of underside of body relative to specified fuselage location

Note: If $ZB = 0$, underside location is coincident with specified fuselage position.

Jet Decay Region

<u>Output Titles</u>	<u>Definitions</u>
DELG/D	Jet ground effect height relative to ground plane
ZPC/RN	Length of potential core
ZFD/RN	Length of potential core and transition regions
Z/RN	Jet axial location measured from nozzle exit

ORIGINAL COPY
OF POOR QUALITY

*** INPUT PARAMETERS ***

MPR= 1.0070 NTR= 2.0000
 MACH NO.= 0.1000 TM/TA= 2.0000
 M/D= 4.00000 S/D= 3.00000 Z/D= 2.00000
 Z/D= 2.00000 DZ/D= 1.00000 ZFINA./D= 4.00000
 BODY LENGTH L/D= 8.00000 WIDTH W/D= 1.00000 DEPTH ZB/D= 0.0

***** JET DECAY REGION *****

JET DEFLECTION HEIGHT DELB/D = 1.19340
 ZPC/RN= 6.81693 ZFD/RN= 12.78302

Z/RN	RJH/RN	RJ/RN	ALPV	UJ/VN	RC/RN	ALPT	RJHT/RN	TM/TM	TM/TA	DTM/DTM	RJHD/RN	DJ/DN
0.0	1.0000	1.0000	0.0	1.0000	1.0000	1.3000	1.3070	1.0000	2.0000	1.0000	1.0000	1.0000
1.7016	1.0181	1.0673	6.0144	1.0000	0.8009	6.0144	1.0181	1.0000	2.0000	1.0000	1.0047	1.0000
3.4033	1.0363	1.1365	6.3209	1.0000	0.5691	6.3209	1.0363	1.0000	2.0000	1.0000	1.0088	1.0000
5.1049	1.0544	1.2085	6.5791	1.0000	0.3035	6.5791	1.0544	1.0000	2.0000	1.0000	1.0120	1.0000
6.8066	1.0726	1.2850	6.7837	1.0000	0.0019	6.7837	1.0726	1.0000	2.0000	1.0000	1.0138	1.0000

***** JET DEFLECTION REGION *****

RGH/RN= 1.07257 RG/RN= 1.28501 RD/RN= 3.86124 VG/VN= 1.00000
 STAGNATION PRESSURE, DPS/DPTJ= 1.00000 GROUND MAX. TEMP., TGS/TA= 2.00000
 STAGNATION MACH NUMBER OF JET= 0.10000
 ALPB= 1.50462

SINGLE JET GROUND PRESSURES

R/RGN	DPS/DPTG	R/RN	DPS/DPTJ
0.0	1.00000	0.0	1.00000
0.15000	0.96689	0.16088	0.96689
0.30000	0.90821	0.32177	0.90821
0.45000	0.83608	0.48265	0.83608
0.60000	0.75619	0.64354	0.75619
0.75000	0.67257	0.80442	0.67257
0.90000	0.58832	0.96531	0.58832
1.05000	0.50592	1.12619	0.50592
1.20000	0.42734	1.28708	0.42734
1.35000	0.35409	1.44796	0.35409
1.50000	0.28731	1.60885	0.28731
1.65000	0.22775	1.76973	0.22775
1.80000	0.17586	1.93062	0.17586
1.95000	0.13175	2.09150	0.13175
2.10000	0.09528	2.25239	0.09528
2.25000	0.06606	2.41327	0.06606
2.40000	0.04350	2.57415	0.04350
2.55000	0.02685	2.73504	0.02685
2.70000	0.01524	2.89592	0.01524
2.85000	0.00771	3.05681	0.00771
3.00000	0.00331	3.21769	0.00331
3.14999	0.00110	3.37858	0.00110
3.29999	0.00023	3.53946	0.00023
3.44999	0.00001	3.70035	0.00001
3.59999	0.00000	3.86123	0.00000

***** WALL JET REGION *****

STAGNATION POINT BOUNDARY LAYER THICKNESS, DELS/RN= 0.03735
 PHI/PA== 1.00373 (PTTOT/PA-1.)= 0.00700 (TOT/TA-1.)= 1.00000
 TMI/TA= 2.00000 VMI/VN= 0.68210
 VELOCITY AT START OF TURBULENT WALL JET, VM/VB= 0.68210
 START OF WALL JET REGION, ALPWO= 0.60408 RWGN/RN= 0.34507 BWO/RN= 2.38600

R81-1622-063D(19 Sheets)

Figure 68 Typical program printout.

ORIGINAL PAGE IS
OF POOR QUALITY

ISOLATED WALL JET PROPERTIES

R/RN	VM/UG	VM/VN	BVM/RN	BW/RN	DELRL/RN	DELFL	RDEL	TM/TN	TM/TA	BWHT/RN	DTM/DTN
0.0	0.0	0.0	0.3451	2.3868	0.0374	1.0000	0.0156	1.0000	2.0000	0.3385	1.0000
0.2500	0.2512	0.2512	0.3451	2.3868	0.0374	1.0000	0.0156	1.0000	2.0000	0.3385	1.0000
0.5000	0.4138	0.4138	0.3451	2.3868	0.0374	1.0000	0.0156	1.0000	2.0000	0.3385	1.0000
0.7500	0.5455	0.5455	0.3451	2.3868	0.0374	1.0000	0.0156	1.0000	2.0000	0.3385	1.0000
1.0000	0.6542	0.6542	0.3451	2.3868	0.0374	1.0000	0.0156	1.0000	2.0000	0.3385	1.0000
1.2500	0.7258	0.7258	0.3483	2.0315	0.0370	0.9818	0.0182	0.9844	1.9687	0.3479	0.9687
1.5000	0.7622	0.7622	0.3529	1.6938	0.0366	0.9376	0.0216	0.9610	1.9219	0.3613	0.9219
1.7500	0.7764	0.7764	0.3575	1.4680	0.0362	0.8799	0.0247	0.9357	1.8715	0.3750	0.8715
2.0000	0.7741	0.7741	0.3620	1.3087	0.0358	0.8153	0.0273	0.9094	1.8193	0.3889	0.8193
2.2500	0.7597	0.7597	0.3664	1.1914	0.0353	0.7492	0.0297	0.8836	1.7473	0.4031	0.7473
2.5000	0.7367	0.7367	0.3712	1.1028	0.0349	0.6853	0.0316	0.8586	1.7173	0.4174	0.7173
2.7500	0.7081	0.7081	0.3758	1.0338	0.0345	0.6259	0.0333	0.8352	1.6701	0.4320	0.6704
3.0000	0.6764	0.6764	0.3803	0.9789	0.0340	0.5722	0.0348	0.8138	1.6274	0.4469	0.6274
3.2500	0.6439	0.6439	0.3849	0.9347	0.0336	0.5245	0.0360	0.7945	1.5889	0.4619	0.5889
3.5000	0.6123	0.6123	0.3895	0.8985	0.0332	0.4827	0.0369	0.7773	1.5545	0.4772	0.5545
3.7500	0.5830	0.5830	0.3941	0.8685	0.0328	0.4461	0.0377	0.7620	1.5239	0.4927	0.5239
4.0000	0.5474	0.5474	0.4103	0.8860	0.0350	0.4023	0.0395	0.7454	1.4907	0.5177	0.4907
4.2500	0.5071	0.5071	0.4360	0.9386	0.0394	0.3520	0.0419	0.7306	1.4612	0.5500	0.4612
4.5000	0.4718	0.4718	0.4614	0.9912	0.0437	0.3102	0.0441	0.7176	1.4352	0.5824	0.4352
4.7500	0.4409	0.4409	0.4873	1.0438	0.0481	0.2753	0.0461	0.7060	1.4120	0.6148	0.4120
5.0000	0.4135	0.4135	0.5129	1.0964	0.0525	0.2458	0.0479	0.6957	1.3913	0.6471	0.3913
5.2500	0.3892	0.3892	0.5386	1.1490	0.0569	0.2207	0.0495	0.6864	1.3727	0.6795	0.3727
5.5000	0.3674	0.3674	0.5642	1.2017	0.0613	0.1991	0.0510	0.6779	1.3558	0.7118	0.3558
5.7500	0.3477	0.3477	0.5899	1.2543	0.0656	0.1804	0.0523	0.6703	1.3405	0.7442	0.3405
6.0000	0.3300	0.3300	0.6155	1.3069	0.0700	0.1642	0.0536	0.6633	1.3265	0.7765	0.3265

***** TWO-JET INTERACTION PROBLEM *****

*** RECIRCULATION EFFECT ON WALL JETS ***

PHI= 0.0 DEGS.

TNEFF= 2.00000 TAEFF= 1.42834

R	VM/VN	TM/TN	TM/TA	BPH/DPN	DTM/DTN
0.0	0.0	1.00000	2.00000	1.00000	1.00000
0.12500	0.14993	1.00000	2.00000	1.00000	1.00000
0.25000	0.25116	1.00000	2.00000	1.00000	1.00000
0.37500	0.33728	1.00000	2.00000	1.00000	1.00000
0.50000	0.41383	1.00000	2.00000	1.00000	1.00000
0.62500	0.48281	1.00000	2.00000	1.00000	1.00000
0.75000	0.54548	1.00000	2.00000	1.00000	1.00000
0.87500	0.60245	1.00000	2.00000	1.00000	1.00000
1.00000	0.65416	1.00000	2.00000	1.00000	1.00000
1.12500	0.69741	0.99740	1.99520	0.99569	0.99520
1.25000	0.72787	0.99185	1.98369	0.98077	0.98359
1.37500	0.75098	0.98587	1.97175	0.96012	0.97175
1.50000	0.76785	0.97962	1.95925	0.93487	0.95925
1.62500	0.77938	0.97312	1.94623	0.90638	0.94623
1.75000	0.78629	0.96641	1.93281	0.87539	0.93281
1.87500	0.78918	0.95954	1.91913	0.84284	0.91913
2.00000	0.78859	0.95265	1.90530	0.80935	0.90530
2.12500	0.78458	0.94574	1.89147	0.77554	0.89147
2.25000	0.77877	0.93888	1.87776	0.74205	0.87776
2.37500	0.77036	0.93213	1.86425	0.70933	0.86425
2.50000	0.76008	0.92553	1.85106	0.67744	0.85106
2.62500	0.74829	0.91913	1.83825	0.64696	0.83825
2.75000	0.73528	0.91294	1.82589	0.61777	0.82589
2.87500	0.72135	0.90701	1.81402	0.59025	0.81402
3.00000	0.70679	0.90133	1.80266	0.56423	0.80266

Figure 68 - Continued

ORIGINAL PAGE IS
OF POOR QUALITY

PHI= 45.0000 DEGS

TNEFF= 2.00000 TAEFF= 1.36561

R	VM/VM	TM/TM	TH/TA	DPH/DPN	DTM/DTN
0.0	0.0	1.00000	2.00000	1.00000	1.00000
0.17678	0.19441	1.00000	2.00000	1.00000	1.00000
0.35355	0.32347	1.00000	2.00000	1.00000	1.00000
0.53033	0.43124	1.00000	2.00000	1.00000	1.00000
0.70711	0.52460	1.00000	2.00000	1.00000	1.00000
0.88388	0.60428	1.00000	2.00000	1.00000	1.00000
1.06066	0.67759	1.00000	2.00000	1.00000	1.00000
1.23744	0.72490	0.99149	1.98298	0.98262	0.98298
1.41421	0.75632	0.98195	1.96390	0.95298	0.96390
1.59099	0.77578	0.97180	1.94360	0.91485	0.94360
1.76776	0.78556	0.96117	1.92233	0.87140	0.92233
1.94454	0.78744	0.95026	1.90051	0.82496	0.90051
2.12132	0.78287	0.93928	1.87857	0.77746	0.87857
2.29809	0.77309	0.92844	1.85688	0.73037	0.85688
2.47487	0.75920	0.91788	1.83577	0.68473	0.83577
2.65164	0.74215	0.90775	1.81550	0.64164	0.81550
2.82842	0.72284	0.89813	1.79626	0.60132	0.79626
3.00519	0.70210	0.88909	1.77818	0.56415	0.77818
3.18197	0.68068	0.88066	1.76132	0.53008	0.76132
3.35875	0.65927	0.87285	1.74570	0.49919	0.74570
3.53552	0.63844	0.86564	1.73128	0.47101	0.73128
3.71230	0.61861	0.85898	1.71796	0.44550	0.71796
3.88907	0.59912	0.85242	1.70484	0.41969	0.70484
4.06585	0.58066	0.84472	1.68944	0.38281	0.68944
4.24263	0.56430	0.83824	1.67648	0.34826	0.67648

PHI= 89.9999 DEGS.

TNEFF= 2.00000 TAEFF= 1.21417

R	VM/VM	TM/TM	TH/TA	DPH/DPN	DTM/DTN
0.0	0.0	1.00000	2.00000	1.00000	1.00000
0.25000	0.25114	1.00000	2.00000	1.00000	1.00000
0.50000	0.41383	1.00000	2.00000	1.00000	1.00000
0.75000	0.54548	1.00000	2.00000	1.00000	1.00000
1.00000	0.65414	1.00000	2.00000	1.00000	1.00000
1.25000	0.72690	0.98828	1.97656	0.98127	0.97656
1.50000	0.76518	0.97072	1.94144	0.93617	0.94144
1.75000	0.78159	0.95177	1.90354	0.87750	0.90354
2.00000	0.78170	0.93210	1.86419	0.81215	0.86419
2.25000	0.76971	0.91246	1.82472	0.74536	0.82472
2.50000	0.74898	0.89349	1.78699	0.68107	0.78699
2.75000	0.72238	0.87567	1.75135	0.62150	0.75135
3.00000	0.69239	0.85929	1.71858	0.56789	0.71858
3.25000	0.66122	0.84449	1.68897	0.52032	0.68897
3.50000	0.63070	0.83124	1.66249	0.47881	0.66249
3.75000	0.60214	0.81944	1.63888	0.44249	0.63888
4.00000	0.56724	0.80654	1.61307	0.39897	0.61307
4.25000	0.52458	0.79499	1.58998	0.34880	0.58998
4.50000	0.49105	0.78474	1.56952	0.30724	0.56952
4.75000	0.45974	0.77544	1.55128	0.27252	0.55128
5.00000	0.43202	0.76746	1.53491	0.24319	0.53491
5.25000	0.40724	0.76007	1.52014	0.21822	0.52014
5.50000	0.38504	0.75336	1.50673	0.19679	0.50673
5.75000	0.36499	0.74725	1.49450	0.17828	0.49450
6.00000	0.34682	0.74166	1.48331	0.16219	0.48331

Figure 68 - Continued

ORIGINAL LISTING
OF POOR QUALITY

PHI=134.9999 DEGS.

TNEFF= 2.00000 TAEFF= 1.06273

R	VM/UM	TM/TN	TM/TA	DPH/DPN	DTH/DTN
0.0	0.0	1.00000	2.00000	1.00000	1.00000
0.25000	0.25116	1.00000	2.00000	1.00000	1.00000
0.50000	0.41383	1.00000	2.00000	1.00000	1.00000
0.75000	0.54548	1.00000	2.00000	1.00000	1.00000
1.00000	0.65414	1.00000	2.00000	1.00000	1.00000
1.25000	0.72616	0.98555	1.97111	0.98166	0.97111
1.50000	0.76313	0.96392	1.92784	0.93718	0.92754
1.75000	0.77798	0.94040	1.88119	0.87914	0.88119
2.00000	0.77641	0.91642	1.83285	0.81436	0.83285
2.25000	0.76272	0.89235	1.78470	0.74799	0.78470
2.50000	0.74041	0.86916	1.73833	0.68397	0.73833
2.75000	0.71242	0.84743	1.69486	0.62450	0.69486
3.00000	0.68128	0.82750	1.65501	0.57087	0.65501
3.25000	0.64917	0.80954	1.61908	0.52317	0.61908
3.50000	0.61792	0.79351	1.58702	0.48147	0.58702
3.75000	0.58883	0.77925	1.55850	0.44494	0.55850
4.00000	0.55361	0.76375	1.52750	0.40128	0.52750
4.25000	0.51303	0.74993	1.49987	0.35097	0.49987
4.50000	0.47768	0.73774	1.47547	0.30930	0.47547
4.75000	0.44663	0.72688	1.45376	0.27443	0.45376
5.00000	0.41915	0.71716	1.43433	0.24497	0.43433
5.25000	0.39467	0.70840	1.41681	0.21988	0.41681
5.50000	0.37274	0.70047	1.40093	0.19835	0.40095
5.75000	0.35299	0.69325	1.38651	0.17974	0.38651
6.00000	0.33512	0.68666	1.37331	0.16355	0.37331

PHI=179.9999 DEGS.

TNEFF= 2.00000 TAEFF= 1.00000

R	VM/UM	TM/TN	TM/TA	DPH/DPN	DTH/DTN
0.0	0.0	1.00000	2.00000	1.00000	1.00000
0.25000	0.25116	1.00000	2.00000	1.00000	1.00000
0.50000	0.41383	1.00000	2.00000	1.00000	1.00000
0.75000	0.54548	1.00000	2.00000	1.00000	1.00000
1.00000	0.65414	1.00000	2.00000	1.00000	1.00000
1.25000	0.72583	0.98437	1.96874	0.98183	0.96874
1.50000	0.76224	0.96097	1.92194	0.93722	0.92194
1.75000	0.77641	0.93575	1.87149	0.87987	0.87149
2.00000	0.77409	0.90963	1.81925	0.81533	0.81925
2.25000	0.75967	0.88364	1.76727	0.74917	0.76727
2.50000	0.73667	0.85863	1.71726	0.68527	0.71726
2.75000	0.70807	0.83522	1.67044	0.62585	0.67044
3.00000	0.67641	0.81378	1.62755	0.57222	0.62755
3.25000	0.64390	0.79447	1.58893	0.52447	0.58893
3.50000	0.61233	0.77725	1.55450	0.48268	0.55450
3.75000	0.58299	0.76196	1.52392	0.44606	0.52392
4.00000	0.54763	0.74536	1.49073	0.40235	0.49073
4.25000	0.50710	0.73061	1.46121	0.35197	0.46121
4.50000	0.47183	0.71759	1.43518	0.31024	0.43518
4.75000	0.44088	0.70602	1.41205	0.27531	0.41205
5.00000	0.41352	0.69567	1.39135	0.24580	0.39135
5.25000	0.38916	0.68636	1.37271	0.22066	0.37271
5.50000	0.36736	0.67792	1.35585	0.19907	0.35585
5.75000	0.34774	0.67026	1.34051	0.18042	0.34051
6.00000	0.33000	0.66325	1.32651	0.16419	0.32651

Figure 68 - Continued

CALCULATION
OF FOOT COUNTS

MAXIMUM GROUND PRESSURE AND TEMPERATURE ALONG UPWASHGROUND STAGNATION LINE

XW/PN	XW/S	DPMAX/DPJ	PMAX/PMAXC	DTMAX/DIJ	TMAX/TMAXU
0.0	0.0	0.56423	1.00000	0.50266	1.00000
0.17473	0.02912	0.56128	0.99478	0.80208	0.99927
0.35045	0.05844	0.55263	0.97944	0.80031	0.99707
0.52698	0.08816	0.53952	0.95443	0.79734	0.99337
0.71101	0.11850	0.51902	0.91987	0.79315	0.98815
0.89814	0.14969	0.49483	0.87701	0.78771	0.98137
1.09191	0.18198	0.46621	0.82629	0.78096	0.97296
1.29407	0.21568	0.43380	0.76884	0.77286	0.96287
1.50665	0.25111	0.39862	0.70348	0.76333	0.95104
1.73205	0.28867	0.36127	0.64028	0.75241	0.93739
1.97313	0.32885	0.32275	0.57202	0.73994	0.92186
2.23341	0.37224	0.28402	0.50337	0.72591	0.90438
2.51770	0.41955	0.24282	0.43036	0.70873	0.88298
2.83035	0.47172	0.19617	0.34768	0.68737	0.85636
3.17981	0.52997	0.15246	0.27198	0.66513	0.82859
3.57525	0.59588	0.11445	0.20439	0.64119	0.79882
4.02969	0.67162	0.08535	0.15127	0.61545	0.76675
4.56127	0.76021	0.06009	0.10650	0.58796	0.73251
5.19614	0.86602	0.04024	0.07149	0.55874	0.69611
5.97346	0.99558	0.0255	0.04531	0.52781	0.65757
6.95473	1.15912	0.01506	0.02673	0.49520	0.61594
8.24235	1.37372	0.00811	0.01438	0.46093	0.57425
10.02056	1.67009	0.00385	0.00683	0.42503	0.52752
12.45775	2.10962	0.00133	0.00272	0.38750	0.48277
17.01334	2.83556	0.00046	0.00082	0.34829	0.43352

UPWASH MOMENTUM FUNCTION: JET RADIUS, INTERACTION CONSTANT, VERTICAL UPWASH SHEET MOMENTUM, AND COALES

RG/RM= 1.29501 ACON= 0.81653 XMGHZ= 0.93884 PHI0(DEGS)= 0.0

UPWASH WIDTH CONSTANT ESTIMATE, CU= 0.29758

*** CALL INTERG ***

SOLUTION OF GROUND PRESSURE DISTRIBUTION HAS BEEN FOUND
 ITERATION CYCLE= 15 EPS= 0.03691 SIGMA= 0.91425
 EPI= 0.03691 CUI= 0.29758 PHIU0= 49.43231 PHI0= 63.52774 DEGREES
 PHI=0.0, DELPM0= 0.67723
 PHI=0.0, PMIN= 0.11929
 PHI=0.0, ALFUB= 2.73835
 UPWASH THICKNESS CONSTANT, (CU) X (SIGMA)= 0.27206

*** COMPUTATION OF TWO-JET GROUND ISOBAR PATTERN ***

10 VALUES OF PRESSURE SPECIFIED FOR PATTERN

PBR= 0 0.10000 0.20000 0.30000 0.40000 0.50000 0.60000 0.70000 0.80000 0.90000
 0.10000 0.05000

Figure 68 - Continued

ORIGINAL PAGE IS
OF POOR QUALITY

GROUND PATTERN IN JET CENTERED COORDINATE SYSTEM

FRAR= 0.90000

JET IMPINGEMENT REGION, IJET= 58

UPWASH DEFLECTION REGION, IU= 0

XISOJ	YISOJ	XISOU	YISOU
0.34791	0.0		
0.34760	0.01472		
0.34665	0.02941		
0.34509	0.04402		
0.34291	0.05852		
0.34012	0.07269		
0.33673	0.08707		
0.33277	0.10105		
0.32823	0.11479		
0.32316	0.12827		
0.31755	0.14145		
0.31144	0.15431		
0.30485	0.16683		
0.29780	0.17899		
0.29031	0.19076		
0.28242	0.20214		
0.27414	0.21310		
0.26551	0.22363		
0.25655	0.23374		
0.24729	0.24339		
0.23774	0.25260		
0.22795	0.26135		
0.21792	0.26965		
0.20769	0.27748		
0.19729	0.28486		
0.18672	0.29178		
0.17601	0.29824		
0.16520	0.30425		
0.15428	0.30981		
0.15428	0.30981		
0.13132	0.31999		
0.10769	0.32846		
0.08353	0.33519		
0.05894	0.34013		
0.03411	0.34328		
0.00911	0.34461		
-0.01590	0.34433		
-0.04679	0.34184		
-0.06544	0.33775		
-0.08970	0.33189		
-0.11347	0.32429		
-0.13660	0.31501		
-0.15859	0.30408		
-0.18052	0.29157		
-0.20108	0.27755		
-0.22056	0.26209		
-0.23887	0.24527		
-0.25591	0.22719		
-0.27160	0.20794		
-0.28585	0.18761		
-0.29860	0.16633		
-0.30978	0.14418		
-0.31934	0.12130		
-0.32722	0.09779		
-0.33339	0.07379		
-0.33783	0.04941		
-0.34049	0.02477		
-0.34139	0.00060		

Figure 68 - Continued

ORIGINAL PAGE IS
OF POOR QUALITY

PBAR= 0.80000

JET IMPINGEMENT REGION: IJET= 58

UPWASH DEFLECTION REGION: IU= 0

X130J	Y130J	X130U	Y130U
0.56735	0.0		
0.56684	0.02401		
0.56530	0.04795		
0.56275	0.07178		
0.55919	0.09543		
0.55464	0.11886		
0.54912	0.14199		
0.54265	0.16479		
0.53526	0.18720		
0.52698	0.20917		
0.51784	0.23067		
0.50788	0.25164		
0.49712	0.27206		
0.48563	0.29188		
0.47342	0.31108		
0.46055	0.32963		
0.44705	0.34751		
0.43298	0.36469		
0.41837	0.38114		
0.40324	0.39691		
0.38770	0.41193		
0.37172	0.42620		
0.35537	0.43973		
0.33869	0.45250		
0.32172	0.46453		
0.30449	0.47581		
0.28703	0.48635		
0.26939	0.49615		
0.25159	0.50522		
0.23415	0.51352		
0.21742	0.52102		
0.19962	0.52763		
0.18261	0.53346		
0.16614	0.53852		
0.14952	0.54280		
0.13285	0.54629		
0.11614	0.54899		
0.09948	0.55090		
0.08285	0.55197		
-0.06593	0.55219		
-0.08652	0.55144		
-0.10671	0.54978		
-0.12628	0.54722		
-0.14503	0.54384		
-0.16276	0.53969		
-0.17928	0.53487		
-0.19439	0.52947		
-0.20791	0.52361		
-0.22068	0.51740		
-0.23254	0.51097		
-0.24332	0.50449		
-0.25390	0.49790		
-0.26415	0.49095		
-0.27494	0.48363		
-0.28517	0.47592		
-0.29575	0.46781		
-0.30561	0.45930		
-0.31485	0.45040		
-0.32348	0.44110		
-0.33150	0.43140		
-0.33890	0.42130		
-0.34568	0.41080		
-0.35185	0.40000		
-0.35740	0.38890		
-0.36230	0.37740		
-0.36655	0.36560		
-0.37005	0.35350		
-0.37290	0.34110		
-0.37600	0.32840		
-0.37835	0.31540		
-0.38000	0.30210		
-0.38090	0.28860		
-0.38100	0.27490		
-0.38030	0.26100		
-0.37880	0.24690		
-0.37640	0.23260		
-0.37310	0.21810		
-0.36810	0.20340		
-0.36180	0.18860		
-0.35450	0.17370		
-0.34520	0.15870		
-0.33400	0.14360		
-0.32090	0.12840		
-0.30600	0.11310		
-0.28930	0.09770		
-0.27080	0.08220		
-0.25050	0.06660		
-0.22850	0.05090		
-0.20480	0.03510		
-0.17940	0.01920		
-0.15230	0.00330		
-0.12360	0.00000		

Figure 68 - Continued

ORIGINAL PAGE IS
OF POOR QUALITY

PBAR= 0.70000

JET IMPINGEMENT REGION, IJET= 58

UPWASH DEFLECTION REGION, IU= 0

XISOU	YISOU	XISOU	YISOU
0.76642	0.0		
0.76573	0.03243		
0.76365	0.06478		
0.76020	0.09697		
0.75540	0.12892		
0.74925	0.16056		
0.74179	0.19181		
0.73306	0.22261		
0.72307	0.25288		
0.71189	0.28257		
0.69954	0.31160		
0.68608	0.33994		
0.67155	0.36751		
0.65602	0.39429		
0.63953	0.42023		
0.62214	0.44529		
0.60392	0.46944		
0.58490	0.49265		
0.56516	0.51490		
0.54475	0.53618		
0.52373	0.55646		
0.50215	0.57574		
0.48007	0.59401		
0.45753	0.61127		
0.43460	0.62752		
0.41133	0.64276		
0.38775	0.65700		
0.36391	0.67024		
0.33987	0.68250		
0.33987	0.68250		
0.28929	0.70491		
0.23724	0.72357		
0.18401	0.73839		
0.12988	0.74929		
0.07513	0.75622		
0.02007	0.75916		
-0.03503	0.75809		
-0.08987	0.75304		
-0.14415	0.74403		
-0.19761	0.73112		
-0.24996	0.71439		
-0.30093	0.69393		
-0.35025	0.66986		
-0.39768	0.64230		
-0.44297	0.61141		
-0.48589	0.57736		
-0.52622	0.54032		
-0.56375	0.50048		
-0.59831	0.45807		
-0.62971	0.41330		
-0.65779	0.36640		
-0.68242	0.31762		
-0.70347	0.26721		
-0.72084	0.21543		
-0.73444	0.16255		
-0.74420	0.10884		
-0.75008	0.05456		
-0.75294	0.00001		

Figure 68 - Continued

ORIGINAL PAGE IS
OF POOR QUALITY

PBAR= 0.60000

JET IMPINGEMENT REGION, IJET= 58

UPWASH DEFLECTION REGION, IU= 11

	XIS0J	YIS0J	XIS0U	YIS0U
	0.96092	0.0	2.75420	0.0
	0.96005	0.04066	2.75724	0.09247
	0.95745	0.08122	2.76042	0.18511
	0.95313	0.12157	2.76592	0.27811
	0.94710	0.16164	2.77408	0.37164
	0.93939	0.20131	2.78552	0.46588
"	0.93004	0.24049	2.80128	0.56104
	0.91909	0.27910	2.82348	0.65729
	0.90657	0.31706	2.85749	0.75486
	0.89254	0.35428	2.93572	0.85395
	0.87706	0.39068	3.00000	0.86662
	0.86018	0.42620		
	0.84198	0.46078		
	0.82250	0.49435		
	0.80183	0.52687		
	0.78003	0.55829		
	0.75717	0.58857		
	0.73333	0.61767		
	0.70859	0.64557		
	0.68300	0.67225		
	0.65664	0.69768		
	0.62958	0.72185		
	0.60189	0.74476		
	0.57364	0.76640		
	0.54489	0.78677		
	0.51571	0.80588		
	0.48615	0.82373		
	0.45626	0.84033		
	0.42612	0.85570		
	0.42612	0.85570		
	0.36270	0.88380		
	0.29744	0.90720		
	0.23070	0.92577		
	0.16283	0.93944		
	0.09420	0.94813		
	0.02516	0.95181		
	-0.04392	0.95048		
"	-0.11267	0.94414		
	-0.18074	0.93285		
	-0.24776	0.91666		
	-0.31339	0.89569		
	-0.37729	0.87004		
	-0.43914	0.83985		
	-0.49840	0.80530		
	-0.55538	0.76658		
	-0.60919	0.72388		
	-0.65976	0.67743		
	-0.70682	0.62749		
	-0.75014	0.57432		
	-0.78951	0.51818		
	-0.82472	0.45939		
	-0.85540	0.39823		
	-0.88199	0.33503		
	-0.90377	0.27011		
	-0.92082	0.20380		
	-0.93306	0.13645		
	-0.94043	0.06841		
	-0.94289	0.00001		

Figure 68 - Continued

ORIGINAL PAGE IS
OF POOR QUALITY

PBAR= 0.5000C
JET IMPINGEMENT REGION, IJF= 58 UPWASH DEFLECTION REGION, IU= 16

XISQJ	YISQJ	XISOU	YISOU
1.15977	0.0	2.65969	0.4
1.15872	0.04907	2.66023	0.09247
1.15558	0.09802	2.66189	0.18511
1.15036	0.14673	2.66471	0.27811
1.14308	0.19509	2.66877	0.37164
1.13379	0.24296	2.67421	0.46588
1.12250	0.29026	2.68121	0.56104
1.10928	0.33686	2.69003	0.65729
1.09417	0.38267	2.70102	0.75486
1.07724	0.42759	2.71472	0.85395
1.05856	0.47153	2.73192	0.95479
1.03819	0.51440	2.75392	1.05763
1.01621	0.55613	2.78312	1.16274
0.99271	0.59665	2.82518	1.27038
0.96775	0.63590	2.90661	1.38087
0.94144	0.67382	3.00000	1.40836
0.91386	0.71036		
0.88509	0.74549		
0.85522	0.77916		
0.82433	0.81136		
0.79252	0.84205		
0.75986	0.87123		
0.72645	0.89888		
0.69235	0.92500		
0.65765	0.94958		
0.62243	0.97265		
0.58675	0.99419		
0.55068	1.01422		
0.51430	1.03277		
0.51430	1.03277		
0.43775	1.06669		
0.35900	1.09493		
0.27844	1.11735		
0.19653	1.13384		
0.11369	1.14433		
0.03036	1.14878		
-0.05301	1.14716		
-0.13599	1.13951		
-0.21814	1.12588		
-0.29903	1.10635		
-0.37824	1.08103		
-0.45537	1.05008		
-0.53001	1.01365		
-0.60178	0.97195		
-0.67031	0.92521		
-0.73525	0.87367		
-0.79628	0.81762		
-0.85308	0.75734		
-0.90537	0.69316		
-0.95289	0.62541		
-0.99538	0.55445		
-1.03265	0.48063		
-1.06451	0.40435		
-1.09079	0.32600		
-1.11137	0.24598		
-1.12615	0.16469		
-1.13504	0.08257		
-1.13801	0.00002		

Figure 68 - Continued

ORIGINAL PAGE IS
OF POOR QUALITY

PBAR= 0.40000

JET IMPINGEMENT REGION, IJET= 58

UPWASH DEFLECTION REGION, IU= 20

XISQJ	YISQJ	XISOU	YISOU
1.37135	0.0	2.58414	0.4
1.37011	0.05802	2.58449	0.09247
1.36439	0.11590	2.58558	0.18511
1.36022	0.17350	2.58741	0.27811
1.35162	0.23067	2.59003	0.37164
1.34062	0.28729	2.59350	0.46588
1.32728	0.34321	2.59791	0.56104
1.31164	0.39832	2.60337	0.65729
1.29378	0.45248	2.61003	0.75484
1.27376	0.50559	2.61807	0.85395
1.25167	0.55755	2.62774	0.95479
1.22758	0.60824	2.63938	1.05763
1.20160	0.65759	2.65343	1.16274
1.17381	0.70550	2.67051	1.27038
1.14430	0.75191	2.69146	1.38087
1.11319	0.79675	2.71766	1.49454
1.08058	0.83996	2.75146	1.61174
1.04656	0.88149	2.79778	1.73292
1.01123	0.92131	2.87355	1.85848
0.97472	0.95937	3.00000	1.92118
0.93710	0.99567		
0.89849	1.03017		
0.85897	1.06286		
0.81866	1.09374		
0.77763	1.12282		
0.73598	1.15009		
0.69379	1.17556		
0.65114	1.19925		
0.60812	1.22118		
0.60812	1.22118		
0.51761	1.26129		
0.42449	1.29468		
0.32924	1.32119		
0.23238	1.34069		
0.13443	1.35704		
0.03590	1.35835		
-0.06268	1.35644		
-0.16079	1.34740		
-0.25793	1.33128		
-0.35358	1.30819		
-0.44725	1.27825		
-0.53844	1.24164		
-0.62670	1.19857		
-0.71156	1.14926		
-0.79259	1.09399		
-0.86939	1.03306		
-0.94155	0.96678		
-1.00871	0.89551		
-1.07054	0.81962		
-1.12672	0.73951		
-1.17697	0.65560		
-1.22104	0.56832		
-1.25871	0.47812		
-1.28979	0.38547		
-1.31412	0.29085		
-1.33159	0.19474		
-1.34211	0.09763		
-1.34562	0.00002		

Figure 68 - Continued

ORIGINAL PAGE IS
OF POOR QUALITY

PBAR= 0.30000

JET IMPINGEMENT REGION: IJET= 58

UPWASH DEFLECTION REGION: IU= 24

XISOJ	YISOJ	XISOU	YISOU
1.40708	0.0	2.51121	0.0
1.40563	0.06800	2.51147	0.09247
1.40128	0.13583	2.51225	0.18511
1.59405	0.20333	2.51357	0.27811
1.58397	0.27033	2.51543	0.37164
1.57108	0.33667	2.51789	0.46588
1.55544	0.40221	2.52099	0.56104
1.53712	0.46679	2.52477	0.65729
1.51619	0.53026	2.52933	0.75484
1.49273	0.59251	2.53476	0.85395
1.46684	0.65339	2.54119	0.95479
1.43861	0.71280	2.54877	1.05763
1.40816	0.77063	2.55770	1.16274
1.37553	0.82678	2.56828	1.27038
1.34101	0.88114	2.58079	1.38087
1.30455	0.93371	2.59566	1.49454
1.26633	0.98433	2.61347	1.61174
1.22644	1.03302	2.63497	1.73292
1.18507	1.07968	2.66119	1.85848
1.14227	1.12429	2.69366	1.98892
1.09819	1.16682	2.73482	2.12481
1.05294	1.20725	2.78971	2.26676
1.00663	1.24557	2.87064	2.41548
0.95939	1.28176	3.00000	2.48979
0.91131	1.31583		
0.86249	1.34779		
0.81305	1.37764		
0.76328	1.40540		
0.71266	1.43110		
0.66259	1.47810		
0.61246	1.51723		
0.56284	1.54830		
0.51333	1.57116		
0.46454	1.58569		
0.41608	1.59185		
-0.36745	1.58962		
-0.31847	1.57902		
-0.26927	1.56013		
-0.22046	1.53306		
-0.17143	1.49798		
-0.12210	1.45508		
-0.07343	1.40461		
-0.02438	1.34682		
-0.02484	1.28205		
-1.01884	1.21064		
-1.10340	1.13297		
-1.18211	1.04945		
-1.25457	0.96051		
-1.32041	0.86663		
-1.37930	0.76830		
-1.43094	0.66601		
-1.47509	0.56071		
-1.51151	0.45174		
-1.54002	0.34085		
-1.56049	0.22921		
-1.57282	0.11441		
-1.57694	0.00002		

Figure 68 - Continued

REGIONAL QUALITY
OF POOR QUALITY

PBAR= 0.20000

JET IMPINGEMENT REGION, IJET= 58

UPWASH DEFLECTION REGION, IU= 27

XISQJ	YISQJ	XISQU	YISQU
1.88819	0.0	2.42495	0.0
1.88648	0.07989	2.42521	0.09247
1.88137	0.15959	2.42596	0.18511
1.87287	0.23889	2.42722	0.27811
1.84103	0.31761	2.42898	0.37144
1.84589	0.39556	2.43124	0.46588
1.82751	0.47256	2.43399	0.56104
1.80598	0.54844	2.43725	0.65729
1.78139	0.62302	2.44103	0.75486
1.75382	0.69615	2.44538	0.85395
1.72341	0.76768	2.45034	0.95479
1.69024	0.83778	2.45600	1.05763
1.65446	0.90542	2.46244	1.16274
1.61620	0.97139	2.46983	1.27038
1.57557	1.03529	2.47830	1.38087
1.53274	1.09703	2.48809	1.49454
1.48783	1.15652	2.49947	1.61174
1.44099	1.21371	2.51281	1.73292
1.39235	1.26853	2.52855	1.85848
1.34207	1.32095	2.54727	1.98892
1.29028	1.37092	2.56971	2.12481
1.23711	1.41842	2.59680	2.26676
1.18271	1.46344	2.62976	2.41548
1.12720	1.50596	2.67830	2.57178
1.07071	1.54599	2.74376	2.73653
1.01336	1.58354	2.83529	2.91985
0.95527	1.61841	3.00000	3.07394
0.89655	1.65123		
0.83731	1.68142		
0.83731	1.68142		
0.71270	1.73665		
0.58447	1.78262		
0.45333	1.81912		
0.31997	1.84598		
0.18510	1.86306		
0.04944	1.87029		
-0.08630	1.86767		
-0.22140	1.85521		
-0.35514	1.83302		
-0.48684	1.80122		
-0.61581	1.76000		
-0.74137	1.70940		
-0.86289	1.65029		
-0.97974	1.58241		
-1.09131	1.50631		
-1.19705	1.42240		
-1.29640	1.33114		
-1.38888	1.23301		
-1.47401	1.12852		
-1.55137	1.01822		
-1.62056	0.90268		
-1.68124	0.78251		
-1.73310	0.65832		
-1.77589	0.53075		
-1.80940	0.40047		
-1.83345	0.26813		
-1.84793	0.13442		
-1.85277	0.00003		

Figure 68 - Continued

ORIGINAL PAGE IS
OF POOR QUALITY

PBAR= 0.10000

JET IMPINGEMENT REGION, IJET= 50

UPWASH DEFLECTION REGION, IU= 50

XIS0J	YIS0J	XIS0U	YIS0U
2.14366	0.74971	2.25500	0.75486
2.11049	0.83772	2.28283	0.85395
2.07389	0.92380	2.30024	0.95479
2.03398	1.00779	2.31383	1.05763
1.99092	1.08955	2.32540	1.16274
1.94487	1.16894	2.33585	1.27038
1.89599	1.24584	2.34567	1.38087
1.84444	1.32013	2.35527	1.49454
1.79040	1.39172	2.36495	1.61174
1.73403	1.46054	2.37505	1.73292
1.67551	1.52651	2.38589	1.85848
1.61500	1.58958	2.39785	1.98892
1.55268	1.64971	2.41139	2.12481
1.48870	1.70688	2.42704	2.26676
1.42323	1.76105	2.44549	2.41548
1.35643	1.81222	2.47136	2.57178
1.28815	1.86039	2.50457	2.73655
1.21944	1.90557	2.54675	2.91086
1.14953	1.94778	2.59936	3.09591
1.07888	1.98703	2.66421	3.29313
1.00739	2.02337	2.74253	3.50416
1.00759	2.02337	2.74253	3.50416
0.85763	2.08982	2.74722	3.52268
0.70333	2.14515	2.75205	3.54132
0.54552	2.18907	2.75702	3.56008
0.38504	2.22138	2.76214	3.57895
0.22274	2.24193	2.76742	3.59791
0.05949	2.25064	2.77285	3.61704
-0.10385	2.24748	2.77847	3.63627
-0.26642	2.23250	2.78426	3.65562
-0.42736	2.20579	2.79024	3.67509
-0.58585	2.16753	2.79644	3.69469
-0.74104	2.11793	2.80284	3.71441
-0.89214	2.05727	2.80949	3.73426
-1.03837	1.98590	2.81638	3.75424
-1.17898	1.90421	2.82354	3.77435
-1.31325	1.81263	2.83100	3.79459
-1.44048	1.71167	2.83877	3.81497
-1.56005	1.60185	2.84690	3.83548
-1.67133	1.48376	2.85541	3.85613
-1.77378	1.35802	2.86436	3.87691
-1.86696	1.22529	2.87379	3.89784
-1.95012	1.08626	2.88380	3.91891
-2.02314	0.94164	2.89446	3.94013
-2.08555	0.79220	2.90592	3.96149
-2.13704	0.63869	2.91838	3.98299
-2.17736	0.48191	2.93216	4.00465
-2.20631	0.32266	2.94785	4.02645
-2.22373	0.16174	2.96686	4.04841
-2.22955	0.00003	2.98881	4.07053

Figure 68 - Continued

PBAR= 0.05000

JET IMPINGEMENT REGION, IJET= 43

UPWASH DEFLECTION REGION, IU= 43

XIS0J	YIS0J	XIS0J	YIS0J
2.08715	1.49384	2.14019	1.49454
2.02600	1.57486	2.22838	1.61176
1.96221	1.65273	2.25469	1.73292
1.89599	1.72738	2.27276	1.85848
1.82752	1.79875	2.28751	1.98892
1.75699	1.86680	2.30084	2.12481
1.68460	1.93148	2.31384	2.26674
1.61051	1.99278	2.32739	2.41548
1.53492	2.05049	2.34467	2.57178
1.45800	2.10520	2.36596	2.73655
1.37990	2.15633	2.39259	2.91084
1.30080	2.20409	2.42590	3.09591
1.22084	2.24851	2.46759	3.29313
1.14018	2.28962	2.51904	3.50416
1.14018	2.28962	2.51904	3.50416
0.97049	2.36482	2.52380	3.55007
0.79588	2.42742	2.52886	3.59449
0.61730	2.47713	2.53426	3.64403
0.43570	2.51369	2.54001	3.69212
0.25205	2.53695	2.54615	3.74097
0.06732	2.54680	2.55249	3.79062
-0.11752	2.54323	2.55947	3.84107
-0.30148	2.52627	2.56712	3.89236
-0.48360	2.49605	2.57508	3.94452
-0.66294	2.45275	2.58360	3.99756
-0.83855	2.39662	2.59270	4.05152
-1.00954	2.32799	2.60246	4.10642
-1.17501	2.24723	2.61291	4.16230
-1.33412	2.15479	2.62414	4.21918
-1.48604	2.05116	2.63621	4.27710
-1.63004	1.93691	2.64922	4.33609
-1.76533	1.81264	2.66325	4.39619
-1.89126	1.67901	2.67844	4.45743
-2.00719	1.53672	2.69493	4.51985
-2.11252	1.38652	2.71290	4.58349
-2.20674	1.22920	2.73257	4.64839
-2.28936	1.06555	2.75423	4.71460
-2.35999	0.89444	2.77828	4.78215
-2.41826	0.72273	2.80529	4.85111
-2.46388	0.54532	2.83615	4.92149
-2.49664	0.36512	2.87247	4.99339
-2.51635	0.18305	2.91795	5.06683
-2.52294	0.00004	2.97761	5.14198

UPWASH DEFLECTION ZONE LINE, PRAR=0 OUTSIDE INTERACTION REGION

XII*	YUP
2.18381	0.0
2.17864	0.33802
2.17211	0.50972
2.16282	0.68473
2.15061	0.86428
2.13528	1.04974
2.11656	1.24264
2.09410	1.44472
2.06745	1.65804
2.03606	1.88502
1.99923	2.12861
1.95605	2.39247
1.90539	2.68096
1.84573	3.00000
1.77513	3.35700
1.69093	3.76187
1.58954	4.22810
1.46590	4.77446
1.31268	5.42806
1.11888	6.22951

Figure 68 - Continued

COMPUTATION OF UPWASH FLOW FIELD

***** COMPUTATION OF UPWASH FLOW FIELD *****

COMPUTATION OF UPWASH STREAMLINE PROPERTIES

PHID= 0.0 DEGS

INU.VEL.= 0.54015 TH/TA= 1.80266 DELPMJ= 0.56423 DELTWJ= 0.80266 BUOH/RN= 0.38034
 ZOU/RN= 1.14102 BUO/RN= 0.46750 BUOHN/RN= 0.20618 TLAMI= 1.22919

Z/RN	VMU/VM	TM/TN	TH/TA	BUH/RN	BU/RN	DFU/DFJ	DTM/DTN
0.38034	0.54015	0.90133	1.80266	0.20618	0.46750	0.56417	0.80266
0.53116	0.60399	0.89130	1.78261	0.25143	0.57009	0.53185	0.78261
0.68198	0.60919	0.87894	1.75791	0.29668	0.67268	0.46950	0.75791
0.83280	0.58224	0.86563	1.73125	0.34192	0.77527	0.40296	0.73125
0.98362	0.54169	0.85313	1.70625	0.38717	0.87786	0.34477	0.70625
1.13443	0.50113	0.84234	1.68467	0.43241	0.98045	0.29014	0.68467
1.28525	0.46613	0.83340	1.66679	0.47766	1.08304	0.26071	0.66679
1.43607	0.43698	0.82573	1.65146	0.52290	1.18563	0.23030	0.65146
1.58689	0.40994	0.81904	1.63812	0.56815	1.28822	0.20517	0.63812
1.73771	0.38694	0.81319	1.62639	0.61340	1.39081	0.18414	0.62639
1.88853	0.36659	0.80799	1.61598	0.65864	1.49340	0.16632	0.61598
2.03935	0.34837	0.80334	1.60668	0.70389	1.59599	0.15107	0.60668
2.19017	0.33198	0.79915	1.59830	0.74913	1.69858	0.13791	0.59830
2.34099	0.31713	0.79536	1.59071	0.79438	1.80117	0.12645	0.59071
2.49180	0.30362	0.79190	1.58381	0.83962	1.90376	0.11641	0.58381
2.64262	0.29126	0.78875	1.57749	0.88487	2.00635	0.10755	0.57749
2.79344	0.27991	0.78584	1.57169	0.93012	2.10894	0.09970	0.57169
2.94426	0.26944	0.78317	1.56634	0.97536	2.21153	0.09270	0.56634
3.09508	0.25974	0.78069	1.56139	1.02061	2.31411	0.08643	0.56139
3.24590	0.25077	0.77819	1.55679	1.06585	2.41670	0.08079	0.55679
3.39672	0.24240	0.77626	1.55251	1.11110	2.51929	0.07570	0.55251
3.54754	0.23459	0.77426	1.54852	1.15634	2.62188	0.07108	0.54852
3.69835	0.22729	0.77239	1.54478	1.20159	2.72447	0.06688	0.54478
3.84917	0.22043	0.77064	1.54127	1.24683	2.82706	0.06305	0.54127
3.99999	0.21399	0.76899	1.53798	1.29208	2.92965	0.05955	0.53798

PHID= 60.0000 DEGS

INU.VEL.= 0.26871 TH/TA= 1.55874 DELPMJ= 0.16135 DELTWJ= 0.55874 BUOH/RN= 0.61550
 ZOU/RN= 1.84649 BUO/RN= 1.11853 BUOHN/RN= 0.49331 TLAMI= 1.05924

Z/RN	VMU/VM	TM/TN	TH/TA	BUH/RN	BU/RN	DFU/DFJ	DTM/DTN
0.61550	0.26871	0.77937	1.55874	0.49331	1.11853	0.16122	0.55874
0.92319	0.32788	0.77604	1.55207	0.55858	1.26653	0.16662	0.55207
1.23087	0.33782	0.76938	1.53876	0.62385	1.41452	0.15529	0.53876
1.53856	0.33358	0.76089	1.52178	0.68912	1.56251	0.13801	0.52178
1.84625	0.30302	0.75283	1.50566	0.75439	1.71051	0.12197	0.50566
2.15393	0.28421	0.74712	1.49424	0.81966	1.85850	0.10812	0.49424
2.46162	0.26772	0.74211	1.48422	0.88493	2.00649	0.09658	0.48422
2.76931	0.25312	0.73768	1.47536	0.95020	2.15449	0.08685	0.47536
3.07699	0.24009	0.73372	1.46744	1.01547	2.30248	0.07857	0.46744
3.38468	0.22840	0.73017	1.46033	1.08074	2.45047	0.07144	0.46033
3.69237	0.21782	0.72695	1.45391	1.14601	2.59846	0.06527	0.45391
4.00005	0.20822	0.72403	1.44807	1.21128	2.74646	0.05988	0.44807
4.30774	0.19946	0.72137	1.44274	1.27655	2.89445	0.05515	0.44274
4.61543	0.19142	0.71893	1.43785	1.34182	3.04244	0.05097	0.43785
4.92311	0.18402	0.71668	1.43335	1.40709	3.19044	0.04725	0.43335
5.23080	0.17719	0.71460	1.42920	1.47237	3.33843	0.04394	0.42920
5.53849	0.17086	0.71267	1.42534	1.53763	3.48642	0.04096	0.42534
5.84617	0.16497	0.71088	1.42176	1.60291	3.63442	0.03829	0.42176
6.15386	0.15949	0.70921	1.41843	1.66818	3.78241	0.03587	0.41843
6.46155	0.15437	0.70765	1.41531	1.73345	3.93040	0.03367	0.41531
6.76923	0.14957	0.70619	1.41239	1.79872	4.07840	0.03168	0.41239
7.07692	0.14506	0.70482	1.40965	1.86399	4.22639	0.02986	0.40965
7.38461	0.14081	0.70353	1.40707	1.92926	4.37438	0.02819	0.40707
7.69230	0.13683	0.70232	1.40464	1.99453	4.52238	0.02666	0.40464
7.99998	0.13307	0.70117	1.40235	2.05980	4.67037	0.02522	0.40235

Figure 68 - Continued

ORIGINAL PAGE IS
OF POOR QUALITY

UPWASH PROPERTIES COMPUTED AT Z LOCATION OF UNDERSIDE OF BODY

BODY CENTERLINE LOCATION AT Z/RN= 4.00000

ZU/RN	RW/RN	PHIB	X/RN	VMU/VN	DPU/PN	BUH/RN	DPU/PUO	DPU/PJS	TH/TA	DTSN/DTH	PSS/PN
4.0000	3.0000	0.0	0.0	0.2140	0.0595	1.2921	1.0000	0.0595	1.5380	0.5380	0.05755
4.0000	3.0024	2.7263	0.3333	0.2139	0.0595	1.2931	0.9991	0.0595	1.5377	0.5377	0.05936
4.0000	3.0136	5.4403	0.6667	0.2136	0.0593	1.2960	0.9965	0.0593	1.5370	0.5370	0.05881
4.0000	3.0305	8.1301	1.0000	0.2130	0.0591	1.3009	0.9923	0.0591	1.5357	0.5357	0.05791
4.0000	3.0539	10.7843	1.3333	0.2122	0.0587	1.3076	0.9863	0.0587	1.5340	0.5340	0.05668
4.0000	3.0837	13.3925	1.6667	0.2113	0.0583	1.3161	0.9785	0.0583	1.5319	0.5319	0.05515
4.0000	3.1198	15.9454	2.0000	0.2101	0.0577	1.3263	0.9692	0.0577	1.5293	0.5293	0.05336
4.0000	3.1623	18.4349	2.3333	0.2087	0.0571	1.3379	0.9582	0.0571	1.5263	0.5263	0.05135
4.0000	3.2103	20.8544	2.6667	0.2071	0.0563	1.3512	0.9456	0.0563	1.5230	0.5230	0.04917
4.0000	3.2639	23.1986	3.0000	0.2053	0.0555	1.3656	0.9316	0.0555	1.5194	0.5194	0.04687
4.0000	3.3228	25.4633	3.3333	0.2033	0.0546	1.3813	0.9163	0.0546	1.5155	0.5155	0.04448
4.0000	3.3866	27.6460	3.6667	0.2012	0.0536	1.3981	0.8997	0.0536	1.5114	0.5114	0.04204
4.0000	3.4553	29.7448	4.0000	0.1990	0.0525	1.4157	0.8822	0.0525	1.5071	0.5071	0.03960
4.0000	3.5283	31.7594	4.3333	0.1966	0.0514	1.4344	0.8636	0.0514	1.5027	0.5027	0.03718
4.0000	3.6055	33.6900	4.6667	0.1941	0.0503	1.4536	0.8445	0.0503	1.4981	0.4981	0.03482
4.0000	3.6867	35.5376	5.0000	0.1915	0.0491	1.4735	0.8248	0.0491	1.4935	0.4935	0.03252
4.0000	3.7715	37.3039	5.3333	0.1889	0.0479	1.4938	0.8047	0.0479	1.4888	0.4888	0.03032
4.0000	3.8598	38.9910	5.6667	0.1862	0.0467	1.5147	0.7843	0.0467	1.4840	0.4840	0.02821
4.0000	3.9517	40.6013	6.0000	0.1833	0.0454	1.5384	0.7626	0.0454	1.4792	0.4792	0.02618
4.0000	4.0457	42.1376	6.3333	0.1803	0.0441	1.5631	0.7407	0.0441	1.4744	0.4744	0.02425
4.0000	4.1429	43.6028	6.6667	0.1773	0.0428	1.5892	0.7185	0.0428	1.4696	0.4696	0.02243
4.0000	4.2426	45.0000	7.0000	0.1743	0.0415	1.6157	0.6966	0.0415	1.4648	0.4648	0.02074
4.0000	4.3448	46.3322	7.3333	0.1713	0.0402	1.6427	0.6750	0.0402	1.4601	0.4601	0.01916
4.0000	4.4493	47.6025	7.6667	0.1683	0.0389	1.6701	0.6538	0.0389	1.4554	0.4554	0.01770
4.0000	4.5558	48.8140	8.0000	0.1654	0.0377	1.6979	0.6331	0.0377	1.4509	0.4509	0.01635

FLAT BOTTOM VEHICLE WITH SHARP CORNERS

UPWASH LIFT FORCE LU/2TJ= 0.08718

BODY WITH CIRCULAR CROSS SECTION

UPWASH LIFT FORCE LU/2TJ= 0.02366

Figure 68 - Continued

ORIGINAL PAGE IS
OF POOR QUALITY

UPWASH PROPERTIES COMPUTED AT Z LOCATION OF UNDERSIDE OF BODY

BODY CENTERLINE LOCATION AT Z/RN= 6.00000

ZU/RN	RW/RN	FRIB	Y/RN	VMU/VN	DPU/PN	BUM/RN	DPU/PUD	DPU/PJS	TM/TA	DTSN/DTN	PDS/PN
6.0000	3.0000	0.0	0.0	0.1544	0.0317	1.8921	1.0000	0.0317	1.5074	0.5074	0.03170
6.0000	3.0021	2.1211	0.3333	0.1545	0.0317	1.8928	0.9995	0.0317	1.5074	0.5074	0.03165
6.0000	3.0082	4.2364	0.6667	0.1544	0.0316	1.8953	0.9981	0.0316	1.5070	0.5070	0.03147
6.0000	3.0185	6.3402	1.0000	0.1542	0.0316	1.8992	0.9957	0.0316	1.5062	0.5062	0.03118
6.0000	3.0327	8.4270	1.3333	0.1539	0.0315	1.9047	0.9923	0.0315	1.5052	0.5052	0.03078
6.0000	3.0510	10.4915	1.6667	0.1535	0.0313	1.9118	0.9879	0.0313	1.5039	0.5039	0.03028
6.0000	3.0732	12.5288	2.0000	0.1530	0.0312	1.9203	0.9826	0.0312	1.5023	0.5023	0.02969
6.0000	3.0992	14.5344	2.3333	0.1524	0.0310	1.9302	0.9763	0.0310	1.5005	0.5005	0.02900
6.0000	3.1289	16.5043	2.6667	0.1517	0.0307	1.9414	0.9690	0.0307	1.4985	0.4985	0.02824
6.0000	3.1623	18.4349	3.0000	0.1510	0.0305	1.9539	0.9608	0.0305	1.4962	0.4962	0.02741
6.0000	3.1992	20.3231	3.3333	0.1501	0.0302	1.9677	0.9516	0.0302	1.4938	0.4938	0.02653
6.0000	3.2394	22.1643	3.6667	0.1492	0.0299	1.9824	0.9416	0.0299	1.4911	0.4911	0.02560
6.0000	3.2830	23.9625	4.0000	0.1482	0.0295	1.9984	0.9308	0.0295	1.4883	0.4883	0.02464
6.0000	3.3296	25.7099	4.3333	0.1471	0.0291	2.0153	0.9191	0.0291	1.4854	0.4854	0.02365
6.0000	3.3793	27.4075	4.6667	0.1460	0.0287	2.0330	0.9067	0.0287	1.4823	0.4823	0.02266
6.0000	3.4319	29.0546	5.0000	0.1448	0.0283	2.0515	0.8937	0.0283	1.4791	0.4791	0.02165
6.0000	3.4871	30.6506	5.3333	0.1435	0.0279	2.0709	0.8801	0.0279	1.4758	0.4758	0.02065
6.0000	3.5451	32.1957	5.6667	0.1422	0.0275	2.0908	0.8659	0.0275	1.4725	0.4725	0.01966
6.0000	3.6055	33.6900	6.0000	0.1400	0.0270	2.1114	0.8514	0.0270	1.4691	0.4691	0.01869
6.0000	3.6683	35.1342	6.3333	0.1394	0.0265	2.1325	0.8364	0.0265	1.4657	0.4657	0.01774
6.0000	3.7334	36.5288	6.6667	0.1380	0.0260	2.1541	0.8212	0.0260	1.4622	0.4622	0.01681
6.0000	3.8006	37.8749	7.0000	0.1365	0.0255	2.1761	0.8057	0.0255	1.4588	0.4588	0.01592
6.0000	3.8698	39.1736	7.3333	0.1350	0.0250	2.1988	0.7901	0.0250	1.4553	0.4553	0.01505
6.0000	3.9409	40.4260	7.6667	0.1334	0.0245	2.2234	0.7737	0.0245	1.4518	0.4518	0.01421
6.0000	4.0139	41.6335	8.0000	0.1319	0.0240	2.2486	0.7573	0.0240	1.4483	0.4483	0.01341

FLAT BOTTOM VEHICLE WITH SHARP CORNERS

UPWASH LIFT FORCE LU/2TJ= 0.05623

BODY WITH CIRCULAR CROSS SECTION

UPWASH LIFT FORCE LU/2TJ= 0.01440

Figure 68 - Continued.

ORIGINAL PAGE IS
OF POOR QUALITY

UPWASH PROPERTIES COMPUTED AT Z LOCATION OF UNDERSIDE OF BODY

BODY CENTERLINE LOCATION AT Z/RN= 8.0000

ZU/RN	RW/RN	PHIB	X/RN	YMU/RN	DFU/RN	BUH/RN	DFU/PGD	DFU/PJS	TM/TA	DTSN/BTN	PBS/PN
8.0000	3.0000	0.0	0.0	0.1212	0.0197	2.4921	1.0000	0.0197	1.4905	0.4905	0.01972
8.0000	3.0014	1.7357	0.3333	0.1212	0.0197	2.4928	0.9997	0.0197	1.4904	0.4904	0.01970
8.0000	3.0055	3.4682	0.6667	0.1211	0.0197	2.4947	0.9988	0.0197	1.4901	0.4901	0.01962
8.0000	3.0124	5.1944	1.0000	0.1210	0.0197	2.4981	0.9972	0.0197	1.4896	0.4896	0.01950
8.0000	3.0220	6.9112	1.3333	0.1209	0.0196	2.5028	0.9951	0.0196	1.4889	0.4889	0.01934
8.0000	3.0342	8.6156	1.6667	0.1207	0.0196	2.5088	0.9922	0.0196	1.4880	0.4880	0.01913
8.0000	3.0492	10.3048	2.0000	0.1204	0.0195	2.5160	0.9888	0.0195	1.4870	0.4870	0.01888
8.0000	3.0668	11.9761	2.3333	0.1201	0.0194	2.5245	0.9847	0.0194	1.4858	0.4858	0.01858
8.0000	3.0869	13.6270	2.6667	0.1198	0.0193	2.5342	0.9800	0.0193	1.4844	0.4844	0.01825
8.0000	3.1096	15.2551	3.0000	0.1194	0.0192	2.5451	0.9747	0.0192	1.4828	0.4828	0.01789
8.0000	3.1347	16.8584	3.3333	0.1189	0.0191	2.5570	0.9687	0.0191	1.4811	0.4811	0.01750
8.0000	3.1623	18.4349	3.6667	0.1185	0.0190	2.5699	0.9622	0.0190	1.4793	0.4793	0.01708
8.0000	3.1922	19.9831	4.0000	0.1179	0.0188	2.5840	0.9550	0.0188	1.4773	0.4773	0.01663
8.0000	3.2244	21.5014	4.3333	0.1174	0.0187	2.5990	0.9472	0.0187	1.4752	0.4752	0.01617
8.0000	3.2588	22.9887	4.6667	0.1168	0.0185	2.6150	0.9389	0.0185	1.4730	0.4730	0.01569
8.0000	3.2954	24.4439	5.0000	0.1161	0.0183	2.6318	0.9299	0.0183	1.4707	0.4707	0.01520
8.0000	3.3340	25.8663	5.3333	0.1154	0.0182	2.6494	0.9205	0.0182	1.4683	0.4683	0.01470
8.0000	3.3747	27.2553	5.6667	0.1147	0.0180	2.6678	0.9105	0.0180	1.4658	0.4658	0.01419
8.0000	3.4173	28.6104	6.0000	0.1140	0.0178	2.6868	0.9002	0.0178	1.4633	0.4633	0.01368
8.0000	3.4617	29.9315	6.3333	0.1132	0.0175	2.7065	0.8894	0.0175	1.4607	0.4607	0.01317
8.0000	3.5080	31.2184	6.6667	0.1124	0.0173	2.7268	0.8783	0.0173	1.4581	0.4581	0.01267
8.0000	3.5559	32.4712	7.0000	0.1115	0.0171	2.7478	0.8668	0.0171	1.4554	0.4554	0.01217
8.0000	3.6055	33.6900	7.3333	0.1107	0.0169	2.7691	0.8550	0.0169	1.4527	0.4527	0.01167
8.0000	3.6568	34.8753	7.6667	0.1098	0.0166	2.7910	0.8430	0.0166	1.4500	0.4500	0.01119
8.0000	3.7095	36.0273	8.0000	0.1089	0.0164	2.8134	0.8307	0.0164	1.4472	0.4472	0.01071

FLAT BOTTOM VEHICLE WITH SHARP CORNERS

UPWASH LIFT FORCE LU/2TJ= 0.03891

BODY WITH CIRCULAR CROSS SECTION

UPWASH LIFT FORCE LU/2TJ= 0.00970

Figure 68 - Concluded.

<u>Output Titles</u>	<u>Definitions</u>
RJH/RN	Half-velocity radius of jet measured from jet center-line
RJ/RN	Half width of jet
ALPV	Exponent of velocity profile
VJ/VN	Centerline velocity
RC/RN	Potential core radius
ALPT	Exponent of temperature profile
RJNT/RN	Half temperature radius
TM/TN	Center line temperature non-dimensionalized by nozzle temperature
TM/TA	Centerline temperature nondimensionalized by ambient temperature
DTM/DTN	$(TM-TA)/(TN-TA)$
RJHQ/RN	Half dynamic pressure radius
QJ/QN	Centerline dynamic pressure

Note: RN, VN, TN, and QN denote nozzle radius, velocity, temperature, and dynamic pressure. TA denotes ambient temperature.

Jet Deflection Region

Single jet impingement characteristics are printed.

<u>Output Titles</u>	<u>Definitions</u>
RGH/RN	Half-velocity radius of jet at ground-effect height
RG/RN	Jet half width at ground-effect height
RO/RN	Deflection zone or pressure recovery radius
VG/VN	Square root of jet ground stagnation pressure
DPS/DPTJ	Jet ground stagnation pressure nondimensionalized by nozzle stagnation pressure
TGS/TA	Stagnation temperature of incident jet at ground-effect height.
ALPG	Exponent of ground pressure distribution
R/RGH	Radial location in deflection region relative to ground stagnation point. Nondimensionalized by ground-effect half-velocity radius of jet

DPS/DPTG	Ground pressure nondimensionalized by ground stagnation pressure
R/RN	Radial location in deflection region nondimensionalized by nozzle radius
DPS/DPTJ	Ground pressure nondimensionalized by nozzle stagnation pressure

Wall Jet Region

Isolated wall jet properties are printed in this set of output.

<u>Output Titles</u>	<u>Definitions</u>
DELS/RN	Boundary layer thickness at stagnation point
VMI/VG	Inviscid maximum velocity at jet half width (RGH) radial location or start of transition to turbulent wall jet
VMI/VN	
ALPWO	Exponent of velocity profile at start of wall jet
BWOH/RN	Half velocity thickness at start of wall jet
BWO/RN	Initial thickness of wall layer
PMI/PR	Initial static pressure in wall layer
TMI/TA	Initial temperature of wall layer
(FTTOT/PR-1.)	Initial total pressure of wall layer
(TOT/TA-1.)	Initial total temperature of wall layer
R/RN	Radial location in wall jet measured from ground stagnation point
VM/VG	Maximum velocity in wall layer nondimensionalized by square root of ground stagnation pressure
VM/VN	Maximum velocity in wall layer referenced to nozzle exit velocity.
BWH/RN	Half velocity thickness of wall layer
BW/RN	Thickness of wall layer
DELBL/RN	Boundary layer thickness
DELPJ	Maximum stagnation pressure in wall layer
KDEL	Ratio of boundary layer to total wall layer thickness
TM/TN	Maximum temperature in wall layer profile
TM/TA	
BWNT/RN	Half temperature thickness of wall layer
DTM/DTN	$(TM-TA)/(TN-TA)$

TWO-JET IMPINGEMENT INTERACTION OUTPUT

Recirculation Effect on Wall Jets

Note: This set of output recomputes the wall jet properties accounting for the interaction of two hot jets.

<u>Output Titles</u>	<u>Definitions</u>
PHI	Azimuthal angle in jet-centered ground polar coordinate system
TNEFF) TAEFF)	Effective nozzle and ambient temperature ratios with recirculation effects taken into account.
R	Radial location in wall jet, measured from ground stagnation point
VM/VN	Maximum velocity in wall layer
TM/TN) TM/TA)	Maximum temperature in wall layer
DPM/DPN	$(P_M - P_A)/(P_N - P_A)$ or $(P_{M-1.})/(P_{N-1.})$
DTM/DTN	$(T_M - T_A)/(T_N - T_A)$ or $(T_{M-1.})/(T_{N-1.})$

Maximum Ground Pressures along Upwash Ground Stagnation Line

<u>Output Titles</u>	<u>Definitions</u>
XW/RN) XW/S)	Coordinate along stagnation line measured from upwash stagnation point
DPMAX/DPJ	Stagnation line pressure nondimensionalized by nozzle stagnation pressure $(P_{MAX} - P_A)/(P_N - P_A)$
PMAX/PMAXO	Stagnation line pressure nondimensionalized by upwash stagnation point pressure
DTMAX/DTJ	Stagnation line temperature nondimensionalized by nozzle stagnation temperature
TMAX/TMAXO	Stagnation line temperature nondimensionalized by upwash stagnation point temperature

Upwash Momentum Function

<u>Output Titles</u>	<u>Definitions</u>
RG/RN	Radius of jet at ground effect height
ACON	Constant in momentum function

XMOMZ Total vertical momentum in upwash sheet non-dimensionalized by the optimum value of $M_J/2\pi$

PHIO Coalescence angle used in upwash momentum model
If PHIO = 0 jets are not coalesced
If PHIO > 0 jets have begun to coalesce

Note: Depending on the value of PHIO (i.e. zero or non-zero) the constant ACON applies to the appropriate upwash momentum model.

CU Nondimensional upwash deflection region width constant

Note: There are two possible outputs that can occur at this point. If the jets are spaced far enough apart the comment:

JET AND UPWASH DEFLECTION REGIONS DO NOT
INTERACT, CU ESTIMATE IS CORRECT

In this case the value of CU is correct and the jet impingement and upwash deflection regions are independent. The perturbation parameters are then defined as:

EPS = 0.0
SIG = 1.0
PHIUO = 0.0
PHIO = 0.0
PMIN = 0.0 along upwash line
ALPUG = 1.50

If the nozzle spacing and height above ground are such that the deflection regions interact, the subroutine INTERG will be called and

CALL INTERG

will be displayed. The following output will be printed.

Note: The ground pressure distributions are computed without temperature effects.

<u>Output Titles</u>	<u>Definitions</u>
Iteration cycle	Number of iterations required to find solution using Newton's method

EPS or EPI	Perturbation parameter for jet impingement pressure distribution
SIGMA or SIG	Perturbation parameter for upwash deflection region pressure distribution
CU or CUI	Upwash width estimate prior to iterative solution
PHIUO	Angles defining the intersection of jet and upwash
PHIO	deflection regions

Note: The following values apply along the line connecting the jet stagnation points on the ground (i.e. $x = 0$).

DELPWO	Pressure at upwash stagnation point nondimensionalized by nozzle stagnation pressure
PMIN	Minimum pressure between jet and upwash deflection regions nondimensionalized by nozzle stagnation pressure
ALPUG	Exponent of upwash ground pressure distribution function
(CU) x (SIGMA)	Final value of upwash thickness constant

Note: If IPBAR = 0, the following output will occur.

Computation of Two-Jet Ground Isobar Pattern

<u>Output Titles</u>	<u>Definitions</u>
PBAR	Input values of pressure, nondimensionalized by nozzle stagnation pressures, will be echoed.

Note: The following will be repeated NU times.

<u>Output Titles</u>	<u>Definitions</u>
IJET	Number of points on jet impingement region isobar
IU	Number of points on upwash deflection region isobar

If IJET = 0 or IU = 0, the specified value of PBAR was not found in ground pressure distribution.

Note: The following coordinates are referenced to the jet stagnation point on the ground.

<u>Output Titles</u>	<u>Definitions</u>
XISOJ	X coordinate of jet isobar
YISOJ	Y coordinate of jet isobar

XISOU X coordinate upwash region isobar
 YISOU Y coordinate of upwash region isobar

The final set of output in this section is the upwash deflection zone line. If the deflection zones do not interact, ambient conditions exist along this line.

XUP X coordinate of upwash line
 YUP Y coordinate of upwash line

COMPUTATION OF UPWASH FLOW FIELD

Upwash Streamline Properties

Note: Two streamlines are printed

<u>Output Titles</u>	<u>Definitions</u>
PHID	Azimuthal angle of upwash streamline referenced to jet ground coordinate system
INV. VEL.	Inviscid turning region maximum velocity
TMI/TA	Inviscid turning region maximum temperature
DELPWJ	Maximum pressure on upwash stagnation line on the ground where upwash streamline originated
BWGH/RN	Half velocity width of incident wall jet streamline
ZOU/RN	Upwash turning region height above ground
BUO/RN	Initial upwash width
BUOHN/RN	Initial upwash half velocity width

Upwash Streamline Decay Properties

<u>Output Titles</u>	<u>Definitions</u>
Z/RN	Upwash Streamline coordinate (ZS)
VMU/VN	Upwash maximum or centerline velocity
TM/TN } TM/TA }	Upwash maximum or centerline temperature
BUH/RN	Half velocity width
BU/RN	Half width of upwash
DPU/DPJ	Upwash maximum or centerline total pressure non-dimensionalized by nozzle stagnation pressure or $(P_{MU} - P_A) / (P_N - P_A)$

Upwash Properties Computed At Z Location of Underside of Body

If $Z_B = 0$, the output will yield the upwash properties at $Z = \text{constant}$ plane above ground.

<u>Output Titles</u>	<u>Definitions</u>
ZU/RN	Upwash coordinate measured from ground plane
RW/RN	Radial coordinate from jet ground stagnation point to upwash stagnation line
PHIB	Azimuthal location of upwash streamline referenced to jet coordinate system
X/RN	X coordinate in upwash sheet or X coordinate on fuselage
VMU/VN	Maximum or centerline upwash velocity
DPU/PN	Maximum or centerline upwash total pressure nondimensionalized by nozzle stagnation pressure $(P_{MU} - P_A) / (P_N - P_A)$
BUH/RN	Half-velocity width of upwash
DPU/PUO	Upwash total pressure nondimensionalized by total pressure on streamline originating from upwash stagnation point ($X = 0, Y = 0$)
DPU/PJS	Upwash total pressure nondimensionalized by jet ground stagnation pressure
TM/TA	Maximum or centerline upwash temperature
DTSM/DTN	$(TM - TA) / (TN - TA)$
PBS/PN	Stagnation pressure on underside of fuselage placed in upwash sheet

Upwash Lift Force

Two values are printed:

FLAT BOTTOM VEHICLE WITH SHARP CORNERS

BODY WITH CIRCULAR CROSS SECTION

<u>Output Title</u>	<u>Definition</u>
LU/2TJ	Upwash lift force nondimensionalized by the total thrust of the two jets

COMPUTER PROGRAM LISTING

Figure 69 shows a Fortran listing of the computer program

FOR QUALITY

```

C*****JET00010
C
C   VTOL TWO-JET IMPINGEMENT INTERACTION COMPUTER PROGRAM   JET00020
C   FOR CLOSELY SPACED JETS                                   JET00030
C   BY M.J.SICLARI                                           JET00040
C   516 575-2207                                             JET00050
C   GRUMMAN AEROSPACE CORPORATION                            JET00060
C   BETHPAGE,NEW YORK 11714                                  JET00070
C   JET00080
C   JET00090
C*****JET00100
C
C   PROGRAM GRUMHOT2                                         JET00110
C   JET00120
C   JET00130
C   REAL KDELFD,KDELO,NFD,NO,N,KDEL                           JET00140
C   REAL MACH,NPR,NTR                                         JET00150
C   COMMON/WALL/DELS,NO,KDELO,ALFG,ALPWO,ALPWF,RO,RGH,VG,BWMO JET00160
C   COMMON/WALL/ TLAMI,BELPS,DELTSR,PSBAR                     JET00170
C   COMMON/NOZZLE/NPR,NTR,TN,GAM,MACH,ACHS,TAEFF,TNEFF       JET00180
C   COMMON/JET/SD,KGU                                         JET00190
C   COMMON/HEIGHT/ HD,IPBAR                                    JET00200
C   FETAMB(ETA,A)=ETA-(4./(A+1.))*ETA**(A+1.)+(6./(2.*A+1.))*ETA**(2.* JET00210
C   IA+1.)-(4./(3.*A+1.))*ETA**(3.*A+1.)+(1./(4.*A+1.))*ETA**(4.*A+1.) JET00220
C   JET00230
C   BODY SHAPE FUNCTIONS FOR FORCE PREDICTION                 JET00240
C   W2...HALF-WIDTH IN NOZZLE RADII                           JET00250
C   ZBODY...HALF DEPTH IN NOZZLE RADII                       JET00260
C   DZDXB...AXIAL SLOPES                                     JET00270
C   THNOSE...NOSE ANGLE OF PARABOLIC BODY                   JET00280
C   JET00290
C   JET00300
C   PARABOLIC BODY WITH CONSTANT CROSS SECTIONAL SHAPE     JET00310
C   JET00320
C   W2(XB)=.5*TAN(THNOSE)*(XL2**2-XR**2)/XL2                  JET00330
C   ZBODY(XB)=.5*TAN(THNOSE)*(XL2**2-XR**2)/XL2             JET00340
C   DZDXB(XB)=TAN(THNOSE)*XB/XL2                             JET00350
C   JET00360
C   CYLINDRICAL BODY WITH CONSTANT CROSS SECTIONAL SHAPE   JET00370
C   JET00380
C   W2(XB)=WCON                                               JET00390
C   ZBODY(XB)=ZCON                                             JET00400
C   DZDXB(XB)=ZSCON                                           JET00410
C   JET00420
C   CYLINDRICAL BODY PARAMETERS IN TERMS OF NOZZLE DIAMTERS JET00430
C   JET00440
C   JET00450
C   ZSCON=0.0                                                 JET00460
C   THNOSE=14.0362*PI/180.                                    JET00470
C   JET00480
C   CIRCULAR CROSS SECTION                                    JET00490
C   POINT OF FLOW SEPARATION                                  JET00500
C   JET00510
C   PI=3.14159265                                             JET00520
C   GAM=1.4                                                    JET00530
C   FHISEP=135.*PI/180.                                       JET00540
C   READ (5,1) NPR,NTR                                         JET00550
C   READ (5,1) HD,SD,ZPLD,DZPL,ZFINAL                          JET00560
C   1 FORMAT (5F10.5)                                           JET00570
C   READ (5,1) XL2,WCON,ZCON                                    JET00580
C   WRITE (6,21)                                                JET00590
C   21 FORMAT ('1',///30X,'*** INPUT PARAMETERS ***'//)       JET00600
C   MACH=SQRT(2.*(NPR-1.)/GAM)                                  JET00610
C   TN=NTR                                                       JET00620
C   WRITE (6,17) NPR,NTR                                         JET00630
C   17 FORMAT (20X,'NPR=',F8.4,2X,'NTR=',F8.4)                JET00640
C   WRITE (6,27) MACH,TN                                         JET00650
C   27 FORMAT (20X,'MACH NO.=',F10.4,2X,'TN/TA=',F10.4)      JET00660
C   WRITE (6,9) HD,SD,ZPLD                                       JET00670
C   9 FORMAT (20X,'H/D=',F10.5,2X,'S/D=',F10.5,2X,'Z/D=',F10.5) JET00680
C   WRITE (6,907) ZPLD,DZPL,ZFINAL                               JET00690
R81-1622-064D(30 Sheets)

```

Figure 69 Program FORTRAN Listing

ORIGINAL FILE IS
OF POOR QUALITY

```

907 FORMAT (/20X,'Z/D=',F10.5,2X,'DZ/D=',F10.5,2X,'ZFINAL/D=',F10.5/) JET00700
      WRITE (6,908) XL2,MCON,ZCON JET00710
908 FORMAT (/20X,'BODY LENGTH L/D=',F10.5,2X,'WIDTH W/D=',F10.5,2X,'DE JET00720
      IFTH ZB/D=',F10.5/) JET00730
      ZPLANE=2.#ZPLD JET00740
C JET00750
C COMPUTE JET STANDOFF DISTANCE AND EFFECTIVE JET DECAY HEIGHT JET00760
C (GIRALT ET AL) JET00770
C JET00780
      IF (MD.LE.6.8) DELG=0.153*7.8 JET00790
      IF (MD.GT.6.8) DELG=0.153*(1.+MD) JET00800
      ZEND=(MD-.50*DELG)*2. JET00810
      WRITE (6,22) JET00820
22 FORMAT (///30X,'***** JET DECAY REGION *****') JET00830
      WRITE (6,7) DELG JET00840
      7 FORMAT (10X,'JET DEFLECTION HEIGHT DELG/D =',F10.5) JET00850
C JET00860
C COMPUTE JET DECAY JET00870
C JET00880
C ALL DIMENSIONS NONDIMENSIONALIZED BY NOZZLE RADIUS JET00890
C JET00900
C SET EMPIRICAL CONSTANTS FOR HALF-WIDTH BEHAVIOR AND LENGTH OF JET00910
C POTENTIAL CORE (HRYCAN,ET AL) JET00920
C JET00930
      A2=.040 JET00940
      B2=.800 JET00950
      FM=1. JET00960
      A3=.09*(1.+ALOG(2./(1.+1./TN*.5)))*(1.0-.16*FM*MACH) JET00970
      B3=0. JET00980
      ZPCO=8.55 JET00990
      FM=0.0 JET01000
      ZPC=.5*ZPCO*(1.+1./(TN*.75))*(1.0+.16*FM*MACH) JET01010
      A1=A2+(B2-1.)/ZPC JET01020
      ZFD=B2/(A3-A2) JET01030
      ALPFD=1.5 JET01040
      WRITE (6,23) ZPC,ZFD JET01050
23 FORMAT (10X,'ZPC/RN=',F10.5,2X,'ZFD/RN=',F10.5) JET01060
      WRITE (6,12) JET01070
12 FORMAT (///3X,'Z/RN',3X,'RJH/RN',3X,'RJ/RN',2X,'ALPV',4X,'UJ/UN',4X JET01080
      ,',RC/RN',3X,'ALPT',3X,'RJHT/RN',2X,'TM/TN',2X,'TM/TA',4X,'DTM/DTN' JET01090
      ,',2X,'RJHD/RN',2X,'QJ/ON') JET01100
C JET01110
C REGION I...POTENTIAL CORE REGION OF JET.. JET01120
C JET01130
      NJPC=5 JET01140
      DNPC=NJPC-1 JET01150
      IF (ZEND.GE.ZPC) DZPC=ZPC/DNPC JET01160
      IF (ZEND.LT.ZPC) DZFC=ZEND/DNPC JET01170
      Z=0. JET01180
      DO 100 I=1,NJPC JET01190
      IF (I.EQ.1) GO TO 102 JET01200
      GO TO 103 JET01210
102 UJ=1. JET01220
      RJH=1. JET01230
      RJHT=1. JET01240
      RJ=1. JET01250
      ALPVC=0. JET01260
      ALPTC=1.5 JET01270
      CV2=.5 JET01280
      RJPC=1. JET01290
      TM=1. JET01300
      DELFMN=1. JET01310
      THB=TN JET01320
      DELTMN=1.0 JET01330
      KC=1. JET01340
      RJHQ=1. JET01350
      GO TO 104 JET01360
103 ETAC=1.-Z/ZPC JET01370
      RJH=A1*Z+1. JET01380
      CALL JETFCY (TN,ETAC,RJH,ALPVC,TLAM,CV2,CT,RV,RT) JET01390
      TLAMPC=TLAM JET01400
      RJ=5JH/KV JET01410
      RJHT=TLAM*RJH JET01420
      TM=1. JET01430
      THB=TN JET01440
      DELTMN=1. JET01450
      DELFMN=1. JET01460

```

Figure 69 - Continued

ORIGINAL RESULTS
OF PROGRAM QUALITY

```

RJPC=RJ
RJHTPC=RJHT
VJ=1.
RC=ETAC#RJ
ALPTC=ALPVC
CALL QHALF (TMB,ETAC,ALPVC,TLAM,RQ)
RJHQ=RJ#RQ
VQ=1.
TQ=1.
THSTAG=THB+VJ#VJ*(NTR-TN)
DTSTAG=(THSTAG-1.)/(NTR-1.)
104 WRITE (6,11) Z,RJH,RJ,ALPVC,VJ,RC,ALPTC,RJHT,TM,TMB,DELTMN,RJHQ,
1 DELPMN
11 FORMAT (1X,4(F7.4,1X),6(F7.4,1X),4(F8.4,1X))
Z=Z+DZPC
100 CONTINUE
C
C TRANSITION REGION II AND FULLY DEVELOPED REGION OF JET
C
IF (ZEND.LE.ZPC) GO TO 998
NJFD=25
DNFD=NJFD-1
ALPVPD=1.5
ALPTFD=1.50
TLAMFD=1.+1.185*TN**5
RCON=(2.-SQRT(2.))/2.
RVFD=RCON**1./ALPVPD
RJFD=(A3#ZFD+B3)/RVFD
RTFD=RVFD
RJHTFD=TLAMFD*(A3+ZFD+B3)
DZ=(ZEND-ZPC)/DNFD
Z=ZPC+DZ
DO 200 I=2,NJFD
IF (Z.GT.ZFD) GO TO 201
RJ=RJPC+(RJFD-RJPC)/(ZFD-ZPC)*(Z-ZPC)
RJM=A2#Z+B2
RV=RJM/RJ
ALPV=ALOG(RCON)/ALOG(RV)
ALPT=ALPV
TLAM=TLAMFC+((TLAMFD-TLAMPC)/(ZFD-ZPC))*(Z-ZPC)
GO TO 202
201 ALPV=ALPVPD
ALPT=ALPTFD
RJM=A3#Z+B3
TLAM=TLAMFD
202 CALL VTSOLV(TN,RJM,ALPV,TLAM,VJ,TM,RV,RT)
RJ=RJM/RV
RJHT=TLAM#RJM
TMB=TH#TN
IF (ABS(TN-1.).LT.1.E-5) DELTMN=1.0
IF (ABS(TN-1.).GT.1.E-5) DELTMN=(TMB-1.)/(TN-1.)
DELPMN=VJ#VJ/TM
CALL QHALF (TMB,O.,ALPV,TLAM,RQ)
RJHQ=RQ#RJ
TQ=TM
VQ=VJ
THSTAG=TMB+VJ#VJ*(NTR-TN)
DTSTAG=(THSTAG-1.)/(NTR-1.)
WRITE (6,11) Z,RJH,RJ,ALPV,VJ,RC,ALPT,RJHT,TM,TMB,DELTMN,RJHQ,
1,DELPMN
Z=Z+DZ
200 CONTINUE
C
C JET DEFLECTION REGION
C JET IMPINGEMENT PRESSURES
C
998 AQCON=-.032026
BQCON=.3354248
CQCON=2.8
IF (MD.GT.3.) AQ=3.6
AQSLH=(3.6-2.9)/(3.-1.2)
IF (MD.LE.3.) AQ=2.9+AQSLH*(MD-1.2)
WRITE (6,79)
79 FORMAT (///30X,'***** JET DEFLECTION REGION *****')
80 FORMAT (10X,'RG/RN=',F10.5,2X,'RG/RN=',F10.5,2X,'PO/RN=',F10.5,2X,
1,'VO/VN=',F10.5/)
C
JET01470
JET01480
JET01490
JET01500
JET01510
JET01520
JET01530
JET01540
JET01550
JET01560
JET01570
JET01580
JET01590
JET01600
JET01610
JET01620
JET01630
JET01640
JET01650
JET01660
JET01670
JET01680
JET01690
JET01700
JET01710
JET01720
JET01730
JET01740
JET01750
JET01760
JET01770
JET01780
JET01790
JET01800
JET01810
JET01820
JET01830
JET01840
JET01850
JET01860
JET01870
JET01880
JET01890
JET01900
JET01910
JET01920
JET01930
JET01940
JET01950
JET01960
JET01970
JET01980
JET01990
JET02000
JET02010
JET02020
JET02030
JET02040
JET02050
JET02060
JET02070
JET02080
JET02090
JET02100
JET02110
JET02120
JET02130
JET02140
JET02150
JET02160
JET02170
JET02180
JET02190
JET02200
JET02210
JET02220
JET02230

```

Figure 69 - Continued

ORIGINAL PAGE IS
OF POOR QUALITY

```

C SET CHARACTERISTIC SCALE LENGTHS FOR IMPINGEMENT REGION
C
  RGH=RJH
  RO=RJ
  RO=AD*RGH
  ETAWG=RGH/RO
  IF (2.*HD.LE.ZPC) GO TO 454
C
C DETERMINE STAGNATION POINT PRESSURE
C
454 WRITE (6,80) RGH,RO,RO,VG
C
C STAGNATION PRESSURE NONDIMENSIONALIZED BY JET TOTAL PRESSURE
C
  ROU=RO
  DELPS=(VG**2)/TG
  PSBAR=1.+DELPS*(NPR-1.)
  ACHS=SQRT(2.*(PSBAR-1.)/GAM)
  TGS=TG*TN
  TGDS=TGS*(NTR-TN)*VG*VG
  WRITE (6,81) DELPS,TGDS
81 FORMAT (10X,'STAGNATION PRESSURE, DPS/DPTJ=',F10.5,2X,2X,'GROUND MACH. TEMP., TGS/TA=',F10.5)
  WRITE (6,801) ACHS
801 FORMAT (/10X,'STAGNATION MACH NUMBER OF JET=',F10.5/)
  CALL QPREST(RO,VG,TD,ALPO,R,CU2)
  WRITE (6,82) ALPO
82 FORMAT (10X,'ALPO=',F10.5)
  NG=25
  RNGH=NG-1
  DR=RO/(RNGH*RGH)
  DETA=1./(RNGH)
  ETA=0.
  R=0.
  WRITE (6,83)
83 FORMAT (30X,'SINGLE JET GROUND PRESSURES'//25X,'R/ROH',6X,'DPS/DPTJ',10X,'R/RN',7X,'DPS/DPTJ'//)
  DO 300 I=1,NG
  DPTG=(1.-ETA**ALPO)**4.
  DPTJ=DPTG*DELPS
  RRN=R*ROH
  WRITE (6,84) R,DPTG,RRN,DPTJ
84 FORMAT (20X,4(F10.5,5X))
  R=R+DR
  ETA=ETA+DETA
300 CONTINUE
C
C INITIALIZE WALL JET REGION
C
  AWJ=.09*(1.+ALPO*(2./(1.+1./TN**5)))*(.1-.16*ACHS)
  TLMFD=1.+1.85*TH**5
  ALPWF=1.5
  KDELFD=.0942
  ALPUG=1.5
  NFD=7.
  CALL SIMW(KDELFD,NFD,ALPWF,RATW,CSV2W,CPW)
  CALL SIMUG(ALPUG,RATUG,CSPUG)
  CU=2.*AWJ*CSV2W/(RATW*CSPUG)
  AS1=.015438
  AS2=.128035
  DELS=2.*AS1*(HD)**AS2
  WRITE (6,26)
26 FORMAT (//30X,'***** WALL JET REGION *****//')
  WRITE (6,86) DELS
86 FORMAT (5X,'STAGNATION POINT BOUNDARY LAYER THICKNESS, DELS/RN=',F10.5)
  NO=14
  KDELO=DELS/(2.*DELO)
  FETAO=(1.-ETAWG**ALPO)**4
  PMBI=1.+(NPR-1.)*DELS*FETAO
  DELPS=(NPR-1.)*DELS
  ACHI=SQRT(2.*(PSBAR/PMBI-1.)/GAM)
  TMBI=TGDS
  VMI=(ACHI/MACH)*SQRT(TMBI/TN)
  DELTSB=DELS-1.0
  WRITE (6,89) PMBI,DELPSE,DELTSB

```

Figure 69 - Continued

ORIGINAL PAGE IS
OF POOR QUALITY

```

89 FORMAT (1X,'PMI/PA=' ,F10.5,2X,'(PTTOT/PA-1.)=' ,F10.5,2X,'(TOT/TA-
11.)=' ,F10.5) JET03000
WRITE (6,92) TMI,VMI JET03010
92 FORMAT (2X,'TMI/TA=' ,F10.5,2X,'VMI/UN=' ,F10.5) JET03020
TMI=TMI/TN JET03030
CALL GNATT(TN,RGH,DELPS,PMI,TMI,VMI,ALPG,KDELO,NO,ETAWG,DELS,
1ALPWO,R,BWO,BWO,TLAMI) JET03040
RATWO=R JET03050
DELSM=BWO*KDELO JET03060
UMG1=VMI/UG JET03070
WRITE (6,91) UMG1 JET03080
91 FORMAT (5X,'VELOCITY AT START OF TURBULENT WALL JET, VM/UG=' ,F10.5) JET03090
1) JET03100
C WRITE (6,87) TLAMFD JET03110
87 FORMAT (5X,'TLAMFD=' ,F10.5) JET03120
WRITE (6,85) ALPWO,BWO,BWO JET03130
85 FORMAT (10X,'START OF WALL JET REGION, ALPWO=' ,F10.5,2X,'BWO/RN='
1,F10.5,2X,'BWO/RN=' ,F10.5) JET03140
JET03150
C JET03160
C MAXIMUM VELOCITY DISTRIBUTION IN DEFLECTION REGION JET03170
C JET03180
C JET03190
NMPT=25 JET03200
XNMPT=NMPT-1 JET03210
REND=2850 JET03220
BR=REND/XNMPT JET03230
BW3HO=AM3R0 JET03240
DELRH=(BW3HO-BWO)/(RO-RGH) JET03250
DELR=(NFD-NG)/(RO-RGH) JET03260
DELAR=(ALPWF-ALPWO)/(RO-RGH) JET03270
ADELBT=.0175 JET03280
ADELBL=(ADELBT*(RO-2.))-DELS/(RO-RGH) JET03290
R=0. JET03300
TLANSL=(TLAMFD-TLAMI)/(RO-RGH) JET03310
WRITE (6,107) JET03320
107 FORMAT(//40X,'ISOLATED WALL JET PROPERTIES'//) JET03330
WRITE (6,97) JET03340
97 FORMAT (//5X,'R/RN',5X,'VM/UG',5X,'UM/UN',5X,'BWH/RN',3X,
1'BW/RN',3X,'DELBL/PN',3X,'DELPJ',3X,'KDEL',3X'TM/TN'
2,1X,'TN/TA',1X,'BWH/FN',1X,'DTM/DTN'//) JET03350
DO 400 I=1,NMPT JET03360
IF (R.GE.RGH) TLAN=TLAMI+TLANSL*(R-RGH) JET03370
IF (R.LT.RGH) TLAN=TLAMI JET03380
IF (R.LE.R0) FETA=(1.-(R/R0)**ALPG)**4 JET03390
IF (R.GT.R0) FETA=0.0 JET03400
IF (R.GT.R0) TLAN=TLAMFD JET03410
PHB=1.+(NPR-1.)*DELPJ*FETA JET03420
IF (R.GT.RGH) GO TO 402 JET03430
ACH=SQRT(2.*(PSBAR/PHB-1.)/OAM) JET03440
TMB=TOBS JET03450
VMN=(ACH/HACH)*SQRT(TMB/TN) JET03460
TM=TMB/TN JET03470
DELPJ=DELPJ JET03480
DELTA=KDELO*BWO JET03490
N=14 JET03500
KDEL=KDELO JET03510
BW=BWO JET03520
BWH=RATWO*BWO JET03530
UMG=VMN/UG JET03540
BWH=TLAMI*BWH JET03550
DELTN=(TMB-1.)/(TN-1.) JET03560
TMSTAG=TMB+VMN*VMN*(NTR-TN) JET03570
DTSTAG=(TMSTAG-1.)/(NTR-1.) JET03580
GO TO 401 JET03590
402 IF (R.GT.R0) GO TO 403 JET03600
BWH=BWO+DELRH*(R-RGH) JET03610
ALPW=ALPWO+DELAR*(R-RGH) JET03620
DELBL=DELS+ADELBL*(R-RGH) JET03630
N=NO+DELR*(R-RGH) JET03640
GO TO 405 JET03650
403 BWH=AM3R JET03660
DELBL=ADELBT*(R-2.) JET03670
N=NFD JET03680
ALPW=ALPWF JET03690
JET03700
JET03710
JET03720

```

Figure 69 - Continued

ORIGINAL PAGE IS
OF POOR QUALITY

```

405 ALAM=((2.-SQRT(2.))/2.)**(1./ALPW) JET03730
KDEL=DELBL/(DELBL+(BWH-DELBL)/ALAM) JET03740
IF (R.LE.4.) FVIS=1.0 JET03750
IF (R.GT.4.) FVIS=1./(R/4.)*.24 JET03760
FMOM=1.-FETA JET03770
DELFM=DELP*FETA JET03780
TAEFF=1. JET03790
TNEFF=TN JET03800
CALL VTWALL (R,BWH,FVIS,FMOM,DELFM,TN,TLAM,PMB,KDEL,N,ALPW, JET03810
1,UMN,TN,TNEFF,TAEFF) JET03820
UMG=UMN/UG JET03830
DELPJ=(PMB-1.)/(NPR-1.)*PMB*UMN*UMN/TN JET03840
RCON=(2.-SQRT(2.))/2. JET03850
RAT=KDEL*(1.-FDEL)*RCON*(1./ALPW) JET03860
BU=BWH/RAT JET03870
DELTA=KDEL*BW JET03880
TMB=TM*TN JET03890
BWHT=TLAM*BWH JET03900
DELTM=(TMB-1.)/(TN-1.) JET03910
THSTAG=TMB+UMN*UMN*(NTR-TN) JET03920
DTSTAG=(THSTAG-1.)/(NTR-1.) JET03930
401 WRITE (6,95) R,UMG,UMN,BWH,BW,DELTA,DELPJ,KDEL,TN,TMB JET03940
1,BWHT,DELTM JET03950
R-R+DR JET03960
95 FORMAT (1X,5(F8.4,2X),8(F7.4,1X)) JET03970
400 CONTINUE JET03980
C JET03990
C UPWASH GROUND MAXIMUM PRESSURE DISTRIBUTION JET04000
C JET04010
C WRITE (6,24) JET04020
24 FORMAT (///30X,'***** TWO-JET INTERACTION PROBLEM *****'//JET04030
1//) JET04040
C JET04050
C WALL JET RECIRCULATION EFFECTS JET04060
C JET04070
IRAY=5 JET04080
AREC=1. JET04090
OMEG=(TGRS-1.)*(RG/SD)**AREC JET04100
IF (RG.GT.SD) OMEG=TGRS-1. JET04110
DRAY=IRAY-1 JET04120
DPHI=PI/DRAY JET04130
PHI=0. JET04140
WRITE (6,710) JET04150
710 FORMAT (//30X,'*** RECIRCULATION EFFECT ON WALL JETS ***'//) JET04160
DO 750 I=1,IRAY JET04170
PHID=PHI*180./PI JET04180
WRITE (6,711) PHID JET04190
711 FORMAT (/50X,'PHI=',F8.4,' DEGS.'/) JET04200
CPHI=COS(.5*PHI) JET04210
TAEFF=1.+OMEG*CPHI*CPHI JET04220
TNEFF=TN*(TAEFF-1.)*(TGRS-TN)/(TGRS-1.) JET04230
WRITE (6,740) TNEFF,TAEFF JET04240
740 FORMAT (/40X,'TNEFF=',F10.5,2X,'TAEFF=',F10.5/) JET04250
IF (PHI.GE..5*PI) GO TO 701 JET04260
XW=SD*TAN(PHI) JET04270
RW=SQRT(XW**2+SD**2) JET04280
IF (RW.GT.2.*SD) RW=2.*SD JET04290
GO TO 702 JET04300
701 RW=2.*SD JET04310
702 NUPT=25 JET04320
XNUPT=NUPT-1 JET04330
DR=RW/XNUPT JET04340
R=0. JET04350
WRITE (6,713) JET04360
713 FORMAT (/37X,'R',7X,'UM/UN',7X,'TM/TN',7X,'TM/TA',7X,'DPH/DPN',5X, JET04370
1'DTH/DTN'//) JET04380
DO 703 IR=1,NUPT JET04390
CALL WALLJT (R,UMN,BWH,DELPW,TN,TMB,PMB,DELTMN,DTSTAG) JET04400
WRITE (6,704) R,UMN,TN,TMB,DELPW,DTSTAG JET04410
704 FORMAT (30X,6(F10.5,2X)) JET04420
R-R+DR JET04430
703 CONTINUE JET04440
PHI=PHI+DPHI JET04450
750 CONTINUE JET04460
WRITE (6,460) JET04470

```

Figure 69 - Continued

ORIGINAL PAGE IS
OF POOR QUALITY

```

460 FORMAT (//5X,'MAXIMUM GROUND PRESSURE AND TEMPERATURE ALONG UPWASH',JET04480
16ROUND STAGNATION LINE'//) JET04490
WRITE (6,470) JET04500
470 FORMAT (14X,'XV/RN',6X,'XU/S',6X,'DPHAX/DFJ',3X,'FMAX/FMAX0',3X,'DJ',JET04510
1THAX/DTJ',3X,'TMAX/TMAX0'//) JET04520
PHI=0. JET04530
PHIN=80.*PI/180. JET04540
DFNI=PHIN/24. JET04550
DO 450 IL=1,25 JET04560
XM=SD*TAN(PHI) JET04570
RM=SQRT(XM**2+SD**2) JET04580
XMS=XM/(2.*SD) JET04590
CPHI2=COS(.5*PHI) JET04600
TAEFF=1.+OMEGA*CPHI2*CPHI2 JET04610
TNEFF=TN+(TAEFF-1.)*(TGPS-TN)/(TGSS-1.) JET04620
CALL WALLJT (RM,VHN,BWN,DELP,TH,TND,PND,DELTMN,DTSTAG) JET04630
PMAXB=(PMB-1.)/(HPR-1.)*PMB+VHN*VHN*COS(PHI)*COS(PHI)/TM JET04640
TSG=TND+(NTR-TN)*VHN*VHN*COS(PHI)*COS(PHI) JET04650
THAXG=(TSG-1.)/(NTR-1.) JET04660
IF (IL.EQ.1) DELPND=PMAXB JET04670
IF (IL.EQ.1) DELTWO=THAXG JET04680
PHAXND=PMAXB/DELPND JET04690
THAXND=THAXG/DELTWO JET04700
WRITE (6,455) XM,XMS,PHAXG,PHAXND,THAXG,THAXND JET04710
455 FORMAT (10X,B(F10.5,2X)) JET04720
PHI=PHI+DPHI JET04730
450 CONTINUE JET04740
ACON=1.-(RG/SD)**2 JET04750
PHIOD=0. JET04760
IF (ACON.GE.0.) PHIO=0.0 JET04770
IF (ACON.GE.0.) GO TO 667 JET04780
PHIO=ARCOS((SD/RG)**.20) JET04790
PHIOD=PHIO*180./PI JET04800
ACON=2./(SIN(.5*PI-PHIO)**2) JET04810
XMONZ=ACON*(1.0+SIN(PHIO))*(SIN(PHIO)-2.0)/3. JET04820
GO TO 668 JET04830
667 XMONZ=ACON+2.*(1.-ACON)/3. JET04840
668 WRITE (6,553) JET04850
553 FORMAT (//5X,'UPWASH MOMENTUM FUNCTION; JET RADIUS; INTERACTION JET04860
1CONSTANT, VERTICAL UPWASH SHEET MOMENTUM, AND COALESCENCE ANGLE'//)JET04870
WRITE (6,551) RG,ACON,XMONZ,PHIOD JET04880
551 FORMAT (15X,'RG/RN=',F10.5,2X,'ACON=',F10.5,2X,'XMONZ=',F10.5,2X,' JET04890
1PHIO(DEGS)=',F10.5//)
CPHI2=1. JET04900
TAEFF=1.+OMEGA*CPHI2*CPHI2 JET04910
TNEFF=TN+(TAEFF-1.)*(TGSS-TN)/(TGSS-1.) JET04920
CALL WALLJT(SD,VHN,BWN,DELP,TH,TND,PND,DELTMN,DTSTAG) JET04930
CALL PGUMAT(CU,DELP,DELPH,RO,SD,ALPG,ALFUG) JET04940
CALL SIMM(KD,LF,NFD,ALPWF,RATW,CSV2W,CFW) JET04950
CALL SIUG(ALPUG,RATUG,CSUG) JET04960
CU=2.*AW3*CSV2W/(RATW*CSFUG) JET04970
WRITE (6,557) CU JET04980
557 FORMAT (25X,'UPWASH WIDTH CONSTANT ESTIMATE , CU=',F10.5) JET05000
READ (5,661) IPBAR JET05010
661 FORMAT (I1) JET05020
C JET05030
C TEST FOR INTERACTION OF DEFLECTION REGIONS JET05040
C " JET05050
C IF (CU*SD+RO.LE.SD) GO TO 222 JET05060
C " JET05070
C COMPUTATION OF DEFLECTION REGION INTERACTION JET05080
C CALL INTERG(XMONZ,DELP,SD,RO,ALPG,EPS,CU,SIG) JET05090
C JET05100
C GO TO 223 JET05110
222 EPS=0.0 JET05120
SIG=1.0 JET05130
PHIU0=0. JET05140
PHIO=0.0 JET05150
WRITE (6,28) EPS,SIG,PHIU0,PHIO JET05160
28 FORMAT (//20X,'JET AND UPWASH DEFLECTION REGIONS DO NOT INTERACT, JET05180
1 CU ESTIMATE IS CORRECT'//)JET05190
1/35X,'EPS=',F10.5,2X,'SIG=',F10.5,2X,'PHIU0=',F10.5,2X,'PHIO=',F10.5,2X, JET05200
1.5) JET05210
WRITE (6,28) ALPUG JET05220

```

Figure 69 - Continued

ORIGINAL
OF POOR QUALITY

```

29 FORMAT (30X,'PHI=0.0 ALONG UPWASH LINE. ALPH= ',F8.4,' IN UPWASH REFLECTION REGION')
IF (IFRAR.NE.0) CALL GPLOT (ALPG,DELPS,SD,RO,EPS,CU,SIG,PHIU,PHIG)
1)
C
C
223 WRITE (6,111)
111 FORMAT (//30X,'***** COMPUTATION OF UPWASH FLOW FIELD *****')
WRITE (6,112)
112 FORMAT (//35X,'COMPUTATION OF UPWASH STREAMLINE PROPERTIES')
PHI=0.0
PHI=0.0
111 FORMAT (//30X,'PHI= ',F8.4,' DEGS')
DO 600 I=1,2
PHI=PHI*180./PI
WRITE (6,114) PHI
ZEND=ZPLANE/COS(PHI)
Y=SD*TAN(PHI)
RW=SQRT(SD**2+Y**2)
IF (RW.LE.RD) RMH=BMH0+DELBRH*(RW-RD)
IF (RW.GT.RD) RMH=AM3*RW
CPHI2=COS(.5*PHI)
TAEFF=1.+OMEGA*CPHI2*CPHI2
TNEFF=TN+(TAEFF-1.)*(TGRS-TN)/(TGRS-1.)
CALL WALLJT(RW,VHN,RWHG,DELPWS,TH,TMB,PHB,DELTMN,DELTWS)
IWR=1
CALL UPWASH(RD,RW,PHI,ZEND,RWHG,DELPS,DELPWS,DELTWS,VUN,DELPJ,
1,TH,TMB,DELTMN,DTSTAG,BUH,ZOUS,IWR)
PHI=PHI+DFHI
600 CONTINUE
MUPT=25
XMUPT=MUPT-1
ALFU=1.5
C
C
C CIRCULAR CYLINDER DRAG FUNCTION
C
DRAG=SIN(PHISEP)*(1.-(4./3.)*(SIN(PHISEP)**2))
DO 700 J=1,23
SUMF=0.0
SUMFC=0.0
XB=0.
DXB=XL2/XMUPT
WRITE (6,116)
116 FORMAT (////30X,'UPWASH PROPERTIES COMPUTED AT Z LOCATION OF UNDERSIDE OF BODY')
WRITE (6,118) ZPLANE
118 FORMAT (/35X,'BODY CENTERLINE LOCATION AT Z/RN= ',F10.5//)
WRITE (6,78)
78 FORMAT (//1X,'ZU/RN',5X,'RW/RN',5X,'PHIB',5X,'X/RN',5X,'VHU/VH',
13X,'DPU/PN',4X,'BUH/RN',2X,'DPU/PUO',1X,'DPU/PJS',3X,'TH/TA',3X,'DTSM/DTN',1X,'PWS/PN')
IWR=0
DO 500 I=1,MUPT
FACT=2.0
IF (I.EQ.1) FACT=1.0
IF (I.EQ.MUPT) FACT=1.
ZB=ZBODY(XB)
PHIB=ATAN(XB/(SD+ZPLANE-ZB))
XW=SD*TAN(PHIB)
RW=SQRT(SD**2+XW**2)
CPHI2=COS(.5*PHIB)
TAEFF=1.+OMEGA*CPHI2*CPHI2
TNEFF=TN+(TAEFF-1.)*(TGRS-TN)/(TGRS-1.)
CALL WALLJT(RW,VHN,RWHG,DELPWS,TH,TMB,PHB,DELTMN,DELTWS)
ZU=ZPLANE-ZB
ZEND=ZU/COS(PHIB)
CALL UPWASH (RD,RW,PHIB,ZEND,RWHG,DELPS,DELPWS,DELTWS,VUN,
1DELPJ,TH,TMB,DELTMN,DTSTAG,BUH,ZOUS,IWR)
THETB=ATAN(DZDXB(XB))
ETAUB=W2(XB)/(3.6*BUH)
IF (ETAUB.GT.1.) ETAUB=1.
FB=FETAUB(ETAUB,ALFU)
DCYL=W2(XB)*DRAG
DFLAT=3.6*BUH*FB
SUMF=SUMF+.5*DXB*FACT*DFLAT*(VUN**2)*(COS(PHIB+THETB)**2)/TH
JET05230
JET05240
JET05250
JET05260
JET05270
JET05280
JET05290
JET05300
JET05310
JET05320
JET05330
JET05340
JET05350
JET05360
JET05370
JET05380
JET05390
JET05400
JET05410
JET05420
JET05430
JET05440
JET05450
JET05460
JET05470
JET05480
JET05490
JET05500
JET05510
JET05520
JET05530
JET05540
JET05550
JET05560
JET05570
JET05580
JET05590
JET05600
JET05610
JET05620
JET05630
JET05640
JET05650
JET05660
JET05670
JET05680
JET05690
JET05700
JET05710
JET05720
JET05730
JET05740
JET05750
JET05760
JET05770
JET05780
JET05790
JET05800
JET05810
JET05820
JET05830
JET05840
JET05850
JET05860
JET05870
JET05880
JET05890
JET05900
JET05910
JET05920
JET05930
JET05940
JET05950
JET05960
JET05970
JET05980

```

Figure 69 - Continued

ORIGINAL SOURCE
OF PROGRAMS

```

SUMFC=SUMFC+.5*DX*FACT*DCYL*(VUN**2)*(COS(PHIB+THETB)**2)/TM      JET05990
ZOU=ZOUS*COS(PHIB)                                                JET06000
PHIB=PHIB*180./PI                                                JET06010
IF (ABS(PHIB).LT.1.E-4) DELPH=DELUJ                               JET06020
IF (DELPH.NE.0.) DELPB=DELUJ/DELPH                                JET06030
IF (DELPH.EQ.0.) DELPB=DELUJ                                       JET06040
DELPUS=DELUJ/DELPS                                               JET06050
PRS=((VUN*COS(PHIB+THETB)**2)/TM)                                  JET06060
WRITE (6,77) ZU,RM,PHIB,XB,VUN,DELUJ,BUN,DELPB,DELPUS,THB,DTSTAB JET06070
1PDS                                                                JET06080
77 FORMAT (1X,11(F8.4,1.),F8.5)                                    JET06090
XB=XB+DXR                                                         JET06100
500 CONTINUE                                                       JET06110
C                                                                      JET06120
C FLAT BOTTOM LIFT FORCE                                           JET06130
C                                                                      JET06140
XLUT=(1./PI)*SUMF                                                JET06150
WRITE (6,77B)                                                       JET06160
77B FORMAT (//30X,'FLAT BOTTOM VEHICLE WITH SHARP CORNERS//')    JET06170
WRITE (6,771) XLUT                                                 JET06180
771 FORMAT (33X,'UPWASH LIFT FORCE',5X,'LU/2TJ=',F10.5//)        JET06190
C                                                                      JET06200
C UPWASH LIFT FORCE FOR CIRCULAR CROSS SECTION                    JET06210
C                                                                      JET06220
XLUT=(1./PI)*SUMFC                                              JET06230
WRITE (6,773)                                                       JET06240
773 FORMAT (//30X,'BODY WITH CIRCULAR CROSS SECTION//')          JET06250
WRITE (6,771) XLUT                                                 JET06260
ZPLANE=ZPLANE+2.*DZPL                                             JET06270
IF (ZPLANE.GT.2.*ZFIMAL) STOP                                     JET06280
700 CONTINUE                                                       JET06290
END                                                                JET06300
C                                                                      JET06310
C                                                                      JET06320
C                                                                      JET06330
C                                                                      JET06340
SUBROUTINE WTSOLV (TM,BVN,ALPV,TLAM,VM,TH,RV,RT)                  JET06350
RCGN=(2.-SQRT(2.))/2.                                             JET06360
WRITE (6,200) TM,BVN,ALPV,ALPT                                    JET06370
200 FORMAT (1X,'TM=',F10.5,2X,'BVN=',F10.5,2X,'ALPV=',F10.5,2X,'ALPT=' JET06380
1,F10.5)                                                           JET06390
DTM=TM-1.                                                         JET06400
REL=.5                                                            JET06410
DELHM=1.E-5                                                       JET06420
RV=(RCGN)**(1./ALPV)                                              JET06430
RT=RV                                                             JET06440
ALPT=ALPV                                                         JET06450
VM=1.                                                             JET06460
TH=1.                                                             JET06470
DO 100 I=1,500                                                    JET06480
CALL SIMTV(TM,TH,ALPV,TLAM,CM,CT,CTM,CTTH)                       JET06490
WRITE (6,203) CM,CT,CTM,CTTH                                      JET06500
203 FORMAT (1X,'CM=',F10.5,2X,'CT=',F10.5,2X,'CTM=',F10.5,2X, JET06510
!'CTTH=',F10.5)                                                 JET06520
F=RV*RV*TH-2.*VM*VM*BVN*DTM*CM                                  JET06530
G=DTM*TH*RV*RV-2.*VM*(TM*TH-1.)*BVN*BVN*CT                    JET06540
FTM=TH-2.*VM*CM*BVN*DTM*CTM                                     JET06550
FVM=-4.*VM*BVN*DTM*CM                                          JET06560
GTM=DTM*RV*RV-2.*VM*(TH*TH-1.)*BVN*BVN*CTTH-2.*VM*BVN*BVN*CT*TM JET06570
GVN=-2.*(TM*TH-1.)*BVN*BVN*CT                                  JET06580
DET=FVM*GTM-GVM*FTM                                             JET06590
DELVM=(G*FTM-F*STM)/DET                                          JET06600
DELTH=(F*GVM-G*FVM)/DET                                          JET06610
VM=VM+REL*DELVM                                                  JET06620
TH=TH+REL*DELTH                                                  JET06630
C                                                                      JET06640
WRITE (6,505) VM,DELVM,TH,DELTH,F,G                               JET06650
505 FORMAT (1X,'VM=',F10.5,1X,'DELVM=',F10.5,1X,'TH=',F10.5,2X,'DTM=' JET06660
110.5,1X,'F=',F10.5,1X,'G=',F10.5)                               JET06670
IF (ABS(F).LT.DELHM.AND.ABS(G).LT.DELHM) GO TO 101              JET06680
100 CONTINUE                                                       JET06690
STOP                                                                JET06700
101 RETURN                                                         JET06710
END                                                                JET06720
C                                                                      JET06730
C                                                                      JET06740
C                                                                      JET06750

```

Figure 69 - Continued

ORIGINAL PAGE IS
OF POOR QUALITY

```

SUBROUTINE WALLJT (R,VMN,BWH,DELPJ,TH,TMB,PHD,DELTMN,DTSTAG)
REAL KDELO,NO,KDELFD,NFD,N,KDEL,NPR,NTR,MACH
COMMON/WALL/ DELS,NO,KDELO,ALPG,ALPWO,ALPWF,RO,RGH,UG,BWHD
COMMON/WALLT/TLAMI,DELPS,DELTSB,PSBAR
COMMON /NOZZLE/ NPR,NTR,TH,GAM,MACH,AC15,TAEFF,TNEFF
RCOH=(2.-SQRT(2.))/2.
NFD=7.0
KDELFD=1./9.
BW3HO=AW3*RO
AWT=.09*(1.+ALGG(2./(1.+1./TN**5)))*(1.-.16*ACHS)
B1J1D=AW3*RO
DELBRH=(BW3HO-BWHD)/(RO-RGH)
DELHR=(NFD-NO)/(RO-RGH)
DELAR=(ALPWF-ALPWO)/(RO-RGH)
ADELBT=.0175
ADELBL=(ADELBT*(RO-2.)-DELS)/(RO-RGH)
TLAMFD=1.+1.185*TN**5
TLAMSL=(TLAMFD-TLAMI)/(RO-RGH)
IF (R.GE.RGH) TLAM=TLAMI+TLAMSL*(R-RGH)
IF (R.LT.RGH) TLAM=TLAMI
IF (R.LE.RO) FETA=(1.-(R/RO)**ALPG)**4
IF (R.GT.RO) FETA=0.0
IF (R.GT.RO) TLAM=TLAMFD
FMR=1.+(NPR-1.)*DELPS*FETA
IF (R.GT.RGH) GO TO 402
TMB=1.+DELTSB
TH=TMB/NTR
ACHI=SQRT(2.*(PSBAR/FMR-1.)/GAM)
VMN=(ACHI/MACH)*SQRT(TMB/NTR)
DELPJ=DELPS
DELTA=KDELO*BWD
N=14
KDEL=KDELO
BW=BWD
BWH=RATWOB*BW
VMG=VMN/UG
BWH=TLAMI*BWH
DELTMN=(TMB-1.)/(NTR-1.)
TMSTAG=TMB
DTSTAG=(TMSTAG-1.)/(NTR-1.)
GO TO 401
402 IF (R.GT.RO) GO TO 403
BWH=BWHD+DELBRH*(R-RGH)
ALPW=ALPWO+DELAR*(R-RGH)
DELBL=DELS+ADELBL*(R-RGH)
N=NO+DELHR*(R-RGH)
GO TO 405
403 BWH=AW3*RO
DELBL=ADELBT*(R-2.)
N=NFD
ALPW=ALPWF
405 ALAM=((2.-SQRT(2.))/2.)**(1./ALPW)
KDEL=DELBL/(DELBL+(BWH-DELBL)/ALAM)
IF (R.LE.4.) FVIS=1.0
IF (R.GT.4.) FVIS=1./(R/4.)**.24
FMOM=1.-FETA
DELPH=DELPS*FETA
CALL UTWALL (R,BWH,FUIS,FMOM,DELPH,TH,TLAM,PHD,KDEL,N,ALPW,
IUMN,TH,TNEFF,TAEFF)
VMG=VMN/UG
RCOH=(2.-SQRT(2.))/2.
RAT=KDEL+(1.-KDEL)*RCOH**(.1/ALPW)
BW=BWH/RAT
DELTA=KDEL*BW
DELPJ=(PHD-1.)/(NPR-1.)+PHD*BWH*VMN/TH
TMB=TMB*NTR
BWH=TLAM*BWH
DELTMN=(TMB-1.)/(NTR-1.)
TMSTAG=TMB
DTSTAG=(TMSTAG-1.)/(NTR-1.)
C 401 WRITE (6,95) R,VMG,VMN,BWH,BW,DELTA,DELPJ,KDEL,TH,TMB
C 1,BWHT,DELTMN,DTSTAG
401 CONTINUE
R=R+DR
95 FORMAT (1X,5(F8.4,2X),6(F7.4,1X))
RETURN
END

```

JET06760
JET06770
JET06780
JET06790
JET06800
JET06810
JET06820
JET06830
JET06840
JET06850
JET06860
JET06870
JET06880
JET06890
JET06900
JET06910
JET06920
JET06930
JET06940
JET06950
JET06960
JET06970
JET06980
JET06990
JET07000
JET07010
JET07020
JET07030
JET07040
JET07050
JET07060
JET07070
JET07080
JET07090
JET07100
JET07110
JET07120
JET07130
JET07140
JET07150
JET07160
JET07170
JET07180
JET07190
JET07200
JET07210
JET07220
JET07230
JET07240
JET07250
JET07260
JET07270
JET07280
JET07290
JET07300
JET07310
JET07320
JET07330
JET07340
JET07350
JET07360
JET07370
JET07380
JET07390
JET07400
JET07410
JET07420
JET07430
JET07440
JET07450
JET07460
JET07470
JET07480
JET07490
JET07500
JET07510
JET07520

Figure 69 - Continued

ORIGINAL PAGE IS
OF POOR QUALITY

```

JET07530
JET07540
JET07550
JET07560
SUBROUTINE VTWALL (R,RWHL,FUIS,FACH,DPH,TN,TLAN,PHB,KDEL,N,ALPV,VM,
JET07570
1TH,TNEFF,TAEFF)
JET07580
REAL KDEL,N
JET07590
VM=1.
JET07600
TM=1.
JET07610
DELMIN=1.E-5
JET07620
REL=.5
JET07630
DO 100 I=1,500
JET07640
TMD=TM*TN
JET07650
CALL SIMTV (TN,TH,TLAN,PHB,KDEL,N,ALPV,CV2,CP,CT,CV2TN,CTTM,
JET07660
1RV)
JET07670
F=RV*FMON*FUIS-R*BWHL*(2.*PHB*VM*VM*CV2/TH+DPH*CP)
JET07680
G=PV*FMON*(TNEFF-TAEFF)*TH-2.*PHB*VM*(TMD-TAEFF)*R*BWHL*CT
JET07690
FVM=-4.*R*BWHL*(PHB*VM*CV2/TH)
JET07700
FTM=2.*R*BWHL*PHB*VM*VM*(CV2/(TH*TM))-CV2TN/TH
JET07710
QVM=-2.*PHB*(TMD-TAEFF)*R*BWHL*CT
JET07720
GTM=RV*FMON*(TNEFF-TAEFF)-2.*PHB*VM*R*BWHL*(CT*TM+(TMD-TAEFF)*CTTM)
JET07730
DET=FVM*GTM-QVM*FTM
JET07740
DELVM=(G*FTM-F*GTM)/DET
JET07750
DELTM=(F*QVM-G*FVM)/DET
JET07760
VM=VM+REL*DELVM
JET07770
TM=TM+REL*DELTM
JET07780
C 1
WRITE (6,705) F,G,VM,TH
JET07790
705 FORMAT (1X,'F=',F10.5,2X,'G=',F10.5,1X,'VM=',F10.5,1X,'TM=',F10.5)
JET07800
IF (ABS(F) .LT. DELMIN.AND.ABS(G).LT.DELMIN) GO TO 101
JET07810
100 CONTINUE
JET07820
STOP
JET07830
101 CONTINUE
JET07840
RETURN
JET07850
END
JET07860
JET07870
JET07880
JET07890
JET07900
SUBROUTINE UPWASH (RO,RWALL,PHI,ZEND,BWGH,DELPS,DELPWS,DELTWS,
JET07910
1VMUN,DELPUS,TM,TMD,DELTM,DTSTAQ,BCH,ZOU,IWR)
JET07920
REAL NPR,NTR,MONU
JET07930
COMMON /JET/ SD,RGH
JET07940
COMMON/NOZZLE/NPR,NTR,TN,GAM,MACH,ACHS,TAEFF,TNEFF
JET07950
REAL MACH
JET07960
C
JET07970
C THIS ROUTINE COMPUTES THE UPWASH STREAMLINE PROPERTIES
JET07980
C
JET07990
AQU=3.
JET08000
PI=3.14159265
JET08010
ALPUP=1.5
JET08020
ALPUM=1.5
JET08030
ACON=1.-(RGH/SD)**2
JET08040
IF (ACON.GE.0.) GO TO 907
JET08050
PHIO=ARCOS((SD/RGH)**.20)
JET08060
ACON=2./(SIN(.5*PI-PHIO)**2)
JET08070
PHIOD=PHIO*100./PI
JET08080
IF (PHI.GE.PHIO) MONU=ACON*SIN(PHI-PHIO)**2
JET08090
IF (PHI.LT.PHIO) MONU=0.
JET08100
GO TO 909
JET08110
907 MONU=ACON+2.*(1.-ACON)*SIN(PHI)**2
JET08120
909 CONTINUE
JET08130
773 FORMAT (1X,'ACON=',F10.5,2X,'MONU=',F10.5)
JET08140
AU3=.30
JET08150
ALU1=.5
JET08160
ALU2=.8
JET08170
ZOU=AQU*BWGH
JET08180
C
WRITE (6,108) SD,RGH,ZOU
JET08190
108 FORMAT (1X,'JET',3F10.5)
JET08200
ZV=ZOU*COS(PHI)
JET08210
ALU=.5
JET08220
ALPU=1.5
JET08230
CALL SIMU(ALPU,RAT,CV2U)
JET08240
C
WRITE (6,111) CV2U
JET08250
111 FORMAT (1X,'SIMU',F10.5)
JET08260
C
JET08270
C DETERMINE DEPARTURE FROM INVISCID DEFLECTION
JET08280

```

Figure 69 - Continued

ORIGINAL PAGE IS
OF POOR QUALITY

```

C DETERMINE INITIAL UPWASH WIDTH JET06290
C JET08300
  DELPWJ=DELPWS JET08310
  ZETAG=BUGH/ZOU JET08320
  FETAGP=(1.-ZETAG**ALPUP)**4 JET08330
C WRITE (6,117) ZETAG,FETAGP JET08340
117 FORMAT (1X,'ZETAG=',F10.5,2X,'FETAGP=',F10.5) JET08350
  FETAGM=(1.-ZETAG**ALPUM)**4 JET08360
  FMOHU=MOHU*(1.-FETAGM) JET08370
  PMBI=1.+(NPR-1.)*DELPWJ*FETAGP JET08380
  DELPWB=(NPR-1.)*DELPWJ JET08390
  PSB=1.+DELPWB JET08400
  DELTSB=(NTR-1.)*DELTWS JET08410
C WRITE (6,107) DELPWB,DELTSB JET08420
107 FORMAT (1X,'DTP=',F10.5,2X,'DTT=',F10.5) JET08430
  ACHI=SQRT(2.*(PSB/PMBI-1.)/GAM) JET08440
  TMBI=1.+DELTSB JET08450
  UHNUI=(ACHI/MACH)*SQRT(TMBI/NTR) JET08460
  THI=TMBI/NTR JET08470
  IF (IWR.NE.0) WRITE (6,55) UHNUI,TMBI,DELPWJ,DELTSB,BUGH JET08480
55 FORMAT (1X,'INV.VEL.',F10.5,3X,'THI/TA=',F10.5,2X,'DELPWJ=',F10.5, JET08490
1,2X,'DELTWJ=',F10.5,2X,'BUGH/RN=',F10.5) JET08500
  RAY=RWALL+BUGH JET08510
  CALL SINUM (TN,THI,TLAMI,FMBI,ALPU,FETAGP,DELPWJ,UHNUI,BUON,RAY, JET08520
IRAT,FMOHU,TNEFF,TAEFF) JET08530
  BUOHN=ZETA*BUON JET08540
  IF (ABS(MOHU).LT.1.E-5) BUON=1.E-5 JET08550
  IF (ABS(MOHU).LT.1.E-5) BUOHN=1.E-5 JET08560
  IF (IWR.NE.0) WRITE (6,10) ZOU,BUON,BUOHN,TLAMI JET08570
10 FORMAT (15X,'ZOU/RN=',F10.5,2X,'BUO/RN=',F10.5 JET08580
1,2X,'BUOHN/RN=',F10.5,2X,'TLAMI=',F10.5//) JET08590
  NUPT=25 JET08600
  XNUPT=XNUPT-1 JET08610
  DZ=(ZEND-BUGH)/XNUPT JET08620
  Z=BUGH JET08630
  IF (IWR.NE.0) WRITE (6,12) JET08640
12 FORMAT (7X,'Z/RN',7X,'UHU:UH',7X,'TH/TN',7X,'TH/TA',7X,'BUH/RN',6 JET08650
1X,'BU/RN',6X,'DPU/DPJ',6X,'DTM/DTN',) JET08660
  TLANFD=1.+1.85*TN**5 JET08670
  TLANSL=(TLANFD-TLANI)/(ZOU-BUGH) JET08680
  TH=THI JET08690
  UHUN=UHNUI JET08700
  DD 100 I=1,NUPT JET08710
  BUH=BUOHN+AU3*(Z-BUGH)*(COS(PHI)**ALUI) JET08720
  BU=BUH/RAT JET08730
  ZETA=Z/ZOU JET08740
  IF (Z.GE.ZOU) ZETA=1. JET08750
  IF (Z.GT.ZOU) TLAN=TLANFD JET08760
  IF (Z.LE.ZOU) TLAN=TLANI+TLANSL*(Z-BUGH) JET08770
  FETAP=(1.-ZETA**ALPUP)**4 JET08780
  FETAM=(1.-ZETA**ALPUM)**4 JET08790
  RAY=RWALL+Z JET08800
  FMOH=MOHU*(1.-FETAM) JET08810
  DPM=DELPWJ*FETAP JET08820
  PMB=1.+(NPR-1.)*DPM JET08830
  CALL UTUPM (RAY,BUH,FMOH,DPM,TN,TLAM,PMB,ALPU,UHUN,TH,TNEFF,TAEFF) JET08840
905 DELPUJ=(PMB-1.)/(NPR-1.)+PMB*UHUN*UHUN/TH JET08850
  TMB=TMBI*NTR JET08860
  DELTMN=(TMB-1.)/(NTR-1.) JET08870
  TMSTAG=TMB JET08880
  TMSTAG=(TMSTAG-1.)/(NTR-1.) JET08890
  IF (IWR.EQ.0) DELPUJ=DELPWJ/DELPS JET08900
  IF (IWR.NE.0) WRITE (6,11) Z,UHUN,TH,TMB,BUH,BU,DELPWJ,DELTMN JET08910
11 FORMAT (2X,9(F10.5,2X)) JET08920
  Z=Z+DZ JET08930
100 CONTINUE JET08940
  RETURN JET08950
  END JET08960
JET08970
JET08980
JET08990
JET09000

```

Figure 69 - Continued

ORIGINAL PAGE IS
OF POOR QUALITY

```

SUBROUTINE UTUPM (R,BUH,FHOM,DFM,TH,TLAM,PHB,ALPV,UM,TH,TNEFF, JET09010
1TAEFF) JET09020
DELMIN=1.E-5 JET09030
REL=.5 JET09040
DO 100 I=1,500 JET09050
THB=TH*TH JET09060
CALL SIMUTV (TN,TH,TLAM,PHB,ALPV,CV2,CF,CT,CV2TH,CTTH,RV) JET09070
F=RV*FHOM-R*BUH*(2.*PHB*UM*UM*CV2/TH+DFM*CP) JET09080
G=RV*FHOM*(1.-1.)*TH-2.*PHB*UM*(THB-1.)*R*BUH*CT JET09090
WRITE (6,111) F,G,TH,UM JET09100
111 FORMAT (1X,'F=',F10.5,2X,'G=',F10.5,2X,'TH=',F10.5,2X,'UM=',F10.5) JET09110
FVH=-4.*R*BUH*(PHB*UM*CV2/TH) JET09120
FTM=2.*F*BUH*PHB*UM*UM*(CV2/(TH*TH))-CV2TH/TH JET09130
GVH=-2.*PHB*(THB-1.)*R*BUH*CT JET09140
GTH=RV*FHOM*(TH-1.)*2.*PHB*UM*R*BUH*(CT*TN+(THB-1.)*CTTH) JET09150
DET=FVH*GTH-GVH*FTM JET09160
DELVH=(3*FTM-F*GTH)/DET JET09170
DELTH=(F*GVH-G*FVH)/DET JET09180
VM=UM+REL*DELVH JET09190
TM=TH+REL*DELTH JET09200
WRITE (6,705) F,G,VM,TH JET09210
705 FORMAT (1X,'F=',F10.5,2X,'G=',F10.5,1X,'VM=',F10.5,1X,'TH=',F10.5) JET09220
IF (ABS(F).LT.DELMIN.AND.ABS(G).LT.DELMIN) GO TO 101 JET09230
100 CONTINUE JET09240
STOP JET09250
101 CONTINUE JET09260
RETURN JET09270
END JET09280
JET09290
JET09300
JET09310
JET09320
JET09330
SUBROUTINE INTERB (XLAM,DELPS,SD,RO,ALPB,EPS,CU,SIG) JET09340
C JET09350
C MAIN ROUTINE FOR COMPUTING GROUND PRESSURE DISTRIBUTION JET09360
C THIS ROUTINE FINDS THE SOLUTION FOR THE UPWASH THICKNESS AND JET09370
C JET IMPINGEMENT PERTURBATION PARAMETER SIGMA AND EPS BY JET09380
C MATCHING PRESSURE INTEGRALS JET09390
C JET09400
COMMON /HEIGHT/ HD,IPBAR JET09410
DIMENSION EP(200),C(200),PHIU(200),PHI(200),CSJ(200),FUI(4),FJI(4) JET09420
CSPJ(ETA,A)=.5*ETA**2-(4./(A+2.))*ETA**A+(3./(A+1.))*ETA**2. JET09430
I**A+2.)-(4./(3.*A+2.))*ETA**3.*A+2.)+(4.*A+2.))*ETA**4.*A+2. JET09440
FETA(ETA,A)=(1.-ETA**A)**4 JET09450
EP(1)=.0 JET09460
WRITE (6,777) JET09470
777 FORMAT (///1X,'*** CALL INTERG ***') JET09480
IFLAG=0 JET09490
C(1)=1. JET09500
PI=3.14159265 JET09510
SIGI=1.0 JET09520
CUI=CU JET09530
ALU=1.0 JET09540
PARH=.01 JET09550
DO 900 J=1,100 JET09560
EPI=EP(J) JET09570
SIGI=C(J) JET09580
DO 1000 ITR=1,4 JET09590
IF (ITR.EQ.2) EPI=EP(J)+PARH JET09600
IF (ITR.EQ.3) EPI=EP(J) JET09610
IF (ITR.EQ.4) SIGI=C(J)+PARH JET09620
C JET09630
C SOLVE FOR INTERSECTION OF PRESSURE BOUNDARIES JET09640
C JET09650
DO 100 I=1,99 JET09660
IF (I.EQ.1) PHIU(I)=1.42 JET09670
YU=SD*TAN(PHIU(I)) JET09680
XUF=SD/(COS(PHIU(I)))**2 JET09690
YU=CUI*SIGI*SD/(COS(PHIU(I))*ALU) JET09700
YUP=-CUI*SIGI*SD*ALU/(COS(PHIU(I))*ALU+1.) JET09710
RUSQ=XU**2+(SD-YU)**2 JET09720
RU=SQRT(RUSQ) JET09730
ROP=RO+EPI*(1.+((SD-YU)/RU)) JET09740
ROPSQ=ROP**2 JET09750
F=RUSQ-ROPSQ JET09760
FP=2.*XU*XUF-2.*(SD-YU)*YUF-2.*EPI*ROP*(SD-YU)* JET09770
1(YUP/RU+(2.*XU*XUF-2.*(SD-YU)*YUF)/RUSQ) JET09780
PHIU(I+1)=PHIU(I)-F/FP JET09790
IF (ABS(PHIU(I+1)-PHIU(I)).LT.1.E-5) GO TO 101

```

Figure 69 - Continued

ORIGINAL PAGE IS
OF POOR QUALITY

```

100 CONTINUE
STOP
101 PHIUD=PHIU(I+1)
PHIUQ=PHIU*180./PI
YUO=CUI*SIGI*SD/(COS(PHIUD)**ALU)
PHIO=ATAN2(SD*TAN(PHIUD),SD-YUO)
PHIOD=PHIO*180./PI
IF (IFLAG.EQ.1) WRITE (6,10) EPI,CUI,PHIUQ,PHIOD
10 FORMAT (15X,'EPI=',F10.5,2X,'CUI=',F10.5,2X,'PHIUQ=',F10.5
1,2X,'PHIOD=',F10.5,2X,'DEGREES')
C
C DETERMINE MOMENTUM INTEGRAL FOR IMPINGEMENT REGION
C
NUPTS=99
IF (J.GT.20) NUPTS=198
XPTS=NUPTS-1.
DFHIU=PHIUQ/XPTS
PHIU(1)=0.
SUMU1=0.
DO 200 IJ=1,NUPTS
FACT=2.0
IF (IJ.EQ.1) FACT=1.0
IF (IJ.EQ.NUPTS) FACT=1.0
RU=SD/COS(PHIU(IJ))
CALL WALLJ (RU,VNM,DUM2,DUM3,DUM4,DELPW)
IF (IJ.EQ.1.AND.IFLAG.EQ.1) WRITE (6,111) DELPW
111 FORMAT (35X,'PHI=0.0, DELPW=',F10.5)
YU=CUI*SIGI*SD/COS(PHIU(IJ))
XU=SD*TAN(PHIU(IJ))
PHI(IJ)=ATAN2(XU,SD-YU)
RU=(SD-YU)/COS(PHI(IJ))
ROP=RO+EPI*(1.+COS(PHI(IJ)))
ETAM=RU/ROP
IF (ETAM.GT.1.) FETAG=0.0
IF (ETAM.GT.1.) GO TO 1011
FETAG=FETA(ETAM,ALPG)
1011 FMIN=DELPS*FETAG
IF (IJ.EQ.1.AND.IFLAG.EQ.1) WRITE (6,775) FMIN
775 FORMAT (35X,'PHI=0.0, FMIN=',F10.5)
PHAX=DELPW-VNM**2+(VNM*COS(PHIU(IJ)))**2
CALL PMATCH (FMIN,PHAX,ALPUG)
IF (IJ.EQ.1.AND.IFLAG.EQ.1) WRITE (6,1055) ALPUG
1055 FORMAT (35X,'PHI=0.0, ALPUG=',F10.5)
CALL SIMUG(ALPUG,RATU,CSPUG)
PHAX=DELPW-VNM**2+(VNM*COS(PHIU(IJ)))**2
FU=DELPS*FETAG+CSPUG*(PHAX-DELPS*FETAG)
FUT=SIGI*FU/(COS(PHIU(IJ)))**3
SUMU1=SUMU1+.5*DFHIU*FACT*FUT
IF (ETAM.GT.1.) ETAM=1.0
CSJ(IJ)=CSJ(ETAM,ALPG)
PHIU(IJ+1)=PHIU(IJ)+DFHIU
200 CONTINUE
XI1UG=CUI*SUMU1*SD**2
SUMI=0.
NUPTSM=NUPTS-1
DO 300 IJ=1,NUPTSM
ROPP=RO+EPI*(1.+COS(PHI(IJ+1)))
ROFFSQ=ROPP**2
ROFM=RO+EPI*(1.+COS(PHI(IJ)))
ROFMSD=ROFM**2
FM=ROFMSD*CSJ(IJ)
FP=ROFFSQ*CSJ(IJ+1)
DPHI=PHI(IJ+1)-PHI(IJ)
SUMI=SUMI+.5*DPHI*(FM+FP)
300 CONTINUE
XI1JG=DELPS*SUMI
CALL SIM(0.0,ALPG,RATU,CSPJG)
XI2JG=CSPJG*DELPS*((PI-PHIQ)-(RO*(RO+2.*EPI)+1.5*EPI**2)
1-2.*EPI*(RO+EPI)*SIN(PHIQ))-25*SIN(2.*PHIQ)*EPI**2)
XJI=XI1JG+XI2JG
FJI(ITR)=XJI-PI
DPHIU=(.5*FI-PHIUD)/XPTS
SUNU2=0.0
PH=PHIUQ
XI2UG=SIGI*(1.-SIN(PHIUD))
FUZ(ITR)=XI1UG+XI2UG-XLAM
JET09800
JET09810
JET09820
JET09830
JET09840
JET09850
JET09860
JET09870
JET09880
JET09890
JET09900
JET09910
JET09920
JET09930
JET09940
JET09950
JET09960
JET09970
JET09980
JET09990
JET10000
JET10010
JET10020
JET10030
JET10040
JET10050
JET10060
JET10070
JET10080
JET10090
JET10100
JET10110
JET10120
JET10130
JET10140
JET10150
JET10160
JET10170
JET10180
JET10190
JET10200
JET10210
JET10220
JET10230
JET10240
JET10250
JET10260
JET10270
JET10280
JET10290
JET10300
JET10310
JET10320
JET10330
JET10340
JET10350
JET10360
JET10370
JET10380
JET10390
JET10400
JET10410
JET10420
JET10430
JET10440
JET10450
JET10460
JET10470
JET10480
JET10490
JET10500
JET10510
JET10520
JET10530
JET10540
JET10550

```

Figure 69 - Continued

ORIGINAL PAGE IS
OF POOR QUALITY

```

IF (IFLAG.EQ.1) GO TO 907
IF (ITR.EQ.1) GO TO 1000
RELAX=.5
DEPI=PARM
DCUI=PARM
IF (ITR.EQ.2) FUIE=(FUI(ITR)-FUI(ITR-1))/DEPI
IF (ITR.EQ.4) FUIC=(FUI(ITR)-FUI(ITR-1))/DCUI
IF (ITR.EQ.3) FJIE=(FJI(ITR)-FJI(ITR-1))/DEPI
IF (ITR.EQ.4) FJIC=(FJI(ITR)-FJI(ITR-1))/DCUI
1000 CONTINUE
DEY=FUIE*FJIC-FJIE*FUIC
DELE=(FJI(1)*FUIC-FUI(1)*FJIC)/DEY
DELC=(FUI(1)*FJIE-FJI(1)*FUIE)/DEY
EP(J+1)=EP(J)+RELAX*DELE
C(J+1)=C(J)+RELAX*DELC
905 FORMAT (15X,'ITERATION CYCLE=',I3,2X,'EPS=',F10.5,2X,'SIGMA=',F10.5)
15)
IF (ABS(DELE).LT.1.E-5)AND.(ABS(DELC).LT.1.E-5) IFLAG=1
IF (IFLAG.EQ.1) WRITE (6,909)
909 FORMAT (20X,'SOLUTION OF GROUND PRESSURE DISTRIBUTION HAS BEEN FOUND')
1ND')
IF (IFLAG.EQ.1) WRITE (6,905) J,EP(J+1),C(J+1)
900 CONTINUE
STOP
907 SIG=C(J)
EPS=EP(J)
CUU=SIG*DCUI
WRITE (6,13) CUU
13 FORMAT (20X,'UPWASH THICKNESS CONSTANT, (CU) X (SIGMA)=',F10.5)
IF (IPBAR.NE.0) CALL GPLOTT,ALPB,DELPS,SD,RO,EPS,CUI,SIG,PHIU,PHIO
1)
RETURN
END

SUBROUTINE GPLOTT (ALPB,DELPS,SD,RO,EPS,CUI,SIG,PHIU,PHIO)
DIMENSION PU(25),RWALL(102),ERR(102),XPLOTU(202),YPLOTU(
1202),XPLOTJ(202),YPLOTJ(202),XAXIS(30),YAXIS(30),XDATA(10),YDATA(
20)
COMMON /HEIGHT/ HD,IPBAR
C
C THIS ROUTINE COMPUTES THE GROUND ISOBAR PATTERN FOR THE TWO-JET
C IMPINGEMENT FLOW FIELD
C
FETA(ETA,A)=(1.-ETA**A)**A
C
C INPUT NUMBER OF ISOBAR VALUES
C
READ(5,51) NU
51 FORMAT (I2)
WRITE (6,53) NU
53 FORMAT ('1',//30X,'*** COMPUTATION OF TWO-JET GROUND ISOBAR PATTE
IRN ***'//32X,I2,' VALUES OF PRESSURE SPECIFIED FOR PATTERN'
2//)
C
C INPUT NU ISOBAR VALUES FOR GROUND PATTERN
C
READ(5,1) (PU(I),I=1,NU)
1 FORMAT (F10.5)
WRITE (6,112) (PU(I),I=1,NU)
112 FORMAT (10X,'PBAR=',8(F10.5,2X))
WRITE (6,121)
121 FORMAT (//25X,'GROUND PATTERN IN JET CENTERED COORDINATE SYSTEM'//
1)
NUPTS=29
CALL PLOT(4.,0.,-3)
C
XLMAX=RO+SD
C
XSC=XLMAX/B.
XSC=1.0
XMIN=0.
DXMIN=-1.
DO 801 IP=1,100
IF (XMIN.LT.-RO) GO TO 802
XMIN=XMIN+DXMIN
801 CONTINUE
JET10560
JET10570
JET10580
JET10590
JET10600
JET10610
JET10620
JET10630
JET10640
JET10650
JET10660
JET10670
JET10680
JET10690
JET10700
JET10710
JET10720
JET10730
JET10740
JET10750
JET10760
JET10770
JET10780
JET10790
JET10800
JET10810
JET10820
JET10830
JET10840
JET10850
JET10860
JET10870
JET10880
JET10890
JET10900
JET10910
JET10920
JET10930
JET10940
JET10950
JET10960
JET10970
JET10980
JET10990
JET11000
JET11010
JET11020
JET11030
JET11040
JET11050
JET11060
JET11070
JET11080
JET11090
JET11100
JET11110
JET11120
JET11130
JET11140
JET11150
JET11160
JET11170
JET11180
JET11190
JET11200
JET11210
JET11220
JET11230
JET11240
JET11250
JET11260
JET11270
JET11280
JET11290
JET11300
JET11310
JET11320

```

Figure 69 - Continued

ORIGINAL PAGE IS
OF POOR QUALITY

802	XMAX=SD	JET11330
	DXAXIS=SD-XMIN	JET11340
	NAPTS=DXAXIS+1	JET11350
	XAXIS(1)=XMIN/XSC	JET11360
	YAXIS(1)=0.	JET11370
	DO 809 IP=2,NAPTS	JET11380
	XAXIS(IP)=XAXIS(IP-1)+1./XSC	JET11390
	YAXIS(IP)=YAXIS(IP-1)	JET11400
809	CONTINUE	JET11410
	DYAX=1./XSC	JET11420
	XAXIS(NAPTS+1)=SD/XSC	JET11430
	YAXIS(NAPTS+1)=0.	JET11440
	DO 805 IP=2,NAPTS	JET11450
	XAXIS(NAPTS+IP)=SD/XSC	JET11460
	YAXIS(NAPTS+IP)=YAXIS(NAPTS+IP-1)+DYAX	JET11470
805	CONTINUE	JET11480
	NPLOT=2*NAPTS	JET11490
C	CALL LINE (XAXIS,YAXIS,NPLOT,1,1,-3,1,1)	JET11500
C	CALL SYMBL4 (-3.,8.,.2,'H/D=14.0, S/D=2.00',0.,18)	JET11510
	PI=3.14159265	JET11520
	XPTS=NUPTS-1.	JET11530
	RELAX=.5	JET11540
	DO 500 I=1,NU	JET11550
	WRITE (6,66) PU(I)	JET11560
66	FORMAT (///45X,'PBAR=',F10.5)	JET11570
	IFLAG=1	JET11580
	XPUF=0.	JET11590
	IJET=1	JET11600
	IU=1	JET11610
	RW=SD	JET11620
	ALPUG=1.5	JET11630
	CALL WALLJ (RW,VMN,DUM2,DUM3,DUM4,DELPW)	JET11640
	PMAX=DELPW	JET11650
	IF (PMAXO.LT.PU(I)) IFLAG=0	JET11660
	RW=SD/COS (PHIU)	JET11670
	CALL WALLJ (RW,VMN,DUM2,DUM3,DUM4,DELPW)	JET11680
	PMAXF=DELPW-VMN**2+(VMN*COS (PHIU))**2	JET11690
	IF (IFLAG.EQ.0) GO TO 502	JET11700
	RWALL(1)=SD	JET11710
	RWALL(2)=SD+.1	JET11720
	DO 400 K=1,100	JET11730
	CALL WALLJ(RWALL(K),VMN,DUM2,DUM3,DUM4,DELPW)	JET11740
	XU=SORT(RWALL(K)**2-SD**2)	JET11750
	PHIU=ATAN2(XU,SD)	JET11760
	PMAX=DELPW-VMN**2+(VMN*COS (PHIU))**2	JET11770
	ERR(K)=PU(I)-PMAX	JET11780
	IF (K.EQ.1) GO TO 400	JET11790
	IF (ABS(ERR(K)).LT.1.E-5) GO TO 501	JET11800
	DRDE=(RWALL(K)-RWALL(K-1))/(ERR(K)-ERR(K-1))	JET11810
	RWALL(K+1)=RWALL(K)-RELAX*DRDE*ERR(K)	JET11820
400	CONTINUE	JET11830
	S*OP	JET11840
501	RW=RWALL(K)	JET11850
	YPUF=SQRT(RW**2-SD**2)	JET11860
	PUF=ATAN2(XPUF,SD)	JET11870
	YUF=CUI*SIGI*SD/COS (PUF)	JET11880
	FUF=PUF*180./PI	JET11890
502	DPHIU=PHIU/XPTS	JET11900
	IF (PHIU.EQ.0.) GO TO 201	JET11910
	PHIU=0.	JET11920
	DO 200 IJ=1,NUPTS	JET11930
	RW=SD/COS (PHIU)	JET11940
	CALL WALLJ (RW,VMN,DUM2,DUM3,DUM4,DELPW)	JET11950
	YU=CUI*SIGI*SD/COS (PHIU)	JET11960
	XU=SD*TAN (PHIU)	JET11970
	PHI=ATAN2(XU,SD-YU)	JET11980
	RU=(SD-YU)/COS (PHI)	JET11990
	ROP=R0+EPS*(1.+COS (PHI))	JET12000
	ETAN=RU/ROP	JET12010
	IF (ETAN.GT.1.) FETAG=0.0	JET12020
	IF (ETAN.GT.1.) GO TO 1011	JET12030
	FETAG=FETA(ETAN,ALPG)	JET12040
1011	PHIN=DELPS*FETAG	JET12050
	PMAX=DELPW-VMN**2+(VMN*COS (PHIU))**2	JET12060
	CALL PHATCH (PHIN,PMAX,ALPUG)	JET12070
	PBAR=(PU(I)-PHIN)/(PMAX-PHIN)	JET12080

Figure 69 - Continued

ORIGINAL PAGE IS
OF POOR QUALITY

```

IF (PHIN.GT.PU(I)) GO TO 509
PBARJ=PU(I)/DELPS
IF (PBARJ.GT.1.) GO TO 509
ETAJ=(1.-PBARJ**.25)**(1./ALPG)
XPLOTJ(IJET)=ROP*ETAJ*DCOS(PHI)
YPLLOTJ(IJET)=ROP*ETAJ*DSIN(PHI)
XPLOTJ(IJET)=XPLOTJ(IJET)/XSC
YPLLOTJ(IJET)=YPLLOTJ(IJET)/XSC
IJET=IJET+1
509 IF (PBAR.GT.1..OR.PBAR.LT.0.) GO TO 506
ETAU=(1.-PBAR**.25)**(1./ALPUG)
XPLOTU(IU)=SD-YU*ETAU
YPLLOTU(IU)=XU
XPLOTU(IU)=XPLOTU(IU)/XSC
YPLLOTU(IU)=YPLLOTU(IU)/XSC
IU=IU+1
506 PHIU=PHIU+DPHIU
200 CONTINUE
201 DPHI=(PI-PHI0)/XPTS
PHI=PHI0
DO 400 IK=1,NUPTS
PBARJ=PU(I)/DELPS
IF (PBARJ.GT.1.) GO TO 400
ETAJ=(1.-PBARJ**.25)**(1./ALPG)
ROP=RO+EPS*(1.+COS(PHI))
XPLOTJ(IJET)=ROP*ETAJ*DCOS(PHI)
YPLLOTJ(IJET)=ROP*ETAJ*DSIN(PHI)
XPLOTJ(IJET)=XPLOTJ(IJET)/XSC
YPLLOTJ(IJET)=YPLLOTJ(IJET)/XSC
IJET=IJET+1
PHI=PHI+DPHI
600 CONTINUE
IF (IFLAG.EQ.0) GO TO 513
IF (PU(I).EQ.0.) GO TO 513
IF (PUF.LT.PHIU0) GO TO 510
GO TO 511
510 XPLOTU(IU)=SD
YPLLOTU(IU)=XPUF
XPLOTU(IU)=XPLOTU(IU)/XSC
YPLLOTU(IU)=YPLLOTU(IU)/XSC
GO TO 800
511 DPHIU=(PUF-PHIU0)/XPTS
PHIU=PHIU0
DO 700 IJ=1,NUPTS
YU=CUI*SIGI*SD/COS(PHIU)
XU=SD*TAN(PHIU)
RU=SD/COS(PHIU)
CALL WALLJ(RU,VHN,DUM2,DUM3,DUM4,DELPW)
PMA=DELPW-VHN**2+(VHN*COS(PHIU))**2
PBAR=PU(I)/PMA
ETAU=(1.-PBAR**.25)**(1./ALPUG)
XPLOTU(IU)=SD-YU*ETAU
YPLLOTU(IU)=XU
XPLOTU(IU)=XPLOTU(IU)/XSC
YPLLOTU(IU)=YPLLOTU(IU)/XSC
IU=IU+1
PHIU=PHIU+DPHIU
700 CONTINUE
513 IU=IU-1
800 IJET=IJET-1
WRITE (6,11) IJET,IU
11 FORMAT (//15X,'JET IMPINGEMENT REGION, IJET=',I4,10X,'UPWASH DEFLECTI
SECTION REGION, IU=',I4//)
IF (IJET.GT.0.OR.IU.GT.0) WRITE (6,552)
552 FORMAT (//34X,'XISOJ',6X,'YISOJ',8X,'XISOU',8X,'YISOU'//)
IMIN=IU
IMAX=IJET
IF (IU.GT.IJET) IMAX=IU
IF (IU.GT.IJET) IMIN=IJET
DO 803 IP=1,IMAX
IF (IM.LE.IMIN) WRITE(6,12) XPLOTJ(IP),YPLLOTJ(IP),XPLOTU(IP),YPLLOTU(IP)
IU(IP)
12 FORMAT (30X,4(F10.5,2X))
IF (IM.GT.IMIN.AND.IMIN.EQ.IU) WRITE (6,15) XPLOTJ(IP),YPLLOTJ(IP)
15 FORMAT (30X,2(F10.5,2X))
IF (IM.GT.IMIN.AND.IMIN.EQ.IJET) WRITE (6,14) XPLOTU(IP),YPLLOTU(IP)
14 FORMAT (54X,2(F10.5,2X))
JET12090
JET12100
JET12110
JET12120
JET12130
JET12140
JET12150
JET12160
JET12170
JET12180
JET12190
JET12200
JET12210
JET12220
JET12230
JET12240
JET12250
JET12260
JET12270
JET12280
JET12290
JET12300
JET12310
JET12320
JET12330
JET12340
JET12350
JET12360
JET12370
JET12380
JET12390
JET12400
JET12410
JET12420
JET12430
JET12440
JET12450
JET12460
JET12470
JET12480
JET12490
JET12500
JET12510
JET12520
JET12530
JET12540
JET12550
JET12560
JET12570
JET12580
JET12590
JET12600
JET12610
JET12620
JET12630
JET12640
JET12650
JET12660
JET12670
JET12680
JET12690
JET12700
JET12710
JET12720
JET12730
JET12740
JET12750
JET12760
JET12770
JET12780
JET12790
JET12800
JET12810
JET12820
JET12830
JET12840
JET12850
JET12860

```

Figure 69 - Continued

ORIGINAL COPY
OF PAPER COPY

```

803 CONTINUE JET12870
C CALL LINE (XPLOTU,YPLOTU,IU,1,1,1,1) JET12880
C CALL LINE (XPLOTJ,YPLOTJ,IJET,1,1,1,1) JET12890
500 CONTINUE JET12900
DPHIU=.5*PI/XPTS JET12910
PHIU=0. JET12920
DO 900 IJ=1,MUPTS JET12930
YU=CUI*SIGI*SD/COS(PHIU) JET12940
XU=SD*TAN(PHIU) JET12950
IF (XU.GT.XLMAX) GO TO 901 JET12960
XPLOTU(IJ)=SD-YU JET12970
YPLOTU(IJ)=XU JET12980
XPLOTU(IJ)=XPLOTU(IJ)/XSC JET12990
YPLOTU(IJ)=YPLOTU(IJ)/XSC JET13000
PHIU=PHIU+DPHIU JET13010
900 CONTINUE JET13020
901 IU=IJ-1 JET13030
WRITE (6,807) JET13040
807 FORMAT (///15X,'UPWASH DEFLECTION ZONE LINE, PBAR=0 OUTSIDE INTERA JET13050
CTION REGION'///) JET13060
WRITE (6,808) JET13070
808 FORMAT (35X,'XUP',8X,'YUP'///) JET13080
DC 813 IM=1,IU JET13090
WRITE (6,811) XPLOTU(IM),YPLOTU(IM) JET13100
813 CONTINUE JET13110
811 FORMAT (30X,2(F10.5,2X)) JET13120
C CALL LINE (XPLOTU,YPLOTU,IU,1,1,1,1) JET13130
C CALL ADRAW JET13140
C CALL PLOT (-99.,-99., 3) JET13150
C READ (5,101) PAUSE JET13160
101 FORMAT (1X,F10.5) JET13170
RETURN JET13180
END JET13190
JET13200
JET13210
JET13220
JET13230
SUBROUTINE WALLJ(R,VNH,BWH,BW,CV2,DELPW) JET13240
REAL KDELO,NO,KDELFD,NFD,N,KDEL JET13250
C THIS COMPUTES THE WALL JET PROPERTIES GIVEN A WALL RADIUS JET13260
C COMMON/WALL/ DELS,NO,KDELO,ALPG,ALPWO,ALPWF,RO,RGH,UG,BWHD JET13270
C MAXIMUM VELOCITY DISTRIBUTION IN DEFLECTION REGION JET13280
C JET13290
AM3=.09 JET13300
NFI=7. JET13310
KDELFD=1./9. JET13320
BW3HO=AM3*RO JET13330
DELRH=(BW3HO-BWHD)/(RO-RGH) JET13340
ALPWF=1.5 JET13350
DELAR=(ALPWF-ALPWO)/(RO-RGH) JET13360
DELR=(NFD-NO)/(RO-RGH) JET13370
ADELBT=.0175 JET13380
ADELBL=(ADELBT*(RO-2.))-DELS/(RO-RGH) JET13390
DKDEL=(KDELFD-KDELO)/(RO-RGH) JET13400
IF (R.LE.RO) FETA=(1.-(R/RO)**ALPG)**4 JET13410
IF (R.GT.RO) FETA=0.0 JET13420
IF (R.LE.RGH) VNG=SQRT(1.-FETA) JET13430
IF (R.LE.RGH) VNH=VNG*UG JET13440
IF (R.LE.RGH) GO TO 401 JET13450
IF (R.LE.RO) BWH=BWHD+DELRH*(R-RGH) JET13460
IF (R.GT.RO) BWH=AM3*P JET13470
IF (R.LE.RO) ALPW=ALPWO+DELAR*(R-RGH) JET13480
IF (R.GT.RO) ALPW=ALPWF JET13490
IF (R.LE.RO) N=N0+DELR*(R-RGH) JET13500
IF (R.GT.RO) N=NFD JET13510
IF (R.LE.RO) DELBL=DELS+ADELBL*(R-RGH) JET13520
IF (R.GT.RO) DELBL=ADELBT*(R-2.) JET13530
ALAM=(2.-SQRT(2.))/2.)*(1./ALPW) JET13540
KDEL=DELBL/(DELBL+(BWH-DELBL)/ALAM) JET13550
CALL SIMW(KDEL,N,ALPW,KAT,CV2,CP) JET13560
IF (R.LE.4.) VISHOM=1.0 JET13570
IF (R.GT.4.) VISHOM=1./(R/4.)**.24 JET13580
F1=VISHOM*RAT*(1.-FETA)/(R*BWH) JET13590
F2=CP*FETA*VG**2 JET13600

```

Figure 69 - Continued

ORIGINAL PAGE IS
OF POOR QUALITY

```

VMN=SQRT((F1-F2)/(2.*CV2))
VMG=VMN/VG
DELPW=FETA*VB**2+VMN**2
PW=BWH/RAT
DELTA=NDEL*BU
401 CONTINUE
IF (R.LT.RGH) DELPW=VG**2
IF (R.LT.RGH) BWH=BWHD
RETURN
END

SUBROUTINE JETPCT (TH,ETAC,BVH,ALPV,TLAM,CH,CT,RV,RT)
DELMIN=1.E-5
CALL JETPCN(ETAC,BVH,ALPVI,RVI,CV2)
C WRITE (6,555) CV2,ALPVI
C CALL JETPC (ETAC,BVH,ALPVI,RVI,CV2)
C WRITE (6,555) CV2,ALPVI
555 FORMAT (1X,'CV2=',F10.6,2X,'ALPVI=',F10.6)
C WRITE (6,123) TH,ETAC,BVH
123 FORMAT (1X,'T,S.6)
ALPV=1.*ALPVI
TLAM=1.
R2=(SQRT(2.))-1./SQRT(2.)
REL=.1000000
DO 100 I=1,999
RV=ETAC*(1.-ETAC)**R2**((1./ALPV)
RVAV=(ETAC-1.)*(RV-ETAC)/(1.-ETAC))*ALOG((RV-ETAC)/(1.-ETAC))/
1ALPV
CALL SIMTPC(TH,ETAC,ALPV,TLAM,CH,CT,CHAV,CHAT,CTAV,CTAT)
F=2.*BVH*BWH*CT-RV*RV
G=2.*BVH*BWH*CH-RV*RV
FAV=2.*BVH*BWH*CTAV-2.*RV*RVAV
FAT=2.*BVH*BWH*CTAT
GAV=2.*BVH*BWH*CHAV-2.*RV*RVAV
GAT=2.*BVH*BWH*CHAT
DET=FAV*GAT-GAV*FAT
DALPV=(G*FAT-F*GAT)/DET
DLAM=(F*GAV-G*FAV)/DET
C WRITE (6,800) BVH,CT,RV,CH,ALPV,ALPT,F,G
800 FORMAT (1X,BF14.6)
C WRITE (6,700) I,DALPV,DALPT
700 FORMAT (1X,I3,2X,2F15.6)
ALPV=ALPV+REL*DALPV
TLAM=TLAM+REL*DLAM
IF (ABS(F).LT.DELMIN.AND.ABS(G).LT.DELMIN) GO TO 200
100 CONTINUE
STOP
C 200 WRITE (6,500) I,ALPV,ALPT
200 CONTINUE
500 FORMAT (1X,I3,2X,'ALPV=',F10.6,2X,'ALPT=',F10.6)
RT=RV
RETURN
END

SUBROUTINE JETPCN (ETAC,RJH,ALPC,R,CV2)
C THIS ROUTINE COMPUTES THE EXPONENT OF THE JET VELOCITY PROFILE
C IN THE POTENTIAL CORE REGION
C
ALP=4.0
DELMIN=1.E-5
REL=.50
DO 100 I=1,500
CALL SIMN(ETAC,ALP,R,CV2,CV2*,RALP)
FUNC=CV2-.5*(R/RJH)**2
FUNCD=CV2A-(R*RALP)/(RJH**2)
ALFN=ALP-FUNC/FUNCD
C WRITE (6,700) ALFN,FUNC
700 FORMAT (1X,'ALF=',F10.5,2X,'FUNC=',F10.5)
ALF=ALP+REL*(ALFN-ALP)
IF (ABS(FUNC).LT.DELMIN) GO TO 101
JET13640
JET13650
JET13660
JET13670
JET13680
JET13690
JET13700
JET13710
JET13720
JET13730
JET13740
JET13750
JET13760
JET13770
JET13780
JET13790
JET13800
JET13810
JET13820
JET13830
JET13840
JET13850
JET13860
JET13870
JET13880
JET13890
JET13900
JET13910
JET13920
JET13930
JET13940
JET13950
JET13960
JET13970
JET13980
JET13990
JET14000
JET14010
JET14020
JET14030
JET14040
JET14050
JET14060
JET14070
JET14080
JET14090
JET14100
JET14110
JET14120
JET14130
JET14140
JET14150
JET14160
JET14170
JET14180
JET14190
JET14200
JET14210
JET14220
JET14230
JET14240
JET14250
JET14260
JET14270
JET14280
JET14290
JET14300
JET14310
JET14320
JET14330
JET14340
JET14350
JET14360
JET14370
JET14380
JET14390

```

Figure 69 - Continued

ORIGINAL PAGE IS
OF POOR QUALITY

```

100 CONTINUE                                     JET14400
      STOP                                       JET14410
101 ALPC=ALPN                                    JET14420
      RETURN                                    JET14430
      END                                       JET14440
                                                JET14450
                                                JET14460
                                                JET14470
      SUBROUTINE SIMN(ETAC,ALP,R,CV2,CV2A,RALP)  JET14480
C
C INTEGRAL OF JET VELOCITY PROFILE FUNCTION=CV2 JET14490
C R=RATIO OF DJH TO BJ                          JET14500
C                                                JET14510
C                                                JET14520
      A1=.5-4./((ALP+2.)) + 3./((ALP+1.))-4./((3.*ALP+7.))+1./((4.*ALP+2.))
      A2=1.-4./((ALP+1.))+6./((2.*ALP+1.))-4./((3.*ALP+1.))+1./((4.*ALP+1.))
      CV2=.5*ETAC**2+A1*(1.-ETAC)**2+ETAC*(1.-ETAC)*A2
      A1ALP=4./((ALP+2.))**2-3./((ALP+1.))**2+12./((3.*ALP+2.))**2
      I=4./((4.*ALP+2.))**2
      A2ALP=4./((ALP+1.))**2-12./((2.*ALP+1.))**2+12./((3.*ALP+1.))**2
      I=4./((4.*ALP+1.))**2
      ETAR1=(1.-ETAC)**2
      ETAR2=ETAC*(1.-ETAC)
      CV2A=ETAB1*A1ALP+ETAR2*A2ALP
      R=ETAC+(1.-ETAC)*((2.-SQRT(2.))/2.))**2*(1./ALP)
      RALP=((ETAC-R)/ALP)*ALOG((R-ETAC)/(1.-ETAC))
      RETURN
      END
                                                JET14530
                                                JET14540
                                                JET14550
                                                JET14560
                                                JET14570
                                                JET14580
                                                JET14590
                                                JET14600
                                                JET14610
                                                JET14620
                                                JET14630
                                                JET14640
                                                JET14650
                                                JET14660
                                                JET14670
                                                JET14680
      SUBROUTINE SIXTFC (TH,ETAC,ALPV,TLAM,CH,CT,CHALP,CHTLAM,CTALP,
      ICTTLAM)
      FUP(ETAP)=(1.-ETAP**ALPV)**2
      FTAP(ETAPT)=(1.-ETAPT**ALPT)**2
      FVAUP(ETAP,FV)=2.*SQRT(FV)*((SQRT(FV)-1.))*ALOG(ETAP)
      FTATP(ETAPT,FT)=2.*SQRT(FT)*((SQRT(FT)-1.))*ALOG(ETAPT)
      FTLAM(ETAPT,ETAP,TLAM)=2.*ALPT*(1.-ETAPT**ALPT)*((ETAPT**ALPT-1.))
      *(ETAP-TLAM*TLAM)
      FUNC(FV,FT)=FV/(FT+(1.-FT)/TH)
      FUN(FT)=FT/(FT+(1.-FT)/TH)
      FUNCT(FV,FT)=FV/((FT+(1.-FT)/TH)**2)
      N=24
C
C WRITE (6,800) TH,ETAC,ALPV,TLAM
      800 FORMAT (5X,4F11.5)
      BTH=(1.-TH)/TH
      N1=N-1
      ALPT=ALPV
      N2=N-2
      DETA=(1.-ETAC)/N1
      ETA=ETAC+DETA
      SUMOM=0.
      SUMOMA=0.
      SUMOMT=0.
      SUMOTA=0.
      SUMOTT=0.
      SUMOT=0.
      DO 100 I=1,N1,2
      ETAP=(ETA-ETAC)/(1.-ETAC)
      ETAPT=ETAP/TLAM
      FV=FUP(ETAP)
      FT=FTAP(ETAPT)
      FVAU=FVAUP(ETAP,FV)
      FTAT=FTATP(ETAPT,FT)
      FTLAM=FTLAM(ETAPT,ETAP,TLAM)
      SUMOM=SUMOM+FV*ETA*FUNC(FV,FT)
      SUMOMT=SUMOMT+FT*ETA*FUNC(FV,FT)
      SUMOMA=SUMOMA+2.*FVAU*ETA*FUNC(FV,FT)+FV*FTAT*ETA*BTH*FUNC(FV,FT)
      SUMOMT=SUMOMT+FV*FTLAM*ETA*FUNC(FV,FT)
      SUMOTA=SUMOTA+FVAU*ETA*FUN(FT)+FTAT*ETA*FUNC(FT,FV)+FTAT*BTH*FUNC
      I(FV,FT)*ETA
      SUMOYT=SUMOTT+FTLAM*ETA*(FUNC(FV,FT)+BTH*FUNC(FV,FT))
      ETA=ETA+2.*DETA

```

Figure 69 - Continued

ORIGINAL PAGE IS
OF POOR QUALITY

```

100 CONTINUE
ETA=ETAC+2.*DETA
SUMEM=0.
SUMET=0.
SUMEMA=0.
SUMEHT=0.
SUMETA=0.
SUMETT=0.
DO 200 I=3,N2+2
ETAP=(ETA-ETAC)/(1.-ETAC)
ETAPT=ETAP/TLAM
FV=FVP(ETAP)
FT=FTP(ETA)
FVAV=FVAVP(ETAP,FV)
FTAT=FTATP(ETAPT,FT)
FTTLAN=FTLAN(ETAPT,ETAP,TLAM)
SUMEM=SUMEM+FV*CTA*FUNC(FV,FT)
SUMET=SUMET+FT*ETA*FUNC(FV,FT)
SUMEMA=SUMEMA+2.*FVAU*ETA*FUNC(FV,FT)+FV*FTAT*ETA*DTM*FUNC(FV,FT)
SUMEHT=SUMEHT+FV*FTTLAN*ETA*FUNC(FV,FT)
SUMETA=SUMETA+FVAU*ETA*FUN(FT)+FTAT*ETA*FUC(FT,FV)+FTAT*DTM*FUNC
1(FV,FT)*ETA
SUMETT=SUMETT+TLAM*ETA*FUNC(FV,FT)+DTM*FUNC(FV,FT)
ETA=ETA+2.*DETA
200 CONTINUE
CM=.5*ETAC*ETAC+(DETA/3.)*(ETAC+4.*SUMEM+2.*SUMEM)
CT=.5*ETAC*ETAC+(DETA/3.)*(ETAC+4.*SUMOT+2.*SUMET)
CHALP=(DETA/3.)*(4.*SUMEMA+2.*SUMEMA)
CHTLAN=(DETA/3.)*(4.*SUMEHT+2.*SUMEHT)*DTM
CTALP=(DETA/3.)*(4.*SUMETA+2.*SUMETA)
CTTLAM=(DETA/3.)*(4.*SUMETT+2.*SUMETT)
C WRITE (6,700) TH,ETAC,ALPV,TLAM,CM,CT,CHALP,CHTLAM,CTALP,CTTLAM
700 FORMAT (1X,10F11.5)
RETURN
END

SUBROUTINE QHALF (TH,ET,ALPV,TLAM,QD)
FVP(ETAP)=(1.-ETAP**ALPV)**2
FTP(ETAP)=(1.-ETAP/TLAM)**ALPT**2
FVETAP(ETAP)=-2.*(1.-ETAP**ALPV)*ALPV*ETAP*(ALPV-1.)
FTETAP(ETAP)=-2.*(1.-ETAP/TLAM)**ALPT**ALPT*((ETAP/TLAM)**(ALPT-1
1.))*(1./TLAM)
REL=.5
ALPT=ALPV
C WRITE (6,700) TH,ETAC,ALPV,ALPT
700 FORMAT (1X,'TH=',F10.5,2X,'ETAC=',F10.5,2X,'ALPV=',F10.5,2X,'ALPT
1=',F10.5)
ETAP=0.
DETAP=1./24.
DO 300 I=1,25
FV=FVP(ETAP)
FT=FTP(ETAP)
QOLD=Q
Q=FV*FV*TH/(1.+FT*(TH-1.))
IF (Q.LT..5.AND.QOLD.GT..5) GO TO 367
ETAC=ETAP+DETAP
300 CONTINUE
STOP
C 367 WRITE (6,557) QOLD,Q
557 FORMAT (2X,'QOLD=',F10.5,2X,'Q=',F10.5)
367 DEDQ=DETAP/(Q-QOLD)
ETAP=ETAP+DEDQ*(.5-Q)
C WRITE (6,375) ETAP
375 FORMAT (2X,'ETAP=',F10.5)
DELIM=1.E-5
DO 100 I=1,500
FV=FVP(ETAP)
FT=FTP(ETAP)
FUETA=FVETAP(ETAP)
FTEA=FTETAP(ETAP)
DEN=1.+FT*(TH-1.)
FUNC=.5-FV*FV*TH/DEN
FUNCD=FV*FV*TH*(TH-1.)*FTEA/(DEN*DEN)-2.*FV*FUETA*TH/DEN
ETAN=ETAC-FUNC/FUNCD
ETAP=ETAP+REL*(ETAN-ETAP)
C WRITE (6,500) ETAP,FINC
500

```

JET15120
JET15130
JET15140
JET15150
JET15160
JET15170
JET15180
JET15190
JET15200
JET15210
JET15220
JET15230
JET15240
JET15250
JET15260
JET15270
JET15280
JET15290
JET15300
JET15310
JET15320
JET15330
JET15340
JET15350
JET15360
JET15370
JET15380
JET15390
JET15400
JET15410
JET15420
JET15430
JET15440
JET15450
JET15460
JET15470
JET15480
JET15490
JET15500
JET15510
JET15520
JET15530
JET15540
JET15550
JET15560
JET15570
JET15580
JET15590
JET15600
JET15610
JET15620
JET15630
JET15640
JET15650
JET15660
JET15670
JET15680
JET15690
JET15700
JET15710
JET15720
JET15730
JET15740
JET15750
JET15760
JET15770
JET15780
JET15790
JET15800
JET15810
JET15820
JET15830
JET15840
JET15850
JET15860
JET15870
JET15880
JET15890

Figure 69 - Continued

ORIGINAL PAGE IS
OF POOR QUALITY

```

500 FORMAT (1X,2F10.5)
IF (ABS(FUNC).LT.1.E-5) GO TO 200
100 CONTINUE
STOP
200 RD=ETAC+(1.-ETAC)*ETAP
RETURN
END ..

SUBROUTINE SINTV (TN, TM, ALPV, TLAN, CM, CT, CMTM, CTTM)
FVP(ETA)=(1.-ETA**ALPV)**2
FTF(ETA)=(1.-ETA/TLAN)**ALPT**2
FUNC(ETA,FV,FT)=FV*ETA/(FT+(1.-FT)/TMB)
FUNCD(ETA,FV,FT)=FV*ETA*((1.-FT)/(TMB*TM))/((FT+(1.-FT)/TMB)**2)
N=24
ALPT=ALPV
C WRITE (6,777) TN, TM, ALPV, ALPT, CM, CT
TMB=TM*TM
N1=N-1
N2=N-2
DETA=1./N1
ETA=DETA
SUMOM=0.
SUMOT=0.
SUMOTM=0.
SUMOCH=0.
DO 100 I=1,N1,2
FV=FVP(ETA)
FT=FTF(ETA)
SUMOM=SUMOM+FV*FUNC(ETA,FV,FT)
SUMOT=SUMOT+FT*FUNC(ETA,F,FT)
SUMOCH=SUMOCH+FV*FUNCD(ETA,FV,FT)
SUMOTM=SUMOTM+FT*FUNCD(ETA,FV,FT)
ETA=ETA+2.*DETA
100 CONTINUE
ETA=2.*DETA
SUMEM=0.
SUMECM=0.
SUMETH=0.
DO 200 I=3,N2,2
FV=FVP(ETA)
FT=FTF(ETA)
SUMEM=SUMEM+FV*FUNC(ETA,FV,FT)
SUMET=SUMET+FT*FUNC(ETA,FV,FT)
SUMECM=SUMECM+FV*FUNCD(ETA,FV,FT)
SUMETH=SUMETH+FT*FUNCD(ETA,FV,FT)
ETA=ETA+2.*DETA
200 CONTINUE
CM=(DETA/3.)*(4.*SUMOM+2.*SUMEM)
CT=(DETA/3.)*(4.*SUMOT+2.*SUMET)
CMTM=(DETA/3.)*(4.*SUMOCH+2.*SUMECM)
CTTM=(DETA/3.)*(4.*SUMOTM+2.*SUMETH)
C WRITE (6,777) TN, TM, ALPV, ALPT, CM, CT
777 FORMAT (1X,6F10.5)
RETURN
END

SUBROUTINE GPRES (RO, VG, TNG, ALPG, R, CPG)
FUNC(ALP)=.5-4./((ALP+2.)*3./((ALP+1.)*4./((3.*ALP+2.)*1./((4.*ALP
1+2.))
FUNCD(ALP)=4./((ALP+2.)*2)-3./((ALP+1.)*2)+12./((3.*ALP+2.)*2)
1-4./((4.*ALP+2.)*2)
C THIS ROUTINE SOLVES GROUND PRESSURE INTEGRAL FOR GROUND PRESSURE
C EXPONENT
C
ALPG=1.5
REL=.5
DELMIN=1.E-5
DO 100 I=1,99
CPG=FUNC(ALPG)
CPGP=FUNCD(ALPG)
F=TNG-RO*RO*VG*VG*CPG
FP=-RO*RO*VG*VG*CPGP
ALPG=ALPG-REL*F/FP
C WRITE (6,500) ALPG, CPG, CPGP.

```

JET15900
JET15910
JET15920
JET15930
JET15940
JET15950
JET15960
JET15970
JET15980
JET15990
JET16000
JET16010
JET16020
JET16030
JET16040
JET16050
JET16060
JET16070
JET16080
JET16090
JET16100
JET16110
JET16120
JET16130
JET16140
JET16150
JET16160
JET16170
JET16180
JET16190
JET16200
JET16210
JET16220
JET16230
JET16240
JET16250
JET16260
JET16270
JET16280
JET16290
JET16300
JET16310
JET16320
JET16330
JET16340
JET16350
JET16360
JET16370
JET16380
JET16390
JET16400
JET16410
JET16420
JET16430
JET16440
JET16450
JET16460
JET16470
JET16480
JET16490
JET16500
JET16510
JET16520
JET16530
JET16540
JET16550
JET16560
JET16570
JET16580
JET16590
JET16600
JET16610
JET16620
JET16630
JET16640
JET16650
JET16660
JET16670
JET16680
JET16690

Figure 69 - Continued

ORIGINAL PAGE IS
OF POOR QUALITY

```

500 FORMAT (1X,F10.5)
IF (ABS(F).LT.DELMIN) GO TO 101
100 CONTINUE
STJF
101 RETURN
END
JET16700
JET16710
JET16720
JET16730
JET16740
JET16750
JET16760
JET16770
JET16780
SUBROUTINE SIMW(KDEL,N,ALPW,R,CV2,CP)
JET16790
C
C THIS ROUTINE COMPUTES THE INTEGRAL OF THE VELOCITY SQUARED PROFILE
JET16800
C AND STATIC PRESSURE PROFILE FOR WALL JET FUNCTIONS
JET16810
C CV2=VELOCITY SQUARED INTEGRAL
JET16820
C CP=STATIC PRESSURE INTEGRAL
JET16830
C R=RATIO OF BWH TO BW
JET16840
C
JET16850
C
JET16860
REAL KDEL,N
JET16870
XN=N
JET16880
XI1=1.-4./(ALPW+1.)+6./(2.*ALPW+1.)-4./(3.*ALPW+1.)+1./(4.*ALPW+1.)
JET16890
1)
JET16900
CV2=(XN/(2.+XN))*KDEL+(1.-KDEL)*XI1
JET16910
CP=KDEL+(1.-KDEL)*XI1
JET16920
F=((2.-SORT(2.))/2.)**(1./ALPW)
JET16930
R=KDEL+(1.-KDEL)*F
JET16940
WRITE (6,500) CV2,CP
JET16950
500 FORMAT (1X,'CV2=',F10.5,2X,'CP=',F10.5)
JET16960
RETURN
JET16970
END
JET16980
JET16990
SUBROUTINE SIMUG(ALPW,R,CV2U)
JET17000
C
C THIS ROUTINE COMPUTES VELOCITY SQUARED INTEGRAL FOR UPWASH
JET17010
C
JET17020
CV2U=1.-4./(ALPW+1.)+6./(2.*ALPW+1.)-4./(3.*ALPW+1.)+1./(4.*ALPW+1.)
JET17030
1.)
JET17040
F=(SORT(2.)-1.)/SORT(2.)
JET17050
R=F*(1./ALPW)
JET17060
RETURN
JET17070
END
JET17080
JET17090
JET17100
JET17110
JET17120
JET17130
JET17140
SUBROUTINE GMATT (TN,RG,DELPS,PMBI,TMI,UMI,ALPG,KDEL,N,ETAWG,DELS
JET17150
1,ALPW,R,BWO,BWH,TLAM)
JET17160
C
C THIS ROUTINE IS USED FOR INITIATING WALL JET REGION
JET17170
C COMPUTES THE INITIAL INVISCID EXPONENT FOR WALL JET PROFILE
JET17180
C
JET17190
C
JET17200
REAL KDEL,N
JET17210
BWO=DELS/KDEL
JET17220
TLAM=1.1
JET17230
ALPW=.5
JET17240
CALL SIMWH (TN,TMI,TLAM,PMBI,KDEL,N,ALPW,ALPG,ETAWG,DELPS,UMI,
JET17250
1,BWO,RG)
JET17260
RCON=(2.-SORT(2.))/2.
JET17270
R=KDEL+(1.-KDEL)*RCON*(1./ALPW)
JET17280
BWH=R*BWO
JET17290
C
JET17300
WRITE (4,709) TLAM,ALPW,BWO,BWH
JET17310
709 FORMAT (1X,'TLAM=',F10.5,2X,'ALPW=',F10.5,2X,'BWO=',F10.5,2X,'BWH',
JET17320
1=' ',F10.5)
JET17330
RETURN
JET17340
END
JET17350
JET17360
JET17370
SUBROUTINE SIMWH(TN,TM,TLAM,PMB,KDEL,N,ALPW,ALPG,ETAWG,DELPS,VM,
JET17380
1,BW,RG)
JET17390
REAL KDEL,N
JET17400
TMB=TM*(N
JET17410
REL=.5
JET17420
DELMIN=1.E-5
JET17430
FETAG=(1.-ETAWG*ALPG)*ALPG
JET17440
FMOM=1.-FETAG
JET17450
WRITE (6,400) FETAG,FMOM,BW,RG
JET17460

```

Figure 69 - Continued

ORIGINAL PAGE IS
OF POOR QUALITY

```

400 FORMAT (1X,'FETAG',4F10.5)
DO 100 I=1,200
CALL SIMUTI (TN,TH,TLAM,PHB,KDEL,N,ALPW,CV2,CP,CT,CV2A,CV2L
1,CPA,CTA,CTL,R,RALP)
C WRITE (6,740) CV2,CP,CT,CV2A,CV2L,CPA,CTA,CTL,R
740 FORMAT (1X,9F10.5)
F=FHON-RG8BU8(2.8PN8*UHS*UHS*CV2/TH+DELPS8FETAG8CP)
G=FHON8TH8(TN-1.)-2.8PH8*UHS(THB-1.)8RG8BU8CT
FALP=-RG8BU8(2.8PH8*UHS*UHS*CV2A/TH+DELPS8FETAG8CPA)
FLAM=-RG8BU8(2.8PH8*UHS*UHS*CV2L/TH)
GALP=-2.8FH8*UHS(THB-1.)8G8BU8CTA
GLAM=-2.8FH8*UHS(THB-1.)8G8BU8CTL
C WRITE (6,750) FALP,FLAM,GALP,GLAM
750 FORMAT (1X,'FA=',F10.5,1X,'FL=',F10.5,1X,'GA=',F10.5,1X,'GL=',F10.
15)
DET=FALP8GLAM-FLAM8GALP
DALP=(G8FLAM-F8GLAM)/DET
DLAM=(F8GALP-G8FALP)/DET
ALPW=ALPW+REL8DALP
TLAM=TLAM+REL8DLAM
C WRITE (6,500) F,G,ALPW,TLAM
500 FORMAT (1X,4F15.5)
100 CONTINUE
STOP
101 CONTINUE
RETURN
END

SUBROUTINE SIMUTI (TN,TH,TLAM,PHB,KDEL,N,ALPW,CV2,CP,CT,CV2A,CV2L
1,CPA,CTA,CTL,R,RALP)
REAL KDEL,N
FUP(ETAP)=(1.-ETAP8ALPV)882
FTP(ETAP)=(1.-ETAP/TLAM)88ALPT882
FVA(ETAP)=-2.8(ETAP8ALPV)8(1.-ETAP8ALPV)8ALOG(ETAP)
FTA(ETAPT)=-2.8(ETAPT8ALPT)8(1.-ETAPT8ALPT)8ALOG(ETAPT)
FPA(ETAP)=-4.8(ETAP8ALPV)8(1.-ETAP8ALPV)8838ALOG(ETAP)
FTL(ETAPT)=-2.8(1.-ETAPT8ALPT)8ALPT8(ETAPT8ALPT)/TLAM
FUNC(FV,FT,FP)=FV8(FP+(1.-FP)/PHB)8FT+(1.-FT)/THB)
FUNC(FV,FT,FP)=FV8(FP+(1.-FP)8(FT+(1.-FT)/THB)882)
FUN(FV,FT)=FT8(FP+(1.-FP)/PHB)8(FP+(1.-FT)/THB)
FUNT(FV,FT)=FV8FT/(FT+(1.-FT)/THB)
NPTS=24
ALPT=ALPV
C WRITE (6,777) TN,TH,ALPW,ALPT,CM,CT
777 FORMAT (1X,10F10.5)
THB=TH8TN
DTM=(1.-THB)/THB
BFM=(PHB-1.)/PHB
N1=NPTS-1
N2=NPTS-2
XN1=N1
DETA=(1.-KDEL)/XN1
ETA=KDEL+DETA
SUMON=0.
SUMOT=0.
SCV2A=0.
SCV2L=0.
SCTA=0.
SCTL=0.
DO 100 I=1,N1+2
ETAP=(ETA-KDEL)/(1.-KDEL)
ETAPT=ETAP/TLAM
IF (ETAPT.GT.1.) ETAPT=1.
FV=FUP(ETAP)
FT=FTP(ETAP)
FP=FV8FU
FVALP=FVA(ETAP)
FTALP=FTA(ETAPT)
FPALP=FPA(ETAP)
FTLAM=FTL(ETAPT)
SUMON=SUMON+FV8FUNC(FV,FT,FP)
SUMOT=SUMOT+FT8FUNC(FV,FT,FP)

```

Figure 69 - Continued

```

SCV2A0=SCV2A0+FUNC(FV,FT,FP)*(2.*FVALP+FV*FPALP*DFM)
1+FUNC(D(FV,FT,FF)*FV*FTALP*DTM
SCV2L0=SCV2L0+FUNC(D(FV,FT,FP)*FV*FTLAM*DTM
SCTA0=SCTA0+FVALP*FUN(FV,FT,FP)+FUNC(FV,FT,FP)*FTALP
1+FUNT(FV,FT)*FFALP*DFM+FUNC(D(FV,FT,FP)*FT*FTALP*DTM
SCTL0=SCTL0+FUNC(FV,FT,FP)*FTLAM+FUNC(D(FV,FT,FP)*FT*FTLAM*DTM
ETA=ETA+2.*DETA
100 CONTINUE
ETA=KDEL+2.*DETA
SUMEM=0.
SUMET=0.
SCV2AE=0.
SCV2LE=0.
SCTAE=0.
SCTLE=0.
DO 200 I=3,N2,2
ETAP=(ETA-KDEL)/(1.-KDEL)
ETAPT=ETAP/TLAM
IF (ETAPT.GT.1.) ETAPT=1.
FV=FVP(ETAP)
FT=FTF(ETAP)
FP=FV*FV
FVALP=FVA(ETAP)
FTALP=FTA(ETAP)
FFALP=FPA(ETAP)
FTLAM=FTL(ETAPT)
SUMEM=SUMEM+FV*FUNC(FV,FT,FP)
SUMET=SUMET+FT*FUNC(FV,FT,FP)
SCV2AE=SCV2AE+FUNC(FV,FT,FP)*(2.*FVALP+FV*FPALP*DFM)
1+FUNC(D(FV,FT,FP)*FV*FTALP*DTM
SCV2LE=SCV2LE+FUNC(D(FV,FT,FP)*FV*FTLAM*DTM
SCTAE=SCTAE+FVALP*FUN(FV,FT,FP)+FUNC(FV,FT,FP)*FTALP
1+FUNT(FV,FT)*FFALP*DFM+FUNC(D(FV,FT,FP)*FT*FTALP*DTM
SCTLE=SCTLE+FUNC(FV,FT,FP)*FTLAM+FUNC(D(FV,FT,FP)*FT*FTLAM*DTM
ETA=ETA+2.*DETA
200 CONTINUE
CV2=N*KDEL/(2.*N)+(DETA/3.)*(1.+4.*SUMEM+2.*SUMET)
CT=N*KDEL/(1.*N)+(DETA/3.)*(1.+4.*SUMOT+2.*SUMET)
CV2A=(DETA/3.)*(4.*SCV2A0+2.*SCV2AE)
CV2L=(DETA/3.)*(4.*SCV2L0+2.*SCV2LE)
CTA=(DETA/3.)*(4.*SCTA0+2.*SCTAE)
CTL=(DETA/3.)*(4.*SCTL0+2.*SCTLE)
CPF=1.-4./(ALPU+1.)*6./(2.*ALFV+1.)*4./(3.*ALFV+1.)*1./(4.*ALPU+1.
1)
CPF0=4./((ALPU+1.)*2)-12./((2.*ALFV+1.)*2)+12./((3.*ALFV+1.)*2)
1-4./((4.*ALFV+1.)*2)
CP=KDEL+(1.-KDEL)*CPF
CFA=(1.-KDEL)*CPF0
RCOM=(2.-SDRT(2.))/2.
R=KDEL+(1.-KDEL)*RCOM*(1./ALFV)
RP=(R-KDEL)/(1.-KDEL)
RALP=(KDEL-1.)*RP*ALOG(RP)/ALFV
WRITE (6,777) TN,TH,ALPU,ALPT,CV2,CP,CT
C 777 FORMAT (1X,7F10.5)
RETURN
END

SUBROUTINE SIMMTV (TN,TH,TLAM,PHB,KDEL,N,ALPU,CV2,CP,CT,CV2TM,CTTM)
1,R)
REAL KDEL,N
FVP(ETAP)=(1.-ETAP**ALFV)**2
FTF(ETAP)=(1.-ETAP/TLAM)**ALPT**2
FUNC(FV,FT,FP)=FV*(FP+(1.-FP)/PHB)/(FT+(1.-FT)/TMB)
FUNC(D(FV,FT,FP))=FV*(1.-FT)/(TMB*TM)*(FP+(1.-FP)/PHB)/((FT+(1.-FT)
1)/(TMB)**2)
NPTS=24
ALPT=ALPU
WRITE (6,777) TN,TH,ALPU,ALPT,CH,CT
C TMB=TM*TN
DTM=(1.-TMB)/TMB
DFM=(PHB-1.)/PHB
N1=NPTS-1
N2=NPTS-2
XN1=N1
DETA=(1.-KDEL)/XN1
ETA=KDEL+DETA
SUMEM=0.

```

Figure 69 - Continued

```

SUMOT=0.
SCV2TO=0.
SCTHO=0.
DO 100 I=1,N1,2
ETAP=(ETA-KDEL)/(1.-KDEL)
ETAPT=ETAP/TLAM
IF (ETAPT.GT.1.) ETAPT=1.
FU=FUP(ETAP)
FT=FTP(ETAP)
FP=FV*FU
SUMOM=SUMOM+FU*FUNC(FU,FT,FP)
SUMOT=SUMOT+FT*FUNC(FU,FT,FP)
SCV2TO=SCV2TO+FUNC(FU,FT,FP)*FU
SCTHO=SCTHO+FUNC(FU,FT,FP)*FT
ETA=ETA+2.*DETA
100 CONTINUE
ETA=KDEL+2.*DETA
SUMEM=0.
SUMET=0.
SCV2TE=0.
SCTHE=0.
DO 200 I=3,N2,2
ETAP=(ETA-KDEL)/(1.-KDEL)
ETAPT=ETAP/TLAM
IF (ETAPT.GT.1.) ETAPT=1.
FU=FUP(ETAP)
FT=FTP(ETAP)
FP=FV*FU
SUMEM=SUMEM+FU*FUNC(FU,FT,FP)
SUMET=SUMET+FT*FUNC(FU,FT,FP)
SCV2TE=SCV2TE+FUNC(FU,FT,FP)*FU
SCTHE=SCTHE+FUNC(FU,FT,FP)*FT
ETA=ETA+2.*DETA
200 CONTINUE
CV2=M*KDEL/(2.+N)+(DETA/3.)*(1.+4.*SUMOM+2.*SUMEM)
CT=M*KDEL/(1.+N)+(DETA/3.)*(1.+4.*SUMOT+2.*SUMET)
CV2TH=(DETA/3.)*(4.*SCV2TO+2.*SCV2TE)
CTTH=(DETA/3.)*(4.*SCTHO+2.*SCTHE)
CPF=1.-4./(ALPV+1.)+4./(2.*ALPV+1.)-4./(3.*ALPV+1.)+1./(4.*ALPV+1.)
1)
CP=KDEL+(1.-KDEL)*CPF
RCON=(2.-SDRT(2.))/2.
R=KDEL+(1.-KDEL)*RCON*(1./ALPV)
WRITE (6,777) TM,TH,ALPV,ALPT,CV2,CP,CT
777 FORMAT (1X,7F10.5)
RETURN
END

SUBROUTINE FGUMAT(CUFD,DELPS,DELPW,RO,SD,ALPG,ALPUG)
DIMENSION ERR(101),SIG(101)

C THIS ROUTINE COMPUTES EXPONENT OF UPWASH GROUND PRESSURE PROFILE
C
SIG(1)=.10
SIG(2)=1.0
ALPUFD=.5
DO 100 I=1,100
PB=(DELPS/DELPW)**(.25)
ETAG=SD*(1.-SIG(I))/RO
ETAU=SIG(I)/CUFD
F1=PB*(1.-ETAG**ALPG)
F2=1.-ETAU**ALPUFD
ERR(I)=F1-F2
IF (I.EQ.1) GO TO 100
S=(SIG(I)-SIG(I-1))/(ERR(I)-ERR(I-1))
IF (ABS(ERR(I)).LT.1.E-5) GO TO 101
SIG(I+1)=SIG(I)-S*ERR(I)
100 CONTINUE
STOP
101 SIGUO=SIG(I)
ETAM=SIGUO/CUFD
IF (ETAM.GT.1.0) ETAM=1.0
PHIN=DELPW*(1.-ETAM**ALPUFD)**4
CALL PHATCH (PHIN,DELPW,ALFUG)
RETURN
END

```

```

JET19000
JET19010
JET19020
JET19030
JET19040
JET19050
JET19060
JET19070
JET19080
JET19090
JET19100
JET19110
JET19120
JET19130
JET19140
JET19150
JET19160
JET19170
JET19180
JET19190
JET19200
JET19210
JET19220
JET19230
JET19240
JET19250
JET19260
JET19270
JET19280
JET19290
JET19300
JET19310
JET19320
JET19330
JET19340
JET19350
JET19360
JET19370
JET19380
JET19390
JET19400
JET19410
JET19420
JET19430
JET19440
JET19450
JET19460
JET19470
JET19480
JET19490
JET19500
JET19510
JET19520
JET19530
JET19540
JET19550
JET19560
JET19570
JET19580
JET19590
JET19600
JET19610
JET19620
JET19630
JET19640
JET19650
JET19660
JET19670
JET19680
JET19690
JET19700
JET19710
JET19720
JET19730
JET19740
JET19750
JET19760
JET19770

```

Figure 69 - Continued

```

SUBROUTINE PMATCH (PMIN,PMAX,ALPUG)
DIMENSION ERR(101),AL(101)
C
C THIS ROUTINE COMPUTES THE EXPONENT OF THE PRESSURE PROFILE FOR
C THE UPWASH DEFLECTION ZONE
C
ALPUFD=1.7
PB=PMIN/PMAX
ETAM=(1.-PB**25)**(1./ALPUFD)
CALL SINUF(ALPUFD,ETAM,CSPUFD)
AL(1)=1.5
AL(2)=3.0
DO 100 I=1,100
CALL SINUF(AL(I),1.0,CSPU)
X1=ETAM*(PB+(1.-PB)**CSPU)
X2=CSPUFD
ERR(I)=X1-X2
IF (ABS(ERR(I)).LT.1.E-5) GO TO 101
IF (I.EQ.1) GO TO 100
S=(AL(I)-AL(I-1))/(ERR(I)-ERR(I-1))
AL(I+1)=AL(I)-S*ERR(I)
100 CONTINUE
STOP
101 ALPUG=AL(I)
RETURN
END

SUBROUTINE SINUF(ALPU,ETA,CSPU)
A1=ETA
A2=-4./(ALPU+1.)*ETA**2
A3=6./(2.*ALPU+1.)*ETA**3
A4=-4./(3.*ALPU+1.)*ETA**4
A5=1./(4.*ALPU+1.)*ETA**5
CSPU=A1+A2+A3+A4+A5
RETURN
END

SUBROUTINE SIN(ETAC,ALP,R,CV2)
C
C INTEGRAL OF JET VELOCITY PROFILE FUNCTION=CV2
C R=RATIO OF BJH TO BJ
C
A1=.5-4./(ALP+2.)*3./(ALP+1.)-4./(3.*ALP+2.)*1./(4.*ALP+1.)
A2=1.-4./(ALP+1.)*6./(2.*ALP+1.)-4./(3.*ALP+1.)*1./(4.*ALP+1.)
CV2=.5*ETAC**2+A1*(1.-ETAC)**2+ETAC*(1.-ETAC)*A2
R=ETAC*(1.-ETAC)*((2.-SQRT(2.))/2.)*1./ALP
RETURN
END

SUBROUTINE SIMU(ALPU,R,CV2U)
CV2U=1.-4./(ALPU+1.)*6./(2.*ALPU+1.)-4./(3.*ALPU+1.)*1./(4.*ALPU+1.)
F=(SQRT(2.)-1.)/SQRT(2.)
R=F**2/ALPU
RETURN
END

SUBROUTINE SIMH(TN,TM,TLAM,FMB,ALPU,FETAG,DELHWS,UM,PU,RG,R,FM
ITNEFF,TAEFF)
C
C WRITE (6,111) FMB,UM
111 FORMAT (1X,'FMB=',F10.5,2X, 'UM=',F10.5)
FMB=FMB*TN
REL=.5
IFLAG=0
DELHIN=1.E-5
TLAM=1.0
TLAMI=TLAM
C
WRITE (6,400) FETAG,FHOM,PU,RG

```

JET19780
JET19790
JET19800
JET19810
JET19820
JET19830
JET19840
JET19850
JET19860
JET19870
JET19880
JET19890
JET19900
JET19910
JET19920
JET19930
JET19940
JET19950
JET19960
JET19970
JET19980
JET19990
JET20000
JET20010
JET20020
JET20030
JET20040
JET20050
JET20060
JET20070
JET20080
JET20090
JET20100
JET20110
JET20120
JET20130
JET20140
JET20150
JET20160
JET20170
JET20180
JET20190
JET20200
JET20210
JET20220
JET20230
JET20240
JET20250
JET20260
JET20270
JET20280
JET20290
JET20300
JET20310
JET20320
JET20330
JET20340
JET20350
JET20360
JET20370
JET20380
JET20390
JET20400
JET20410
JET20420
JET20430
JET20440
JET20450
JET20460
JET20470
JET20480
JET20490
JET20500
JET20510
JET20520
JET20530
JET20540
JET20550
JET20560

Figure 69 - Continued

```

400 FORMAT (1X,'FETAG',4F10.5) JET20570
DO 100 I=1,50 JET20580
CALL SIMUTI (TN,TH,TLAM,PHR,ALFU,CV2,CP,CT,CV2L,CTL,R) JET20590
IF (I.EQ.1) BU=FHOM/(RG*CV2*(2. JET20600
(SVM**2+DELPWS*FETAG)) JET20610
IF (I.EQ.1) BUI=BU JET20620
C WRITE (6,740) CV2,CP,CT,CV2L,CTL,R JET20630
740 FORMAT (1X,6F10.5) JET20640
C IF (I.EQ.1) WRITE (6,103) BU JET20650
103 FORMAT (1X,'BU EST.',F10.5) JET20660
F=FHOM-RG*(2.*PHB*UHM*UHM*CV2/TH+DELPWS*FETAG*CF) JET20670
G=FHOM*TH*(TH-1.)-2.*PHB*UHM*(THB-1.)*RG*BU*CT JET20680
FBU=-RG*(2.*PHB*UHM*UHM*CV2/TH+DELPWS*FETAG*CP) JET20690
FLAM=-RG*BU*(2.*PHB*UHM*UHM*CV2L/TH) JET20700
GRU=-2.*PHB*UHM*(THB-1.)*RG*CT JET20710
GLAM=-2.*PHB*UHM*(THB-1.)*RG*BU*CTL JET20720
C WRITE (6,750) FBU,FLAM,GRU,GLAM JET20730
750 FORMAT (1X,'FA=',F10.5,1X,'FL=',F10.5,1X,'GA=',F10.5,1X,'GL=',F10. JET20740
15) JET20750
DET=FBU*GLAM-FLAM*GRU JET20760
IF (ABS(DET).LT.1.E-10) ILFLAG=1 JET20770
IF (ABS(DET).LT.1.E-10) GO TO 101 JET20780
DBU=(G*FLAM-F*GLAM)/DET JET20790
DLAM=(F*GRU-G*FBU)/DET JET20800
RU=BU*REL*DBU JET20810
TLAM=TLAM*REL*DLAM JET20820
IF (TLAM.LT.0.) IFLAG=1 JET20830
IF (TLAM.LT.0.) GO TO 101 JET20840
C WRITE (6,500) F,G,RU,TLAM JET20850
IF (ABS(F).LT.DELMIN.AND.ABS(G).LT.DELMIN) GO TO 101 JET20860
500 FORMAT (1X,4F15.5) JET20870
100 CONTINUE JET20880
STOP JET20890
101 IF (IFLAG.EQ.1) BU=BUI JET20900
IF (IFLAG.EQ.1) TLAM=TLAM JET20910
RETURN JET20920
END JET20930
JET20940
JET20950
JET20960
JET20970
SUBROUTINE SIMUTI (TN,TH,TLAM,PHR,ALFU,CV2,CP,CT,CV2L,CTL,R) JET20970
FUP(ETAP)=(1.-ETAP**ALFU)**2 JET20980
FTP(ETAP)=(1.-(ETAP/TLAM)**ALPT)**2 JET20990
FTL(ETAPT)=2.*(1.-ETAPT**ALPT)*ALPT*(ETAPT**ALPT)/TLAM JET21000
FUNC(FU,FT,FP)=FU*(FP+(1.-FP)/PHR)/(FT+(1.-FT)/THB) JET21010
FUNC(FU,FT,FP)=FU*(FP+(1.-FP)/PHB)/(FT+(1.-FT)/THB)**2 JET21020
NPTS=24 JET21030
ALPT=ALFU JET21040
C WRITE (6,777) TN,TH,ALFU,ALPT,CM,CT JET21050
777 JET21060
THB=TH*TN JET21060
DTH=(1.-THB)/THB JET21070
DPH=(PHR-1.)/PHB JET21080
N1=NPTS-1 JET21090
N2=NPTS-2 JET21100
XN1=N1 JET21110
DETA=1./XN1 JET21120
ETA=DETA JET21130
SUMOM=0. JET21140
SUMOT=0. JET21150
SCV2LO=0. JET21160
SCTL0=0. JET21170
DO 100 I=1,N1+2 JET21180
ETAP=ETA JET21190
ETAPT=ETAP/TLAM JET21200
IF (ETAPT.GT.1.) ETAPT=1. JET21210
FU=FUP(ETAP) JET21220
FT=FTP(ETAP) JET21230
FP=FU*FU JET21240
FTLAM=FTL(ETAPT) JET21250
SUMOM=SUMOM+FU*FUNC(FU,FT,FP) JET21260
SUMOT=SUMOT+FT*FUNC(FU,FT,FP) JET21270
SCV2LO=SCV2LO+FUNC(FU,FT,FP)*FU*FTLAM*DTH JET21280
SCTL0=SCTL0+FUNC(FU,FT,FP)*FT*FTLAM*DTH JET21290
ETA=ETA+2.*DETA JET21300

```

Figure 69 - Continued

ORIGINAL PAGE IS
OF POOR QUALITY

```

100 CONTINUE
ETA=2.*DETA
SUMEN=0.
SUMET=0.
SCV2LE=0.
SCTLE=0.
DO 200 I=3,N2,2
ETAP=ETA
ETAPT=ETAP/TLAM
IF (ETAPT.GT.1.) ETAPT=1.
FU=FUP(ETAP)
FT=FTP(ETAP)
FP=FV*FU
FTLAM=FTL(ETAPT)
SUMEN=SUMEN+FU*FUNC(FV,FT,FP)
SUMET=SUMET+FT*FUNC(FV,FT,FP)
SCV2LE=SCV2LE+FUNC(FV,FT,FP)*FU*FTLAM*DTM
SCTLE=SCTLE+FUNC(FV,FT,FP)*FTLAM+FUNC(FV,FT,FP)*FT*FTLAM*DTM
ETA=ETA+2.*DETA
200 CONTINUE
CV2=(DETA/3.)*4.*(1.+4.*SUMON+2.*SUMFM)
CT=(DETA/3.)*4.*(1.+4.*SUMOT+2.*SUMET)
CV2L=(DETA/3.)*4.*(4.*SCV2LO+2.*SCV2LE)
CTL=(DETA/3.)*4.*(4.*SCTLO+2.*SCTLE)
CP=1.-4./(ALPV+1.)*6./(2.*ALPV+1.)*4./(3.*ALPV+1.)*1./(4.*ALPV+1.
)
RCON=(2.-SORT(2.))/2.
R=RCON**2/(ALPV)
C WRITE (6,777) TN,TH,ALPV,ALFT,CV2,CP,CT
777 FORMAT (1X,7F10.5)
RETURN
END

SUBROUTINE SIMUTV (TN,TH,TLAM,PHB,ALPV,CV2,CP,CT,CV2TH,CTH,R)
FUP(ETAP)=(1.-ETAP**ALPV)**2
FTP(ETAP)=(1.-(ETAP/TLAM)**ALPT)**2
FUNC(FV,FT,FP)=FV*(FP+(1.-FP)/PHB)/(FT+(1.-FT)/THB)
FUNC(FV,FT,FP)=FV*(1.-FT)/(THB*TH)**(FP+(1.-FP)/PHB)/((FT+(1.-FT)
1)/THB)**2)
NPTS=24
ALPT=ALPV
C WRITE (6,777) TN,TH,ALPV,ALFT,CH,CT
THB=TH*TH
DTM=(1.-THB)/THB
DPH=(PHB-1.)/PHB
N1=NPTS-1
N2=NPTS-2
XN1=N1
DETA=1./XN1
ETA=DETA
SUMOH=0.
SUMOT=0.
SCV2TD=0.
SCTHO=0.
DO 100 I=1,N1,2
ETAP=ETA
ETAPT=ETAP/TLAM
IF (ETAPT.GT.1.) ETAPT=1.
FU=FUP(ETAP)
FT=FTP(ETAP)
FP=FV*FU
SUMOH=SUMOH+FU*FUNC(FV,FT,FP)
SUMOT=SUMOT+FT*FUNC(FV,FT,FP)
SCV2TD=SCV2TD+FUNC(FV,FT,FP)*FU
SCTHO=SCTHO+FUNC(FV,FT,FP)*FT
ETA=ETA+2.*DETA

```

JET21310
JET21320
JET21330
JET21340
JET21350
JET21360
JET21370
JET21380
JET21390
JET21400
JET21410
JET21420
JET21430
JET21440
JET21450
JET21460
JET21470
JET21480
JET21490
JET21500
JET21510
JET21520
JET21530
JET21540
JET21550
JET21560
JET21570
JET21580
JET21590
JET21600
JET21610
JET21620
JET21630
JET21640
JET21650
JET21660
JET21670
JET21680
JET21690
JET21700
JET21710
JET21720
JET21730
JET21740
JET21750
JET21760
JET21770
JET21780
JET21790
JET21800
JET21810
JET21820
JET21830
JET21840
JET21850
JET21860
JET21870
JET21880
JET21890
JET21900
JET21910
JET21920
JET21930
JET21940
JET21950
JET21960
JET21970
JET21980

Figure 69 - Continued

ORIGINAL PAGE IS
OF POOR QUALITY

100 CONTINUE	JET21990
ETA=2.*DETA	JET22000
SUMEM=0.	JET22010
SUMET=0.	JET22020
SCV2TE=0.	JET22030
SCTME=0.	JET22040
DO 200 I=3,N2,2	JET22050
ETAP=ETA	JET22060
ETAPT=ETAP/TLAM	JET22070
IF (ETAPT.GT.1.) ETAPT=1.	JET22080
FV=FVP(ETAP)	JET22090
FT=FTP(ETAP)	JET22100
FP=FV*FV	JET22110
SUMEM=SUMEM+FV*FUNC(FV,FT,FP)	JET22120
SUMET=SUMET+FT*FUNC(FV,FT,FP)	JET22130
SCV2TE=SCV2TE+FUNC(FV,FT,FP)*FV	JET22140
SCTME=SCTME+FUNC(FV,FT,FP)*FT	JET22150
ETA=ETA+2.*DETA	JET22160
200 CONTINUE	JET22170
CV2=(DETA/3.)*(1.+4.*SUMEM+2.*SUMET)	JET22180
CT=(DETA/3.)*(1.+4.*SUMOT+2.*SUMET)	JET22190
CV2TH=(DETA/3.)*(4.*SCV2TO+2.*SCV2TE)	JET22200
CTTH=(DETA/3.)*(4.*SCTHO+2.*SCTHE)	JET22210
CPF=1.-4./(ALPV+1.)+6./(2.*ALPV+1.)-4./(3.*ALPV+1.)+1./(4.*ALPV+1.)	JET22220
1)	JET22230
CP=CPF	JET22240
RCON=(2.-SQRT(2.))/2.	JET22250
R=RCON*(1./ALPV)	JET22260
WRITE (6,777) TN,TH,ALPV,ALPT,CV2,CP,CT	JET22270
777 FORMAT (1X,7F10.5)	JET22280
RETURN	JET22290
END	JET22300
	JET22310
	JET22320
	JET22330

Figure 69 - Concluded.

8 - REFERENCES

1. Full-Scale Tests of Grumman Design 698-411 Tilt-Nacelle V/STOL Model at the NASA-Ames Research Center, Grumman Report PDR 698-53, December, 1981.
2. Hill, W.G., Jr., and Jenkins, R.C., "Experimental Investigation of Multiple Jet Impingement Flows Applicable to VTOL Aircraft in Ground Effect", Grumman Research Department Memorandum RM-605, November 1975.
3. Migdal, D., Hill, W.G., Jr., Jenkins, R.C. and Siclari, M.J., "VTOL in Ground Effect Flows for Closely Spaced Jets", NASA CR 152321, Dec. 1979.
4. Jenkins, R.A. and Hill, W.G., Jr., "Investigation of VTOL Upwash Flows Formed by Two Impinging Jets," Grumman Research Department RE-548, November 1977.
5. Platzer, M.F. and Margason, R.J., "Prediction Methods for Jet V/STOL Propulsion Aerodynamics", Jr. of Aircraft, Vol. 15, No. 2, pp. 69-77, Feb. 1978.
6. Siclari, M.J., Migdal, D., and Palcza, J.L., "The Development of Theoretical Models for Jet-Induced Effects on V/STOL Aircraft", AIAA Paper No. 75-1216, AIAA/SAE 11th Propulsion Conference, Anaheim, Cal., Sept. 29-Oct. 1, 1975.
7. Siclari, M.J., Hill W.G., Jr., and Jenkins, R.C., "Investigation of Stagnation Line and Upwash Formation", AIAA Paper No. 77-615, AIAA/NASA, Ames V/STOL Conference, June 1977.
8. Schlichting, H., Boundary Layer Theory, McGraw Hill, 1960
9. Reichardt, H., Gesetzmer Bigkeiten der freien Turbulenz, VDI - Forschungsheft, 414 (1942), 2 ed. 1951.
10. Abramovich, G.H., The Theory of Turbulent Jets, MIT Press, 1963.
11. Harsha, P.T., "Free Turbulent Mixing: A Critical Evaluation of Theory and Experiment", AEDC-TR-71-36, Feb. 1971.

12. Schauer, J.J., and Eustis, R.H., "The Flow Development and Heat Transfer Characteristics of Plane Turbulent Impinging Jets", NSF 69705, Sept. 1963.
13. Corrsin, S. and Uberoi, M., "Further Experiments on the Flow and Heat Transfer in a Heated Turbulent Air Jet", NACA Report 998, 1947.
14. Giralt, F.G., Chia, C.J., and Trass, O., "Characterization of the Impingement Region in an Axisymmetric Turbulent Jet", Industrial Engineering Chemistry, Fundamentals, Vol. 16, No. 1, 1977.